2019

HIDRAULICA

HYDRAULICS-PNEUMATICS-TRIBOLOGY-ECOLOGY-SENSORICS-MECHATRONICS

No. 1

ISSN 1453-7303
ISSN-L 1453-7303

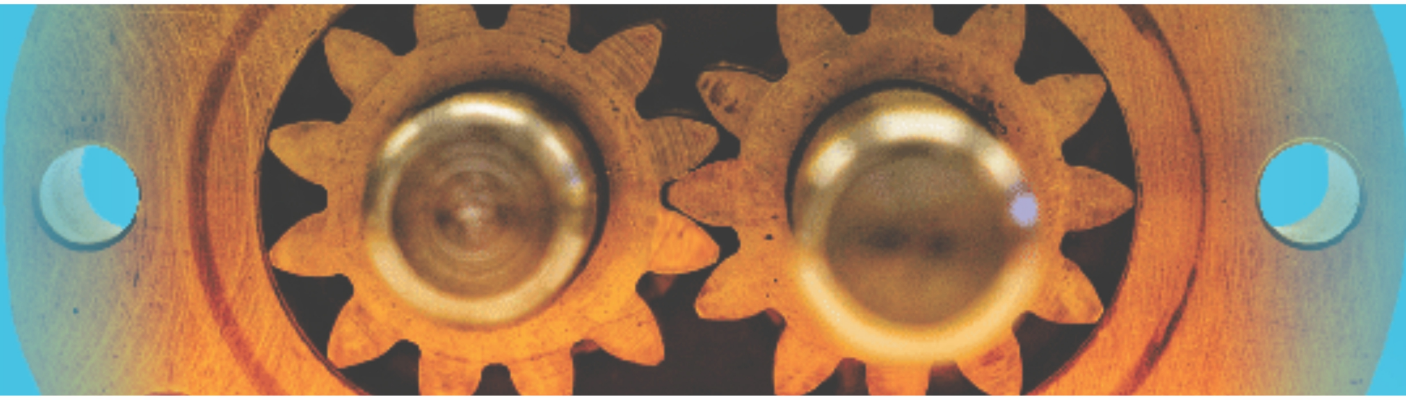

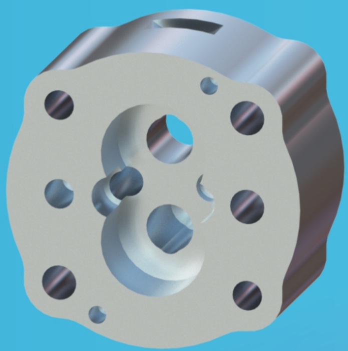

Computer-aided design (CAD)

Computer-aided engineering (CAE)

Computer-aided manufacturing (CAM)

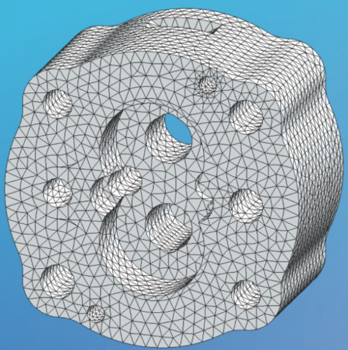

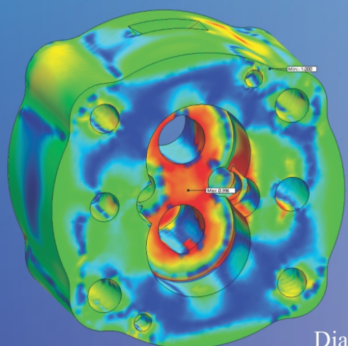

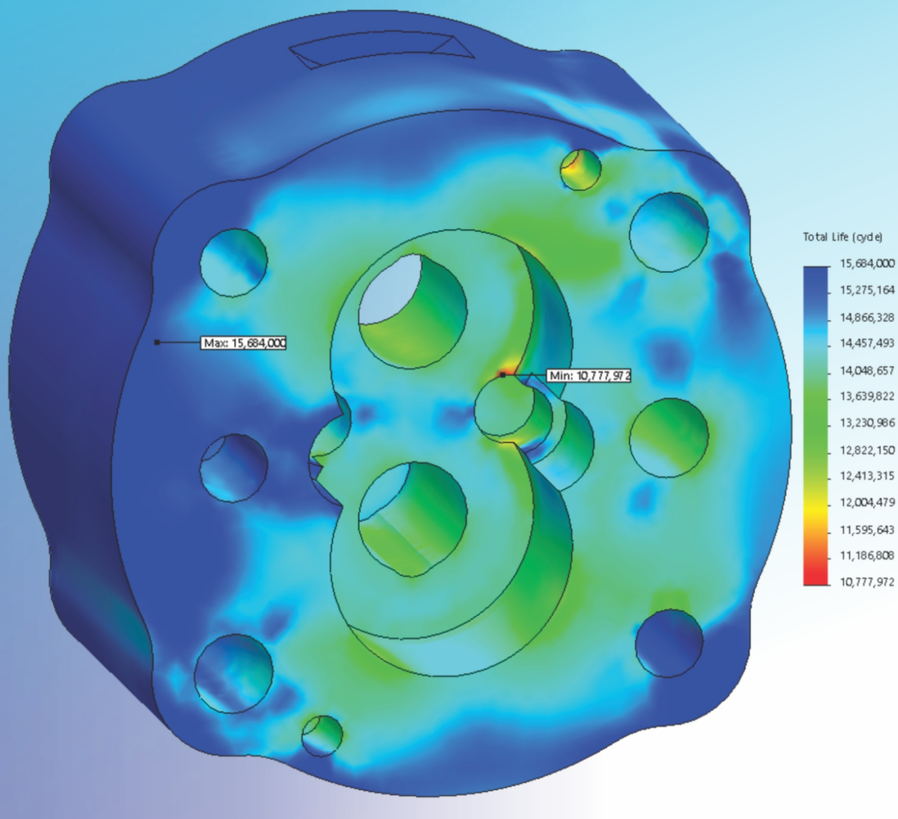

Diagrams from the paper on page 88.

hidraulica.fluidas.ro

CONTENTS

Published by:
Hydraulics and Pneumatics Research Institute, Bucharest-Romania
Address: 14 Cuţitul de Argint, district 4, Bucharest, 040558, Romania
Phone: +40 21 336 39 91; Fax: +40 21 337 30 40; e-Mail: ihp@fluidas.ro; Web: www.ihp.ro
with support from:
National Professional Association of Hydraulics and Pneumatics in Romania - FLUIDAS
e-Mail: fluidas@fluidas.ro; Web: www.fluidas.ro

HIDRAULICA Magazine is indexed by international databases

ISSN 1453 – 7303; ISSN – L 1453 – 7303

EDITORIAL

How do we complete a repair? A point of view.

Ph.D.Eng. Petrin DRUMEA
MANAGING EDITOR

Repairs in hydraulics are usually difficult and quite expensive, even though many of the beneficiaries consider that they can only offer up to 2-3 percent of the initial price for a repair service. Of course, the problem of repairs is neither simple nor easy, but it is not the most complicated activity in the technical - technological field, too.

The first difficult issue is finding the fault, since basically we have to fix what does not work, that is to intervene where there is an irregularity that influences the proper functioning of the machine. Therefore, it has to be determined right from the beginning whether the failure is caused by the wear and tear of a piece of equipment or by a mechanical, electrical or cleaning accident.

After the malfunction is determined, the specialist determines how to remedy it, and he / she also indicates by whom and where the repair should be done. As a general recommendation, I believe that the repair is to be done by industry specialists who have tools and devices, as well as a properly equipped laboratory. Such a laboratory shall be equipped with stands and devices to certify the quality of the repair. I do not think it is acceptable to check the correctness of the repair of a piece of hydraulic equipment directly on the machine in which it is included. Under these conditions, the conclusion is that the repair will be completed with a separate functional test, conducted in a specialized laboratory.

Being a repair, the level and complexity of the tests do not have to cover the whole range of parameters checked in the case of type testing, not even in batch testing; they shall only be limited to achieving operation, reaching the flow rate and reaching the working pressure specified in the product catalog.

The test stands and devices should not be equipped with computer control systems and sensing technology of a too high level, either, because this would lead to a non-rewarding increase in repair which will include the costs of control tests and checking. It is important that following this laboratory check there is a certainty of proper functioning and at the performance level required to ensure the working parameters of the machine to which the hydraulic system belongs.

This material refers mainly to corrective maintenance rather than predictive maintenance, that is, to faults that have occurred and not to those that might occur in running of a machine over time.

In conclusion, we note that it is not right to make repairs without performing final tests and functional checks in a dedicated laboratory.

Heavy Duty Machine Tools – Hydraulic Balancing of the Kinematic Chains

Prof. PhD Eng. **Dan PRODAN**[1], Prof. PhD Eng. **Anca BUCUREȘTEANU**[1],
Assoc. Prof. PhD Eng. **Adrian MOTOMANCEA**[1]

[1] University POLITEHNICA of Bucharest, prodand2004@yahoo.com, ancabucuresteanu@gmail.com, adrian.motomancea@deltainfo.ro

Abstract: *The authors of this paper introduce some of the hydraulic balancing systems for the large rams, cross-rails and housings which travel vertically. These systems are used for the feed and/or positioning kinematic chains of the heavy-duty machine tools. The paper presents the hydraulic basic diagrams, the methodology of calculation and the manufactured units. These low-cost systems are equipped with usual hydraulic devices. The balancing hydraulic units can be used for DC or CNC machines.*

Keywords: *Heavy duty machine tools, feed/positioning kinematic chain, hydraulic balancing*

1. Necessity of balancing

In the case of heavy duty machine tools (vertical lathes, gantry type milling machines, boring and milling machines), there are different sub-assemblies such as housings, rams and cross-rails that are moved vertically by means of the feed/positioning kinematic chains [1, 2, 3]. The mass of these sub-assemblies ranges from 500 to 15000 kg. Their drive kinematic chain is shown in Figure 1.

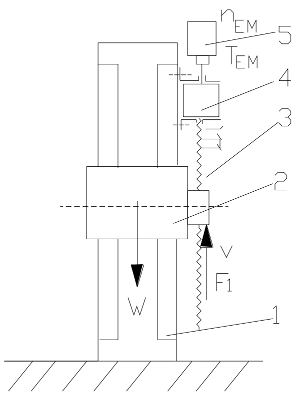

Fig. 1. Kinematic diagram of the vertical feed kinematic chain without balancing

The load 2 is moved on the guideways 1 by the feed kinematic chain which includes the leading screw 3, the reducer 4 and the electric motor 5. The transfer ratio of the reducer 4 is i (i<1) and the screw pitch is l [2, 3, 4].
For going up, if the electric motor develops the rotational speed n_{EM} and the torque T_{EM}, taking into account the weight of the entire assembly as W and neglecting the frictions, in stationary conditions, it is possible to determine the force F_1 and the speed v by means of the relations:

$$F_1 = W = \frac{2\pi}{il} T_{EM} \quad (1)$$

$$v = il n_{EM} \quad (2)$$

For example, for W = 50000 N, i = 1/2, v = 9 m/min, l = 20 mm, the motor should have the rotational speed n_{EM} = 900 RPM and the torque T_{EM} = 80 Nm. The power required in this case is P = 7.5 KW.
In order to unload the feed kinematic chain, which entails the use of feed motors with reduced torque and reduced power implicitly, it is necessary to use mechanical balancing, with

counterweight or hydraulic balancing. Mechanical balancing involves the use of counterweights as shown in Figure 2.

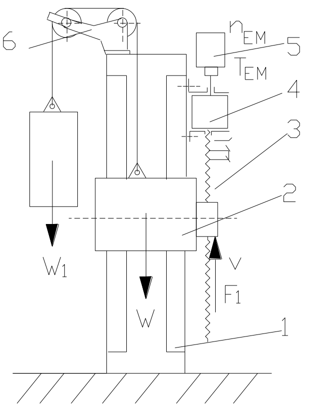

Fig. 2. Kinematic diagram of the vertical feed kinematic chain balanced with counterweight

In this case, the counterweight W_1 balances totally or partially the weight W through the agency of the pulley system 6. The force developed in the feed kinematic chain, in stationary regime, will be equal to the difference between W and W_1.

The mechanical balancing has a series of disadvantages:

- it doubles the mass of the system, so that the performances are diminished in dynamic conditions. The acceleration of a mechanical system is inversely proportional to its mass. When the mass is doubled, it is obvious that the acceleration decreases accordingly;
- the structure of the machine has the size necessary for a large system, so it will be a solid one, made of a large amount of material;
- the counterweight requires a guiding and safety system;
- faulty pulley system entails the risk of an uncontrolled fall of the counterweight that could damage the entire machine.

2. Hydraulic balancing

In the case of a hydraulic balancing, the counterweight shown in Figure 2 will be replaced by the hydraulic cylinder 7 with the useful cross section S as in Figure 3. This one is supplied from a hydraulic source at a pressure p with the proper flow, marked with Q. The other notations in Figure 3 are similar to the notations used in the previous figures.

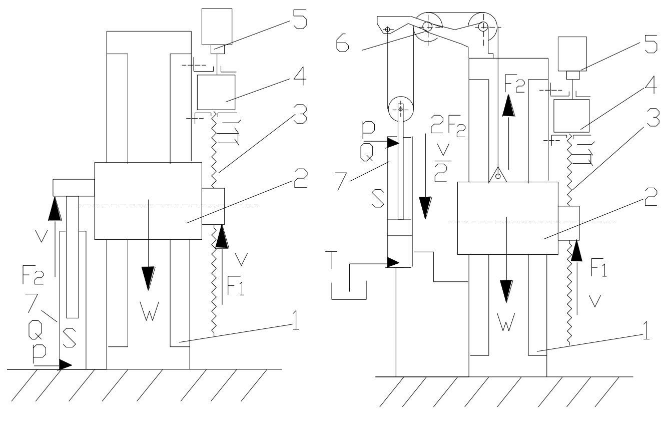

a. b.

Fig. 3. Balancing systems with hydraulic cylinders

In both cases, the sub-assembly 2 is moved by the feed kinematic chain formed of the screw 3, reducer 4 and motor 5 but also by the hydraulic cylinder 7 [1]. The possible losses of oil are recovered by the drainage on path T.

2.1 Mathematical models in stationary regime

Figure 3a shows the case in which cylinder 7 is directly connected to the balanced sub-assembly **2**. In this case, we shall consider:

$$F_1 = W - F_2 = \frac{2\pi}{il} T_{EM} \tag{3}$$

$$F_2 = pS \tag{4}$$

$$Q = Sv = Siln_{EM} \tag{5}$$

If the balancing is made as shown in Figure 3b, the relations above become:

$$F_1 = W - F_2 = \frac{2\pi}{il} T_{EM} \tag{6}$$

$$F_2 = S\frac{p}{2} \tag{7}$$

$$Q = S\frac{v}{2} = S\frac{iln_{EM}}{2} \tag{8}$$

If the travels are shorter, usually up to 1000-2000 mm and the weights are smaller (the rams of the vertical lathes or Gantry-type machines) it is possible to use the variant shown in Figure 3a. In the case of the machines with large masses to be balanced along travels over 2500-3000 mm, such as the boring and milling machines, it is recommended to use the balancing variant shown in Figure 3b. Thus, it is possible to use cylinders with halved lengths in comparison with the cylinders used in the Figure 3a variant.

In stationary conditions, the good operation of the machine requires a hydraulic unit able to provide the necessary flow Q and the working pressure p. The velocity is ensured by the feed kinematic chain and the load (or part of it) is taken over by the hydraulic system. As for the CNC machines, the velocity is commanded and controlled by the equipment.

Regardless the balancing variant selected, the necessary power of the feed kinematic chain is significantly reduced thanks to the hydraulic unit with an available theoretical power P_H:

$$P_H = pQ \tag{9}$$

2.2 Mathematical models in dynamic regime

It is considered that the feed kinematic chain can ensure a maximum velocity v_{MAX} in an acceleration time t_A according to the characteristics shown in Figure 4.

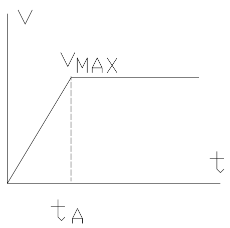

Fig. 4. Time dependence of velocity ensured by the feed kinematic chain

Taking into account the travel shown above, the loading diagram is the one presented in Figure 5.

The mass of the system is obtained by dividing the weight W by the gravitational acceleration (g), the friction forces in the two guideways are considered equal ($F_F/2$). The acceleration of the system is the second derivative of space; the first derivative is the velocity.

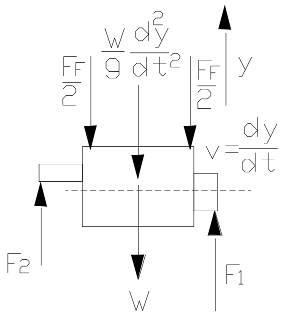

Fig. 5. The loading diagram

Regarding the diagram in Figure 3a, the following mathematical model can be taken into consideration in dynamic regime:

$$\frac{W}{g}\frac{d^2y}{dt^2}+b\frac{dy}{dt}+sgnvF_F+W=F_1+pS \tag{10}$$

$$Q=S\frac{dx}{dt}+ap+\frac{V_0+yS}{E_O}\frac{dp}{dt} \tag{11}$$

If the balancing system is the one shown in Figure 3b, the mathematical model in dynamic regime becomes:

$$\frac{W}{g}\frac{d^2y}{dt^2}+b\frac{dy}{dt}+sign(v)F_F+W=F_1+S\frac{p}{2} \tag{12}$$

$$Q=S\frac{1}{2}\frac{dx}{dt}+ap+\frac{V_0+\frac{y}{2}S}{E_O}\frac{dp}{dt} \tag{13}$$

Other notations used in the relations (10) - (13): b - linearization coefficient of force losses proportional to velocity (damping coefficient), sign - (signum function), a - linearization coefficient of flow losses proportional to pressure, V_0 - oil inactive volume in cylinder and feed pipe, E_O - elastic modulus of oil. On the basis of mathematical models, it is possible to make the analysis of the operation in dynamic regime by simulation, using specialized programs.
If the average volume under pressure in the cylinder is V_M = SC/2, where C is the cylinder stroke, it can be concluded that the own frequency of the cylinder is V_M = SC/2 in both cases:

$$f=\frac{1}{2\pi}\sqrt{\frac{E_O g S^2}{W V_M}} \tag{14}$$

In these conditions, it is recommended that the acceleration time t_A checks the condition [5]:

$$t_A \geq \frac{2.4}{f} \tag{15}$$

The control equipment of feed kinematic chain will provide acceleration consistent with the condition shown by the relation (15). So, in the case of a vertical lathe with the ram having the weight W = 20000 N, balanced by a cylinder with the useful surface S = 20 cm^2 and the total stroke C = 1000 mm, it results a minimum acceleration time of 0.4 s. The maximum acceleration will be a_{MAX} = 0.33 m/s^2 in order to reach the maximum velocity imposed v_{MAX} = 8 m/min.
The hydraulic source must provide the necessary pressure and flow in any phase: going up, STOP or going down. The necessary flow for the ram of the vertical lathe mentioned above, in maximum velocity regime, is Q = 16 l/min. Considering that a total balancing is made, the operating pressure in stationary regime is p = 100 bar.

In real conditions, the balancing is done so that the hydraulic unit does not take over exactly the balanced weight. If such a balancing was done when starting or stopping the operation, the movement would entail positioning and machining errors and also the wear of the kinematic chain elements because of the backlash occurred in the nut-screw mechanism. An over-balancing ($F_2 > W$) is recommended. In this case, the contact on only one flank of the lead screw must be maintained in order to reduce the return backlash.

3. Simulation of the balancing hydraulic systems running

In the design stage of a balancing unit, the simulation programs can be really helpful [5].
Let's consider a kinematic chain with the following values: W = 20000 N, i = 1/2, l = 10 mm, v_{Max} = 8 m/min. The actuation is made as in Figure 3a. Balancing cylinder has S = 20 cm^2, the stroke is C = 1000 mm.
Given these conditions, if the frictions are neglected and an acceleration time t_A is imposed, the necessary torque at the electric motor T_{EM}, for an unbalanced system, is:

$$T_{EM} \geq \left(W + \frac{W v_{MAX}}{g t_A}\right)\frac{il}{2\pi} \tag{16}$$

After making the replacements in the relation (16), for an acceleration time t_A = 0.5 s, checking condition (15), we shall obtain the condition $T_{EM} \geq 17$ Nm. The maximum rotational speed of the motor will be:

$$n_{EM} = \frac{v_{MAX}}{il} \tag{17}$$

Following up the replacements, it will be obtained n_{EM} = 1600 RPM.
In the case of the above-mentioned kinematic chain, the balancing is considered actuated at the adjusted pressure of 110 bar, thus leading to the over-balancing.
Figure 6 shows the evolution of the pressure in the balancing cylinder and the evolution of the velocity of the subassembly 2 in Figure 3a. The acceleration time imposed at the electric motor is t_A = 0.5 s too and its maximum rotational speed n_{EM} = 1600 RPM.

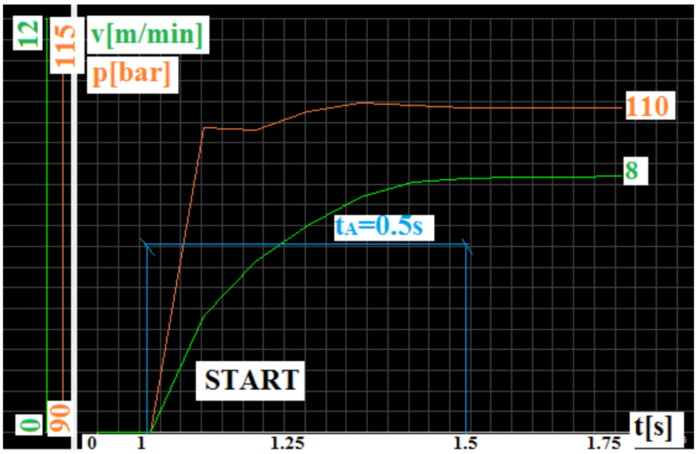

Fig. 6. Evolution of pressure and velocity in the balancing unit

The characteristics in Figure 6 were obtained for an electric motor that develops the theoretical maximum torque T_{EM} = 2 Nm. In these conditions, the system stabilizes after 0.5 s approximately. It is worth mentioning that the initial pressure in the cylinder must ensure the load taking over before the start of the feed kinematic chain.
By using a well-sized balancing unit, the efforts of the feed kinematic chain are diminished, therefore the behavior of the system is improved during rapid travel or when it operates in coordination with the travels on other axes (in the case of interpolation).

4. Balancing hydraulic units

There are several balancing diagrams used for the actuation of the vertical kinematic chains of the heavy duty machine-tools. The most frequently used three variants are presented hereby [6].

4.1 Balancing units with 3-way pressure reducing valve

The basic diagram of such unit is presented in Figure 7.

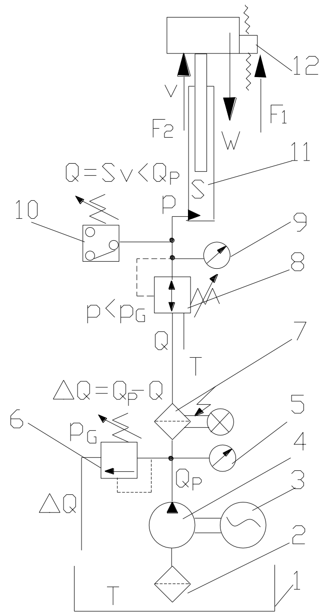

Fig. 7. Balancing hydraulic system with pressure reducing valve

The electric motor 3 drives the constant flow pump 4 which sucks the oil from the tank 1 (T) through the suction filter 2. The oil is filtered by the filter with clogging indicator 7. General pressure p_G is adjusted by means of the pressure relief valve 6. The balancing pressure p is adjusted at the pressure reducing valve 8. The two pressures p_G and p are read by means of the pressure gauges 5 and 9. Other notations used in Figure 7, in addition to the notations already presented, are:10 - pressure switch, 11 - balancing cylinder, 12 - feed kinematic chain, ΔQ - flow directed through the pressure relief valve 6. The flow supplied by the pump is Q_P and the flow used by the balancing system is Q.

The general conditions of operation are:

$$Q = Sv \tag{18}$$

$$v \in [-v_{MAX}, v_{MAX}] \tag{19}$$

$$Q \in [0, Sv_{MAX}] \tag{20}$$

$$\Delta Q = Q_P - Q \tag{21}$$

$$p < p_G \tag{22}$$

In the phases where the balanced assembly must not go upwards, the unit can also achieve other functions at the general pressure p_G. In the case of the CNC machines, the pressure switch 10 is the one that confirm the presence of the pressure required by the balancing. This diagram is relatively simple, it uses ordinary items and the price is low. The use of gear pumps is a simple and cheap solution, but has the disadvantage of a high consumption of energy even during the phases when the feed kinematic chain is not actuated. This energy consumption has also negative effects as for the system heating. For these reasons it should be used at pressures up to 40 bar and for flows smaller than 20 l/min. Therefore, some vertical lathes use this system that operate at the pressure p_G = 35 bar while the pump passes a flow Q_P = 16 l/min. In this case, 1.5 KW of the power supplied by the electric motor is used for the balancing. The hydraulic tank (with a volume of 220 l) is placed inside the machine bed and is used by the lubrication unit too.

4.2 Closed circuit balancing units

Figure 8 shows the hydraulic diagram of balancing in closed circuit for AF127 machine.

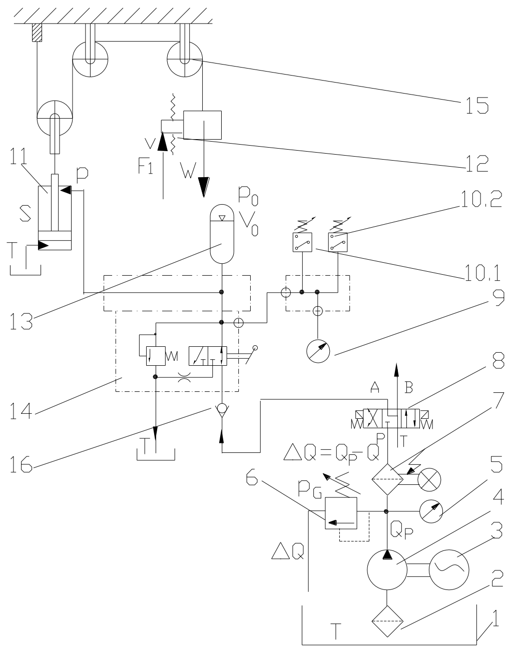

Fig. 8. Balancing system in closed circuit

The notations W, F_1, p, S, T, p_G, Q, ΔQ, 1 - 7, 9, 11 and 12 in Figure 8 are the same as the ones in Figure 7. Supplementary notations: 8 - hydraulic distributor, 10.1 – pressure switch for minimum pressure (p_m), 10.2 - pressure switch for maximum pressure (p_M), 13 - accumulator (accumulators), 14 - safety block, 15 - pulley system, 16 - check valve.
The closed circuit includes cylinder 11, accumulator 13, pressure switches 10.1 and 10.2 and check valve 16. Accumulator 13 has the volume V_0 and is loaded with nitrogen at the initial pressure p_0. After making the circuit with the cylinder piston in low position, the distributor 8 is clutched in the position that makes possible the circulation of the oil P→A and B→T. The closed circuit is fed through the check valve 16 up to a pressure equal to p_m. When this pressure is reached, the circuit is considered to be loaded, thus the distributor is declutched, path P is closed and paths A and B are connected to the tank (T).
The nitrogen was submitted to an isothermal transformation in the accumulator, according to the relation [7, 8];

$$p_0 V_0 = p_m V_M \tag{23}$$

An amount of oil entered the accumulator, entailing the decrease of the initial volume of nitrogen from the value V_0 to the value V_M.
In this phase, the feed kinematic chain is unloaded with a force F_2 expressed as follows:

$$F_2 = \frac{p_m S}{2} \tag{24}$$

If we consider that the balanced assembly 12 gets down by the quantity y, the nitrogen in the accumulator suffers an isothermal or adiabatic transformation. The transformation is an adiabatic one if the travel is made with high velocity, in the range of seconds. The isothermal transformation is made in a slow pace, in the range of minutes [7]. The relations that describe these transformations are listed below:

$$p_m V_M^{\gamma} = p_{(y)}\left(V_M - \frac{yS}{2}\right)^{\gamma} \quad (25)$$

$$p_m V_M = p_{(y)}(V_M - \frac{yS}{2}) \quad (26)$$

$$y \in [0,2C] \quad (27)$$

In these relations, C is the stroke of the cylinder 11. For nitrogen, it can be considered that γ = 1.4.
We can notice that the balancing force is variable and it increases when the load goes downwards:

$$F_{2(y)=}\frac{p_{(y)}S}{2} \quad (28)$$

The maximum value of this pressure p_M is reached when the cylinder rod gets in the higher end of the travel. This pressure is signaled by the pressure switch 10.2. The unit is able to operate by the charge and discharge of the accumulator towards and coming from the cylinder, even if the pump does not supply this circuit. If the connections P→B and A→T are made, the pump can supply other consumers too, through the path B. When the pressure drops under the adjusted value p_m, as shown by the pressure switch 10.1, the recharge of the circuit (P→A and B→T) shall be commanded.
The unit is relatively simple: it includes usual devices; the pump has constant flow and the energy consumption is very low (it occurs practically only when the circuit is charged). These are the main advantages of such systems. There are also some disadvantages, like:
- only one accumulator is not usually enough; batteries of accumulators are needed; therefore, the price of the unit gets bigger;
- the balancing force (F_2) is variable. It has a minimum value when the load is up and a maximum value when the load is down. These variations are felt by the feed kinematic chain and entail variations of the motor torque;
- the failure of the accumulator (accumulators) leads to the instantaneous immobilization of the machine because the feed kinematic chain is overstressed.

4.3 Balancing units with pumps with pressure regulator

A balancing unit with pressure regulator pump used for modern vertical lathes, Gantry-type machines and also for horizontal boring and milling machines (HBM-s) is presented in Figure 9.
The motor 2 actuates the pump with variable flow 3 which sucks the oil from the tank 1 (T). The general pressure p_1 is adjusted by means of the pressure switch of the pump. The pressure p_2 is regulated at the pressure relief valve 6 and it is usually higher by 5-10 bar than pressure p_1. The two pressures p_1 and p_2 can be read on the pressure gauges 4 and 8. The one-way check valve 5 closes if the pressure downstream exceeds the value p_1. The pressure switch 7 is set at a pressure p_3, smaller by 5 bar at the most related to p_1. This switch confirms the presence of pressure in circuit and in cylinder 9 too, making possible the actuation of the feed kinematic chain 10. The circuit also includes an accumulator 11 and the safety block of this one 12. The filtering of the oil in circuit is made by the return filter 13. When the unit starts operating, the circuit reaches the pressure p1. If no movement is commanded, the pressure regulator sets the pump in null flow position. In this case, the accumulator is charged at the pressure p_1. If the load travels upwards, the pump supplies the necessary flow depending on the velocity. When the load travels downwards, the one-way check valve 5 closes, the pump regulator passes the pump to the null flow position and the oil of the cylinder runs into the tank through the pressure relief valve 6 and the return filter 13. In this phase, the balancing is made at the pressure p_2. Actually, the pump supplies the circuit only during the moving upwards phases. In STOP phase and moving downwards phase, the pressure regulator declutches the pump, thus the consumed energy and the unit heating are reduced considerably.

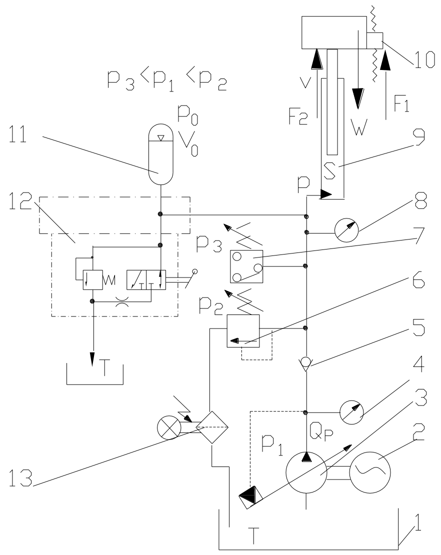

Fig. 9. Balancing unit with pump provided with pressure regulator

The pressure achieved in each one of these phases and the respective flows are shown in Figure 10 [5, 6].

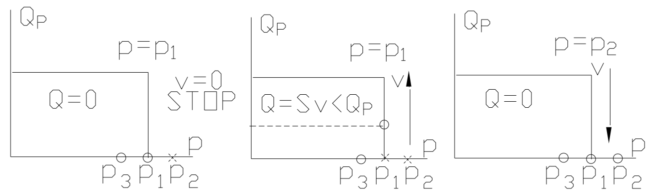

a. STOP b. Going upwards c. Going downwards
Fig. 10. Flow-pressure characteristics in the three phases of operation

If the STOP phase occurs after the going upwards phase, the pressure is p_1 and the flow ensured by the pump is 0. If the STOP phase occurs after the going downwards phase, the pressure downstream the check valve and in the accumulator has value p_2; the pressure upstream the check valve has the value p_1 and the flow supplied by the pump is 0. In the going upwards phase, the pressure in the entire unit is p_1 and the pump supplies enough flow to achieve the imposed velocity but smaller than the maximum flow. In the going downwards phase, the pressure downstream the check valve and in the accumulator has value p_2; the pressure upstream the check valve has the value p_1 and the flow supplied by the pump is 0. The accumulator 11 operates between the pressures p_1 and p_2, making possible the flow peaks required by the acceleration phases. Due to this accumulator, the balancing unit operates as a locking unit too during the STOP phases. Figure 11 shows such a unit manufactured with usual devices [5].

Fig. 11. Balancing hydraulic unit with pump with pressure regulator

Figure 11 kept the same notations used in Figure 9. The tank has a volume of 230 l and is equipped with a temperature probe and an electronic level gauge. The pump ensures a maximum flow Q_P = 20 l/min; the adjusted pressures are p_1 = 75 bar, p_2 = 85 bar and p_3 = 70 bar. The electric motor has the power 4 KW. The cylinder – not shown in Figure 11 – has an active cross-section of 20 cm^2. The maximum velocity imposed in the feed kinematic chain is v_{MAX} = 8 m/min and the balanced weight is W = 14000 N.
Because these units use the pressure regulator and also an accumulator, it is recommended to use them for balancing big loads, over 100000 N, with maximum velocities up to 10 m/min. Thus, in the case of a machine AFP 200 type, such balancing unit ensures the vertical displacement of a housing with W = 150000 N with maxima velocity of 8 m/min. Pump has a maximum flow Q_P = 100 l/min and the working pressure p_1 = 105 bar, p_2 = 115 bar, p_3 = 100 bar.

5. Conclusions

In the case of the vertical feed kinematic chains for heavy duty machines it is recommended that the load (slide, housing, ram) is balanced hydraulically. The hydraulic balancing should be preferred instead of the mechanical one given its higher performances, especially dynamic regime. In order to choose the hydraulic balancing variant, a study of the necessary power should be done. In a first phase, this power can be estimated as equal to the product of the weight to be balanced (W) and the maximum velocity of the respective kinematic chain. For small powers, up to 2-3 KW, it is possible to use balancing systems with pressure reducing valves and debit constant flow pump. The systems in closed circuit or the pumps with pressure regulator could be used in the case of higher powers, over 20000 N.
The systems in closed circuit use pumps with constant flow but need high volume accumulators. The balancing force in these systems is not constant and depends on the load position. The systems with regulator pumps can achieve the balancing of big loads but they need more expensive devices. The presence of an accumulator in this unit improves its behavior in transient regime and also ensures the operation of the system for locking the load during the STOP phases.
Regardless of the variant selected, the kinematic chain will be driven in such way to be in dynamic compliance with the hydraulic unit, providing a proper acceleration time.

References

[1] Prodan, Dan. *Heavy machine tools. Mechanical and Hydraulic Systems/Maşini-unelte grele. Sisteme mecanice si hidraulice*. Bucharest, Printech Publishing House, 2010.
[2] Perovic, Bozina. *Machine tools handbook/Handbuch Werkzeug-Maschinen*. Munchen, Carl Hanser Verlag, 2006.
[3] Joshi, P. H. *Machine tools handbook*. New Delhi, McGraw-Hill Publishing House, 2007.
[4] Teixido, C., J-C. Jouanne, B. Bauwe, P. Chambraud, G. Ignatio and C. Guerin. *Guide de Construction Mecanique*. Paris, Delagrave Edition, 2000.
[5] *** Catalogues and leaflets BOSCH REXROTH, BERARMA, ATOS.
[6] Prodan, Dan, Anca Bucuresteanu, Adrian Motomancea and Emilia Balan. "Balancing Hydraulic Units. General Considerations." *International Journal of Engineering and Innovative Technology (IJEIT)* Vol. 3, Issue 5, (November 2013): 234-237.
[7] Bucuresteanu, Anca. *Pneumatic Hydraulic Accumulators. Use and Modeling/Acumulatoare pneumohidraulice. Utilizare si modelare*. Bucharest, Printech Publishing House, 2001.
[8] Prodan, Dan, Anca Bucuresteanu, Tiberiu Dobrescu and Adrian Motomancea. "Mathematical Models on the Closed Circuit Balancing Systems in Machine Tools." *Applied Mechanics and Materials.* Vol. 859, (2017):170-176.

Automatic Processing Station Actuated by Pneumatic Drive

Ph.D. Eng. **Ionel Laurentiu ALBOTEANU**[1]

[1] University of Craiova, Faculty of Electrical Engineering, lalboteanu@em.ucv.ro

Abstract: *The paper presents an automatic processing system made on a small scale. The entire structure is integrated in an electro-pneumatic drive system with linear actuators and rotary pneumatic motors, supplied by the solenoid valves. The system is controlled by a PLC in accordance with the required operating protocol.*

Keywords: *Automatic, PLC, pneumatic, processing station.*

1. Introduction

The advantages, qualities and flexibility of the pneumatic drives, the facilities offered by the interface elements have allowed a rapid improvement and adaptation to the new requirements imposed by the specifics of the processes in which they are integrated [1].
The rapid paces of technology development and advances in electronics have today enabled the development of highly efficient drive equipment and a high degree of "intelligence" built into it. Thus, the main direction of current research is to improve the control of pneumatic drives by incorporating "intelligence" [2].
Robots and manipulators are the most complex and flexible machines that have been created and used by man so far that incorporate pneumatic drives. Taking into account these considerations the paper presents an automatic processing system using a manipulator robot and a pneumatic actuation system purpose in [3].

2. Structure of processing station

The processing station consists of a machine tool (MT) with a stock of raw input pieces and a stock of output semi-finished products (Fig.1) and a manipulator robot (MR) transferring the work pieces from the stock Input to the machine tool [3].

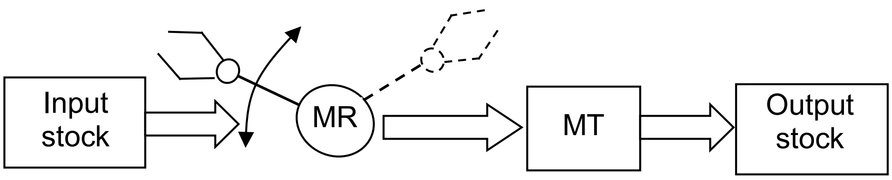

Fig. 1. Structure of processing station

It is considered that the MT performs a single operation (for example, pressing, stamping, drilling, threading, etc.) on a single ingots. It is also considered that both input and output stocks have a limited capacity at a semi-finished product.
The entire structure is integrated in an electro-pneumatic drive system with linear actuators (pneumatic cylinder) and rotary (rotary pneumatic motors), controlled by monostable and bistable valves [4].
Thus, the manipulator robot- MR comprises four modules and machine tool- MT comprises a main processing module and the outlet module machined semi-finished products (Fig. 2).
A complete working cycle of pneumatic drive involves following sequences:

1. Advance C4→ Advance C1→Retraction C4→ Retraction C1;
2. Advance C3→ Left rotation MP2→ Advance C1→ Advance C4;
3. Retraction C1→ Retraction C4→Right rotation MP2→ Retraction C3;
4. Advance C5→ Retraction C5→ Advance C6→ Retraction C6

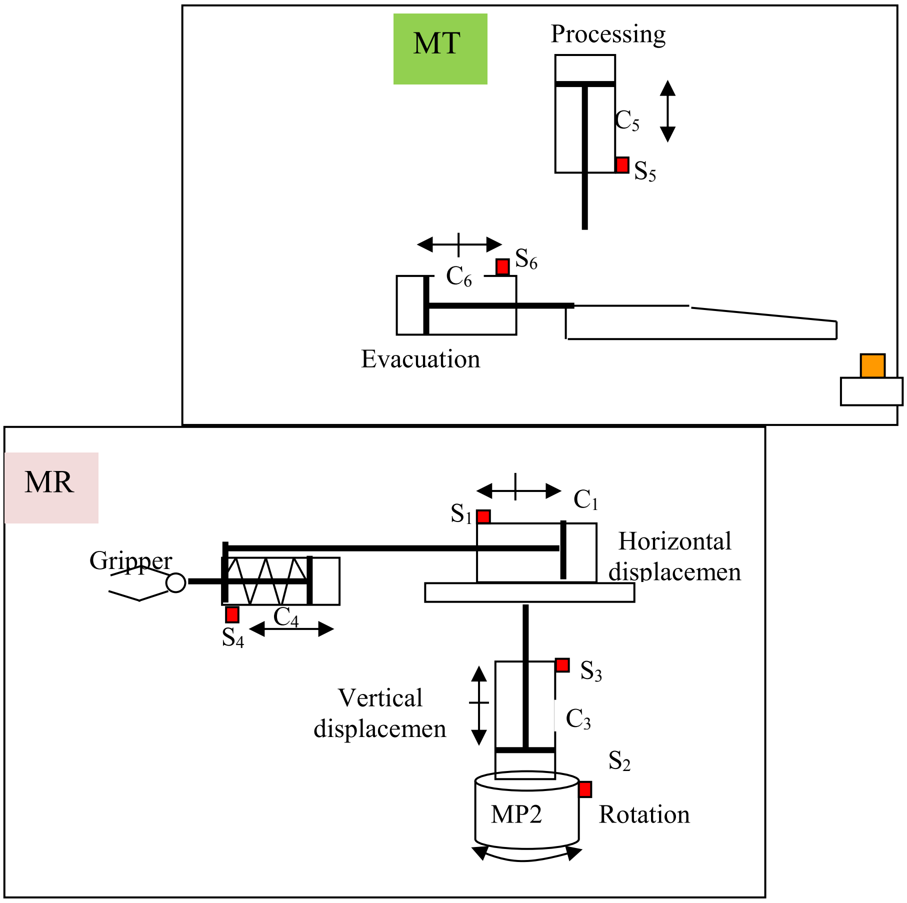

Fig. 2. Structure of pneumatic drive of the processing station

Based on the structure of the pneumatic drive was carried general scheme of the automatic processing station (Figure 3).

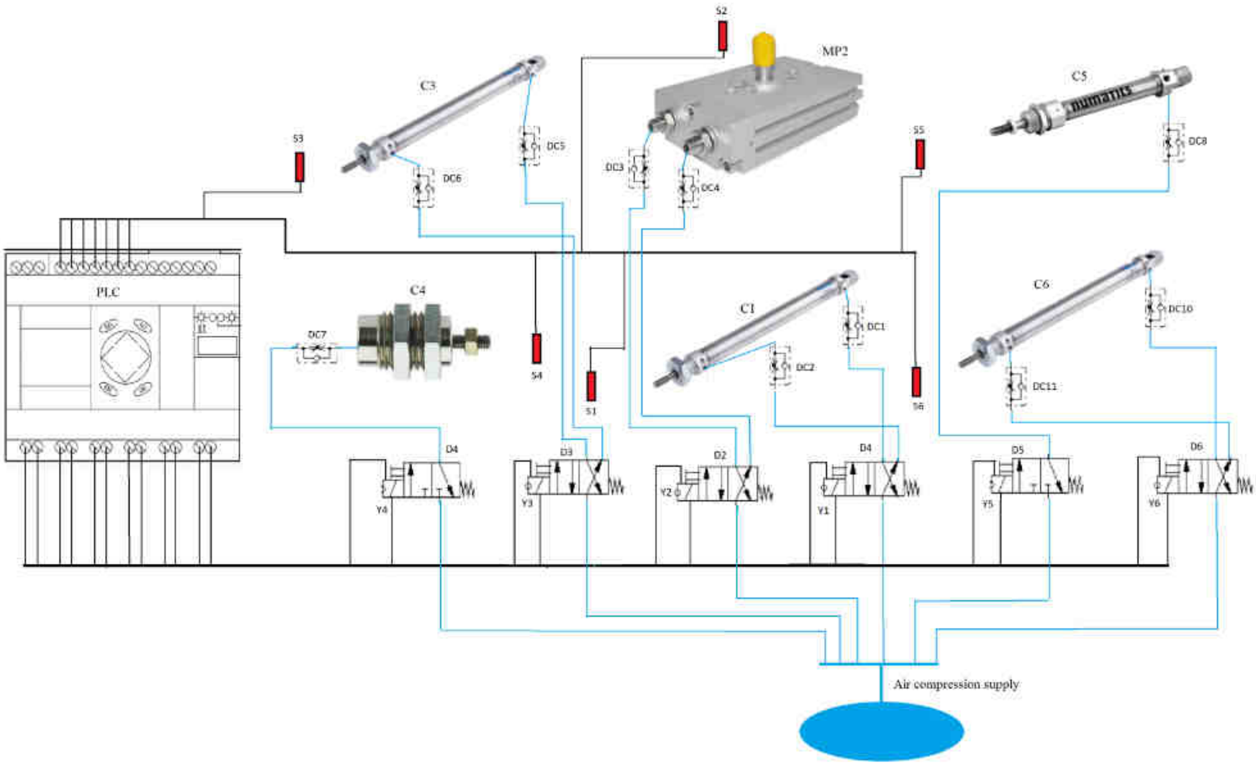

Fig. 3. General scheme of automatic processing station

The meaning of the elements used in the scheme is as follows:
PLC- programmable logic controller;
D1...D6 – pneumatic valve;
C1...C6 – pneumatic cylinders;
MP2 – rotary pneumatic motor;
DC1...DC11 – one-way flow control valve;
S1...S6 – sensors;
Y1...Y6 – relays valve control.

3. Achievement the automatic processing station

3.1. Achievement of the control system

The following aspects were taken into account in the implementation of the control system:
- simplifying the hard drive and using as few components as possible;
- the possibility of easy system programming;

To meet the above requirements, a PLC control system has been designed. For this purpose, the Moeller Easy AC-RC-819 programmable controller was selected.
It offers a number of facilities including:
- small size
- direct power supply to the 220V network;
- Keyboard and screen presence.
- a total of 14 entries.

3.2. Achievement the power and protection circuit

For application operation, it is necessary to 220V power supply of the PLC as well as a 24V source so that the coils of the 6 valves and the sensors used operate at a voltage of 24V. Figure 4 shows the electrical circuit diagram of the processing station.

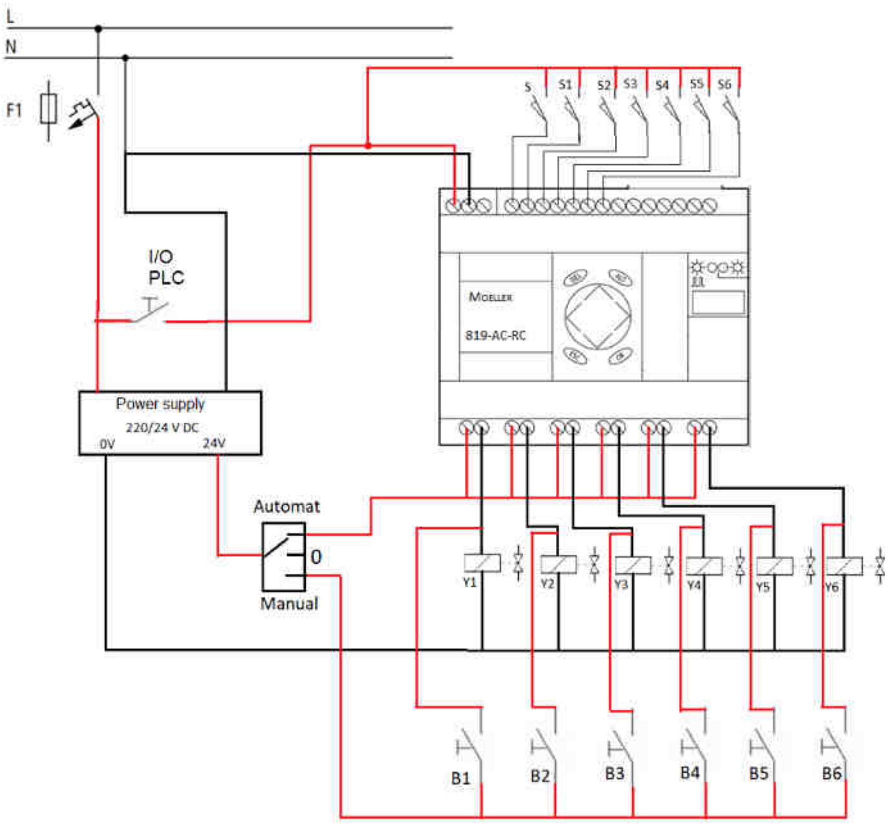

Fig. 4. Electrical circuit diagram of the processing station

3.3. Achievement the user communication system

At the core of the control process lays the command and control unit that manages the entire process as well as the human-machine interface.
Based on the operating principle of a closed-loop control system, the command and control unit takes over the position information of the system sensors from the position sensors and the presence piece sensor. After processing the information, after a predetermined schedule, control signals are generated to the pneumatic actuators.
The user communication system consists of the PLC keypad, a three-way switch, 6 buttons for manual control and the automatic display screen where you can see the activation of inputs (figures 4 and 5).
The keyboard allows the user to enter programs without a computer or modify certain parameters within an already created program.
The three-way switch is used to switch the mode of operation of the processing station. It allows switching from automatic mode to manual mode but also stops all pneumatic drive.
To avoid the dual simultaneous control, a separate PLC power supply switch was used which disconnects its power when the drive is operating in manual mode.
The 6 manual control buttons allow the control of the solenoid valves in the pneumatic drive.

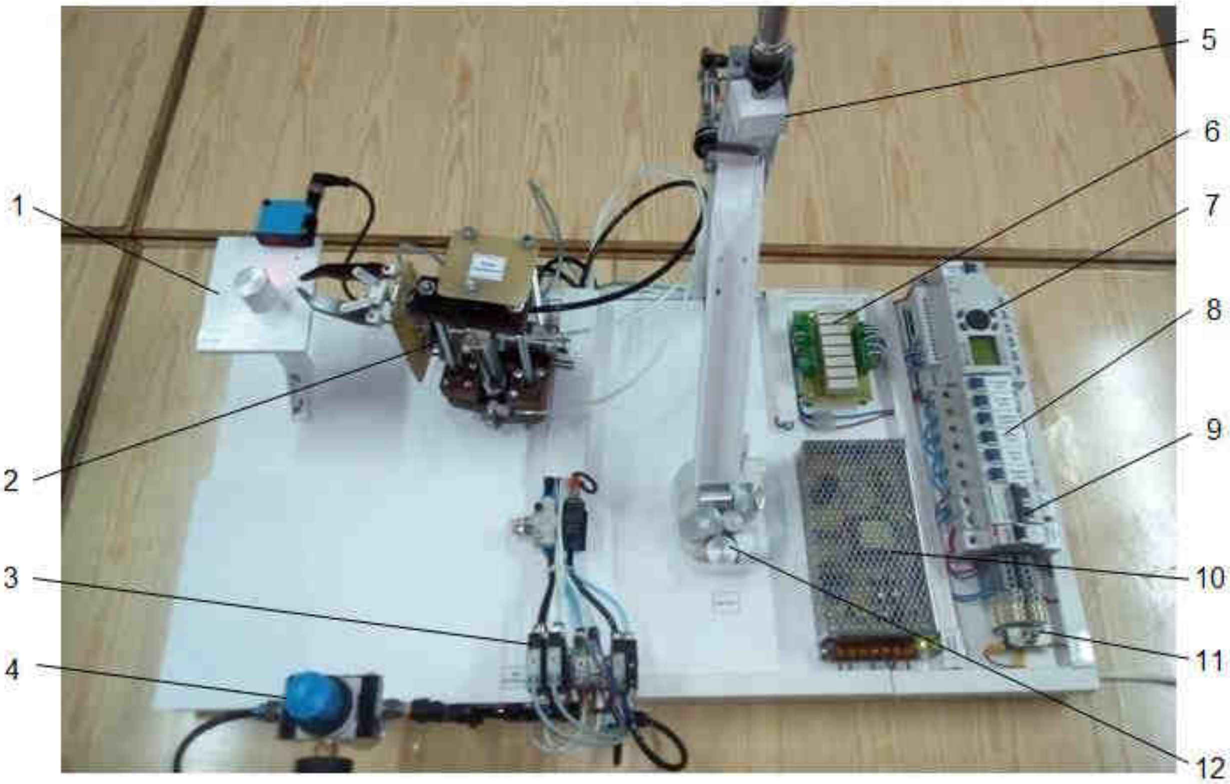

Fig. 5. Accomplished processing station:
1- input piece stock; 2- manipulator robot; 3- pneumatic valves; 4- air preparation group; 5- machine tool; 6- relay module for adapting signals from sensors; 7- Easy 819 AC-RC PLC; 8- switch for manual control mode; 9- electrical protection; 10- DC power supply; 11- three-way switch for operation mode selection; 12- output piece stock.

The air preparation group is FR type produced by SMC. This combination minimizes space and pipelines by integrating the two units into one. Standard features include a regulator that can be quickly locked by pushing the adjustment knob down. A pressure gauge is mounted on the control group. The filter cartridge provides a filtration rate of up to 5 microns/m.
Waircon URG 5/8 type regulators have been used to control actuator speed. The "URG" series flow regulators are produced in in-line, unidirectional versions.

The "URG" model has a built-in control valve to control the flow in one direction, while the reverse flow is free. They are high precision regulators and can provide a high flow rate ratio and are very compact.
For MK5100 IFM sensors were used to determine the position of pneumatic cylinders.
Closed open positions of the gripper are given by a pressure relay type: Festo SDE5-D10-O-Q6-P-M8 inserted into the pneumatic actuator of the gripper.
SICK K3L-P3216 type sensor was used to detect the presence of the piece to input stock.

4. Experimental results

Experimentation actually consists of correct working verification according to the protocol and conditions imposed by design. In figures 6 a)…6 f) there are captured the 6 operating states in a work cycle.

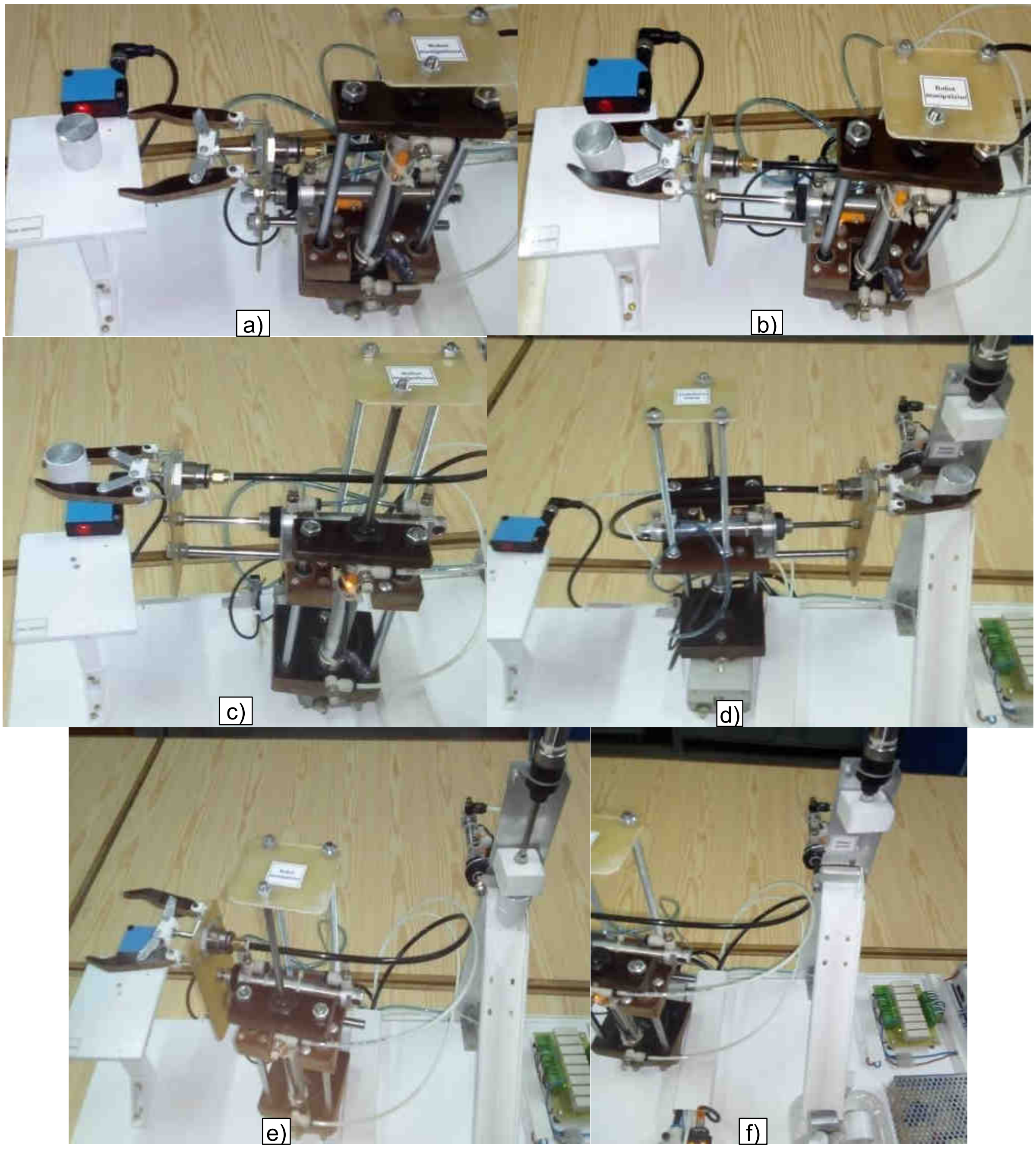

Fig. 6. Working states of processing station: a) piece detection; b) piece grip; c) lifting the piece; d) putting the piece on the tool machine; e) processing the piece; f) piece evacuation.

Other experiments consisted of visualizing command signals generated by the PLC for supplying valves to actuators. Figure 7 shows the diagrams of the two working cycles.

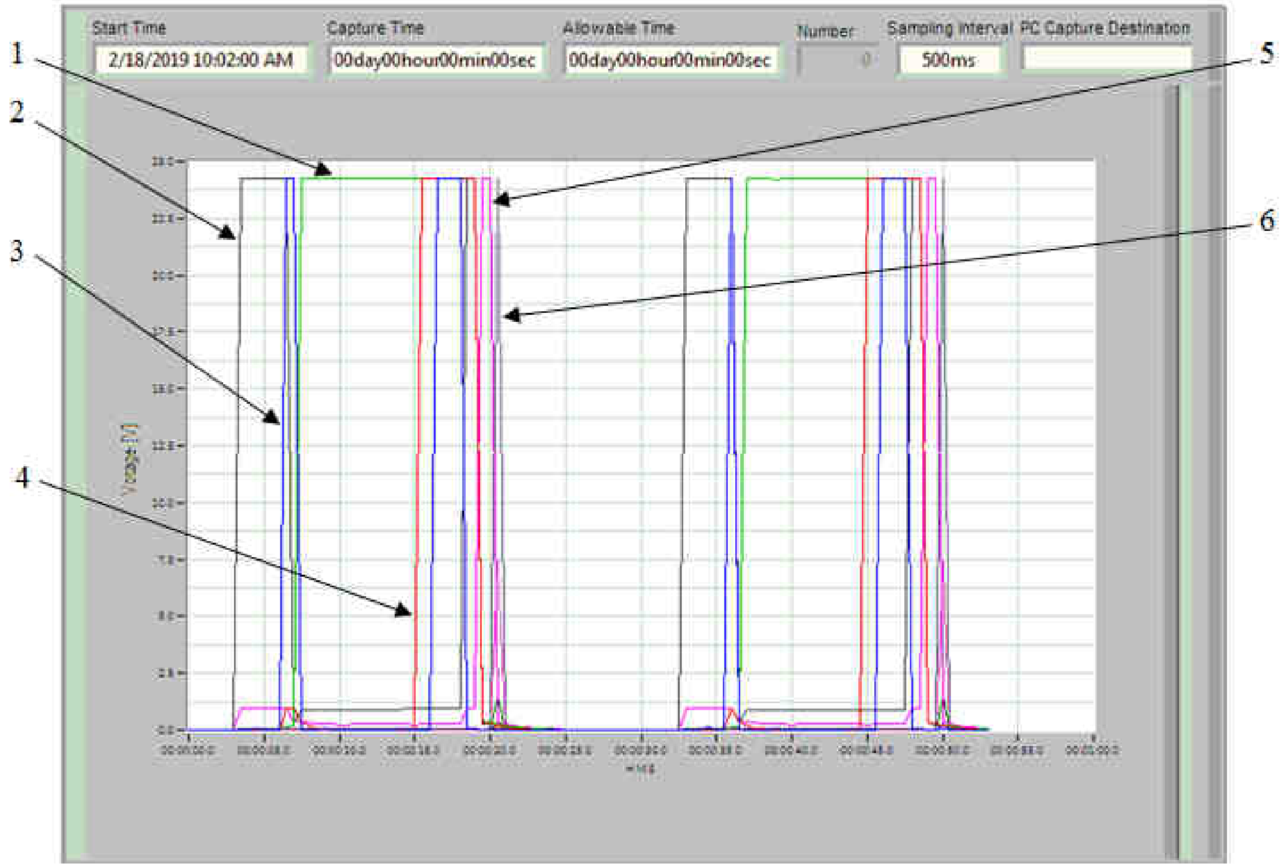

Fig. 7. Recording of command signal diagrams generated by PLC: 1- lifting arm of robot; 2- opening gripper; 3- robot arm pushing; 4- robot rotation; 5- piece processing; 6- piece evacuation.

Based on the diagrams, an optimization of the automatic processing system can be done. For example, working times can be reduced.

5. Conclusions

In the paper was designed and developed an automated processing station that respond to the requirements of a flexible manufacturing system.

Infrastructure hardware and software used allows monitoring and control of a processing station.

Sensors, electrical equipment and electronic components used for automatic system design have a high degree of accessibility and performance. Both the pneumatic part of performed processing station as well as electrical and command part was proven correct functioning according to the solution and protocol required.

The system designed, developed and tested can be used both in educational applications in electrical engineering and in industrial applications.

References

[1] Drighiciu, M.A. *Hydro pneumatic drive and automation/Acţionări şi automatizări hidropneumatice*, Craiova, Publishing House of University of Craiova, 2003.
[2] Alboteanu, L., Gh. Manolea, and F. Ravigan. "Automatic sorting and handling station actuated by pneumatic drive." *Annals of the University of Craiova, Electrical Engineering Series,* no. 1 (2018): 1-8.
[3] Alboteanu, L. "Modeling an Automatic Processing Station Using Fluidsim Software." *Hidraulica-Magazine of Hydraulics, Pneumatics, Tribology, Ecology, Sensorics, Mechatronics*, no. 3 (September 2017): 27-30.
[4] Van Varseveld, Robert B., and Gary M. Bone. ˝Accurate Position Control of a Pneumatic Actuator Using On/Off Solenoid Valves.˝ *IEEE/ASME Transactions on mechatronics* 2, no. 3 (September 1997): 195-204.

[5] Lazăr, C., O. Păstrăvanu, E. Poli, and F. Schonberger. *Computer-assisted management of technical processes /Conducerea asistată de calculator a proceselor tehnice*. Bucharest, Matrix Rom Publishing House, 1996.
[6] Alboteanu, I.L. ˝Pneumatic Tracking System for Photovoltaic Panel.˝ *Hidraulica-Magazine of Hydraulics, Pneumatics, Tribology, Ecology, Sensorics, Mechatronics*, no. 1 (March 2015): 32-39.
[7] Alboteanu, I.L., Gh. Manolea, and A. Novac. ˝Automation of a pumping station for low power applications.˝ *Hidraulica-Magazine of Hydraulics, Pneumatics, Tribology, Ecology, Sensorics, Mechatronics*, no. 1 (March 2014): 58-64.
[8] Avram, M., C. Bucşan, and V. Banu. ˝Innovative Systems for Incremental Positioning in Pneumatics.˝ *Hidraulica-Magazine of Hydraulics, Pneumatics, Tribology, Ecology, Sensorics, Mechatronics*, no. 2 (June 2015): 53-56.
[9] Nawrocki, W. *Measurement Systems and Sensors.* London, Artech House, 2005.
[10] Toma, L. *Acquisition and digital signal processing systems/Sisteme de achiziţie şi prelucrare numerică a semnalelor.* Timişoara, West Publishing House, 1996.
[11] http://www.smcromania.ro.
[12] http://www.festo.com/net/startpage.

Testing of Operating Characteristics with Powershift Multi-disc Clutches

Lect. Dipl. Eng. **Attila SZEGEDI**[1]

[1] University of Nyíregyháza, szegedi.attila@nye.hu

Abstract: *The diverse requirements pose complex demands on today's agricultural tractors. Effective work requires a modern diesel engine to have an efficient and versatile drivetrain, since the engine's performance must be transmitted to the ground and the wheel with minimal loss. At the same time, the activated gear ratio ensures optimum engine load in the otherwise wide range of speeds to reach low fuel consumption. For this reason, powershift transmissions are most often used under modern loads. The critical point of their operation is the gear shifting under load - the gear shifting process which is achieved by the controlled sliding of multidisc wet clutches. The research work focuses primarily on these clutches, starting from the electric signal controlling the shift, due to the displacement of the hydraulic actuation elements, taking into account the change in the drawbar force exerted.*

Keywords*: Tractor drivetrain, powershift transmission, multidisc clutch*

1. Introduction

Climate change and energy efficiency that are linked to each other are among the challenges of the present and the future.
Nowadays, transportation is the biggest branch causing greenhouse gases, that is why energy saving and low emission vehicles and prime movers are needed. In the case of vehicles, energy efficiency and emission are not simply a question of motorization, but it is also a machine development problem that includes drivetrain solutions providing efficient transmission.
The most frequent purpose of researches on the development of gear boxes is the reduction of power transmission loss. While earlier developments mostly aimed at the optimal use of engine power and meeting the expectations regarding the ergonomic demands of operation, nowadays, the minimization of performance loss is the most typical goal.
The results of researches on the energy losses of tractor transmissions can be found in various literature. *Mc Carthy and Kolozsi* [5] already dealt with the research method based on preliminary calculations of transmission energy loss and and actual tests in late 20th century. Their calculation principles are valid to this day. Based on the simulated examinations of the characteristics of the continuously variable tractor transmissions *Joóri et al.* [2] found that the continuously variable tractor transmissions can be more widely used than the stick shift transmissions and due to the more optimal transmission of engine performance, they provide lower specific fuel consumption. In subsequent researches, *Kerényi and Farkas* [3] found that the continuously variable, power branching engines provide the most optimal, $\eta=0,90\text{-}0,94$ transmission efficiency in the $i=0,85\text{-}2,4$ variation range.
Based on their research aiming at detecting kinetic energy losses of tractors, *Molari and Sedoni* [1] pointed out that beyond the friction losses of the mechanical power transmission parts - especially in case of higher travelling speed -, losses due to lubricant viscosity as well as due to the operation of the gearshift's own hydraulic system itself are significant.
In their publications, *Molari and Sedoni* [1] and *Bietresato et al.* [6] refer to the fact that the hydraulic system of the powershift transmission consumes 4% of the input power even when unloaded. Their researches also pointed out that half of that results from the losses due to oil filling viscosity.
In the process of gear shifting, the transmitted power is reduced by the friction losses depending on the time passing during the variation of transmission. The passage of time is influenced by the hydraulic accumulators built in the system to stabilize the supply pressure *D. Prodan and A. Bucuresteanu* [7]. During gear shifting, the energy transmission between the driving shaft and the driven shaft ceases and with the increase of the gear shifting time, the kinetic energy loss of the prime mover increases due to the decrease of the travelling speed.
Considerable losses occur in the connection of the wheel to the ground as well. *Kiss and Laib* [4]

examined the components of the rolling resistance and paid special attention to extent of work necessary for the deformation of the soil.
In the light of all the foregoing, it can be assumed that the energy losses on prime movers and vehicles due to gear shifting can be decreased by the optimization of the shifting time of transmissions.
The research objectives can be determined on the basis of my assumption. Objective of this research: exploring the possibilities of decreasing loss on prime mover transmissions based on the theoretical analyses and practical examinations. As far as the execution methods of the examinations are concerned, they are in accordance with the work of *Hristea Al. et al.* [8].
In order to explore the connections, the passage of time during the shifting process, that can be described with the changes of regulating signals, has to be examined. The conclusions drawn from results based on analyses and measurements support the proposals for decreasing loss in prime mover transmissions.

2. The losses of tractor transmissions

Based on the results in literature, the losses of transmissions can be divided into two main groups on the basis of their source:

First, the mechanical losses of transmission that are caused by the friction loss at the gear connections, bearings and shaft sealings
- In addition to these, in case of power branching transmissions, there are the losses of the power transmission parts (variator, toroidal friction disc).
- In case of underload gear shifting, the friction losses of the multidisc clutch (at start and underload transmission)

Secondly, the hydraulic losses which, in most tractor transmissions occur due to the viscosity of oil filling, also used as hydraulic fluid. By moving and mixing it, they cause the heating of the transmission. As the transmission losses are accounted for more than half of the transmission losses according to literature sources, this is what will be examine in more detail.

2.1 Hydraulic losses in the gear shift

- Losses of the transmission’s own hydraulic circuit
    - for the flow and vaporization of the lubricant
    - for the operation of clutches (TLT, POWERSHIFT)
    - for operation of steering and braking
- The fluid friction between the released brake and the clutch lamellae

Nowadays, hydraulically (and hydro-pneumatically) actuated multidisc clutches (Figure 1) are used in high performance prime movers and vehicles.

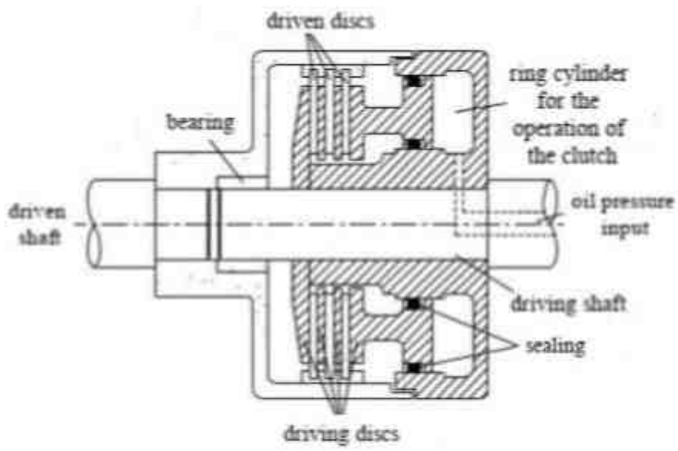

Fig. 1. The structure of a hydraulically actuated multidisc clutch [9]

Torque is transmitted from the drive shaft to the driven shaft by the friction occurring on the discs fixed to them. When the clutch is engaged, transmission is provided by the hydrostatic pressure that presses the discs against each other. The pressure transfer medium is hydraulic oil (fluid). However, even with this it takes time for the pressure necessary for the torque transmission of the drive shaft to be built up.

3. The method and toolset of measurement

Measurements were carried out to explore the operation characteristics of powershift clutches, paying special attention to under load gear shifting.
The measurements to be carried out aim at supporting the possibilities for decreasing losses that occur on the clutches of prime movers.
The measuring method to be applied is based on the fact that at gear shifting, torque transmission between the drive shaft and the driven shaft of the clutch stops for a measurable time and this fluctuation results in a detectable drawbar force fluctuation as well.
Experimental toolset:

Prime mover:
Type: New Holland T7040
Gear Shift: Full Powershift, multiplication system 3x2x3=18 and one direct gear
Tow: HW 80.11 trailer
Total weight during the examination: 9800 kg
Equipment: hydraulic cylinder built in towing device and pressure transmitters (Figure 2)

Fig. 2. Measurement of indirect drawbar force with hydraulic cylinder

Table 1: Features measured and their measurement tools

Nr.	Feature measured	Unit of measurement	Frequency	Measurement tool
1.	PWM valve operating current	mA	200 Hz	Scan Tool software
2.	Operating pressure of clutch B	bar	100 Hz	HydacHMD3444
3.	Operating pressure of clutch D	bar	100 Hz	HydacHMD3444
4.	Operating pressure of clutch E	bar	100 Hz	HydacHMD3444
5.	Chamber pressure of cylinder built in the drawbar eye	bar	100 Hz	HydacHMD3444

Number of repetitions: 2
Location of measurements: Periphery of the town Szerencs

3.1. The relevant characteristics of the experimental toolset

The detailed examination was carried out on a New Holland T7040 type tractor with a Full Powershift clutch.
The clutch makes 19 forward and 6 reverse gears shiftable under load. This clutch provides speeds of 3-9 km/h and 5-13 km/h during field, and a speed of about 40 km/h during transportation.
Gear shifting is done by 9 hydraulically actuated multidisc wet clutches. A characteristic of the gear shift is the fact that during transportation in 19th gear, optimal efficiency direct drive can be transmitted from the flywheel through the TLT drive shaft, thus decreasing heat development and friction losses [1].

Presentation of the measurements carried out

The measurements were carried out during road towing, with the loaded prime mover being accelerated continuously. In the acceleration cycle, the indirect drawbar force measurement was carried out by recording the pressure values built up in the chamber of the hydraulic cylinder placed in the towing structure. During the measurement process, the pressure values of the operating current and the hydraulics operating the gear shifting clutch were recorded against time. The measurements were carried out at fixed throttle position. The rotational speed of the tractor engine had been set to 1500 1/min beforehand.
The measurement was carried out in two phases.

As a first step, the electric signal of the actuator operating he hydraulics was read from the control circuit of the actuator through the CAN network of the tractor, with New Holland's original software (New Holland Electronic Service Tool). The amount of current that passed through the solenoid of the hydraulically shifted multidisc wet clutch was saved with this software.

In the second measurement phase, the changes were examined in hydraulic pressure. A Hydac analysis tool /meter+data collector/ was applied to measure the pressure operating the clutch during gear shifting. The ***Hydac HDA 3444-A-600-000*** pressure transmitters were connected to the pressure measuring service ports of clutch B C and D on the control blocks of the transmitter. These can be found in the hydraulic control circuit right after the PWM valves, so the amount of pressure operating each clutch can be directly examined. Data were retrieved on the time and course differences between the controlling current and the pressure it passed through.
The measured pressure values were recorded by a Hydac HMG 2020 data recorder from which data was imported to a PC and could be processed.

Fig. 3. Connection of the pressure transmitters and the data collector to the control block, valve C, D and E.

3. Analysis of the measurement results

The control signals, the number of which reached 8000 during the examination, were recorded in the case of every clutch. The current changes during the gear shifting process based on the measured data are presented in Figure 4.

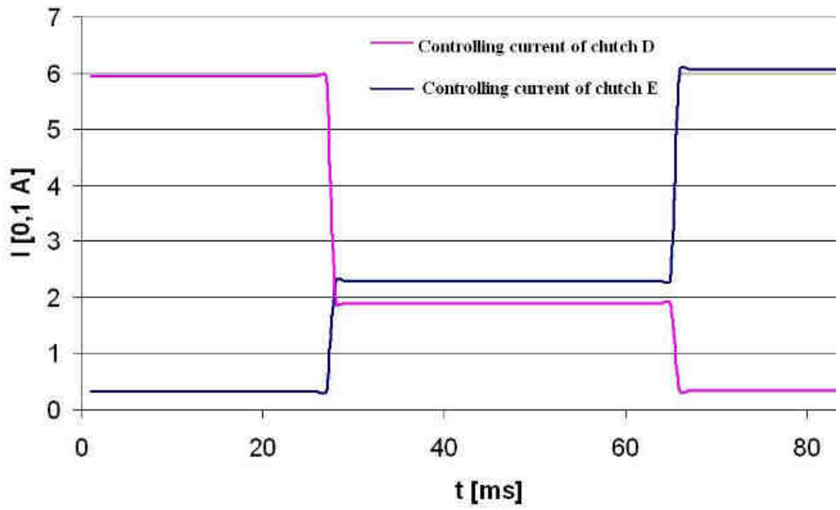

Fig. 4. Time course of the electrical control signals of the subsequent gears during gear shifting

The amount of control current of the hydraulic system decreased from 0.6 A to 0.2 A during gear shifting when the clutch D was engaged, while the same amount of current starts to switch the control valve of the hydraulic clutch in order to reach the next gear. After the time (in this case 47 ms) that can be set in the software which operates the interconnected system, clutch D completely stops, meanwhile its controlling current decreases to 0.05 A. On the contrary, clutch E becomes completely engaged, thus its controlling current increases to 0,6 A. It was found important to note that as I was preparing for this series of measurements, preliminary control measurements were carried out in non-loaded mode, without a tow and at 1200 1/min and 1800 1/min engine speeds as well. The current of the electronic signals and the controlled time of the gear shift were the same as the values measured in underload mode.

For the analysis of the relations of the operation process, the electronic signal at the particular clutch and the hydraulic control pressure was presented on an identical time scale.

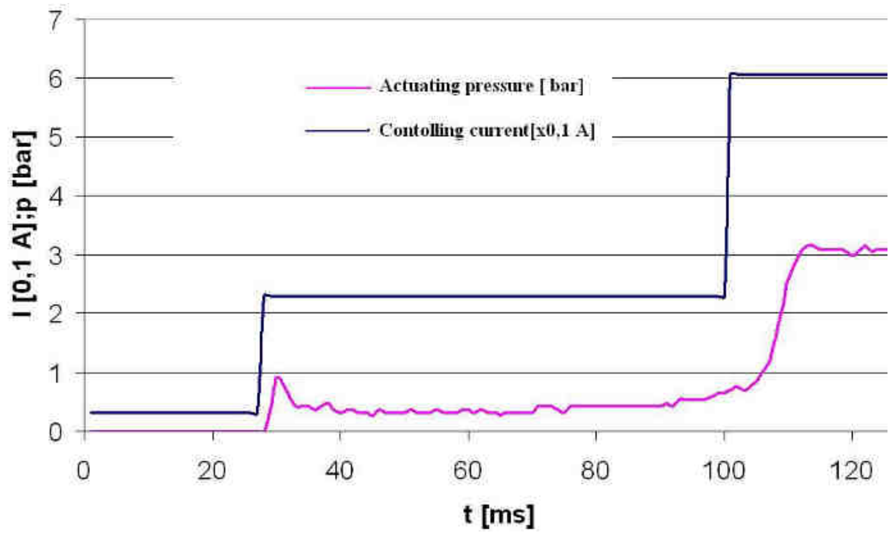

Fig. 5. Time course of the pressure of the electronic signal at clutch D and the hydraulic actuator during gear shifting

On Figure 5 it is clear that pressure of the hydraulic system builds up with a 10-15 ms delay, following the changes of the control signal. The explanation to this is that certain moving occurs during the compression of the lamellae, which takes time to happen. In addition, the accumulator built in the system also has to charge for a smooth gear shift.

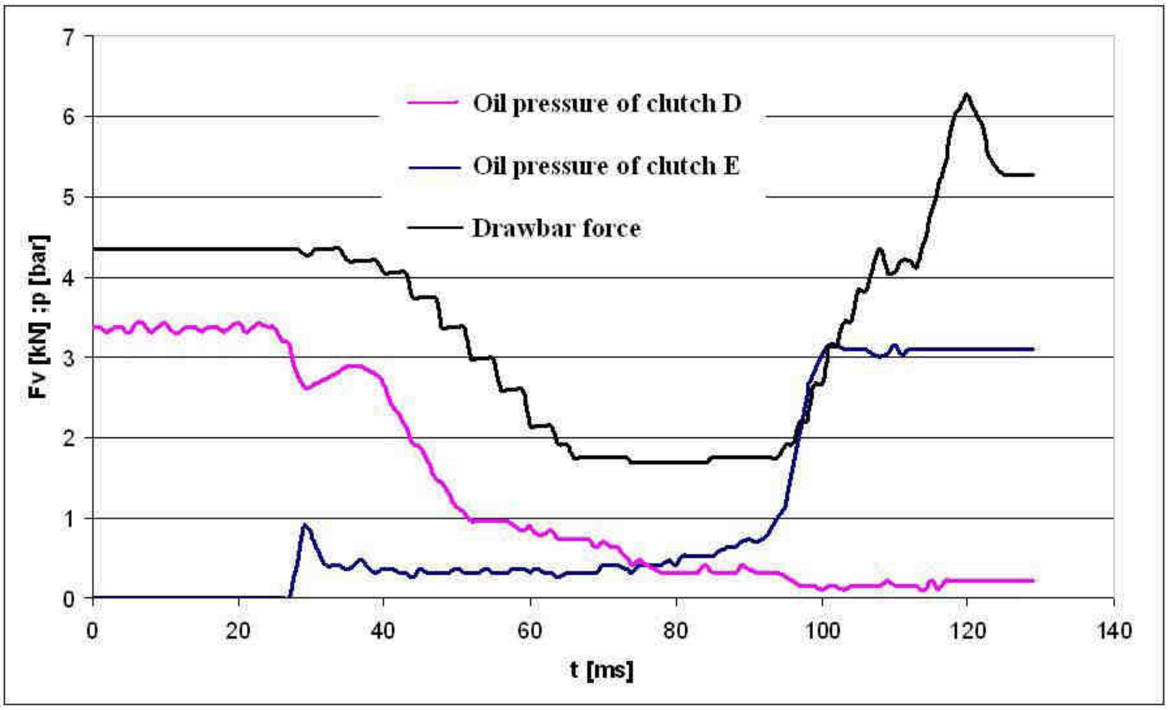

Fig. 6. Time course of the hydraulic control pressure and the drawbar force during gear shifting

Figure 6 shows the change of the measured drawbar force. From this, it can be ascertained that the control pressure of the clutch is closely followed by the drawbar force exerted by the prime mover.
The few ms delay is primarily due to the inertia of the prime mover as the drawbar force in the wheel-soil interaction was not examined, but between the prime mover and the tow. The drawbar force peak at the end of the shift clearly presents the extra force necessary for the prime mover to accelerate again.

4. Conclusions, proposals

Prime movers have to exert a variable amount of drawbar force in a wide speed range. Based on the measured data, the relations between the electronic control signal and the course of the shifting process can be detected. It can be found that the examined prime mover works with the same duration and current of control signals independently from the speed and the exerted drawbar force. From an energetic point of view, it would be advisable to differentiate the hydraulic pressure that controls the course of the under-load gear shifting depending on the drawbar force and the travelling speed. With the modified control, in addition to the expected (otherwise slight) fuel saving, the lifespan of the clutch parts may considerably increase, the operating temperature of the lubricant may decrease and depending on the operating conditions, the shifting comfort improves.
With the analysis of the construction and the operating conditions of the multidisc clutch, the following relations can be determined the connection between the control pressure and the transmitted torque.
From the geometric and friction characteristics of hydraulically (and pneumatically) operated clutches, a coefficient can be derived (specific torque transmission). Multiplied by the control pressure, it provides the amount of the momentary gear ratio.

The specific transmission coefficient (C_{MP}):

$$C_{MP} = \left(D_h^2 - d_h^2\right) \cdot \pi \cdot z \cdot \mu \cdot D_k \tag{1}$$

Where:

D_h is the outside diameter of the ring plunger;
d_h is the inside diameter of the ring plunger;
D_k is the average diameter of the friction discs;
z is the number of friction discs.

Due to the dynamic viscosity of the lubricant, friction occurs between the friction discs even when multidisc wet clutches are released.

Friction between the discs when multidisc wet clutches are released (F):

$$F = \eta \cdot \frac{dv}{dx} \cdot A \tag{2}$$

Where:

η is the dynamic viscosity of the lubricant;
Dv is the average speed difference of the friction discs;
Dx is the average gap between the discs of the released clutch;
A is the the frontal area of the friction disc.

The average speed difference of the discs (dv):

$$dv = q_i \cdot n \cdot \left(D - d\right) \cdot \pi \tag{3}$$

Where:

q_i is the quotient of the gear of examined clutch and the transmission of current gear;
N is the input speed;
D is the outside diameter of the friction disc;
d is the inside diameter of the friction disc.

The average gap between the friction discs (dx):

$$dx = \frac{x_z}{z} \tag{4}$$

Where:

X_z is the operating travel of the ring cylinder;
z is the number of friction discs.

The total surface of the friction discs (A):

$$A = \frac{(D^2 - d^2) \cdot \pi \cdot z}{4} \tag{5}$$

By substituting relations (3), (4), (5) described in detail above in the equation (2), multiplying by the medium radius of the clutch after simplification, with the help of the following relation and based on the construction characteristics of the clutch and the viscosity characteristics of the lubricant, the amount of fluid friction transmission occurring on the released clutch can be calculated.

$$M_S = \frac{n \cdot q_i \cdot (D^2 - d^2) \cdot (D^2 - d^2) \cdot \pi^2 \cdot z \cdot \eta \cdot \varphi}{8 \cdot x_z} \tag{6}$$

Where the fill factor φ, the value of which can be between 0 (dry clutch) and 1 (completely submerged in oil), was introduced as a supplement to describe the oil filling between the friction surfaces.

From the relations described, the following solutions can be suitable for reducing hydraulic losses:

- application of dry clutches;
- lower viscosity lubricant;
- lower oil filling (+ active lubrication);
- bigger lamellae gap;
- application of fewer clutches.

References

[1] Bietresato, M., et al. "Assessment of the efficiency of tractor transmissions using acceleration tests." *Biosystems Engineering* 112, no. 3 (July 2012): 171-180.
[2] Joóri, J.I., Gy. Kerényi, and Zs. Farkas. "The application and modelling possibilities of CVT in tractor." Paper presented at the 5th International Multidisciplinary Conference, Baia Mare, Romania, May 23–24, 2003.
[3] Kerényi, Gy., and Zs. Farkas. "Power flows an efficiency analysis of out- and input coupled IVT." *Periodica Politechnica*, *Mechanical engineering* 53, no. 2 (2009): 61-68.
[4] Kiss, P., and L. Laib. "Determination of the adsorbed energy of the soil in the soil-tyre interaction." Paper presented at the 13th ISTVS Conference, Munich, Germany, September 14-17, 1999.
[5] Mc Carthy, T.T., and Z. Kolozsi. "The measurement of tractor transmission losses." *Journal of Agricultural Engineering Research* 19, no. 1 (March 1974): 71-75.
[6] Molari, G., and E. Sedoni. "Experimental evaluation of power losses in a power shift agricultural tractor transmission." *Biosystems Engineering* 100, no. 2 (June 2008): 177-183.
[7] Prodan, D., and A. Bucuresteanu. "Determining the times of charging and discharging of hydro-pneumatic accumulators." *Hidraulica-Magazine of Hydraulics, Pneumatics, Tribology, Ecology, Sensorics, Mechatronics*, no. 1 (March 2017): 8-15.
[8] Hristea, Al., R. Radoi, B. Tudor, and I. Balan. "Mobile equipment for testing the power steering of cars." *Hidraulica-Magazine of Hydraulics, Pneumatics, Tribology, Ecology, Sensorics, Mechatronics*, no. 4 (December 2017): 84-88.
[9] https://www.slideshare.net/mirhadizadeh/chapter10-clutches-and brakes.

Reducing Pollutant Emissions by Integrating Flue Gas Treatment Systems into a Corn Coal Fired Coating Plant

Assoc. Lecturer PhD. Eng. **Adrian ȚENCHEA**[1], PhD Student. Eng. **Dănuț TOKAR**[2], Assoc. Prof. PhD. Eng. **Adriana TOKAR**[3]

[1] "POLITEHNICA" University of Timișoara, adi_tenchea@yahoo.com

[2] "POLITEHNICA" University of Timișoara, tokardanut@yahoo.com

[3] "POLITEHNICA" University of Timișoara, adriana.tokar@upt.ro

Abstract: *The European Union's 2020 greenhouse gas reduction targets bring solid biomass to the attention of specialists as one of the renewable energies on which Europe can rely. The technical potential for biomass use is about 8-10% of the primary energies in Europe. The amount of heat from the energy recovery of biomass, in Romania, has different weights in the balance of primary resources, depending on the type of waste used or the destination. The rational use of biomass involves knowledge of the physical-chemical characteristics and knowledge of the technological characteristics without which rational design and exploitation storage, transport and grinding would not be possible.*

Keywords: *Biomass, corn cobs, combustion, pilot plant, scrubber, reactor*

1. Introduction

The technical potential for biomass use is about 8-10% of the primary energies in Europe [2]. Some very large countries, such as China and India, have significant biomass potential and, as a result, its use for energy purposes would significantly relieve the national and global energy balance.

The amount of heat from the energy recovery of biomass in Romania has different weights in the balance of primary resources, depending on the type of waste used or the destination. Thus, 54% of the heat produced from biomass is obtained from the burning of forest residues or 89% of the heat required for the heating of the dwellings and the preparation of the food (rural area) is the result of the consumption of residues and vegetal waste.

Intensive cultivation of "energy plants" is not recommended because in this case chemical fertilizers are used in the manufacture of which indirect CO_2 is emitted. It is preferable to use biogenic resources and energy plants that develop naturally without the use of chemical fertilizers.

The main categories of biogenetic fuels (biomass) are: containing wood, containing straw, oil plants and animal biomass (sludge, slaughterhouse residues, etc.). While the straw-containing biomass has a cellulosic composition ($C_6H_{10}O_5$), the biomass has a composition with a slightly increased carbon content ($C\ H_{1,23}\ O_{0,38}$), and the biomass with protein and oleaginous content has a low content of carbon, but has N and S in relatively high proportion compared to woody or perennial biomass.

Biomass can be used as fuel in the form of "pellets", which have the advantage of improving ignition and combustion stability [3]. The pelleting technology consists of pre-drying, grinding (if necessary) and then pressing with or without a binder. These, for example those made from wood waste (sawdust, chips, chips, etc.) in Germany, are in the form of small cylinders with a diameter of 6 mm and a length of 24 mm, having density δ_{pel} = 650 kg / m^3, the calorific power of about H = 5,0 kWh / kg = 18 MJ / kg at a moisture content of W_{pel} = 8%. The production of pellets, which have a higher energy density than their biomass, contributes to the reduction of transportation and storage costs.

2. Potential of biomass as a renewable source

The rational use of biomass involves knowledge of the physical-chemical characteristics and knowledge of the technological characteristics (density, granulometric composition, sliding

capacity, mechanical strength, milling capacity, hardness, self-ignition tendency, etc.) without which rational design and exploitation storage, transport and grinding would not be possible.
Density for biomass can be in the form of real and apparent density, as the mass is related to the volume of fuel including or exclusively pore volume. Next to these two sizes is the density in the heap, which is the ratio between the mass of biomass and its gross volume. Gross volume refers to the volume of non-combustible fuel, including the volume of voids between pieces, grains or dust particles. Density in the heap depends on the type of biomass, its humidity, its granulation and its leaching. Its value is used for the sizing of bunkers or fuel silos.
Of great importance in choosing the burning mode, the type of grate and the biomass preparation machine is its granulometric composition, which indicates the distribution of their weight by size. The method for determining the granulometric composition is standardized and is based on the passage of a representative sample through horizontal screens made of standard mesh woven fabric.
The chemical elements that come into the biomass (in fact, any solid fuel) are: carbon (C), hydrogen (H), oxygen (O), nitrogen (N) and organic sulphur), humidity (W) and non-combustible mineral mass (which also includes sulphide sulphide) from which the ashes result. Mineral mass and humidity form the so - called "ballast" of fuel.
The elemental composition of a biomass sample, expressed as a percentage by mass, is reported under the following conditions [4], [5], [6], [7]:

- initial state:

$$C^i + H^i + O^i + N^i + S_c^i + A^i + W_t^i = 100\ [\%] \tag{1}$$

- dry air condition:

$$C^u + H^u + O^u + N^u + S_c^u + A^u + W_h^u = 100\ [\%] \tag{2}$$

- state of analysis:

$$C^a + H^a + O^a + N^a + S_c^a + A^a + W_a^a = 100\ [\%] \tag{3}$$

- anhydrous state:

$$C^{anh} + H^{anh} + O^{anh} + N^{anh} + S_c^{anh} + A^{anh} = 100\ [\%] \tag{4}$$

- fuel state:

$$C^{mc} + H^{mc} + O^{mc} + N^{mc} + S_c^{mc} = 100\ [\%] \tag{5}$$

- organic state:

$$C^o + H^o + O^o + N^o + S_o^o = 100\ [\%] \tag{6}$$

- total sulphur:

$$S_t = S_c + S_{SO4}\ [\%] \tag{7}$$

The total moisture content of the biomass composition is divided into humidity and hygroscopic humidity.
Humidity or external moisture W_i represents the amount of water lost by drying in the oven at 50˚C for about 3 hours or at room temperature of 20˚C for about 24 h to a practically constant weight. If the mass of the initial sample is m [kg], and after drying it reaches m_1 [kg], the moisture content is given by:

$$W_i^i = \frac{m - m_1}{m} 100[\%] \tag{8}$$

Humus hygroscopic or internal (W_h^u) moisture originates from the water found in plant capillaries and cells (biomass). W_h^u is determined by drying in the oven at 105ºC to practically constant weight. If m_1 is the initial mass and m_2 of the final mass, hygroscopic humidity results from the relationship:

$$W_h{}^u = \frac{m_1 - m_2}{m_1} 100[\%] \tag{9}$$

If the dry state of the air coincides with the state of analysis, then obviously $W_h^a = W_a^a$.

3. Biomass preparation and combustion concept

Generally, biomass, due to its properties, falls into the category of solid fuels with medium calorific value, low ash content and high moisture content. As a result, it can be burned in installations used to burn coal, especially the lower ones, with some constructive and functional adaptations.
Due to the low energy density of biomass compared to conventional fuel, it is desirable to use it at the place of production or in small installations, with long-distance transport being economically inefficient.
Ash deposition on heat exchange surfaces when biomass is burned can occur to a greater or lesser extent than coal combustion. When combustion of the biomass and coal mixture, ash deposition occurs to a lesser extent than the combustion of only one of the fuels. The adherence and hardness of biomass burning deposits are higher than those encountered during coal combustion.
For these reasons it is recommended to co-incinerate biomass together with a fossil fuel. The participation of biomass in energy plants where it is burnt together with coal can reach up to 20% of the nominal power of the energy group.

There are three situations of co-incineration of biomass with a fossil fuel:

1) Combustion in the same furnace [8], [9], [10], [11], [12], [13], [14] when the resulting combustion gases cede the heat of a working fluid (usually water) which turns into steam, in turn being released into a turbine that drives an electric generator or is used for district heating. This process is used in high-power power plants.

2) Combustion in different flames when the combustion gases mix after exiting the furnace, their energy being used as in the previous case. The advantage of this process lies in better combustion and safer operation;

3) Combustion in different installations operating in parallel, the electrical and / or thermal energy being supplied together. In this case the costs are higher than in the first two, but there is the possibility of simultaneous or consecutive use of the two installations depending on the energy demand (electrical or thermal).

As far as fuel preparation is concerned, they were milled with a knife mill after grinding of between 0 and 4 mm. The Fig.1 show the type of waste biomass analysed, before and after grinding.

Fig. 1. Corn stalks forward (left) and after (right) grinding

Corn stumps, the waste biomass used to carry out the measurements, has a density of 337 kg/m^3.

4. Integration of the scrubber and reactor into the fluidized bed combustion plant

The pilot plant of the Multifunctional Laboratory of Thermal Machines and Unconventional Laboratories from U. P. Timişoara presented in Fig. 2 has the following components:
- stationary fluidized bed combustion of solid fuel particles (biomass, coal) equipped with a fluidised air distributor, an ash cooler, two solid fuel systems with adjustable speed springs, a natural gas burner a burner outlet, and a pressure measuring outlet;
- the convective body in which there are mounted coils of pipes through which the cooling water circulated with the circulation pump from a cooling tank;
- the cyclone in which it occurs most of the dust reduction from the combustion gases;
- the scrubber, which defines the process of degreasing the combustion gases by washing them with industrial water dispersed by means of a sprayer mounted on the top cover;

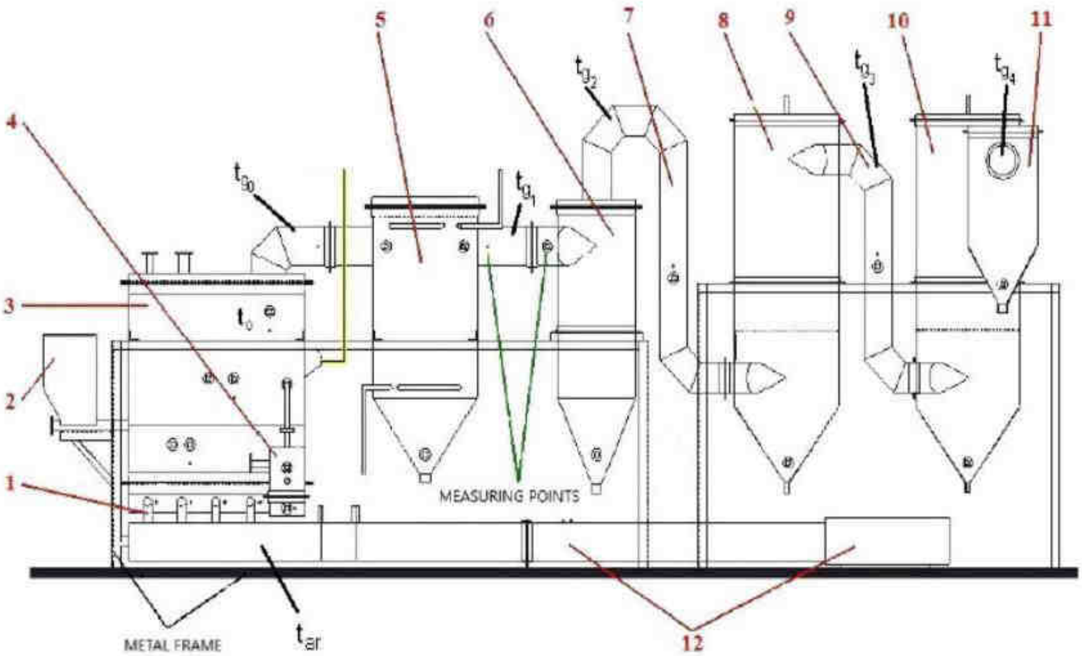

Scrubber

Reactor

Fig. 2. Pilot Station Principal Scheme
1 - Air distributor, 2 - Fuel hopper, 3 - Fireplace, 4 - Cooler, 5 - Convective body, 6 - Cyclone, 7 - Cyclone-scrubber connection, 8 - Scrubber, 9 - Scrubber reactor connection, 10 - Reactor, 11 - Drop separator, 12 - Air supply system, 13 - Smoke chimney connection

- a reactor with a 100 mm thick bottom layer of glass Rasching rings, permanently wetted with a water solution having, where appropriate, a certain concentration of the active substance for desulphurisation of the flue gases such as calcium hydroxide Ca $(OH)_2$ or sodium hydroxide;
- the separator of droplets trapped by the waste gas stream upon leaving the reactor;
- the chimney with a height of 15 m and a diameter of 150 mm.

Where:
t_{ar} - the temperature of the air introduced into the furnace;
$t_0 = t_{g0}$ - the temperature of the combustion gases when leaving the furnace [°C]:
- at the out of the furnace: $t_0 = tg_0 = 900$ °C;
- the temperature of the combustion gases when leaving the convective body: $tg_1 = 300$ °C;
- the temperature of the flue gases at the cyclone outlet: $tg_2 = 290$ °C;
- the temperature of the flue gases at the outlet of the scrubber: $tg_3 = 90$ °C;
- the temperature of the combustion gases at the reactor outlet: $tg_4 = 70$ °C;
- the temperature of the flue gases to the chimney: $tg_c = tg_4 = 70$ °C.

Determination of the composition of the combustion gases is made in three points: before and after the scrubber, respectively after the reactor. For this purpose, three TESTO 300 gas analysers are used to determine the volumetric or mass content (as adjusted) of the components (O_2, CO, NO, NO_x, SO_2, CO_2) in the dry combustion gases. The concentration of dust in the flue gases is determined using the Ströhlein STE 4. The construction and operation of these measuring devices are presented in [15], [16].

5. Experimental results and conclusions on pollutant emissions before and after the integration of exhaust gas cleaning elements in the pilot plant

Experimental measurements were made using corn cob biomass. The sampling and determination of the concentration of noxes from combustion gases, resulting from the burning of corn cobs, was carried out using the TESTO 300XXL gas analyser.
For the type of fuel used, in terms of gas emissions, measurements were made at three distinct points, namely:
- before the flue gas treatment system (ante SEGA);
- between the scrubber and the reactor (intermediate point);
- after the flue gas treatment system (post SEGA).

The results were recorded for a period of 30 minutes, in every minute, from the moment the plant has entered the stationary thermal operating regime. The measurements obtained for the fuel used are shown in Fig. 3. Only the variations for temperature, carbon monoxide, nitrogen oxides and sulphur dioxide are considered to be the most representative [1].

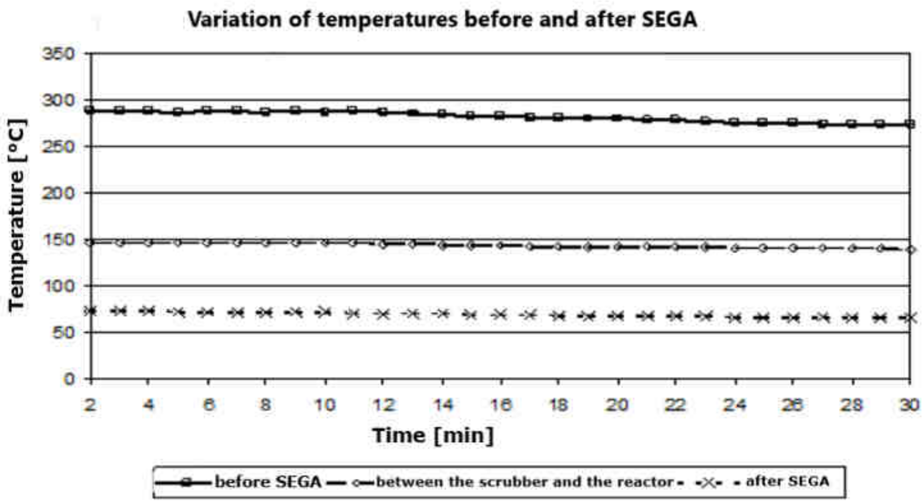

Fig. 3. a. Temperature variation before and after SEGA to burning corn cobs

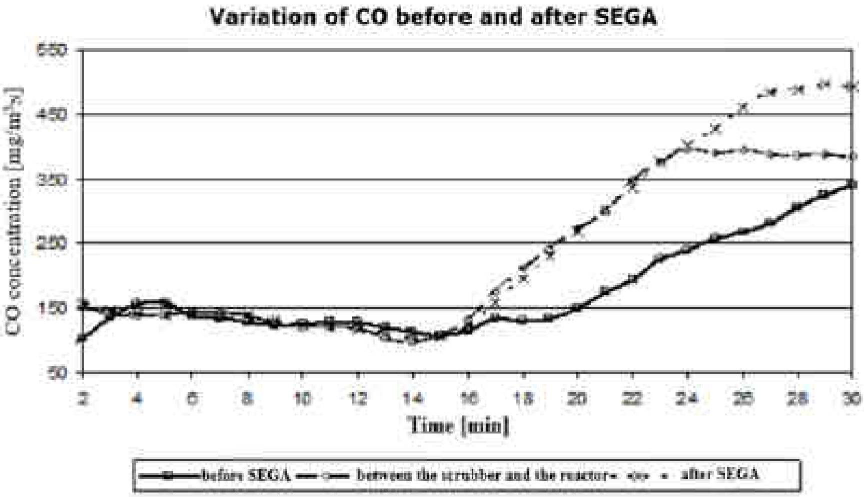

Fig. 3. b. Variation of CO before and after SEGA to burning corn cobs

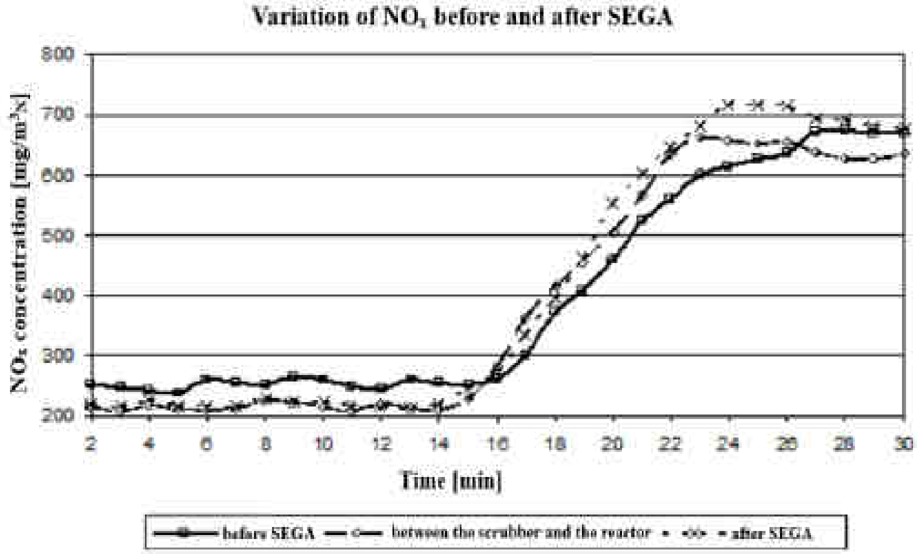

Fig. 3. c. Variation of NO_x before and after SEGA to burning corn cobs

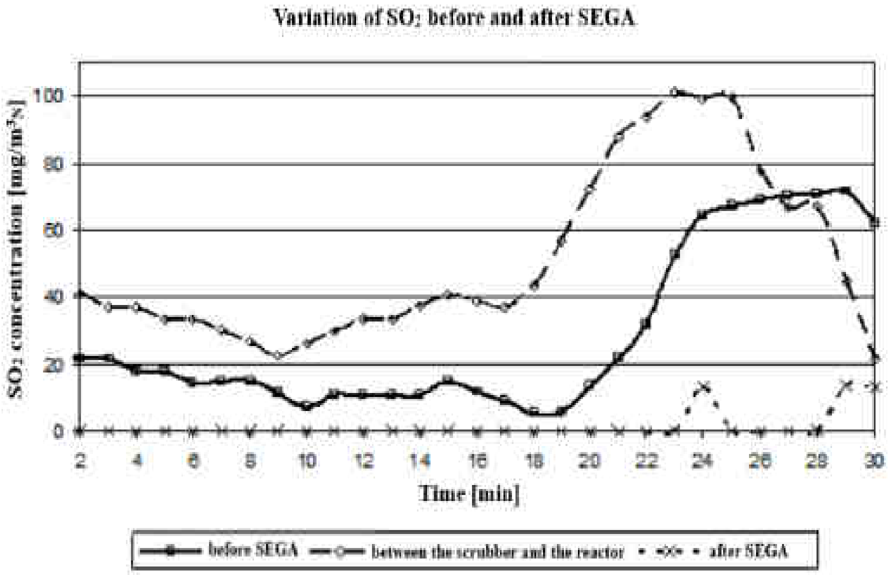

Fig. 3. d. Variation of SO_2 before and after SEGA to burning corn cobs

Current legislation does not provide for limit values related to 11% of reference oxygen for pollutant emissions from combustion gases from combustion of waste biomass, which is why the data obtained from the combustion of waste biomass from corn cobs could not be compared to fixed values.
For corn cobs the CO concentration values are higher, the temperature conditions (760 - 920) °C and the excess air coefficient (1.6 - 2.25) recommended by the literature are not met in the combustion zone.
The reported average values for corn cobs of NO_x concentrations are between 94.94 and 72.37 [mg/m^3_N] and for SO_2 between 4.40 and 0.10 [mg/m^3_N].

References

[1] Țenchea, Adrian. *Contribuţii privind cercetarea arderii în strat fluidizat a biomasei.* Timișoara, Politehnica Publishing House, 2008.
[2] Kaltschmitt, M., and H. Hartmann. *Energie aus Biomasse, Grundlagen*. Techniken und Verfahren, Springer Verlag Berlin, Heidelberg, New – York, 2001.
[3] Malamatenios, Ch., coordinator. *Energii regenerabile & Eficienţa enegetică, Ghid de instruire*. Bucureşti, Nic Vox Publishing House, 2007.
[4] Mihăescu, L., et al. *Cazane de abur şi apă fierbinte*. Bucureşti, Perfect Publishing House, 2007.
[5] Pănoiu, N. *Cazane de abur*, Bucureşti, E.D.P. Publishing House, 1982.
[6] * * *. *Manualul inginerului termotehnician vol.I*. Bucureşti, E.T. Publishing House, 1986.
[7] Pănoiu, N., et al. *Instalaţii de ardere a combustibililor solizi*. Bucureşti, Technical Publishing House, 1985.
[8] Trif-Tordai, G., V. Gruescu, and A. Ţenchea. "Operational and design variables affecting the biomass combustion process." *Buletinul Ştiinţific al UPT*, seria Mecanică, 49 (63), 2004.
[9] Trif-Tordai, G., Ioana Ionel, V. Gruescu, and A. Ţenchea. "Instalaţie demonstrativă în cogenerare de ardere a biomasei. Stadiu actual şi perspective." A XIV-a Conferinţă Naţională de Termotehnica, Bucureşti, Romania, November 25 – 26, 2004.
[10] Ungureanu, C., Ioana Ionel, G. Trif-Tordai, Al. Savu, V. Gruescu, and A. Ţenchea. *Instalaţie pentru arderea combinată a deşeurilor*. Timişoara, Politehnica Publishing House, 2004.
[11] Ionel, Ioana, G. Trif-Tordai, Vasile Gruescu, and Adrian Ţenchea. "Biomass utilization in Romania." *Buletinul Ştiinţific al UPT*, seria Mecanică, 51 (65), 2006.
[12] Ionel, Ioana, Al. Savu, V. Gruescu, G. Trif-Tordai, Adrian Ţenchea, and Corneliu Ungureanu. "Co-combustion of biomass in a Romanian fluidized bed combustion facility." *Buletinul Ştiinţific al UPT*, seria Mecanică, Tom 51 (65), 2006.
[13] Ionel, Ioana, Al. Savu, C. Ungureanu, G. Trif-Tordai, A. Ţenchea, N. Lontiş, and C. Bulzu. "Co-combustion of waste in a Romanian fluidized bed combustion facility." Paper presented at the World Renewable Energy Congress WREC IX, Florence, Italy, August 19-25, 2006.
[14] Ionel, Ioana, Al. Savu, V. Gruescu, M. Savu, and A. Ţenchea. "Instalaţie de ardere combinată." Omul si mediul 2005, Zilele Academice Timisene ed. a IX-a, Timisoara, Romania, May 27, 2005.
[15] ***. *Testo – Prospect de firmă* TESTO 300 XXL.
[16] ***. *Ströhlein – Manual de utilizare*. Ströhlein STE 4.

Using Complex Liquid-Measuring Devices in Fire Hoses

Assist. Prof. PhD. Stud. Eng. **Nikolett FECSER**[1], Master teacher **Filomena HAROMI**[2], Associate. Prof. PhD. **Rajmund KUTI**[3]

[1] Széchenyi István University, Department of Mechatronics and Machine Design H-9026 1 Egyetem tér, Győr, fecser.nikolett@sze.hu

[2] Széchenyi István University, Centre of Foreign Languages H-9026 Győr, Egyetem Square 1., haromi.filomena@sze.hu

[3] Széchenyi István University, Department of Mechatronics and Machine Design H-9026 1 Egyetem tér, Győr, kuti.rajmund@sze.hu

Abstract: *Up to now, it is still very common to use water for extinguishing fire. To be able to ensure the adequate water supply, it is essential to examine the parameters of the water supply system, especially in the case of firefighting devices, which are sometimes used under extreme conditions. To ensure the proper amount of firewater and to carry out the necessary modifications, it is vital to examine the firewater supply system from the pump including the pipes to the nozzle. We aim at making such a complex measuring instrument that provides accurate measurements in the pipes and at the nozzles used by firefighters and presenting its practical applications. First, we demonstrate the water supply system used during the process of firefighting, then we describe the measuring task, the applied instruments and devices. Our goal is to contribute to the increase of the efficiency of providing water supply required for firefighting.*

Keywords: *Firefighting pipe, water, nozzle, complex measuring instrument*

1. Introduction

During firefighting one of the most important tasks is carried out by firefighters handling nozzles at the end of the hose out of which the discharging water puts out the fire. These firefighters completing their task to be able to extinguish the fire fast and efficiently are constantly on the move, they change their positions both horizontally and vertically. Despite the fact that firefighters change their positions frequently, an adequate amount of firewater at a suitable pressure is expected to be provided. Ensuring these factors is a complex task, especially when the pump is required to operate multiple streams from the supply hoses. Therefore, examining the system providing water for firefighting and performing the necessary fluid mechanics measurements are essential. Several measurements can be carried out under laboratory conditions, however, the system providing water for firefighting is advised to be examined in 1:1 in field tests. We compiled a group of combined instruments measuring liquids necessary for the measurements and adapted it for practical application. We present our experience and measurement results in this study.

2. The elements of a firewater supply system

First, we find it important to introduce the elements of a firewater supply system before presenting the actual measuring task. The list of system elements can be extended with various parts, among which the elements used the most commonly, such as the pump, the hose, the manifold and the nozzle, are going to be presented below.

2.1. Firefighting pumps

The operation of a water supply system is mainly ensured by vortex pumps or in other names, centrifugal pumps. A vortex pump is primarily a machine travelling fluids and using up the mechanical energy driven into the pump and the angular momentum, it enhances the working capacity (its energy) of the travelled fluid with the extent necessary for forwarding the liquid to its place of use. Among the vortex pumps, firefighting pumps are a special class, which - due to their design - can even withstand being operated under not optimal conditions to a certain extent, however, it may lead to failures in the longer term. Most frequently, 2-5 multi staged pumps are used for firefighting purposes, whose performance is highly influenced by reaching the water supply or water source. The inappropriate installation of the pump onto the water source or a sudden extra water extraction may cause cavitation. The physical process of cavitation is related to the phenomenon of boiling water in which the forming vapour cavities in the liquid delivered suddenly implode. This process takes place at those locations in the pump where the pressure is under the vapour-pressure of the pumped medium. [1] Signs referring to cavitation are the various noises and the suddenly developing resonance followed by degradation in performance. Cavitation can occur in the course of operating pumps used by firefighters. In the initial phase well-detectable noises develop, then stronger and stronger shockwaves and vibrations are forming in the fluid and the travelling systems. Since the fluid has a minimum pressure at the leading edge of the impeller from the direction of the suction pipe, this is the location where cavitation may occur the earliest. The decrease of suction depth, applying suction pipes with a narrow diameter, resistance emerged in the suction pipe or an increase in the temperature of the fluid all contribute to the emergence of the phenomenon. [2]

2.2. Firehoses

In most cases lay-flat fire hoses of standard diameters (52-75 mm) fitted with standard Storz couplings and of unit length (20m) are used for firefighting. The hose with a diameter of 75 mm is called hose "B", while the one of 52 mm is called hose "C". A lay-flat fire hose is a soft wall hose which, when unpressurized internally, collapses to such an extent that the inner faces of the inside diameter make contact and the hose takes up a flat cross-sectional appearance making it easy to store and delivered reeled up. Essentially, lay-flat fire hoses are produced with an external jacket and a flexible impermeable lining. [3]

2.3. Manifolds

Manifolds are firefighting devices applied for distributing firewater flowing in the hose. In most cases, four-way valve manifolds are used which come with 1 Storz inlet of 75 mm in diameter, 1 Storz outlet of 75 mm and 2 Storz outlets of 52 mm. All outlets are fitted with manually operated mechanical fittings allowing the outlets to operate independently. [3]

2.4. Nozzles

One of the most important devices of extinguishing fire with water is the nozzle, which allows the water delivered in the firefighting system to be discharged onto the seat of fire. The nozzle itself is two confusers in line, [4], between which a combined closing device got installed. The multitude of nozzles not only allows the discharge of water, but they make it possible to vapourise the water into the required size and to form various stream types in order to ensure the optimal use of water. In the case of jet streams, nozzles are produced with various exit diameters according to the different uses. The most commonly used exit diameters of nozzles are d = 12 mm, 14 mm and 16 mm. [3]

3. Losses in firewater supply system

Carrying out firefighting tasks, in most cases, the conditions expected from the water supply system are not fulfilled in practice. The stream's change in height compared to the position of the pump and the changes of suction and total head when applying an external water source can show significant deviations with centrifugal pumps. It implies that the amount of the delivered firewater may decrease within a given time. Although creating optimal operating conditions in the course of firefighting is essential, field conditions and equipment available on the spot do not always make their creation possible, thus the actual pressure and amount of water fall short of expectations. Regardless of external factors, some elements of the water supply system show losses during operation. The pressure of the liquid exiting the fire pump discharge can be expressed as the sum of the following pressure losses: [5]

$$\Delta p = \Delta p_L + \Delta p_t + \Delta p_h + \Delta p_0 \tag{1}$$

In the equation:

- Δp: pump pressure

- Δp_L:pressure at the nozzle tip
- Δp_t: friction loss in hoses
- Δp_h: pressure loss due to change in height
- Δp_0: pressure loss of devices (e.g. manifold, restrictor, pressure equalizer unit)

Studying the available literary sources dealing with pressure loss in hoses, we concluded that the data show differences, therefore the hoses' pressure loss per meter in the function of flow rate should be calculated in each case. It should be noted that although the hoses are to meet the standards, these values may vary slightly depending on the manufacturers and the age of the hoses.
The pressure loss-flow rate data of the nozzles are included in the relevant standards in a spreadsheet. Taking a nozzle tip of 12 mm with Q=206 l/min=0,00343 m^3/s flow rate as an example, it states exactly $\Delta p_L = 5 \cdot 10^5$ Pa pressure drop.[3] It must be added that the pressure differential is not a huge loss since the pressure and kinetic energy at intake diameter of the nozzle is converted into kinetic energy at the discharge diameter. When no relevant pressure-flow rate data is available for the required nozzle, it can be calculated using only the geometric data with a reasonable approximation. Writing the Bernoulli equation between the intake and discharge diameters of the nozzle, the pressure and kinetic energy turns into clearly kinetic energy [4]:

$$\frac{\Delta p_L}{\rho} + \frac{v_{L1}^2}{2} = \frac{v_{L2}^2}{2} \qquad (2)$$

In the case of the pressure loss coming from raising water, 1 bar per meter ie. 10^5 Pa can be calculated. The manufacturers generally do not or only in certain cases indicate the Resistance Coefficient of the fittings, so it needs to be calculated later [3]. According to the source cited, in the case of manifolds the pressure drop is taken into consideration with 10 PSI ie. 0.69 bar.
As shown above, during the operation of a firewater supply system several losses occur and their calculation is not simple even in the case of a static system, but when the firefighter handling the stream constantly changes his position or multiple streams are to be operated simultaneously, determining the momentary flow rates and the amount of the discharge water becomes extremely complicated. For the reasons given above, we decided to choose measuring, since applying measurement instruments which do not change the flow conditions of the water supply system, valid results can be gained.

4. Assembling the complex measuring device

Preparing our complex measuring device, we took similar equipment used in practice as a starting point allowing each measurement sub-task to be carried out individually, however the simultaneous measurement of the flow in the hose and the parameters of the water discharging from the nozzle was not possible. The elements of the complex measuring device being able to be applied individually in the firewater supply system and being able to measure the characteristics of the flowing fluid connected to each other and to the end of the fire hose raised as a requirement as well. As the streams used in firefighting activities are mainly operated with "C" hoses of 52 mm and the most commonly used nozzles are also fitted with Storz couplings may be connected to "C" hoses, each component of our complex measuring device was fitted with Storz couplings compatible with "C" fire hoses. First, we had to choose a flow meter which is capable of measuring the parameters of the fluid travelling through so as not to modify its flow characteristic and not to cause any turbulence. The device is expected to be able to carry out measurements under non-laboratory conditions and to determine the flow parameters of the water gained from fire water sources. Considering the abovementioned facts, we chose a flow meter type Arad Octave 50 for our purposes. The instrument itself, seen in the figure 1., was not suitable for being applied in firewater supply system by default.

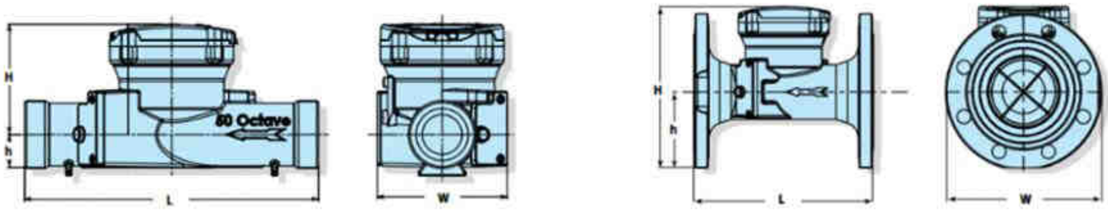

Fig. 1. Flow Meter type Arad Octave 50 (Source: Factory catalogue with authors' additions)

To obtain accurate measurement results, the device had to be fitted with a connector, a semi-rigid discharge hose and Storz couplings for the ideal application. The technical drawing made by dimensioning - based on which the supplementary hoses got manufactured - can be seen in the figure 2.

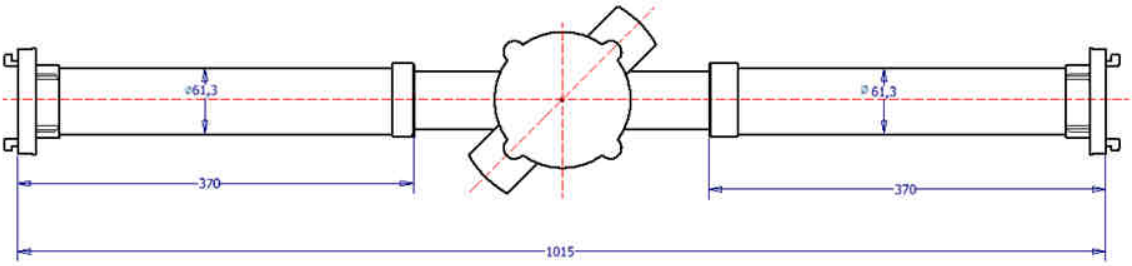

Fig. 2. Ultrasonic Flow Meter type Arad Octave 50 (Source: prepared by the Authors)

The next part of the measuring device is made up of a pressure gauge that can be connected to a "C" type fire hose, a nozzle with two confusers whose tip is replaceable making it possible to use it for measuring with a nozzle of 12, 14 and 16 mm in diameters. A Storz coupling for "C" type fire hose was mounted to the sleeve on the intake. In the figure 3. the pressure gauge and the measuring nozzle can be seen connected to each other.

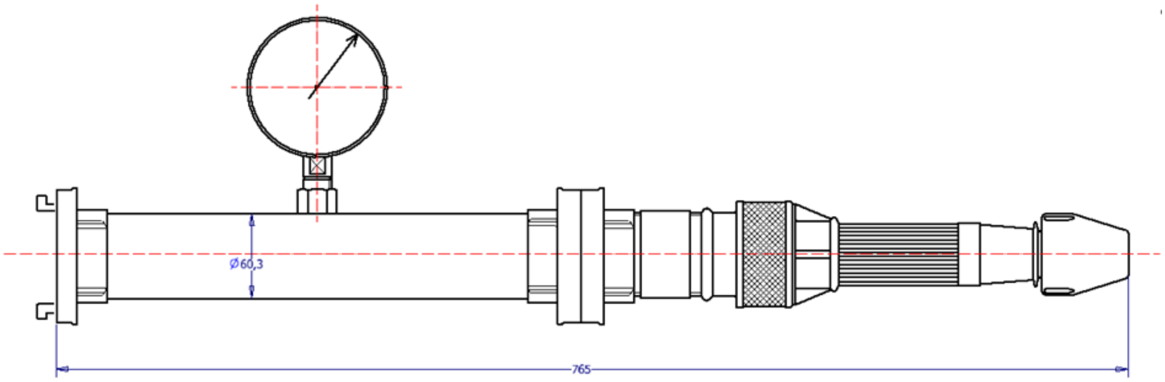

Fig. 3. The connected pressure gauge and measuring nozzle (Sources: prepared by the Authors)

The pressure gauge presented in the figure can be used individually built into the hose system as well. The measuring nozzle cannot be used for firefighting tasks, it was specifically designed for measuring purposes. When coupled, the unit fitted to the end of the hose is perfectly suitable for determining the water discharging from the nozzle of whichever size against pressure.

5. The measurement

We made in field measurements and operated two manifolds with a two-storey difference in height, whose water supply was provided by a heavy-duty Steyr Rosenbauer TLF 4000 fire engine. An RB NH 30 centrifugal pump was installed into the fire truck, whose drive is ensured by the engine through the driving mechanism mounted on the gear box. During our measurements, the outlet pressure of the pump was set for 5 bar, which is the most commonly used pressure in firefighter activities. In accordance with the regulations applied by fire departments, standard fire-fighting equipment and pressure hoses were used during the measurement. We operated the pump in suction mode, its water supply was ensured by 2 pieces of "A" type suction hoses of d=110mm and a suction strainer. 2 pcs of "B" type pressure hoses of d=75 mm internal diameter, 4 pcs of "C" type pressure hoses of d = 52 mm inner diameter and 2 pcs of 75/52 four-way valve manifolds were applied during the installation. The amount of water flowing through the examined hoses was measured by an ultrasonic flow meter type Arad Octave 50, meanwhile the amount of water discharging from the nozzle was measured by the pressure gauge we constructed combined with the measuring nozzle with a nozzle tip of 14 mm diameter. As for the rest of the streams, we applied standard reel nozzles with a nozzle tip of 14 mm in diameter. A separate measurement was performed with the stream at ground-level and the stream on the second storey. The figure 4. shows how the water supply system serving firefighting purposes was installed and operated.

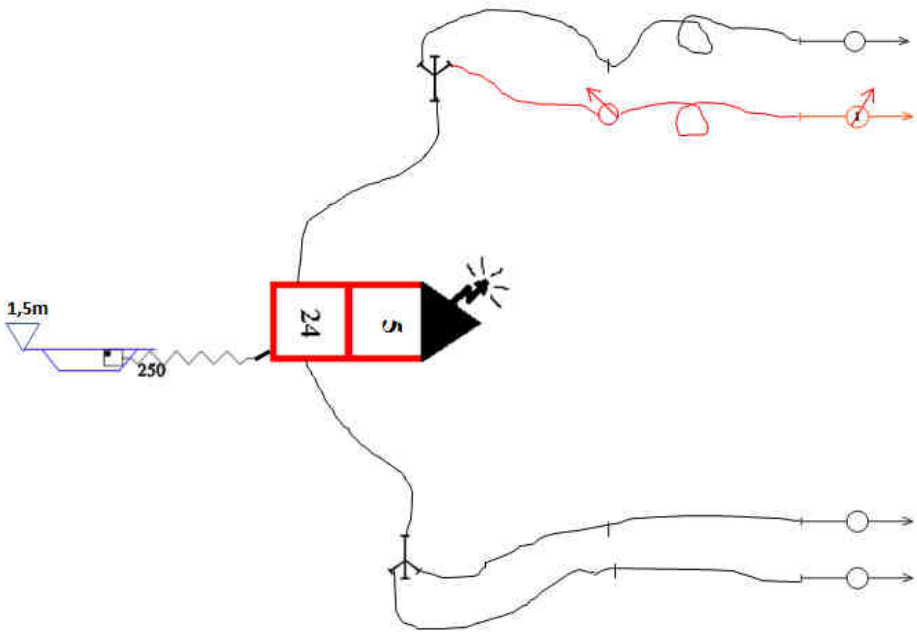

Fig. 4. The firefighting system design for our measurements (Source: Compiled by the Authors)

Performing the measurement, we first sucked water with the pump, then we activated the streams one by one. First, we installed the complex measuring device into the stream placed on the storey. We installed the ultrasonic flow meter type Arad Octave 50 behind the first 'C' type fire hose and the measuring nozzle connected to the pressure gauge at the end of the second "C" type fire hose. Our next step was to activate the other streams as well, then we continuously increased the performance of the pump reaching 5 bar outlet pressure on the measured stream. At that time, the outlet pressure of the pump was 6 bar. The data were recorded continuously and prepared for validation. We calculated the amount of water discharging from the nozzle with 14 mm of diameter at the different pressures. Up to 5 bar outlet pressure, the changes of water discharge in the stream placed on the storey are shown in the table 1.

Table 1: The changes of discharge water in the stream positioned on the storey (Source: Compiled by the Authors)

Pressure at the nozzle-Storey 2 [bar]	Discharge water at the nozzle [l/min]	Pressure at the pump [bar]	Flow rate [l/min]
1	163.528	1.8	164.67
1.5	200.280	3	207.67
2	231.263	3.9	243
2.5	258.560	4.5	273.5
3	283.238	5	303.5
3.5	305.932	5.5	322.17
4	327.055	5.9	339.83
4.5	346.895	6.5	356.33
5	365.659	7.2	377.83

Next, the changes of discharge water in the ground stream were measured. The complex measuring unit was installed into the system as previously. The measurement results are indicated in the table 2.

Table 2: The changes of discharge water in the ground positioned on the storey (Source: Compiled by the Authors)

Pressure at the nozzle- Groundfloor [bar]	Discharge water at the nozzle [l/min]	Pressure at the pump [bar]	Flow rate [l/min]
1	163.528	1	164.33
1.5	200.280	1.6	204.17
2	231.263	2.2	238.67
2.5	258.560	2.9	262.17
3	283.238	3.5	291
3.5	305.932	4.2	315.17
4	327.055	5	337.5
4.5	346.895	5.9	353.67
5	365.659	6.5	369.5

Finishing the measuring process, the performance of the pump was continuously decreased and finally stopped. After that we disassembled the system.

6. Conclusions

Our research project was to examine the operating parameters of a firewater supply system. In order to keep the measurement procedure simple and to gain accurate results, we constructed a complex measuring device. We conducted our measurements in an infield 1:1 experiment creating a realistic firefighting environment. Analysing our measurement results, we concluded that the amount of water obtainable at different heights show differences, so it must be taken into consideration during the firefighting process. We also concluded that during operation significantly high losses occur inside the fire hoses, which can be demonstrated without complicated calculations only by applying our complex measuring device. Our measuring nozzle assembled with a pressure gauge and fitted with a replaceable tip is suitable for performing accurate discharge water measurements, furthermore, with a simple calculation method the water flows belonging to the outlet pressure values can be determined and demonstrated in a table. The table format makes it easy to identify the discharge water values belonging to the relevant outlet pressure, which simplifies the measuring process. The size of the replaceable nozzle tips in our measuring nozzle equals to of the most commonly used ones, therefore, our measurement results can be used in practice during firefighting activities.

References

[1] Józsa, I. *Vortex Pumps in practice / Örvényszivattyúk a gyakorlatban*. Budapest, Invest-Marketing Bt., 2013: 108-196.
[2] Fecser, N., and R. Kuti. "Examining Fire Pump Metz Fp 24/8 on Cavitation." *Hidraulica*, no. 4 (December 2017): 98-104.
[3] Szabó Béla, L. *Water Supply Studies/ Vízellátási ismeretek*. Budapest, BM Könykiadó, 1983: 244.
[4] Lajos, T. *The basics of hydrodynamics /Az áramlástan alapjai*. Budapest, Műegyetemi Kiadó, 2004: 571.
[5] Spurgeon, P. "Every Pump Operator's Basic Equation." *Fire Engineering* 165, no. 10 (October 2012): 51-64.

The Correlation between the Composition of the Gas Mixture Injected into Water and the Concentration of Dissolved Oxygen in Water

PhD Student **Nicoleta Dorina ALBU**[1], As. Dr. Eng. **Elena Beatrice TĂNASE**[1], PhD Student **Nicolae Vlad SIMA**[1], Prof. Dr. Eng. **Nicolae BĂRAN**[1], Eng. **Corina MOGA**[2]

[1] Politehnica University of Bucharest, n_baran_fimm@yahoo.com

[2] DFR Systems SRL, Bucharest, corinamoga@yahoo.com

Abstract: *The paper presents three versions of gas mixtures: atmospheric air, atmospheric air and oxygen from a cylinder, air with low nitrogen content supplied by oxygen concentrators. These mixtures are successively introduced into a water tank and the theoretical and experimental determination of the change in the dissolved oxygen concentration in water is determined. The most favourable option for water oxygenation is chosen.*

Keywords: *Water aeration, oxygen dissolved in water, water oxygenation.*

1. Introduction

The process of water oxygenation is based on a transfer between air and water; the oxygen in the air is transferred by various processes to the water. The air bubbles generated by the installations that form them are introduced into a water volume. The most effective water oxygenation systems are those that generate very fine bubbles. A classification of the gas bubbles is shown in Figure 1.

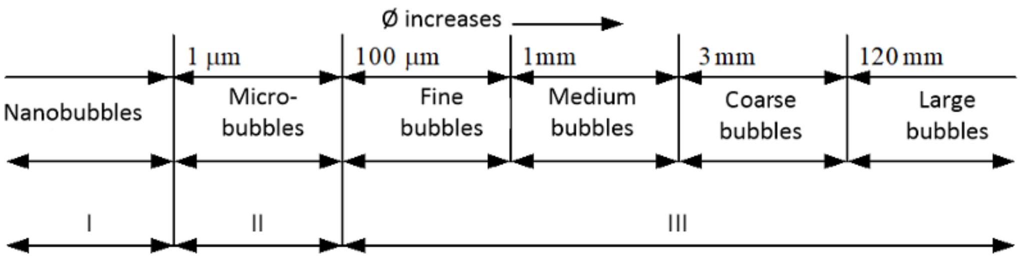

Fig. 1. Classification of gas bubbles according to their diameter
I - the area where the gas bubbles can be observed under the microscope;
II - the area where gas bubbles can be observed with difficulty;
III - the area where gas bubbles can be observed with the naked eye.

In the water treatment and purification processes, oxygenation, referred to as aeration in some specialty works, is the basic operation in ensuring proper water quality. As a result of the researches carried out in the laboratories of POLITEHNICA University of Bucharest, it was found that the two processes should be distinguished:
I) Water Aeration;
II) Water oxygenation.
- In the case I) only atmospheric air (21% O_2 + 79% N_2) is introduced into the water.
- In the case II), a mixture of gases consisting of:
• air + oxygen from a cylinder in different volumetric volumes;
• air with low nitrogen content supplied by oxygen concentrators.
Aeration is used:
- In water treatment processes, removal of dissolved inorganic substances or chemical elements such as iron, manganese, etc., by oxidation and formation of sedimentable compounds or which may be retained by boiling;
- In the biological treatment of wastewater, either through the activated sludge process or with bio filters;

- In the disinfection processes, by ozonizing the raw water captured from a source for the purposes of its drinking;
- In separating and collecting emulsified fats from wastewater.

Water oxygenation is a mass transfer process with wide application in water treatment and purification. Oxygenation equipment's are based on the dispersion of one phase into the other, for example, a gas into liquid, an energy consuming process.

Dissolved oxygen is an important parameter in assessing water quality due to its influence on living organisms in a water volume. In Limnology (the study of lakes), dissolved oxygen is an essential factor [1]. A too high or too low dissolved oxygen level can affect water life and affects water quality.

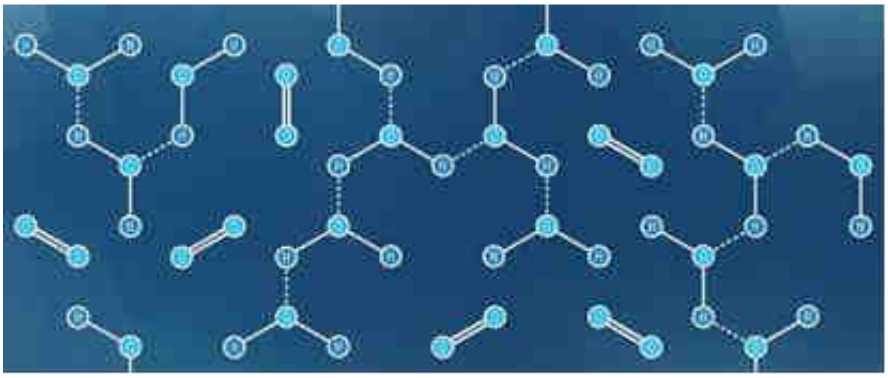

Fig. 2. Non-bonded oxygen molecules in water

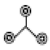 **-** oxygen molecule bound in water;  - oxygen dissolved in water.

Non-compound oxygen or free oxygen is the oxygen that is not bound to any other element (Fig. 2). Dissolved oxygen is the presence of those free oxygen molecules into water. Water-bound oxygen molecules (H_2O) are a compound and are not considered in the determination of dissolved oxygen level [2].

2. The introduction of gas mixtures in water to increase the dissolved oxygen concentration in water

These gas mixtures can be made in the following versions:
I - Atmospheric air (21% O_2+ 79% N_2);
II - Atmospheric air + oxygen from a cylinder (the following cases are considered:
case 1: r_{O2} = 25%;
case 2: r_{O2} = 50%;
case 3: r_{O2} = 75%;
case 4: r_{O2} = 100%;
r- volumetric participation).
III - Air with low nitrogen content (95% O_2 + 5% N_2) supplied by oxygen concentrators.
In the studied versions, the concentration of oxygen dissolved in water (C_{O2}) will increase in time.
The gas mixture is continuously fed into the tank for 120 minutes, so the regime is non-stationary and the initial concentration of oxygen dissolved in water increases in time.
In non-stationary regime the measured amount is the concentration of dissolved oxygen in water, in time.
The water tank in which the researches are carried out is shown in Figure 3.

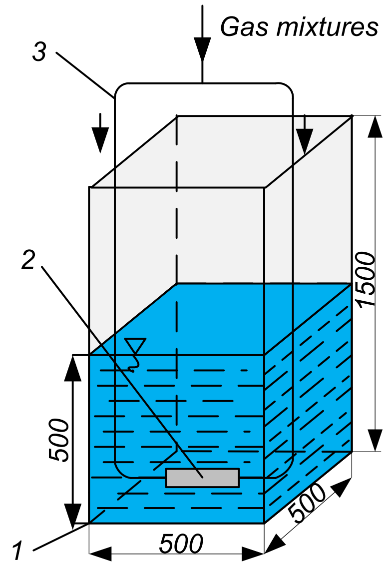

Fig. 3. Water tank into which the microbubbles generator is inserted; the generator is fixed
$V_{useful} = 0.375\ m^3$; $V_{H2O} = 0.125\ m^3$
1 - transparent plexiglass tank; 2 - microbubbles generator (M.B.G.); 3 - different gas mixtures supply pipes.

The following are measured: water and air temperature, gas flow rate at the inlet to the tank and gas pressure in the body of the microbubbles generator [1].

3. Numerical integration of the equation of oxygen transfer rate into water

The oxygen transfer speed equation in water is [1]:

$$\frac{dC}{d\tau} = a \cdot k_L \left(C_s - C\right) \tag{1}$$

where:
C - The dissolved oxygen concentration at the time τ;
ak_L -The volumetric mass transfer coefficient;
C_s -The oxygen concentration in water at saturation.
The values of ak_L and C_s are constant with time. If the boundary conditions $C = C_0$ for $\tau = 0$ are imposed, the equation (1) can be integrated [2]:

$$\frac{\mathrm{dC}}{\mathrm{C_s - C}} = \mathrm{a \cdot k_L\, d\tau} \tag{2}$$

Assuming $C < C_s$, after integration, results:

$$-\ln\left(\mathrm{C_s - C}\right) = \mathrm{a \cdot k_L \cdot \tau + ct} \tag{3}$$

The ct. term is obtained from the limit condition:

$$C = C_0 \text{ for } \tau = 0 \tag{4}$$

and has the value

$$ct = -\ln\left(C_s - C_0\right). \tag{5}$$

Inserting (5) into (3):

$$-\ln\left(C_s - C\right) = a \cdot k_L \cdot \tau - \ln\left(C_s - C_0\right), \tag{6}$$

$$\ln\left(C_s - C\right) = \ln\left(C_s - C_0\right) - a \cdot k_L \cdot \tau, \tag{7}$$

$$\ln\left(C_s - C\right) = \ln\left(C_s - C_0\right) + \ln e^{-a \cdot k_L \cdot \tau}, \tag{8}$$

$$\ln\left(C_s - C\right) = \ln\left(\left(C_s - C_0\right) \cdot e^{-a \cdot k_L \cdot \tau}\right),$$

$$C_s - C = \left(C_s - C_0\right)\cdot e^{-a\cdot k_L\cdot \tau}\ , \tag{9}$$

$$C = C_s - \left(C_s - C_0\right)\cdot e^{-a\cdot k_L\cdot \tau}\ , \tag{10}$$

initial: $\tau = 0$.

In this equation the following values must be known: C_0 - the initial concentration of dissolved O_2 in water; C_s - saturation concentration of dissolved O_2 in water for a given water temperature; ak_L - the volumetric mass transfer coefficient [s^{-1}] or [min^{-1}] determined by one of the chemical or electrical methods. The values of C = f (τ) are calculated based on a computing program presented below (Fig. 4) [4] [5]:

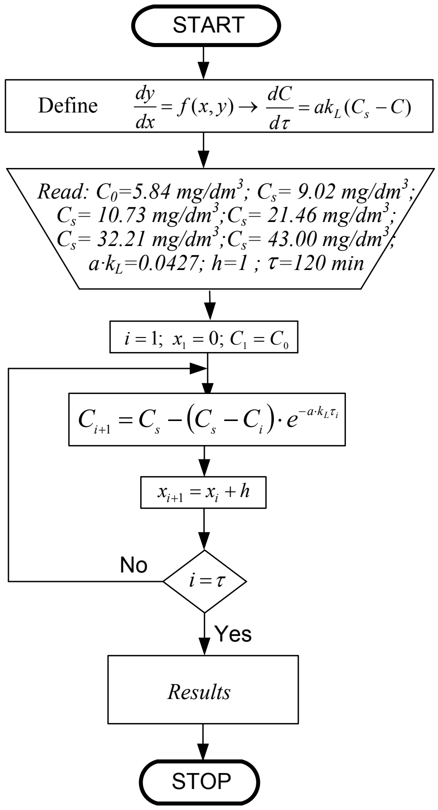

Fig. 4. The logical scheme for the function: C = f (τ) in the case of the injection of some gas mixtures into the water tank

This logical scheme is completed for each studied variant, i.e. separately:
- air (O_2 + N_2);
- air / oxygen mixture (air + O_2);
- air with low nitrogen content.

4. Data on the analysed gas mixtures

In the theoretical study, the following assumptions are made:
- the air flow rate or the mixing rate (air + oxygen), (air with low nitrogen content) is equal to 600 dm^3/h;
- gas mixture pressure 573 mm H_2O;
- the height of the water layer remains constant: H = 500 mmH_2O;
- working time, i.e. duration of an experiment: τ = 120 minutes;
- water temperature, t_{H2O} = 23.7 °C;
- the value of the initial dissolved oxygen concentration in the water is to be the same: C_0 = 5.84 mg / dm^3.

Theoretically, the following versions of gas mixtures in water are analysed:
Version I: air (21% O_2 + 79% N_2);

Version II: gas mixture: air + gas cylinder gas ($r_{O_2} = 25\ \%, r_{O_2} = 50\ \%, r_{O_2} = 75\ \%, r_{O_2} = 100\ \%$);
Version III: air with low nitrogen content (95% O_2 + 5% N_2) air.
For the three gas mixtures, some input data into the computation program are the same. It is specified that the value of oxygen concentration at saturation is different in each version I, II, III.

5. Computation results regarding the introduction of gas mixtures in the water

5.1 Version I. Injection of atmospheric air into the water

Input data in the computation program: C_0 = 5.84 mg / dm^3; H = 500 mmH_2O; t_{H2O} = 23.7 °C, t_{air} = 24.1 °C; $\dot{V} = 600$ dm^3/h; τ = 120 min, C_s = 8.4 [mg / dm^3].
To represent the evolution of dissolved oxygen concentration in water, computational programs were performed using the MatLab simulation program and the results obtained were displayed graphically.

Table 1: Theoretical operating conditions of the fine bubble generator in version I

τ [min]	0	15	30	45	60	75	90	105	120
$\dot{V}_{air}$ [dm^3/h]	600	600	600	600	600	600	600	600	600
$\dot{V}_{IO_2} = 0.21 \cdot 600 = 126$ [dm^3/h]	126	126	126	126	126	126	126	126	126
$\dot{V}_{O_2}$ from other sources	0	0	0	0	0	0	0	0	0

Based on the theoretical data in Table 1 and the obtained results following the computation program, the function C = f (τ) was represented in figure 5.

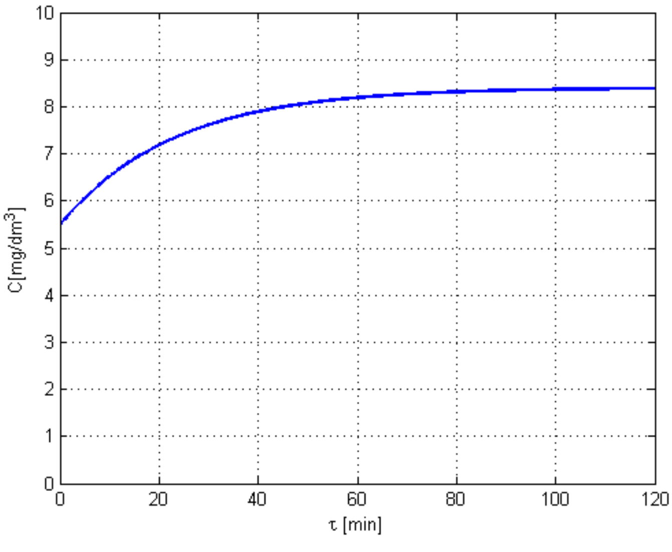

Fig. 5. Graphical representation of the variation of dissolved oxygen in water in version I.

5.2 Version II. Injection of a mixture of atmospheric air and oxygen from a cylinder

When oxygen-enriched air is used for oxygenation, the saturation concentration is corrected by the factor "k" according to the relation [8], [9]:

$$C_s = C \cdot \frac{k\ \%}{21\ \%}\ , \tag{11}$$

where k% is the oxygen concentration in the diffusing gas.

For t = 20 °C and p = 760 torr, for water, the saturation concentration is C = 9.02 mg / dm^3.

Taking into account the evolution of saturation concentration of dissolved oxygen in water for different values of the gas mixture between air and pure oxygen results: case I: - for k = 25% result:

$$C_{s,25} = C \cdot \frac{k\ \%}{21\ \%} = 9.02 \cdot \frac{25}{21} = 10.73\ \text{mgO}_2/\text{dm}^3 \tag{12}$$

C_s for case 2, 3, 4, the results are shown in table 2.

Table 2: Saturation concentration values C_s for the four cases of version II

Nr. crt	$\dot{V}$ [dm^3/h]	$\dot{V}_{air}$ [dm^3/h]	r_{i,O_2}	$\dot{V}_{O_2}$ [dm^3/h]	C_0 [mg/dm^3]	C_s [mg/dm^3]
1	600	450	25	150	5.84	10.73
2	600	300	50	300	5.84	21.46
3	600	150	75	450	5.84	32.21
4	600	0	100	600	5.84	43.00

The following are theoretical calculation results for the four cases of version II.
1. Version II, case 1 (r_{O2} = 25%)
Atmospheric air $\dot{V}_1 = 0,75\ \% \cdot V_I = 0.75 \cdot 600 = 450$ dm^3/h and oxygen $\dot{V}_{O_2,b}$ =150 dm^3/ h from a cylinder of with the same pressure are injected. As a result, the oxygen flow rate introduced into water is (Table 3).

$$\dot{V}_{1,O_2} = 0.21 \cdot \dot{V}_1 + \dot{V}_{O_2,b} = 0.21 \cdot 450 + 150 = 94.5 + 150 = 244.5\ \text{dm}^3/\text{h}$$

Table 3: Theoretical operating conditions of the fine bubble generator in case 1

τ [min]	0	15	30	45	60	75	90	105	120
$\dot{V}_{air}$ [dm^3/h]	450	450	450	450	450	450	450	450	450
$\dot{V}_{1O_2} = 0.21 \cdot \dot{V}_{air} = 94.5$ [dm^3/h]	94.5	94.5	94.5	94.5	94.5	94.5	94.5	94.5	94.5
$\dot{V}_{O_2}$ from a cylinder [dm^3/h]	150	150	150	150	150	150	150	150	150
$\dot{V}_{O_2,total}$ [dm^3/h]	244.5	244.5	244.5	244.5	244.5	244.5	244.5	244.5	244.5

Based on the data in Table 3 and the obtained results following the computation program, the graph in Figure 6 was plotted.

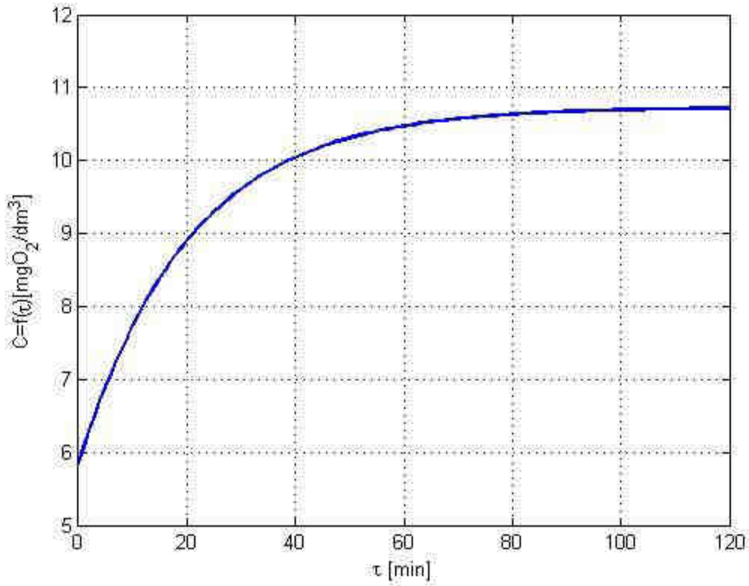

Fig. 6. Graphical representation of the variation of dissolved oxygen concentration in water in case 1.

The obtained values are similar to the data from the literature [10], [11].
2. Version II, case 2 (r_{O2} = 50%)
Atmospheric air is introduced: $\dot{V}_2 = 0.5\ \% \cdot V_I = 0.5 \cdot 600 = 300$ dm^3/h t_{air} = 24.10 ° C, t_{H2O} = 23.7 ° C and $\dot{V}_{O_{2,b}} = 300$ dm^3/h. As a result, the oxygen flow rate introduced into water is (Table 4):

$$\dot{V}_{2,O_2} = 0.21 \cdot \dot{V}_2 + \dot{V}_{O_2,b} = 0.21 \cdot 300 + 300 = 63 + 300 = 363 \text{ dm}^3/\text{h}$$

Table 4: Theoretical operating conditions of the fine bubble generator in case 2

τ [min]	0	15	30	45	60	75	90	105	120
$\dot{V}_{air}$[dm^3/h]	300	300	300	300	300	300	300	300	300
$\dot{V}_{2O_2} = 0,21 \cdot \dot{V}_{air} = 63$ [dm^3/h]	63	63	63	63	63	63	63	63	63
$\dot{V}_{O_2}$ from a cylinder [dm^3/h]	300	300	300	300	300	300	300	300	300
$\dot{V}_{O_2,total}$ [dm^3/h]	363	363	363	363	363	363	363	363	363

Based on the data in Table 4 and the obtained results following the computation program, the graph in Figure 7 was plotted.

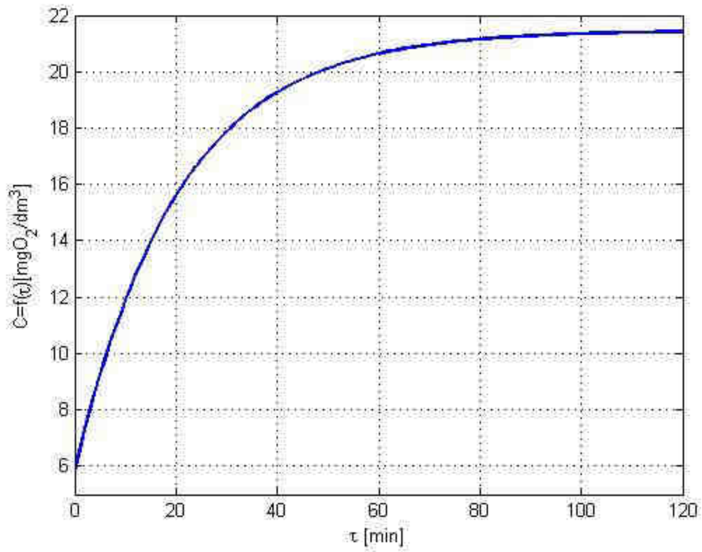

Fig. 7. Graphical representation of the variation of dissolved oxygen concentration in water in case 2.

3. Version II, case 3 (r_{O2} = 75%)
Atmospheric air is introduced: $\dot{V}_3 = 0.25\,\% \cdot V_I = 0.25 \cdot 600 = 150$ dm^3/h and $\dot{V}_{O_{2,b}} = 450$ dm^3/h . As a result, the oxygen flow rate introduced into water is (Table 5):

$$\dot{V}_{3,O_2} = 0.21 \cdot \dot{V}_3 + \dot{V}_{O_2,b} = 0.21 \cdot 150 + 450 = 31.5 + 450 = 481.5 \text{ dm}^3/\text{h}$$

Table 5: Theoretical operating conditions of the fine bubble generator in case 3

τ [min]	0	15	30	45	60	75	90	105	120
$\dot{V}_{air}$[dm^3/h]	150	150	150	150	150	150	150	150	150
$\dot{V}_{3O_2} = 0.21 \cdot \dot{V}_{air} = 31.5$ [dm^3/h]	31.5	31.5	31.5	31.5	31.5	31.5	31.5	31.5	31.5
$\dot{V}_{O_2}$ from a cylinder [dm^3/h]	450	450	450	450	450	450	450	450	450
$\dot{V}_{O_2,total}$ [dm^3/h]	481.5	481.5	481.5	481.5	481.5	481.5	481.5	481.5	481.5

Based on the data in Table 5 and the obtained results following the computation program, the function C = f (τ) (figure 8) was represented.

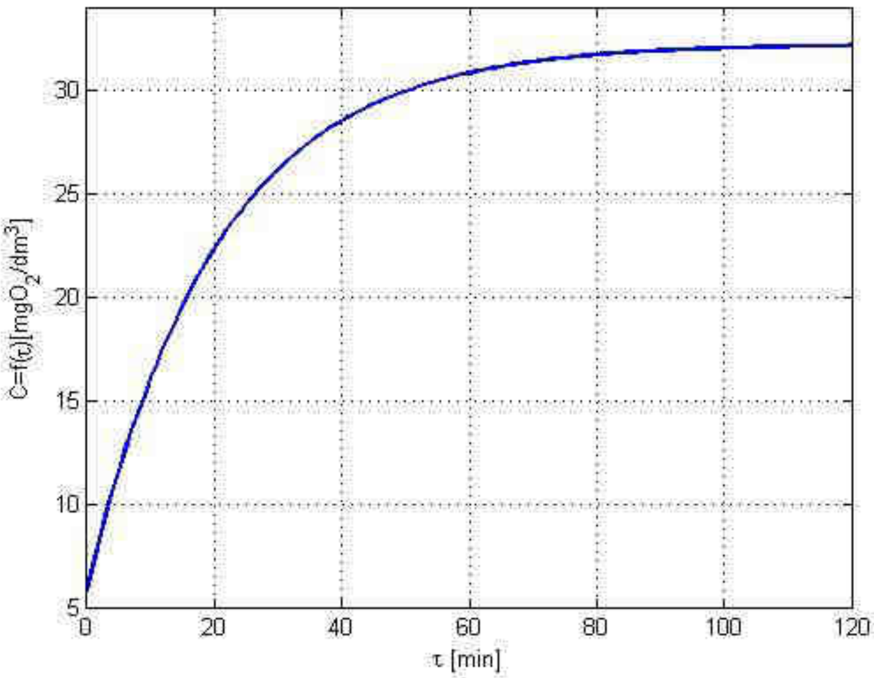

Fig. 8. Graphical representation of the variation of dissolved oxygen concentration in water in case 3.

4. Version II, case 4 (r_{O2} = 75%)
Atmospheric air is introduced: $\dot{V}_4 = 0$ dm^3/h and $\dot{V}_{O_2,b} = 600$ dm^3/h. As a result, the oxygen flow rate introduced into water is (Table 6):

$$\dot{V}_{4,O_2} = 0 + \dot{V}_{O_2,b} = 0 + 600 = 600 \text{ dm}^3/\text{h}$$

Table 6: Theoretical operating conditions of the fine bubble generator in case 4

τ [min]	0	15	30	45	60	75	90	105	120
$\dot{V}_{air}$ [dm^3/h]	0	0	0	0	0	0	0	0	0
$\dot{V}_{4O_2} = 0.21 \cdot \dot{V}_{air} = 0$ [dm^3/h]	0	0	0	0	0	0	0	0	0
$\dot{V}_{O_2}$ from a cylinder [dm^3/h]	600	600	600	600	600	600	600	600	600
$\dot{V}_{O_2,total}$ [dm^3/h]	600	600	600	600	600	600	600	600	600

Based on the data in Table 6 and the obtained results following the computation program, the function C = f (τ) (figure 9) was represented.

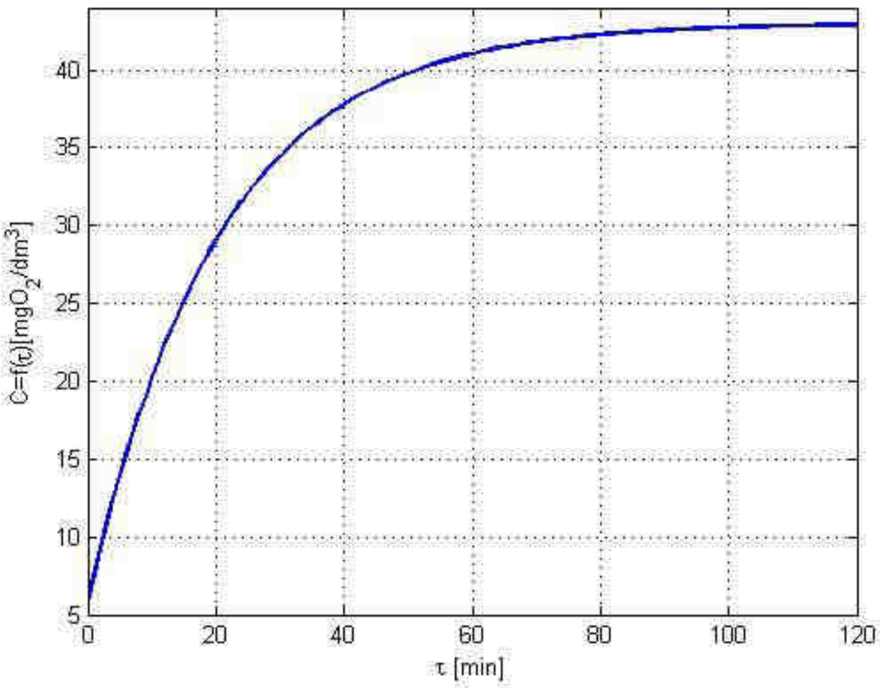

Fig. 9. Graphical representation of the variation of dissolved oxygen concentration in water in case 4.

The comparison of the C = f (τ) function for version I and the four cases of version II presented above can be seen in Figure 10.

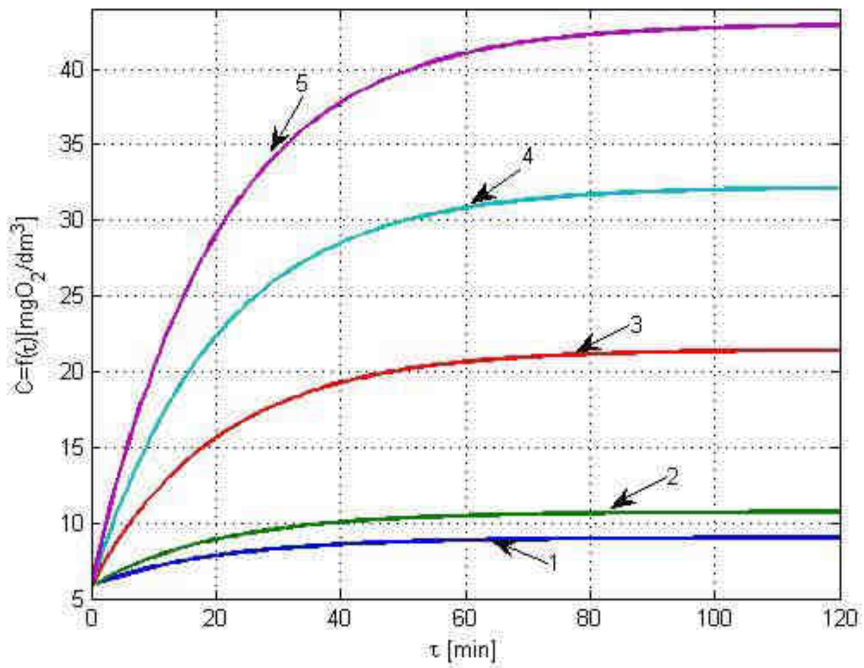

Fig. 10. The graphical representation of the variation of dissolved oxygen concentration in water for the I version and the four cases of version II
1 - the I version; 2 - version II, case 1; 3 - version II, case 2; 4 - version II, case 3; 5 - version II, case 4.

Figure 10 shows that with the increase in oxygen from the cylinder, the amount of dissolved oxygen in water increases.

5.3 Injection of air with low nitrogen content (version III)

In the process of water oxygenation, the use of air with low nitrogen content is investigated.
For t = 29 °C and p = 760 torr, the saturation concentration is 7.7 mg / dm³.

$$C_s = 7.7 \cdot \frac{95\ \%}{21\ \%} = 34.8\ \text{mg O}_2/\text{dm}^3\,. \tag{13}$$

The values C = f (τ) are shown in Table 7.
Of the total of 600 dm³ / h, 95% is O_2 (i.e. 570 dm³ / h), and 5% (i.e. 30 dm³ / h) is nitrogen.

Table 7: Theoretical operating conditions of the fine bubble generator in version I

τ [min]	0	15	30	45	60	75	90	105	120
$\dot{V}_{N_2}$ [dm³/h]	30	30	30	30	30	30	30	30	30
$\dot{V}_{O_2} = 95\ \%$[dm³/h]	570	570	570	570	570	570	570	570	570

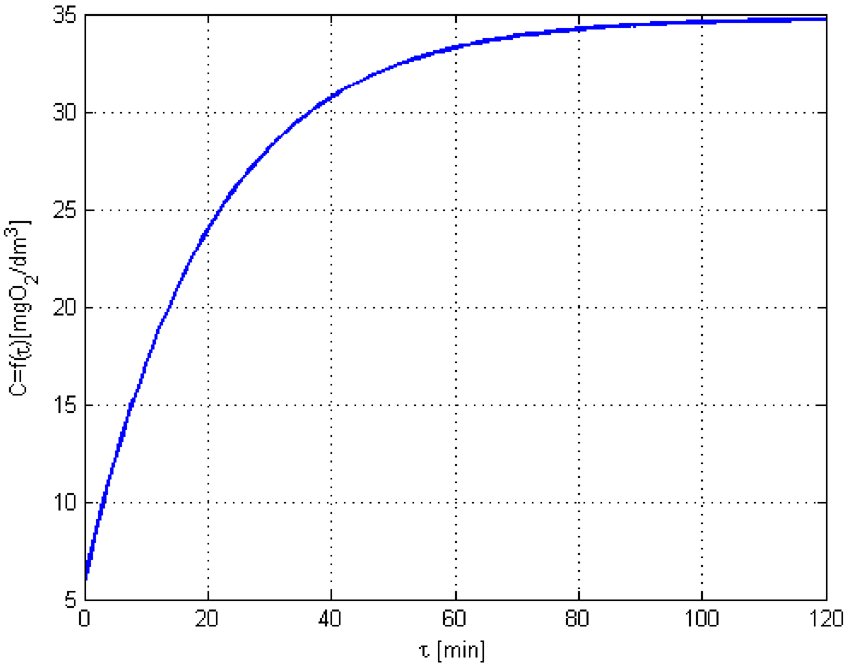

Fig. 11. Graphical representation of the variation of dissolved oxygen in water in version III.

Following the running of the computation program, the graph in Figure 11 was plotted.

6. Conclusions

- The most advantageous method of water oxygenation is presented in version II, case 4, when pure oxygen is pumped into the water.
- The variation speed, namely the increase of the dissolved oxygen concentration in water, increases from the version I to the version II, case 4.
- An efficient oxygenation process is also achieved with the use of air with low nitrogen content.
- Following an economic calculation, it can be determined which process is most effective among the most advantageous solutions, namely:

a) Case 4 when pure oxygen is introduced or a mixture of air and oxygen from the cylinder;
b) Version III where air with low nitrogen content is introduced.

Taking into account the costs of purchasing oxygen and operating costs, it was concluded that the most cost-effective water oxygenation process consists of introducing into the water a mixture of atmospheric air and 25% oxygen from a cylinder.

References

[1] Tănase, Elena Beatrice. *Influenţa compoziţiei gazului insuflat în apă asupra conţinutului de oxigen dizolvat*. PhD. Thesis. Bucharest, Politehnica University of Bucharest, 2017.
[2] Oprina, G., I. Pincovschi, and Gh. Băran. *Hidro – gazo – dinamica sistemelor de aerare echipate cu generatoare de bule fine*. Bucharest, Politehnica Press, 2009.
[3] Pătulea, Al.S. *Influenţa parametrilor funcţionali şi a arhitecturii generatoarelor de bule fine asupra eficienţei instalaţiilor de aerare*. PhD. Thesis. Bucharest, Politehnica University of Bucharest, 2012.
[4] Călușaru, I. *Influenţa proprietăţilor fizice ale lichidului asupra eficienţei proceselor de oxigenare*. PhD. Thesis. Bucharest, Politehnica University of Bucharest, Faculty of Mechanical Engineering and Mechatronics, 2014.
[5] Căluşaru-Constantin, M., E.B. Tănase, N. Băran and Rasha Mlisan-Cusma. "Researches Regarding the Modification of Dissolved Oxygen Concentration in Water." *IJISET - International Journal of Innovative Science, Engineering & Technology* 1, no. 6 (August 2014): 228-231.
[6] Căluşaru, I., N. Băran and A. Pătulea. "The influence of the constructive solution of fine bubble generators on the concentration of oxygen dissolved in water." *Advanced Materials Research* 538-541 (July 2012): 2304-2310.
[7] Băran, N., A. Pătulea, and M. Căluşaru. "Computation of performance and efficiency of the water oxygenation process in non-stationary conditions." Paper presented at the Sixième édition du Colloque Francophone sur L'Energie –Environnement- Economie et Thermodynamique COFRET 2012, Sozopol, Bulgaria, June 11-13, 2012.
[8] Tănase, E.B., N. Băran, and R. Mlisan. "An Efficient Solution for Water Oxygenation." *Asian Engineering Review* 1, no. 3 (2014): 36-40.
[9] Barnhart, E.L. "Transfer of oxygen in aqueous solutions." *J. Sanit. Eng. Div.* 95, no. 3 (1969): 645 – 661.
[10] Băran, N., M. Vlăsceanu, M. Băran, and E.B. Tănase. "Increasing the performance of oxygenation installations." *Termotehnica* 18, no. 1 (2014): 16-21.
[11] Vlăsceanu, M., N. Băran, and M. Băran. "Decrease of Energy Consumption in the Case of Water Oxygenation Processes." *Energy Procedia* 50 (2014): 454-459.

2D Numerical Model of a River Sector Flow in Case of Hypothetical Side Flooding Due to Embankment Failure

Lect.dr.eng. **Albert Titus CONSTANTIN**[1], Assoc.prof.dr.eng. **Gheorghe I. LAZĂR**[2], Lect.dr.eng. **Şerban-Vlad NICOARĂ**[3]

[1] POLITEHNICA University Timişoara, albert.constantin@upt.ro

[2,3] POLITEHNICA University Timişoara

Abstract: *The paper presents a 2D numerical modelling of water flow on a sector of about 7800m of Timiş River downstream of Lugoj Town, west of Romania, in case of accidental highwaters produceing side flooding due to a hypothetical embankement breach. The numerical simulation, assimilating the special high-flow values that occurred on site along the April 4th to 11th hydrological event of 2005, aims to estimate the possible water levels on the river sector and the flood development, meaning the flood area contour and its eventual threaten with respect to an economic objective (important logistic warehouse) existing on the right river plain.*

Keywords: *River flow, high water flow, embankment failure, side flooding, numerical model.*

1. General considerations

The numerical modelling of the analysed river site is based on a flooding study on Timiș River, covering a sector of about 7800m outside of Lugoj Town, west of Romania, downstream towards Coșteiu Water Arrangements, looking to estimate the eventual implications upon the accomplishment of a logistic warehouse in the immediate vicinity of the river right flooding plain [1]. In the same time, the present approach considers a 1D numerical modelling performed by HEC-RAS ver.4.1 [2,3] that looked to retrace the special high waters passing by the considered river sector during the exceptional hydrological event of the spring of 2005.

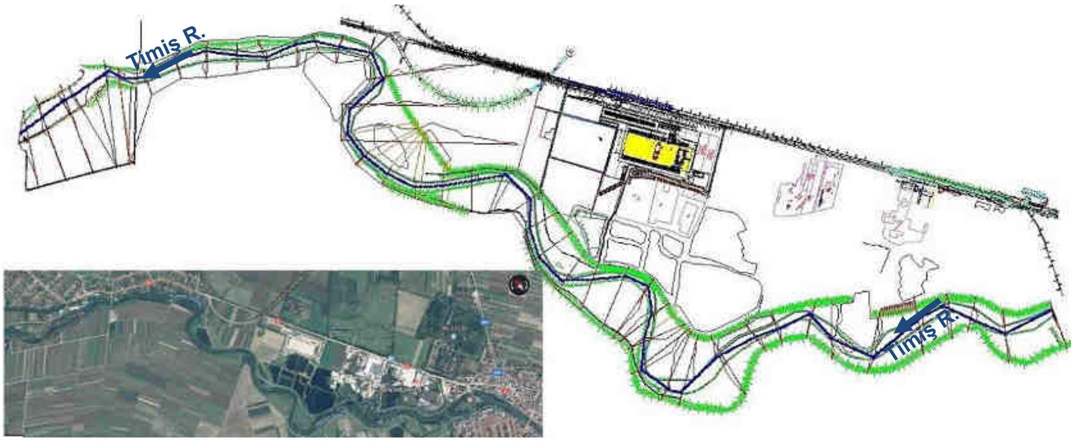

Fig. 1. General plan view of analysed Timiş River area (warehouse located) based on the topographical measurements downstream of Coșteiu Water Arrangements

As considering the mentioned river sector with its side areas, a data base objectified by a general site plan (Stereo70 standardized topographical measurement) comprising 49 short cross-view profiles (framed by flood protection embankments and pointing out the streambed morphology) and 49 long cross-view profiles (covering the possible affected floodplain between the left protection dike and the railway embankment, and respectively the right dike and the national road structure) was created. The specified economic objective, consisting from the actual warehouse, the administration / operation office building and the sanitary and traffic infrastructure, is placed at about 300m from the side embankment on the right flood plain of Timiș River. The specific developed area covering about 180 m^2 in total is situated at a mean level of about 115.30 meters with respect to the Sea Level.

The graphic accomplishment of a 3D terrain representation is usually performed by the help of the additional satellite application Earth Explorer. A useful and comfortable methode of topographical data graphical processing is presented by Nicoara & al., 2018 [4]. The methode employes a specialized topography application for 2D graphical interpolation on two directions – 0x and 0y – by which a 3D shape surface can be generated as a .shx extention file.

The created surface is then loaded with ArcMAP 9.3 [5] where is to be divided in discrete spatial areas of triangularly shapes leading to a digital final outline asa 3D real space of Triangulated Irregular Network (TIN) type (figure 2). In order to be acknowledged by the RAS Mapper module in HEC-RAS 5.0.6 the outline had to be converted as a grid loadable file of Digital Terrain Model type [4,6].One can accept that by the help of "satellite" model, terrain results quite accurate as a meshed domain even if it was based on a relatively reduced number of topographic measured points – 6045 points for the considered area – and so suitable fulfilling the usual requirements of a 3D graphic representation. Still the model can not truly generate nither the flood protection embankments configuration and nor the underwater streambed.

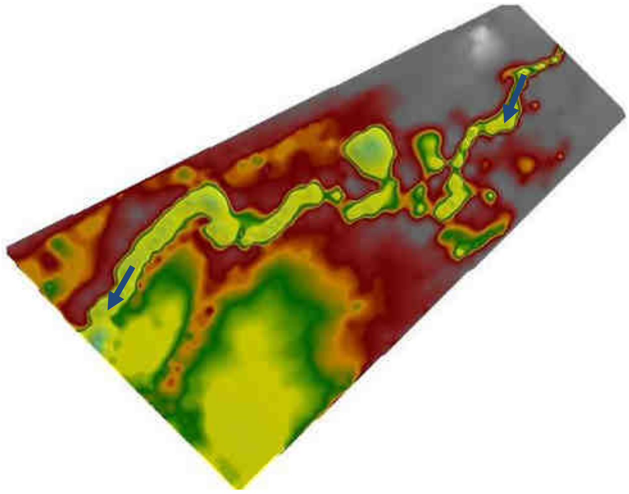

Fig. 2. 3D terrain representation of the studyed Timiş River sector with its adjoining flooding plains protected by embankments

As so, the 3D representation model reached by bidimensional interpolation was afterwards enhanced in HEC-RAS 5.0.6 [6] by upgrading the streambed ground geometry and the embankments top configuration according to the available topographic cross-sections. HEC-RAS 5.0.6 offers a usefull and casual facility that may be considered also for surface geometry updating operations [6,7]. A given water course can be overlaid as defined by a series of successive cross-sections specifying the side structures geometry. This known procedure is described by Kiers, 2015 [8], while a specific application was performed by Nicoara & al., 2018 [4].

2. Accomplishment of 2D numerical model

The 3D model reached by bi-dimensional interpolation and imported to HEC-RAS 5.0.6 was so geometricaly upgraded by adding the particular sector of Timiș River course defined by a double series of discrete points following the axes along the top of the two flood protection embankments.
First, the 2D surface domain – timis_lugoj_costei – was generated for the initial terrain model. The 2D Flow Areas facility is considered in the Explorer Window (figure 3) and the domain contour named S2D is established. There was adopted a grid defined by Dx = Dy = 25m, following to generate the associated points (Generate Computations Points) with their corresponding properties tables (Compute Property Points).
Similarly, the paths of the two embankments top were defined in River facility – right and left river banks as supplyed by topographical measurements – and distinctly saved as mal_drept_dig and mal_stâng_dig. Two perimeter fields covering the two paths are defined right away in the 2D Flow Areas facility in order to perform an automatic additional grid thickening to Dx = Dy = 3.5m. Further on the embankments cross sections types were successively inserted along the two paths. The actual procedure of accesing the Geometry Data facility in the main menu is presented by Kiers, 2015 [8], the cross-section types being attached one by one to the paths bending points.
Returning to RAS Mapper window, the Interpolation Surface option is to be considered in Cross Sections menu. The embankments geometry, both for the right and left banks, is considered in the Explorer Window and so is exported by the Export Layer facility as engaging the Create Terrain GeoTiff from XS' s (Overbanks and Channel) option.

A terrain image type file – maluri_dig – was so obtained and saved. Based on this "maluri_dig" image and the "Terrain_neact" image (supplied by the Terrain option in 2D Flow Areas facility), a new and final terrain image – Terrain_dum_final – was than defined [3] and selected by a check mark (figure 3). Once the geometry upgrading operations are fulfilled, the overlaid given river sector (meaning the embankment top paths with the associated cross-sections) can be eliminated. There results a clean but sharpened with respect to elevations 2D numerical model. Figure 3 aims to present the final 3D type terrain configuration bearing the river bed and side embankments enhancements.

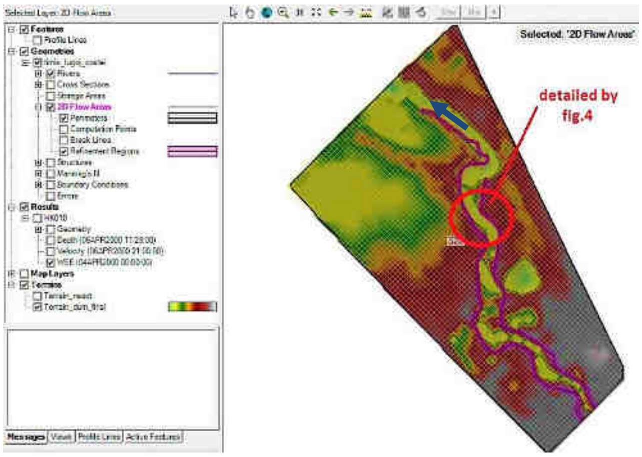

Fig. 3. 3D type view of the analysed site of Timiş River sector and side floodplains with upgraded geometry of riverbed and embankments

As about the river site hydrological conditions, the standard flow values of various overrunning probabilities that may occur on the analysed sector of Timiş River, downstream of Lugoj Town towards Coştei Water Arrangement, as provided by the Banat Regional Water Branch of Romanian Waters National Administration, are presented by the following table:

Table 1: Hydrological data

River	Station	F [km²]	Qmax [m³/s]					
			0.1%	0.5%	1%	2%	5%	10%
Timiş	logistic warehouse Lugoj	2827	2520	1540	1266	1100	860	695

As a result of two exceptional hydrological events that occurred on the highwaters seasons of April 2000 and April 2005, a long breach of about 154m in length and a minimum level of about 114.55mSL got developed on the left-side embankment of Timiş River (located on figure 3 and detailed by figure 4). At a highwater phenomenon defined by a water flow of already 5% overrunning probability, the river water level would overcome the left embankment lower crest level and volumes would start spill towards the adjoining floodplain.

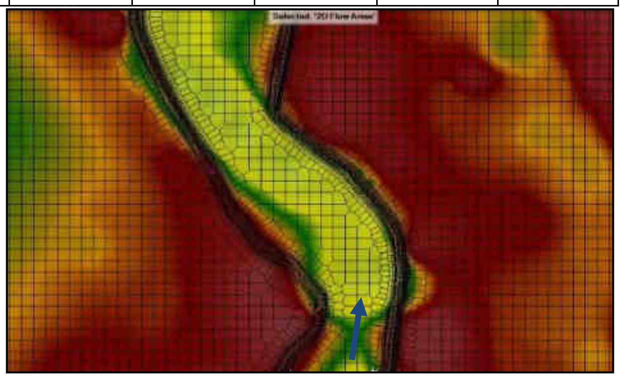

Fig. 4. Detailed terrain configuration in the area of the top breached left embankment

The final stage of the 2D numerical model development is the initial / boundary conditions definition. The SA/2D Area BC Lines option is to be considered by the boundary conditions (BC Line) facility in Geometric Data main menu (figure 5). Three zones were considered for the employed 2D domain, one on the upstream side (BC_S2D_11) upon which the highwaters hydrograph of a given water energy gradient was applied, and two on the downstream side (BC_S2D_22 and BC_S2D_33) upon which the corresponding water hydro-dynamic gradient was considered. As reported by the competent authority after the spring of 2000 and so attached to the upstream BC_S2D_11 boundary line, the highwaters hydrograph on the analyzed sector of Timiş River reached a maximum value of 1241.295 m3/s with an accompanying water energy gradient of 0.000475 (value for which the engaged HEC-RAS 5.0.6 software will settle the entering flow distribution). As for the downstream BC_S2D_22 and BC_S2D_33 boundary lines, the resembling value of 0.000375 was assigned as hydro-dynamic gradient.

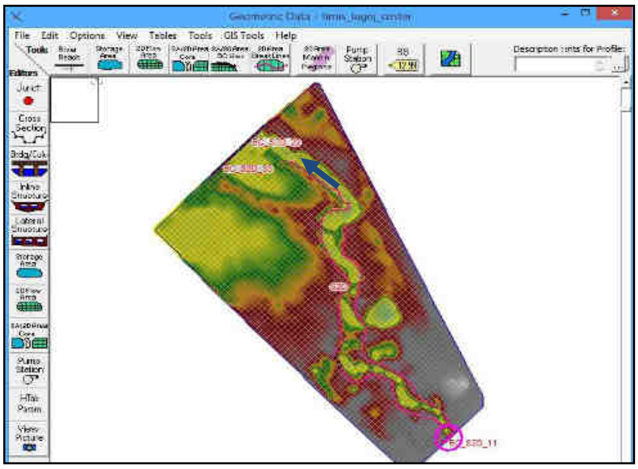

Fig. 5. Upstream and downstream zones assigned with boundary conditions of the analysed river sector

Looking to estimate the consequences of a hypothetical but still possible event, the actual numerical simulation of water flow transit was performed over a time period as corresponding to the special hydrologic phenomenon that actualy occurred on the spring of 2000, meaning from April 4th, 00:00 hours, to April 6th, 23:00 hours. There was set an analysis running step of Δt = 10 secunde, while the results recording moment was set to each 10 minutes.

3. Numerical simulation and output processing

Specific steady or time dependent parameters – water levels, velocity and flow – were reached for each grid cell of the 2D model by running the numerical simulation. Following the postprocessing operations, the numerical output is stored in designated files that can be further on visualized by employing the facilities of RAS Mapper [9], either regarding specific grid cells or defined paths.
Several significant options were considered, specifically levels, particles trajectories and velocity distributions along the flow or crossways. Figure 6 points out the eventual particles trajectories as overlaid to the corresponding water surface elevation (in mSL) by graphic representations at some considered noteworthy moments along the simulation period.

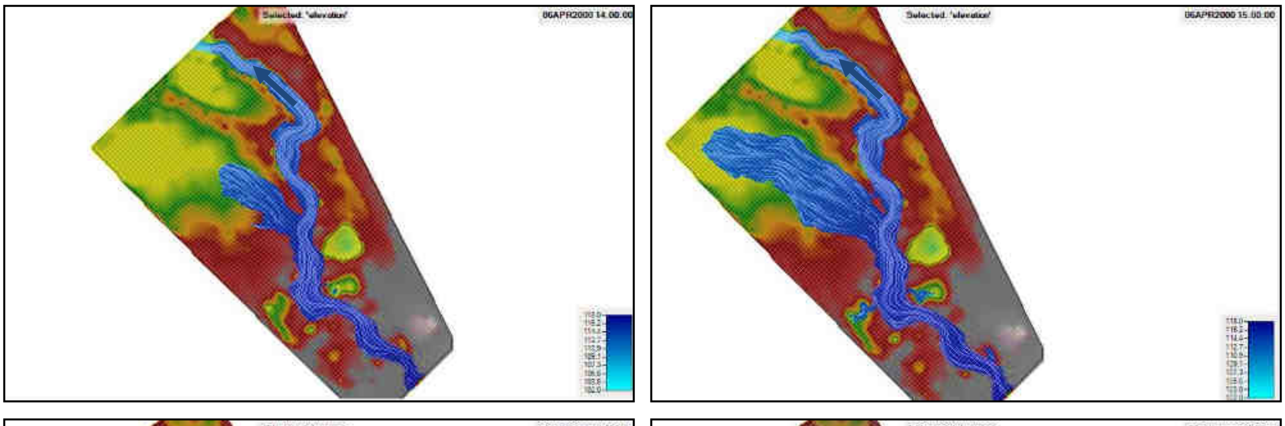

Fig. 6. Particles trajectories overlaid on surface elevation at 14:00 – 870.998 m^3/s corresponding flow, 15:00 – 1006.375 m^3/s, 18:00 – 1227.355 m^3/s and 20:00 – 1241.295 m^3/s, on April 6th, 2000

The following figures 7 and 8 show the water surface longitudinal eventual developments, the first one along the Timiș River sector thalweg and the second one through the adjoining left-side floodplain, both at the given moment of maximum flow 1241.295 m^3/s, i.e. 21:00 on April 6th, 2000.

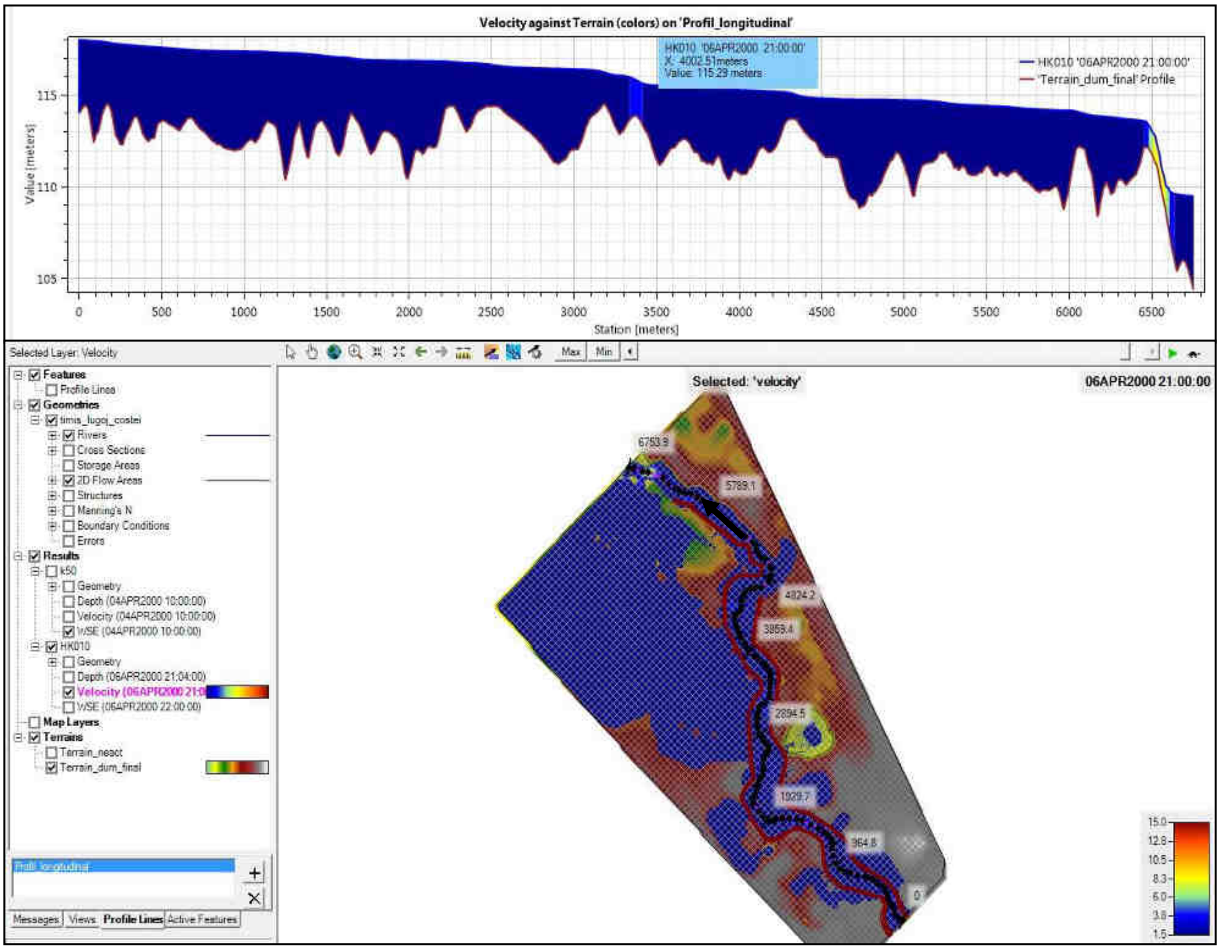

Fig. 7. Water surface elevation (mSL) longitudinal profile and spread along the river sector thalweg at 21:00 on April 6th, 2000, the corresponding moment of maximum flow of 1241.295 m^3/s

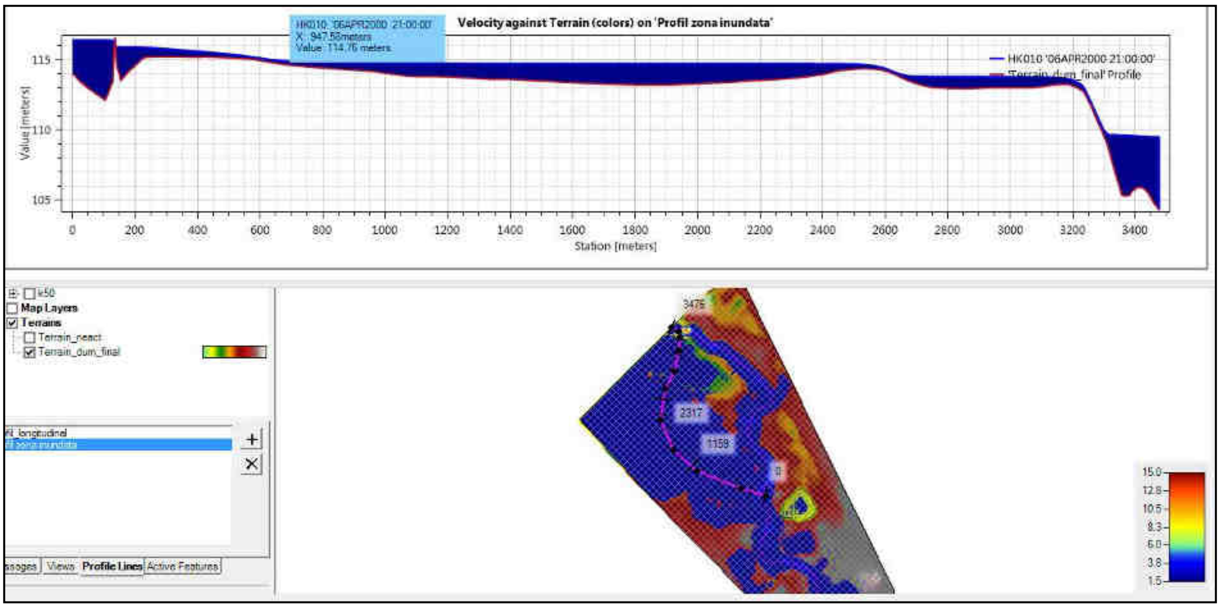

Fig. 8. Water surface elevation (mSL) longitudinal profile and spread along the river sector adjoining floodplain at 21:00 on April 6th, 2000

Figure 9 brings the piezometer line and water flow time developments on the upstream entering BC_S2D_11 and downstream outgoing BC_S2D_22 boundary lines as related to the river course.

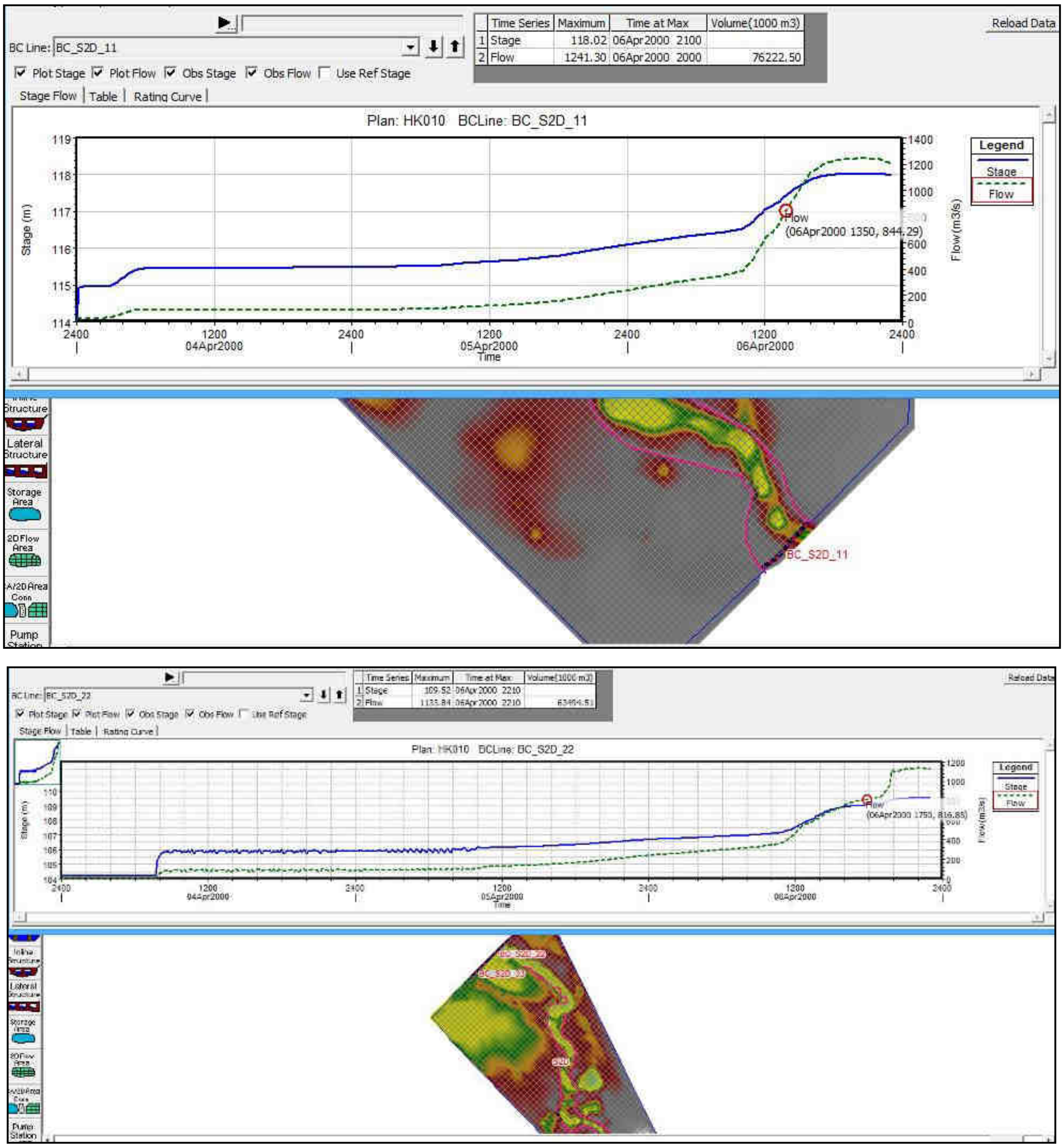

Fig. 9. Piezometric line and water flow time development on the river course sector upstream and downstream boundary lines

As considering an overall flow balance, it results that to an entering flow of the accidental highwaters at about its maximum value 1241.30 m^3/s corresponds a later on maximum outgoing flow of 1132.84 m^3/s. As about the velocity regime, the maximum value on the main path along the river sector goes up to about 10 m/s, towards Coșteiu overflowing structure, and to about 1.5 m/s in the flooded area on the left bank.
Consequently, one can also say that the flooding area over the left side protection embankment works as a given polder that determines an attenuation of the special highwater by cutting its flow maximum value with about 108.46 m^3/s.

4. Conclusions

The performed 2D numerical modeling of the concerning Timiş River sector show that under the given geometry circumstances and for a possible hydrological special event, the flow transit would

unfold both by the framed riverbed but also over the left-side embankment through a considerable gap (going from about 350m to 1493m) into the adjoining floodplain, either for the checking flow value of 1% overrunning probability ($Q_{1\%}$ = 1266m^3/s) and even for the dimensioning value of 5% overrunning probability ($Q_{5\%}$ = 860m^3/s).
There can be also confirmed that under foreseen and also regulations stipulated hydrological extreme conditions, the right-side embankment of the analysed Timiş River sector ensures the flood protection of the entire area covering correspondingly the site of the logistic warehouse investment.
In the same time, there can be concluded that the time developed gap – erosions under previous overspillings – along the top of the left-side framing embankment of the river sector might act favorable (on professional monitoring) at dimensioning and cheking values of transited water flow, since the idle (except for farming) adjacent floodplain can be employed as a highwaters atenuating polder.

References

[1] ∗∗∗. *Flooding study associated to a 7800m sector on Timiş River in the area of Coșteiu – Lidl warehouse construction site / Studiu de inundabilitate pe un sector cu lungimea de 7800m a cursului de apă Timiş în zona Coșteiu – amplasament depozit Lidl*. Politehnica University of Timişoara, Contract no.768/2007.
[2] Ghitescu, M.A., Gh.I. Lazăr, A.I. Popescu-Buşan, A.T. Constantin, and Ş.V. Nicoară. "Numerical modelling of high water flow transit for a specific river reach." *Scientific Bulletin of the Politehnica University of Timişoara, Transactions on Hydrotechnics* 60 (74), no. 2 (2015): 29-36.
[3] Brunner, G.W. *HEC–RAS 4.1*, *River Analysis System Hydraulic Reference Manual*. US Army Corps of Engineers, November 2002.
[4] Nicoară, Ş.V., Gh.I. Lazăr, and A.T. Constantin. "Comparative study of a 1D and 2D numerical analysis modelling a water flow at a river confluence under accidental high waters." *Hidraulica Magazine*, no. 4 (December 2018): 90-97.
[5] ∗∗∗. *HEC–GeoRAS GIS Tools for Support of HEC-RAS using ArcGIS User's Manual, Version 4.3.93*. US Army Corps of Engineers, Institute for Water Resources Hydrologic Engineering Center, February 2011.
[6] Brunner, G.W. *HEC–RAS 5.06*., US Army Corps of Engineers, November 2018.
[7] ∗∗∗. *HEC-RAS River Analysis System, Supplemental to HEC- RAS Version 5.0 User's Manual Version 5.0.4*. US Army Corps of Engineers, April 2018.
[8] Kiers, G. *Lifting Terrain in HEC-RAS 5.0*. VIZITERV Consult Kft., Hungary. Copyright © The RAS Solution and Gerrit Kiers, 2015.
[9] Brunner, G.W. *Combined 1D and 2D Modelling with HEC–RAS, v.5*. US Army Corps of Engineers, 2016.

Theoretical Characteristics of Fluid Flow within a Pneumatic System

Assistant professor **Fănel Dorel ȘCHEAUA**[1]

[1] "Dunărea de Jos" University of Galați, fanel.scheaua@ugal.ro

Abstract: *There are numerous applications in industry branches that use pneumatic drive to achieve various imposed movements for the working body. Here the working fluid is represented by a gaseous medium that is influenced by the temperature, humidity and pressure values. With regard to the flow pattern, a clear distinction must be made between the fluid volume at inlet and the discharge volume due to air compressibility properties. Specific parameters regarding the state of the working fluid are given by volume, pressure and temperature and any momentary modification of these specific values depends on the transformation mode to which the fluid is subjected at a given time. Theoretical flow aspects of the working fluid through a pneumatic installation model as well as the transformations to which the working fluid is subjected during operation are presented. Numerical flow analysis on a virtual model is used in order to highlight the primary flow parameters values for the pattern model containing distinct flow orifices paths used usually in pneumatic drive systems.*

Keywords*: Pneumatic system, air flow, circulation orifices, three-dimensional modelling, CFD*

1. Introduction

It is known that the bonds between the fluid molecules are weaker than the solids causing the flow, but in the case of gases the molecular bonds action has a virtually non-existent effect, causing rather a rejection between the molecules within the free space so that the distances between them become larger. This creates an environment that, unlike liquids, has a strong compressibility property at varying external pressure forces and at different temperature values.
The compressed air gaseous medium is used in pneumatically operated low pressure and force transmission systems as compared to hydraulic systems. General laws of fluid flow can be applied also to pneumatic drive with the particularity that the gaseous medium is directly influenced by temperature, humidity and pressure. Air density values decrease with temperature and humidity affects directly the transformations that occur in the gaseous fluid volume so that specific state parameters which can modify the working process based on energy transmission through pneumatic drive are influenced.
The pneumatic system is based on the compressed air circulation through the working equipment components with specific velocity and pressure values. This continuous fluid movement is inevitably accompanied by pressure losses and variations in the air flow rate due to the crossing of different network sections at a given time. Friction forces of the gaseous medium with different installation elements are encountered so that a part of the mechanical work produced for the fluid circulation is consumed to overcome these resistances. Energy consumption values results as a heat amount that is taken up by the gaseous medium. The flow pattern is considered to be in permanent mode with the same features as hydrostatic drive systems.

2. Specific transformations to the air mass within the pneumatic drive system

- Isocorous transformation or air conversion to a constant volume $\left(V_a = ct;\ dV_a = 0\right)$.
It is the case that the air mass is retained in an enclosure and receives or dissipates an amount of heat, in which case the mechanical work is zero and consequently the variation of the energy value is given by the amount of heat ceded or received by the air amount.
For two states of the gaseous medium (I and II) it can be write the state relation for the isocorous transformation in which the pressure variation is proportional to the absolute temperature: 0

$$\frac{p_I}{p_{II}} = \frac{T_I}{T_{II}} \tag{1}$$

$$\frac{p}{T} = ct. \tag{2}$$

- isobar transformation is specific to the case where a mass of air enclosed in a piston or membrane enclosure upon which a constant load is applied. At constant pressure values heat exchange with the external environment is achieved.

The thermal equation for two states of the gaseous medium corresponding to the isobar transformation shows that the volume variation is directly proportional to the absolute temperature: 0

$$\frac{V_I}{V_{II}} = \frac{T_I}{T_{II}} \tag{3}$$

$$\frac{V}{T} = ct. \tag{4}$$

- isothermal transformation is obtained when the temperature of the gaseous medium remains constant following the mechanical and heat exchange.

The internal energy of the fluid environment is constant and the heat amount is fully transformed into mechanical work. The state equation for two states of the gaseous medium (I and II) is: 0

$$p_I V_I = p_{II} V_{II} \tag{5}$$

$$pV = ct. \tag{6}$$

- adiabatic transformation describes where the mass of air receives and shares mechanically work but without exchanging heat with the outside environment.

$$pV^x = ct;\ T \cdot V^{x-1} = ct. \tag{7}$$

This is the case for pneumatic drives in which the working process takes place in a very short time so that heat exchange is not recorded.

- polytropic transformation is the general case where the specific heat is constant.

$$pV^{\kappa} = ct. \tag{8}$$

$$\kappa = \frac{C_p}{C_V} \tag{9}$$

3. Theoretical aspects for a fluid flow within a pneumatic installation

The pneumatic actuations practice involves the use of variable compressed air masses in order to achieve the proper work process. This change within the fluid mass used in the actuation determines changes in the state of specific parameters based on the thermodynamic process taking place within the pneumatic installation.
The use of a pneumatically-actuated linear motor involves considering the status of the gaseous medium at the inlet, inside the cylinder and at the device outlet.
The air flow through the installation takes place with pressure losses and changes in flow rates due to the resistance encountered inside the installation network. These losses need to be considered when designing and dimensioning the network elements by the design engineer.
For two flow sections considered on the network (I and II) the energy conservation equation for an M mass of air can be written: 0

$$E_{II} - E_I = Q_{I,II} - A\left(p_{II}V_{II} - p_I V_I\right) - \frac{AM}{2g}\left(\omega_{II}^2 - \omega_I^2\right) - AL_{fr\,I,II} - L_{ex} \quad (10)$$

Where:
E_I, E_{II} - internal energy values for section I and II;
ω_I, ω_{II} - medium values of air velocity for section I and II;
L_{ex} - mechanical work for exterior produced by kinetic energy of air for pneumo-dynamic actuation;
Taking into account the enthalpy of the gas used in the drive system, the state equation can be written as follows: 0

$$I_{II} - I_I = Q_{I,II} - \frac{AM}{2g}\left(\omega_{II}^2 - \omega_I^2\right) - AL_{fr\,I,II} - AL_{ex} \quad (11)$$

where:
I_I, I_{II} - air enthalpy for section I and II;
For a 1 kg air mass unit used in a pneumatic drive system, the conservation equation can be written as follows: 0

$$dE = dQ - Ad\left(pV\right) - Ad\left(\frac{\omega^2}{2g}\right) - AL_{fr} \quad (12)$$

Where considering the relation for fluid volume with specific weight $\left(V = \frac{1}{\gamma}\right)$ it can be written:

$$d\left(\frac{\omega^2}{2g}\right)+\frac{dp}{\gamma}+dL_{fr}=0 \tag{13}$$

Relationship that describes the possibility of changing the air kinetic energy and the mechanical workload in order to overcome the friction forces in the network together with the change in system pressure values.
By integrating into various types of transformations considered for the gaseous medium can be obtained the following relations:
- For adiabatic transformation: 0

$$\frac{\omega_{II}^2-\omega_I^2}{2g}+\frac{\kappa}{\kappa-1}\cdot\frac{p_I}{\gamma}\left[\left(\frac{p_{II}}{p_I}\right)^{\frac{\kappa-1}{\kappa}}-1\right]+L_{fr}=0 \tag{14}$$

- For isothermal transformation: 0

$$\frac{\omega_{II}^2-\omega_I^2}{2g}+\frac{p_I}{\gamma}\cdot\ln\frac{p_{II}}{p_I}+L_{fr}=0 \tag{15}$$

- For polytropic transformation: 0

$$\frac{\omega_{II}^2-\omega_I^2}{2g}+\frac{n}{n-1}\cdot\frac{p_I}{\gamma}\left[\left(\frac{p_{II}}{p_I}\right)^{\frac{n-1}{n}}-1\right]+L_{fr}=0 \tag{16}$$

Particular flow characteristics occur in the air flow through the conduits of the pneumatic drive system and through different diameters orifices necessary to make the couplings between the pipes or with various appliances used in the installation assembly.

4. Air flow inside a circuit selector device virtual model

By analyzing the flow of the working fluid on the virtual model (figure 1), important details can be obtained regarding the occurrence of the fluid flow resistance and the areas in which it occurs, whether we are talking about pipes of different diameters, orifices or component devices used for adjusting the pressure or fluid flow rate values.
The use of fluid flow analysis methods provides the possibility to improve the fluid region shape inside the device model so as to minimize the losses due to the resistances occurring in the flow paths so as to manage and optimize the pumping needs and overall the costs of installation using.
The three-dimensional model of a circuit selector device is chosen to perform the flow analysis, as shown in figure 1 along with the mesh network model.

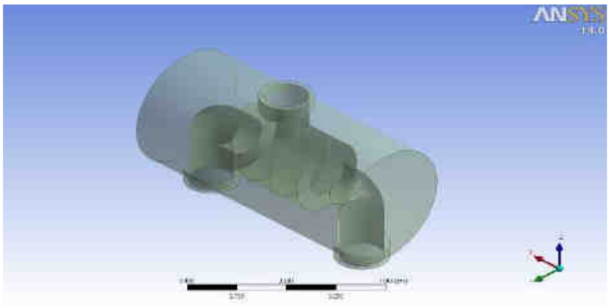

a) imported model

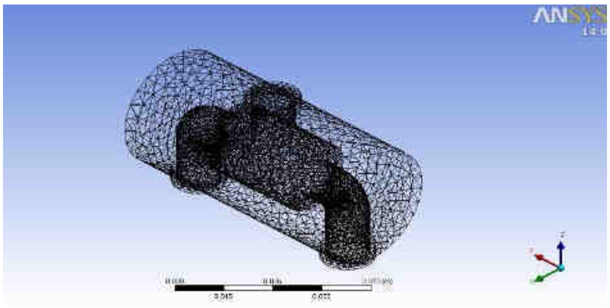

b) mesh network of triangular elements

Fig. 1. Three-dimensional assembly model taken into consideration for flow analysis

It is highlighted the operating principle for this particular device used to select a higher-pressure signal value within the working fluid that circulates from the inlet orifice that to the device outlet.
The analysis is based on the declared fluid velocity values at the inlet port and the axial displacement of the adjusting element positioned inside the model, which has the possibility of moving in one direction or another in order to provide the momentary connection of two orifices function of the higher fluid pressure value.
The main domains of the analysis are represented by the solid model or the device casing declared as outer walls, the fluid region positioned inside the device and the regulating element being declared as immersed solid within the fluid region.
The meshing network was made with triangular shape elements, with 42533 nodes and 221592 elements.
The working fluid is represented by air at 25 degrees Celsius with the k-Epsilon turbulence option for the fluid region.
The analyzed model has two inlet ports for the working fluid and one outlet. The adjusting element is represented by a centrally positioned cylindrical drawer that has the ability to perform translational movement within the selector device body.
In the set of initial values, the air inlet velocity is declared with a value of 3 m/s for the first case and then with a value of 5 m/s for the second case.
Also, for the immersed solid regulator element an axial directional movement is declared at a velocity value of 1 cm/s.
This device performs the selection of the high-pressure values, the fluid signal being sent further to the circuit by choosing the branch with the highest pressure at the two inlet ports.
Figure 2 shows the main domains of the analysis on the imported virtual model.

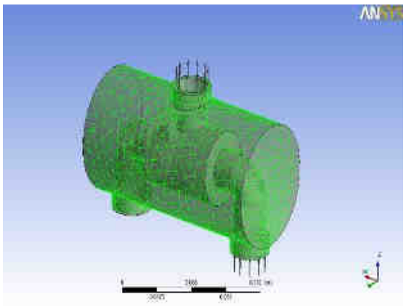

a) Device body

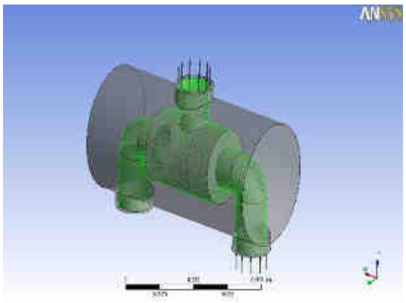

b) Fluid region

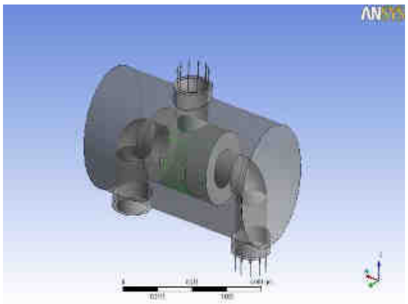

c) Immersed solid

Fig. 2. Flow analysis main domains

Thus, when the pressure value at one of the two inlet orifices is greater, the locking element is forced in translational motion opening the outlet, connecting in this way the two orifices and allowing the fluid to circulate along this new created path. The other branch is automatically blocked due to the position of the adjustment element.

The airflow analysis is performed with the Ansys CFX program.
The results are presented in terms of total pressure and fluid velocity values recorded for both analysed cases, (figure 3).

Case 1

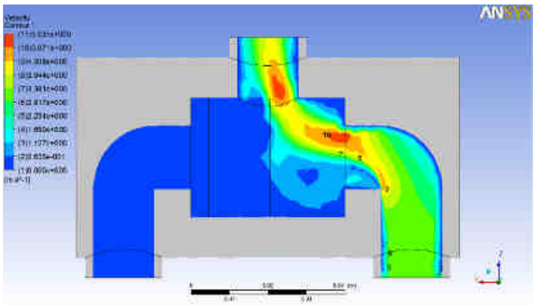

a) Fluid velocity values

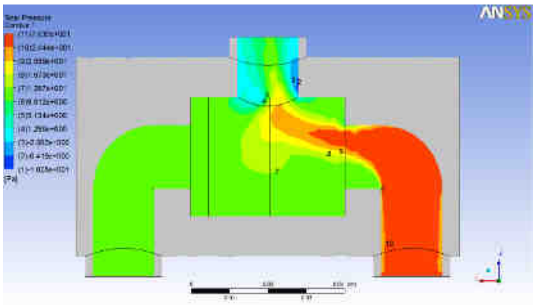

b) Total pressure values

Case 2

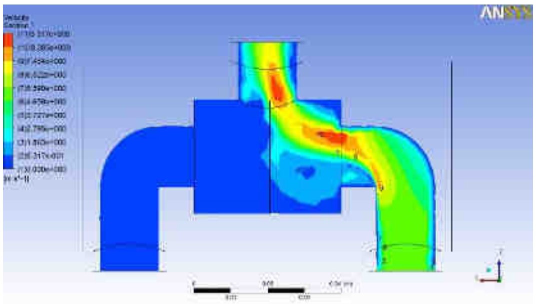

c) Fluid velocity values

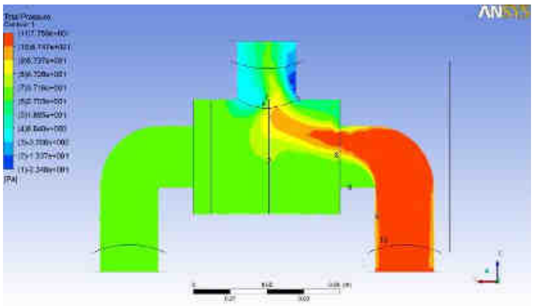

d) Total pressure values

Fig. 3. The flow analysis obtained result values

On the obtained results, can be observed the trajectory described by the working fluid inside the selection chamber, which due to the movement of the adjusting element (immersed solid) to the left direction has the possibility to circulate between the inlet and outlet orifice.
The distribution of velocity values and total pressure values on the active branch of the device model are presented.
Table 1 shows the variation diagrams for the total pressure component represented by the dynamic pressure. The exponential growth model for dynamic pressure is shown based on the operating fluid velocity values recorded for the fluid region in the two analysed cases.

Table 1

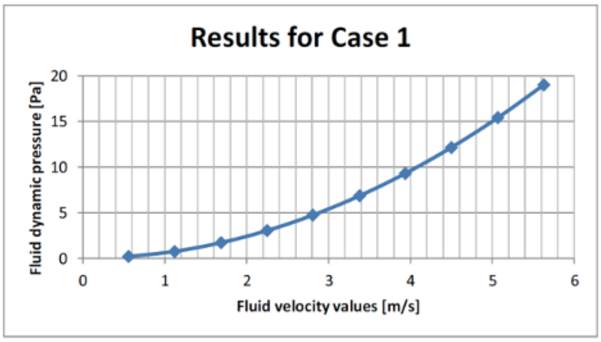

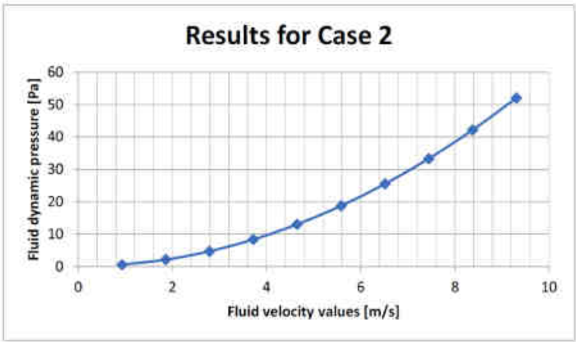

5. Conclusions

Pneumatic actuator drives are used in industry for a much lower range of pressures and powers compared to hydraulic drives.
For pneumatic drive, the compressor is used as a primary energy source in order to provide the compressed air demand for transport in the working circuit.
Specific industrial applications are using pneumatic drive and the required compressed air flow rate necessary to be supplied by the compressor can be estimated.
The air flow rate value supplied by the energy source must also take into account the losses within the installation that need to be defeated. These losses are due to the friction forces of the fluid with the crossed pipes walls, but also the various devices that are interposed on the circuit.
Such a device is also the selection valve whose model is presented and analyzed in the paper.
It represents a constructive solution for a device that is able to send forward in the circuit a signal of higher-pressure value.
Analysis of the air flow as working fluid is achieved on the valve virtual model.
The velocity distribution and pressure values recorded at the fluid region level are presented for the two analysed cases.
High fluid velocity values are noted in areas where the fluid is forced to circulate (reduced section), and the total pressure values are higher on the device inlet area to the adjustment drawer area. On the diagrams made for the total pressure component represented by the dynamic pressure in relation to the fluid velocity it can be noticed an exponential increase for both analyzed cases. Based on the results obtained from fluid flow analysis on the virtual model of the selection valve, are created the premises of optimizing the constructive shape of the apparatus in order to allow uniformity of the velocity and pressure values during operation, thus improving the values for the operating efficiency of the entire actuation drive.

References

[1] Axinti, G., and A.S. Axinti. *Hydraulic and pneumatic drives – Components and systems, Functions and features/Acţionări hidraulice şi pneumatice – Componente și sisteme, Funcții și caracteristici*. Vol. 1. Chişinău, Tehnica-Info Publishing House, 2008.
[2] Axinti, S., and F.D. Scheaua. *Introduction to industrial hydraulics/Introducere în hidraulica industrială*. Galati, Galati University Press, 2015.
[3] Axinti, G., and A.S. Axinti. *Hydraulic and pneumatic drives – Bases of Calculation, Design, Operation, Reliability and Drive Diagrams/Acţionări hidraulice şi pneumatice – Baze de Calcul, Proiectare, Exploatare, Fiabilitate și Scheme de Acționare*. Vol. 3. Chişinău, Tehnica-Info Publishing House, 2009.
[4] Florea, J., and V. Panaitescu. *Fluid Mechanics/Mecanica Fluidelor*. București, Didactic and Pedagogical Publishing House, 1979.
[5] Axinti, G., and A.S. Axinti. *Hydraulic and pneumatic drives – Equipment and systems dynamics /Acţionări hidraulice şi pneumatice – Dinamica echipamentelor și sistemelor*. Vol. 2. Chişinău, Tehnica-Info Publishing House, 2008.
[6] Vasilescu, Al.A. *Fluid Mechanics/Mecanica Fluidelor*. Romanian Ministry of Education / Ministerul Educației și Învățământului, Galați, University of Galati, 1979.

New Actuator Type Using Magnetically Controlled Rheological Properties of Fluids

Assoc. Prof. Dr. Eng. **Dan SCURTU**[1]**,** Prof. Dr. Eng. **Doru CĂLĂRAȘU**[2]

[1]Technical University of Iasi e-mail address scurtud@yahoo.com

[2]Technical University of Iasi e-mail dorucalarasu@yahoo.com

Abstract *The paper presents the concept of new type of actuator that uses the specific properties of a magneto rheological fluid. The proposed actuator allows controlling the speed of a mechanical element and its positioning. The paper gives details about the structure of the actuator and functions of elements, ongoing program of experiments and results obtained.*

Keywords: *Magneto rheological fluids, actuator, magnetic control*

1. Introduction

Based on space researches, the research field concerning on magnetic controllable fluids is widened from laboratory curiosity to the production of ferro-fluid components with that can be used in industrial application.
The first publications about ferro-fluids are made by Knight, Bitter, Elmore, Neuringer, and Rosensweig, founded the American company "Ferro fluidics Corporation", the first company who managed the industrial production of magnetic fluids. Studies made on magnetic fluids showed a series of sensational fluid-mechanical phenomena that make possible new settlements of the problems of science and technology. There are two scientific papers [1] and [2] who present the first technical achievements obtained using magnetic properties of ferro-fluids.
According to [3] and [4; 5; 6] magnetically controllable fluid scan be classified into two classes: ferro-fluids and magneto rheological fluids. They are characterized by the fact that the IR energy is performed by means of an external magnetic field.
Both types of liquid scan are classified as smart fluids. Magnetic fluids are colloidal suspensions of magnetic particles in different liquids. These fluids, in addition to an obvious magnetic behaviour, preserve and exhibit characteristics of liquids.
As shown by [6], ferro-fluids are colloidal suspensions of ultra-stable magnetic nanoparticles (whose order of magnitude is up to hundreds of Armstrong) dispersed in a liquid base. They are characterized by the following basic properties: the sedimentation is zero even in the presence of magnetic field, are quasi-homogenous magnetisable fluids and their magnetic behaviour are of Langevin type. From the point of view of viscosity, their behaviour is approximately Newtonian even in the presence of a magnetic field and have a reduced magneto-viscous effect.
The magnetically controllable fluids viscosity [7] is subject to the base liquid viscosity, to the shape of particles, to the dispersed phase volume and the degree of salvation. Einstein elaborated a formula that is being used in the study of spherical-colloidal liquid solutions $\eta_s = \eta_0 \left(1 + k_\varepsilon\right)$, where η_s is the liquid solution's viscosity, η_0 is the base liquid viscosity, ε is the overall volume of colloidal particles dispersed within the unit of volume, whereas k is a constant.
Magneto rheological fluids [8] comprise magnetisable solid particles, a prevailing liquid environment whose role is of carrier fluid, a surfactant whose role is to prevent the separation of the two constituents. The dimensions of the particles may vary between 0.1 to 500 μm. The solid content within the liquid varies between 31 and 90% (weight ratio).
Magneto rheological fluids are characterized by the fact that their energy derives from an external magnetic field. These liquids fall within the category of non-Newtonian fluids - Bingham type plastic fluids [9] and [10]
Magneto rheological fluids modify their apparent viscosity much faster and more dramatically by comparison to ferro fluids.

Thixotropic magneto rheological fluids [11] (www.liquidsresearch.com) are capable of providing high shear stress when subjected to comparatively weak magnetic fields. That class of magneto rheological fluids is conducive to major changes in the rheology of fluids when subjected to a relatively weak external magnetic field.
Considering the complexity of magnetically controllable fluid systems, it is difficult to achieve a thorough investigation of the latter.
The scientific literature is offering calculation models for the flow of non-Newtonian fluids.
The Herschel-Bulkley model is allowing for the calculation of τ stress for positive values of the magnetic induction.
For the laminar flow [12], is suggesting a model for the calculation of pressure drop. For the turbulent flow, the authors are proposing a method which requires that the wall shear stress is known, yet they do not provide a formula for the respective calculation. The latter model was completed by Hathoot. The Buckingham-Reiner model is giving a formula for calculating magneto-rheological fluids flow rate through circular pipes.
The size of magnetic particles distributed throughout the magnetic fluid [13] is of crucial importance for the case when the liquid is subjected to shear stress under the influence of an applied magnetic field.
For the analysis of magnetically controllable fluid systems, one should utilize notions and calculation formulae specific to ferromagnetism.
The dynamic viscosity η for a magneto-rheological fluid has two components, a η_0 component, in the absence of the magnetic field, and a η_c component respectively, which depend on the intensity of the magnetic field, H.
Experimental studies that have been undertaken [12], on various shear stresses have shown that an increase in the intensity of the magnetic field causes a rise in the fluid's viscosity, the so-called magneto-viscous effect, whereas the increase in shear velocity is conducive to a decrease in viscosity (shear-thinning effect).
Considering that the magnetic induction $B = \mu \cdot H$, where $\mu = \mu_0 (1+\chi)$ is the environment permeability, there results that the magneto rheological fluid viscosity $\eta(B) = \eta_0 + \eta_c(B)$ depends on the value of the magnetic induction *B*. In case the magnetic field is generated by a coil, the value of magnetic induction depends on the electric current *I* that pass the coil spirals, $B = B(I)$ respectively.
There derives that one may control a magneto rheological fluid flow through a circular pipe fitted with a coil traversed by an electric current I. By adjusting the intensity of the electric current I the η_c value of the dynamic viscosity is being altered in the presence of the magnetic field.
The applications of magneto rheological fluids related to every field (areas) where high shear stresses are being required: vehicle suspension systems, suspension chairs and rehabilitation exercise equipment's.
The present paperwork provides a new technical application for magnetic fluids, therefore a new type of actuator that makes use the rheological properties of magneto rheological fluids. The actuator that was built is allowing the velocity control of a mechanical component, as well as for positioning the latter by controlling the liquid flow velocity subjected to an external applied magnetic field. Thus, one may obtain a driving element that utilizes the fluid's rheological properties.
Our paperwork is presenting the conceptual model of the new type of actuator, construction data, calculation elements, the schedule of carrying-out experiments, the results attained, and the conclusions.

2. The actuator conceptual model

The schematic diagram of the new type of actuator is being illustrated in Figure 1.

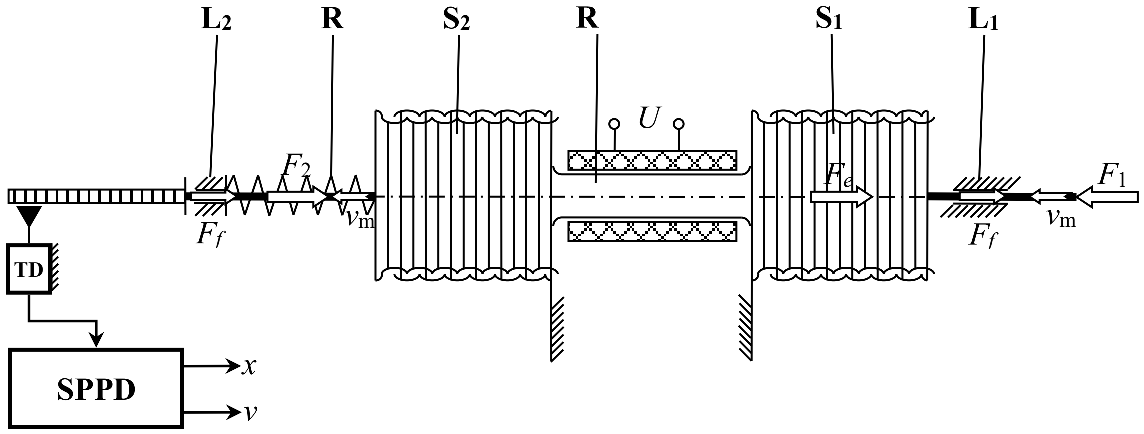

Fig. 1. The actuator schematic diagram

The watertight hydraulic system made of the identical bellows S_1 and S_2 and the tubular hydraulic resistance RH, of diameter *d*, contains a MRHCCS4-B type magneto rheological fluid made by the company Liquids Research Limited. The advantage of using the bellows consists in the complete lack of relative movement parts, and the lack of sealing components. The bellows present a linear characteristic of axial deformation when subjected to a variation in a certain domain of the applied external force.

The value of hydraulic resistance RH is being controlled by the value of the external magnetic field, of intensity H, generated by the coil under the electric tension U. Thus, the magnetic induction B is being modified, and, subsequently, the magnetic fluid viscosity, η.

The flow velocity of the magneto rheological fluid V_{RH}through the hydraulic resistance RH and implicitly the axial deformation velocities of the bellows V_{s1} =V_{s2} = V_m depend on the viscosity of the fluid.

Since the fluid dynamic viscosity η is being influenced by the intensity of the external applied magnetic field H, there results the loss of pressure function Δp[η(H)].

By controlling the fluid's flow velocity subjected to the external applied magnetic field one may obtain an actuator that allows for controlling the speed, as well as he positioning of a working part that supports the S_2 bellow axial deformation. The actuator is therefore a command element that makes use of the magnetic fluid rheological properties.

The value of the pressure p_1 from the chamber of the S_1 bellow is given by Equation 1:

$$p_1 = \frac{F_1 - F_{f1} - F_{es}}{S_s} = \frac{F_1 - F_{f_1} - k_s \cdot \frac{x}{2}}{S_s} \tag{1}$$

where F1 is the external applied force, F_{f1}represents the friction force present in the bearing L_1, whereas F_{es} is the elastic force corresponding to an x axial deformation of the S_1 bellow of S_s transversal section.

The value of the pressure p_2 from the S_2 bellow chamber is given by Equation 2:

$$p_2 = \frac{F_2 + F_{f2}}{S_s} = \frac{F_{es} + F_{ea} + F_{f2}}{S_s} = \frac{k_{sa} \cdot \frac{x}{2} + F_{f2}}{S_s} \tag{2}$$

Where F_2 is the operational charge of the system, from which there derives the p_2 counter-pressure in the S_2 bellow chamber. That force is caused by the cumulated elastic forces of the spring load Rand of the S_2 bellow.

For the elastic constants corresponding to the components utilized, we've used the notations k_s=k_{s1}=k_{s2}, for elastic constants corresponding to the $S_1$and S_2 bellows, k_a the elastic constant of

the spring load R. The elastic constant equivalent to the 2 springs connected in series (S_2 and R), was marked k_{sa}. We are also naming the overall sum of friction forces $F_f=F_{f1}+F_{f2}$ ($F_{f2}$is the friction force present in bearingL_2*)*.
Given the hydraulic resistance RH, the flow of the magnetic fluid occurs when the difference in pressure is the one expressed by Equation 3.

$$\Delta p = \frac{F_1 - F_f - \frac{x}{2}(k_s + k_{sa})}{S_s} \tag{3}$$

For the purpose of measuring the parameters of the motion, it is required that the magneto-rheological fluid characteristics be known and that the fluid may be characterized as Bingham fluid. The manufacturing company is offering the physical properties, for the MRHCCS4-B magneto rheological fluid, as well as the characteristics of the variation of induction B (H) and of tension τ [Pa] according to the shear velocity $\dot{\gamma}$ [s^{-1}] at various temperatures.
From the linear zone of the characteristics induction- magnetic field intensity B(H), one may calculate the magnetic permeability coefficient of the magneto rheological fluid $\mu = \frac{B}{H}$.
By knowing the magnetic permeability in conditions of vacuum, there derives the magneto rheological fluid relative permeability $\mu_r = \frac{\mu}{\mu_0}$.
In the case of the coil that induces the magnetic field H applied to the magneto rheological fluid from the hydraulic resistance RH, the magnetic induction B is being calculated with the formula given by Equation 4.

$$B = \mu \frac{NI}{L} \tag{4}$$

WhereN is the number of spirals of the coil, I [A] is the electric current intensity, whereas *L* [m] is the length of the coil.
The displacementand the average velocity at the exit from bellow S_2 are obtained from the SPPD system that takes over and processes the data as shown in fig. 1. Once we've calculated the average velocity and the bellow transversal section S_s, the flow rate transiting the actuator is $Q= V_m S_s$
In processing the experimental data we've utilized the following values: D= *26 mm* - the average value of the diameters of bellows S_1 and S_2, the section of bellow S_s = *5.3 cm²*, d = *2.5mm* - the diameter of hydraulic resistance, l= *0.14 m* - the length of hydraulic resistance, k_s = *1522* N/m - the elastic constants corresponding to bellows S_1 and S_2, k_a = *110 N/m* - the elastic constant of the spring load, k_{sa} = *103 N/m* - the equivalent elastic constant, L = *0.056 m* - the length of the coil, N = *1480* - the number of spirals of the coil, $\mu = 5\ 10^{-6}$ *Tm/A* - the magnetic permeability, $\mu_0 = 4\pi\ 10^{-7}$ *Tm/A* - the magnetic permeability of vacuum, μ_r= *3.9*- the relative magnetic permeability, F_f *= 0.6 N* - the sum of friction forces.
The experimental measurements were made for six values of the applied external force, F_1= *5 N; 10 N; 15 N; 20 N; 25 N; 30 N*. For each value of force, by adjusting the tension Usupplied to the coil, distinct magnetic fields were obtained, for which there correspond values of the magnetic induction B, as seen in table 1.

Table 1: Magnetic induction related to tension supplied to the coil

U [V]	0	1	2	3	4	5	6	7	8	9	10	15	20
B [T]	0	0.017	0.033	0.055	0.075	0.094	0.114	0.132	0.151	0.170	0.193	0.288	0.383

3. Experimental results

Figures 2, 3 and 4 are presenting the characteristics of the variation of mean velocity $V_s(B)$,of the variation of the difference in pressure *Δp(Q)* and of the variation of the distance of travel x(B)for different values of applied external force F_1 = constant, at the output of the actuator.

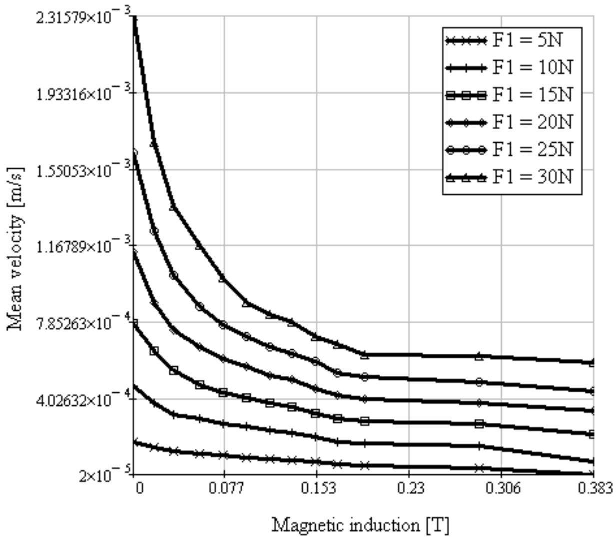

Fig. 2. The variation of the axial deformation speed for bellow S_2 according to the magnetic induction B

By analyzing the mean velocity $V_s(B)$characteristics of variation (Figure 2), at the actuator output, and according to the applied force F_1, we've observed:

- at the actuator output, the velocity decreases according to the value of the magnetic field applied, for F_1 = constant.
- The$V_s(B)$ characteristic, for F_1 = constant, is nonlinear.
- the velocity gradient according to the magnetic induction, for F_1 = constant, increases according to the value of the induction.

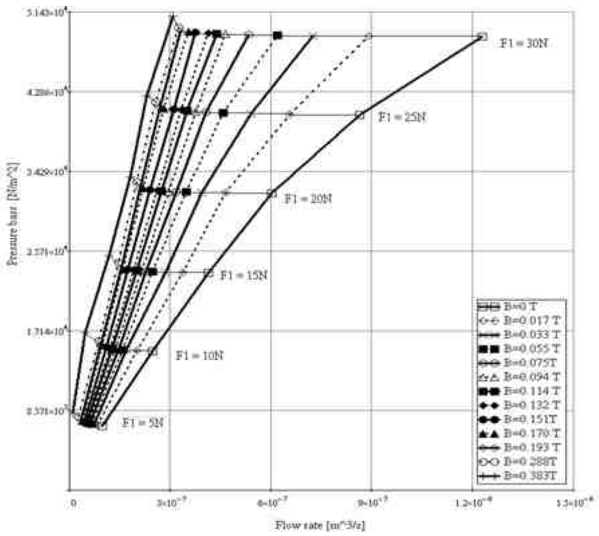

Fig. 3. The variation of pressure drop Δp according to flow rate Q

By analyzing the characteristics of the variation in pressure drop according to the flow rate Δp(Q) (Figure 3), for different values of the magnetic field Bit is established that:

- the loss of pressure increases according to the increase in flow rate.
- the loss of pressure, at the same flow rate, is greatest in elevated magnetic fields.

- the gradient of the increase in pressure loss according to the velocity is increasing according to the values of the applied magnetic field.

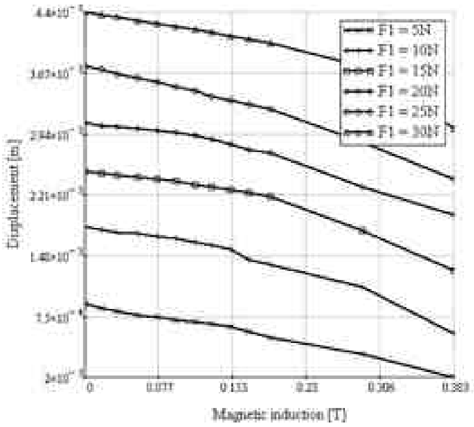

Fig. 4. The variation of axial deformation x according to magnetic induction B

By analyzing the characteristics of the variation of the displacement at the actuator output x(B) (Figure 4), it is established that:
- the displacement xincreases according to the value of the applied force for B = constant.
- the increase in the magnetic field applied is conducive to a reduction in the displacement xfor applied force F_1 = constant.
- for an applied force F_1 = constant, and through the variation in the intensity of the magnetic field one may gain control over the displacement, and a control of the positioning at the actuator output.

4. Technical application

A possible application for making use of the studied actuator is controlling the displacement of the drawer of a hydraulic distributor by varying the tension Usupplied to the coil, and of the induction B, respectively. One may obtain controlled openings of the slot the distributor. One may therefore adjust the flow and the velocity of the hydraulic working part.
The testing of the actuator was carried out on an experimental stand whose schematic principle diagram is presented in figure 5. The actuator 3 was commanding the opening of the hydraulic distributor 2 and the supply flow rate of the hydraulic rotating motor 4, at whose exiting the rpm should be *n*, interpreted by the transducer 5. The value of force F_1 applied at the actuator input was decided based on analysing the experimental characteristics x(B) - Figure 4. For the value F_1= *20 [N],* one is able to control the value of the displacement up to $3\ 10^{-3}$ *[m],* value that covers the maximum displacement of the distributor’s piston.

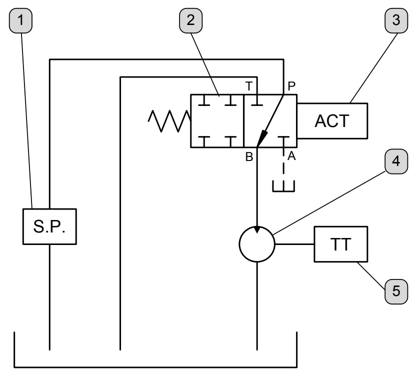

Fig. 5. The hydraulic scheme of the experimental stand

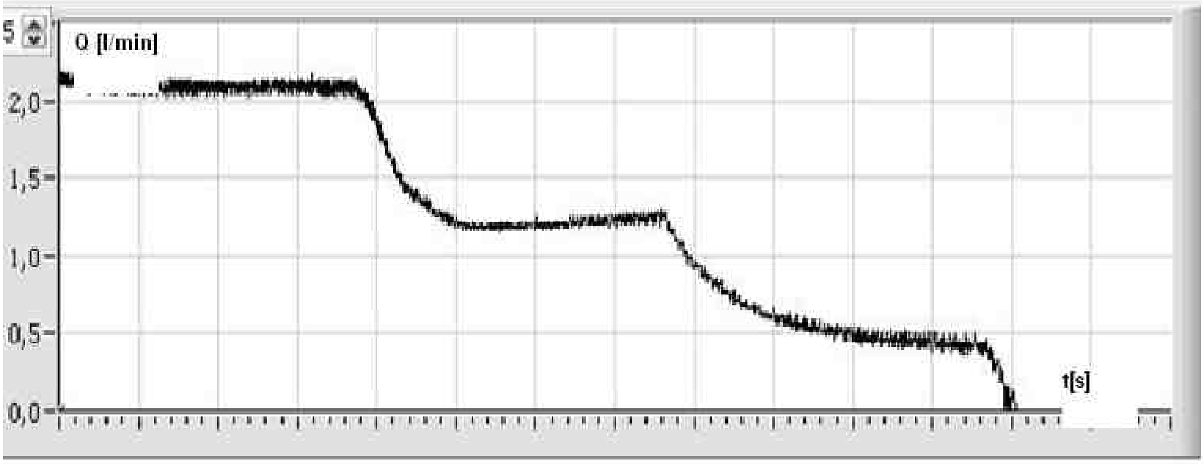

Fig. 6. The step response Q(t).

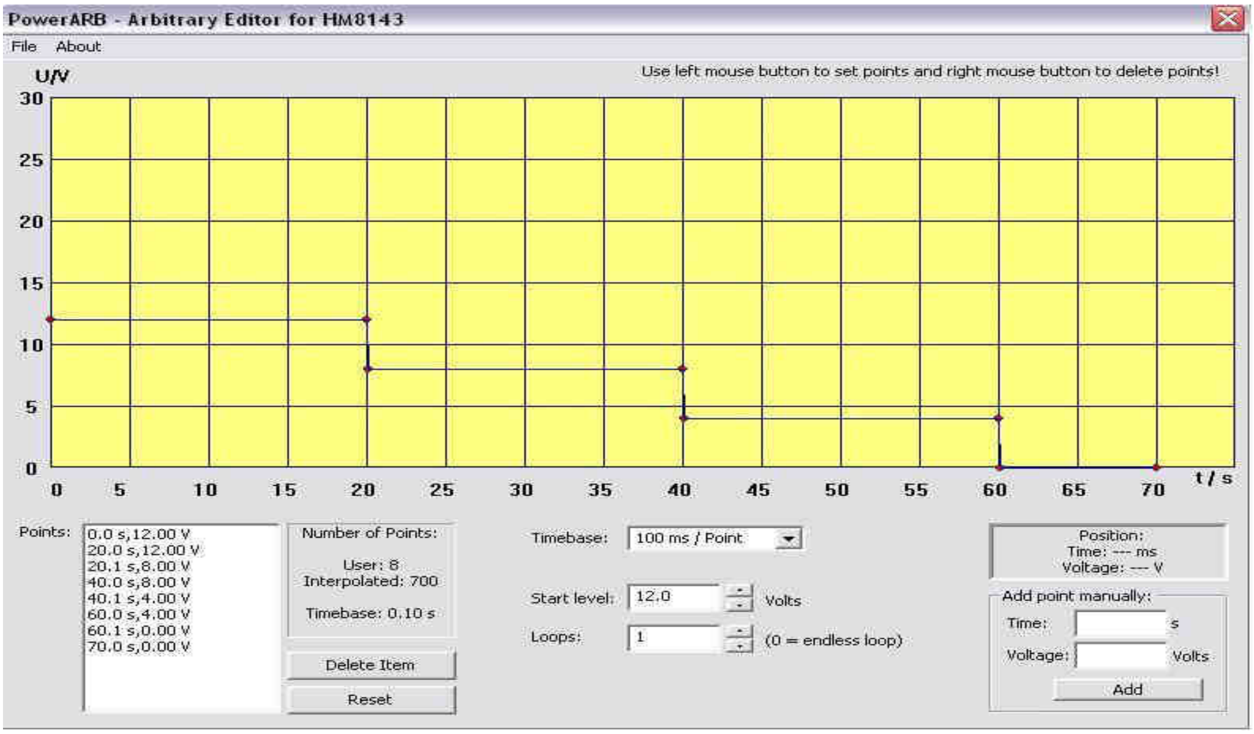

Fig. 7. The system response due to the variation in power supply for an applied force F_1 = 20 [N], at the time the piston of the distributor is executing a closing movement.

The system is dynamically stable. The step responses are non-periodical.

5. Conclusions

The proposed actuator version is a watertight design, simple and reliable, that does not require additional internal sealing components compatible to the magnetic-rheological fluid.
The actuator does not comprise mechanical components in relative motion, thus removing any corresponding friction and therefore reducing wear.
By analysing the experimental results there derives that the drive element of a linear actuator type, using magnetic-rheological fluid, is easily exerting control of kinematic and mechanical parameters (velocity, force), by utilizing the external applied magnetic field.
The actuator is capable of electrically controlling through a non-contact method and allows for precise positioning of the driven element.

The actuator is capable of electrically controlling through a non-contact method and allows for precise positioning of the driven element.
The actuator-based technical application using magnetic-rheological fluid is a dynamically stable system.
The use of different diameter bellows may extend the actuator's control capabilities.

References

[1] O'Connor, T.L. *Belgian Patent* 613, 716, 1962.
[2] Papell, S. *US Patent* 3.215.572, 1965.
[3] Susan-Resiga, D., D, Bica and L. Vékás. "Flow behaviour of extremely bidisperse magnetizable fluids." *Journal of Magnetism and Magnetic Materials* 322, no. 20 (October 2010): 3166-3172.
[4] Olaru, R., A. Salceanu, D. Calarasu, et al. "Magnetic fluid actuator." *Sensor and Actuators A: Physical* 81, no. 1-3 (April 2000): 290-293.
[5] Luca, E., Gh. Călugăru, R. Bădescu, et al. *Ferro fluids and their applications in the industry / Ferofluidele* şi *aplicaţiile lor în industrie*. Bucharest, Technical Publishing House, 1978.
[6] Olaru, R., C. Petrescu, and R. Hertanu. "A novel double-action actuator based on ferrofluid and permanent magnets." *Journal of Intelligent Material Systems and Structures* 23, no. 14 (September 2012): 1623–1630.
[7] Einstein, Albert. *Annals of Physics* / *Annalen der Physik*, vol. 19: 289-306. Leipzig, 1906.
[8] Pop, L.M., S. Odenbach, A. Wiedenmann, et al. "Microstructure and rheology of ferrofluids." Paper presented at the 10th International Conference on Magnetic Fluids (ICMF10), Guaruja, Sao Paulo, Brazil, August 2-6, 2004.
[9] Wiliams, E.W., S.G. Rigby, J. Sproston, and R. Stanway. "Electrorheological fluids applied to an automotive engine mount." *Journal of Non Newtonian Fluid Mechanics* 47 (June 1993): 221-238.
[10] Dimock, G.A., J.E. Linder, and N.M. Wereley. "Bingham biplastic analysis of shear thinning and thickening in magneto rheological dampers." Paper presented at the SPIE's 7th International Symposium on Smart Structures and Materials, Newport Beach, CA, United States, March 6-9, 2000.
[11] www.liquidsresearch.com.
[12] Thurm, S., and S. Odenbach. "Magnetic separation of ferrofluids." Paper presented at the International Conference on Magnetic Fluids (ICMF9), Bremen, Germany, July 23-27, 2001. *Journal of Magnetism and Magnetic Materials* 252 (November 2002): 247-249.
[13] Chilton, R.A., and R. Stainsby. "Pressure loss equations for laminar and turbulent non-Newtonian pipe flow." *Journal of Hydraulic Engineering* 124, no. 5 (May 1998): 522-529.

Simulation of the Cargo Tank Cleaning Plant for an Oil Tanker

Prof.PhD.Eng. **Mariana PANAITESCU[1],** Prof.PhD.Eng. **Fănel-Viorel PANAITESCU[2]**

[1] Constanta Maritime University, panaitescumariana1@gmail.com

[2] Constanta Maritime University, viopanaitescu@yahoo.ro

Abstract: *In order to achieve the modeling of the sea water system through the freight tanks installation, the Ansys-Fluent v.14.5 programme was used. The help of the Design Modeler option offered by Ansys Fluent program has been performed by the geometry of a sealer from the tanning-washing plant. The discretization was initiated by the help of the "Mesh" interface of the Ansys Fluent program resulted 2586712 Cells and 886324 knots. It was followed: a) Determination of the parameters and boundary conditions; b) view results: local pressure and speed variations on certain seers, and on the entire installation. The results obtained from the simulation were: the static pressure max 3.9 · 108 Pa; dynamic max pressure 2.28 · 109 Pa; total pressure max 1.99 · 109 Pa. The ANSYS simulation program has been used to provide the best value of the parameters variation for the tank washing installation investigation.*

Keywords: *Simulation, flow, plant, cargo, tank, oil, pressure, parameter*

1. Introduction

Taking into account the large volume of oil transported worldwide and the variety of petroleum products, oil vessels must perform the following basic functions: a) the cargo space to ensure the required load capacity transport in economic conditions of crude oil and petroleum products with specific weight ranging from 0.7 g/cm^3 to 0.96 g/cm^3; b) to have a flexibility corresponding to the diversity of the products transported, that is, to be able to carry at least two freight sorts at the same time; c) the cargo-tanks are sealed between them and between the groups forming the sections, to avoid contamination of the freight transported simultaneously; d) cargo tanks have sufficient surplus space to ensure product expansion, when passing through high temperature areas; e) at the maximum transport capacity and at different loading states, ensure that a proper trim and proper weight distribution are maintained in order to avoid overstressing the vessel's body; f) the piping system allows for the easiest distribution of the different products, on the sections, both in loading and unloading.

2. Material and methods

The reference vessel is an oil/chemical tanker with a capacity of 40400 Tdw and double bridge (Figure 1, Figure 2) [1].

Fig. 1. Oil vessel-Histria Gemma [1]

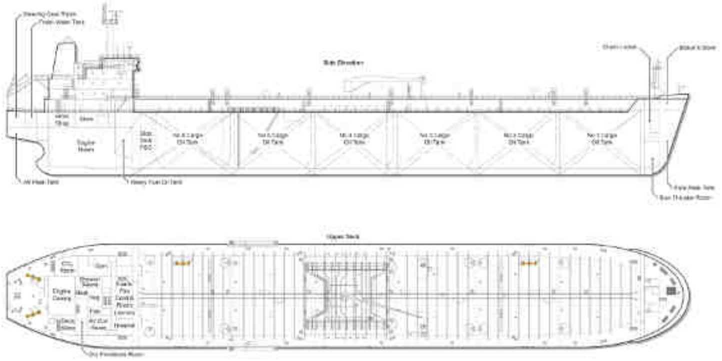

Fig. 2. Histria Gemma- Graphical representation of the ship [1]

2.1 Deadweight and capacities

- Gross tonnage: 25864;
- Net tonnage: 11369;
- Cargo Tanks: 10 tanks with a total volume of 47803 m^3.
- Tank filling is carried out by 10 pumps with total flow of 500 m^3/hour.
- The weight of the empty vessel shall comprise:

- Weight of body, machinery and electrical equipment; Inventory
- Spare parts.

The Deadweight will include:

- Heavy fuel, diesel, oil, water technique in systems and piping, drinking water in tanks;
- Freight
- Ballast
- Spare parts; Other than those required by the rules;
- Crew with luggage;
- Food.

2.2 The main dimensions of the vessel

- Maximum length L max = 179.96 m ;
- Length between perpendiculars LPP = 172 m ;
- Width B = 32.20 m ;
- Draught at the summer load line d = 11.00 m ;
- Construction Height D = 16.79 m ;
- Dead Weight DWT = 40400 TDW ;
- Speed: 18 knots.

2.3 The characteristics of the vessel body

- Builder: Constanţa, Romania ;
- Material: Steel ;
- Joint: Welding .

2.4 The transport features

- Transport capacity: 47803 m^3 ;
- Tank No.: 10 + 1 Slop ;
- Charging installation: 10 Framo SD-300 pumps of 500 m^3 (freight tanks) and 2 Framo SD-100 pumps of 200 m^3 (slop tank).

2.5. Main propulsion engine characteristics (Figure 3)[2]

Builder: MAN B & W ;

- Type: 6S50MC-C Mk7 ;
- Operating principle: diesel-reversible – 2 strokes ;
- Power (MCR): 9480 KW at 127 rpm ;
- Power (NCR): 8044 KW at 120.3 rpm ;
- Cylinders: 6 L ;
- Transmission: Direct ;
- Cylinder Diameter: 500 mm ;
- Piston Race: 2000 mm ;
- Actual consumption: 126 g/CPH.

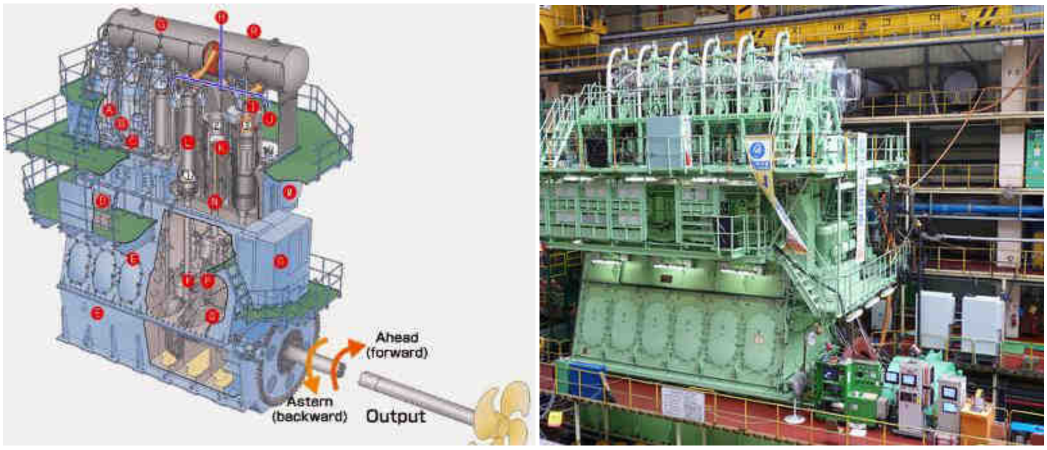

Fig. 3. Main propulsion engine [2]

2.6. Diesel characteristics of main generators

- Diesel Generators: 3 pcs (Figure 4) [3] ;
- Builder: Hyundai Himsen ;
- Type: 6h21/32 ;
- Diesel engine power: 960 kW ;
- Speed: 900 rpm ;
- Cylinders: 6L ;
- Cylinder Diameter: 210 mm ;
- Piston Race: 320 mm ;
- Engine power: 787 kW ;
- Generator Type: Himsen, HFC7 ;

- Power generator: 925 KVA ;
- Voltage generator: 450 V ;
- Intensity generator: 1186.8 A ;
- Generator frequency: 60 Hz.

Fig. 4. Diesel main generator [2]

3. Description of the structure of the fuel tank cleaning plant

The ship is equipped with 10 cargo tanks (5 on the starboard board and 5 on the port board), and 1 slop tank. In the tank washer plant, ballast pumps, fire pumps and slop tank pumps are used (Table 1).

Table 1: Cargo and Slop tank capacity

CARGO OIL AND SLOPS TANKS							
Compartment	Location Frame	Volume			VCG From BL m	LCG from Midship m	Max. Moment of Inertia m^4
		100% m^3	98% m^3	98% (Barrel US)			
No.1 Cargo Tank (P)	162 - 187	3,069.8	3,008.4	18,922.3	9.853	66.15	1,971
No.1 Cargo Tank (S)	162 - 187	3,069.8	3,008.4	18,922.3	9.853	66.15	1,971
No.2 Cargo Tank (P)	138 - 163	3,666.3	3,593.0	22,599.3	9.678	44.97	2,877
No.2 Cargo Tank (S)	138 - 163	3,666.3	3,593.0	22,599.3	9.678	44.97	2,877
No.3 Cargo Tank (P)	114 - 139	3,670.8	3,597.4	22,627.0	9.677	23.18	2,881
No.3 Cargo Tank (S)	114 - 139	3,670.8	3,597.4	22,627.0	9.677	23.18	2,881
No.4 Cargo Tank (P)	90 - 115	3,670.8	3,597.4	22,627.0	9.678	1.31	2,884
No.4 Cargo Tank (S)	90 - 115	3,670.8	3,597.4	22,627.0	9.678	1.31	2,884
No.5 Cargo Tank (P)	66 - 91	3,670.8	3,597.4	22,627.0	9.677	-20.50	2,881
No.5 Cargo Tank (S)	66 - 91	3,670.8	3,597.4	22,627.0	9.677	-20.50	2,881

3.1. Pumps used in the tank cleaning plant

Ballast Pump (2 pcs)-flow rate 750 m^3/ h, 242 l/min; Height of discharge-25 m; pressure-193 bar.
Slop pump (2 pcs)-flow rate 150 m^3/ h, 173 l/min; Height of discharge-120 m; pressure-200 bar (Figure 5) [3].
Salt water Pump (3 pcs)- flow rate 380 m^3/ h, 173 l/min.

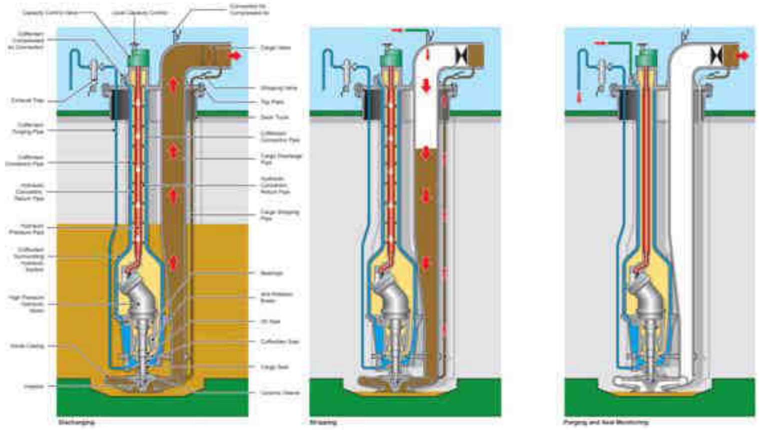

Fig. 5. Slop pumps [3]

3.2. Description of the calculation route

The buses of the ballast water tubing, sea water from the fire plant and the piping of the slop pump are connected to the cargo tanks washing buses. The circulation of water is carried out through a wide variety of pipelines. Also, depending on the pressure is chosen the pipe type, respectively the material. Due to the high corrosivity of seawater, the pipes are made of galvanised steel (Table 2).

Table 2: Diameters nominal piping installation of cargo tanks

Mainline	Nominal diameter
Salt water, freshwater and crude oil wash line	200 mm ; length 120 m
Salt water, freshwater and crude oil wash line	250 mm ; length 70 m
Salt water, freshwater and crude oil wash line	300 mm ; length 130 m
Salt water, freshwater and crude oil wash line	350 mm ; length 30 m

For hydraulic calculation We will consider as seawater washing agent. The analysis of the flow of seawater is intended, the determination of variable pressures, to understand the dimensioning of the pipes and the correct choice of water flow. Establishing the components of the plant and calculating the linear and local load losses, i.e. pressure losses, we can determine the total losses, but also carry out a study on fluid flow through the installation. Developing the calculation for each sector of the cooling plant, depending on the speed of the water resulted the following values, presented to the Table 3.

Table 3: Local load and pressure losses

Speed Flow	Reinforcement	Number of Fittings	Coefficient of friction	Local load loss	Local pressure loss
[m/s]				[m]	105 [Pa]
			ξ	$h_{f\,loc} = \xi \frac{v^2}{2g}$	$\Delta_p = h_{f\,l,oc} * \rho * g$
6,62	Elbows at 90°	4	1.3	5.81	57826.30
	Filter with Sieve	2	1.10	4.91	48929.94
	T-Connections	2	1.20	5.36	53378.12

	Coolers	2	1.40	6.25	62274.47
	One-way throttle valves	2	1.80	8.04	80067.18
	Reduction	2	1.90	8.49	84515.36
	Elbows at 90°	5	1.30	5.96	59303.61
	Filter with Sieve	2	1.10	2.02	20071.99
	T-Connections	6	1.20	6.60	65690.15
4,24	Coolers	3	1.40	3.85	38319.25
	One-way throttle valves	4	1.80	6.60	65690.15
	Reduction	4	1.90	6.96	69339.60
	Elbows at 90°	2	1.30	1.15	11405.23
	Filter with Sieve	4	1.10	1.94	19301.16
	T-Connections	4	1.20	2.11	21055.81
2,94	Coolers	4	1.40	2.47	24565.11
	One-way throttle valves	4	1.80	3.17	31583.71
	Reduction	4	1.90	3.35	33338.37
	Elbows at 90°	5	1.30	1.55	15390.65
	Filter with Sieve	4	1.10	1.05	10418.28
	T-Connections	8	1.20	2.28	22730.80
2,16	Coolers	8	1.40	2.66	26519.27
	One-way throttle valves	4	1.80	1.71	17048.10
	Reduction	8	1.90	3.61	35990.44
TOTAL				97.89	974753.06

4. Simulation of the cargo tank cleaning plant

The ANSYS simulation program has been used to provide the best value of the parameters variation for the tank washing installation investigation [4].

4.1. Realization of the installation plan

The help of the Design Modeler option offered by Ansys Fluent program has been performed by the geometry of a sealer from the tanning-washing plant (Figure 6).

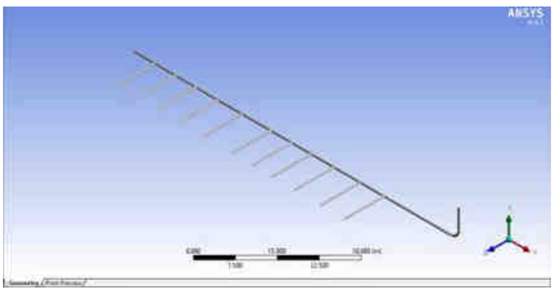

Fig. 6. Tank Washing Plant Plan

The cut-off from the diameter of 250 mm to 200 mm was made using a truncated cone, with the bases of diameters for two dimensions of tubing (Figure 7, Figure 8).

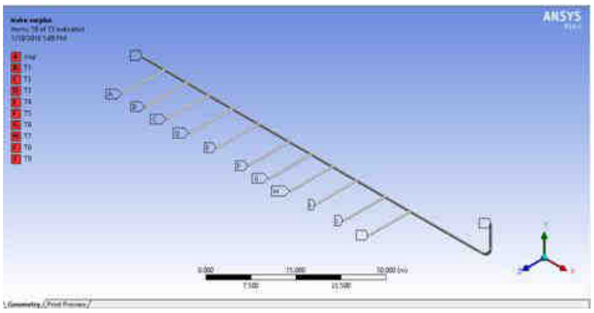

Fig. 7. Installation inputs and outputs

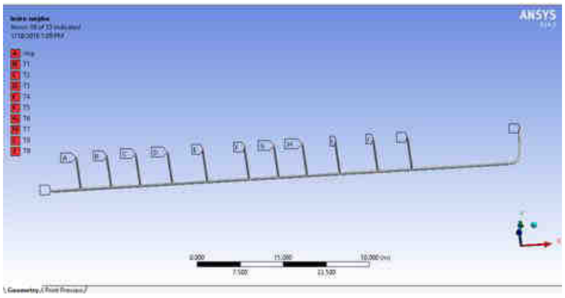

Fig. 8. Cargo tank cleaning plant

The elbow 90° was assembled by combining two perpendicular cylinders one against the other and the laying of a sphere in the jointing of the joint.
In order to achieve ramification in the "T", it was necessary to introduce a cylinder on the "X" axis, which has been intersected with the previous one (Figure 9).

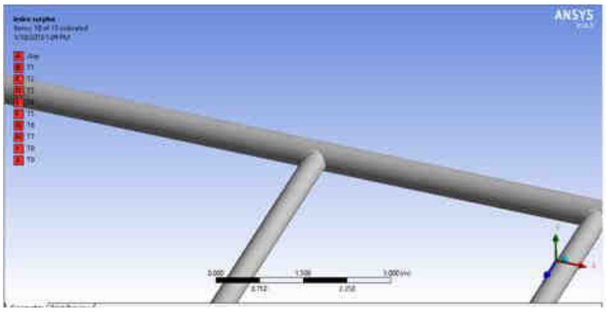

Fig. 9. T -connections

4.2. The discretization of the domain

The discretization of domain was initiated by the help of the "Mesh" interface of the Ansys Fluent. Following the structural analysis 2586712 Cells and 886324 knots resulted (Figure 10).

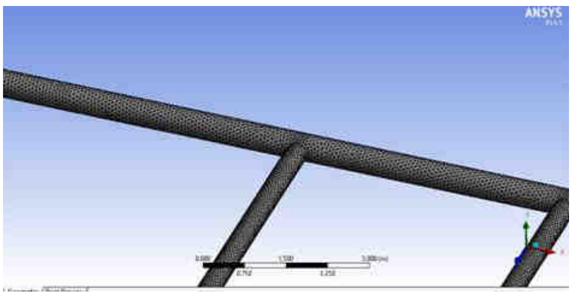

Fig. 10. The discretization of the plant's domain

4.3. Determination of the parameters and boundary conditions

In the first stage, the input and output bags of the fluid were established. Thus, 1 entry and 11 exits were noted (Figure 11).

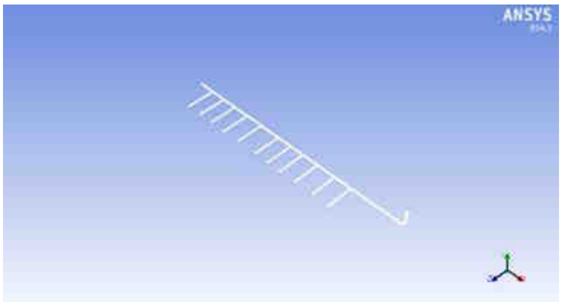

Fig. 11. Running simulation

4.4. Results and interpretations

As a result of the use of ANSYS Fluent numeric programme there are presented the local pressure and speed variations on certain spheres, as well as the entire installation (Figure 12, Figure 13, Figure 14, Figure 15, Figure 16).

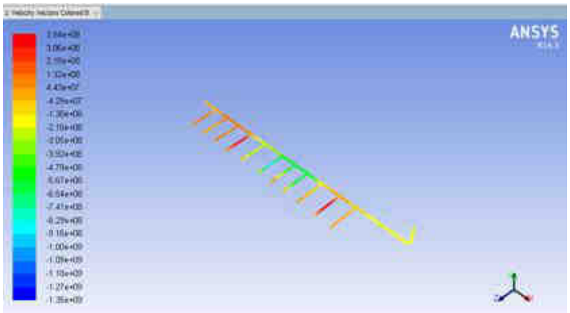

Fig. 12. Static pressure [Pa]

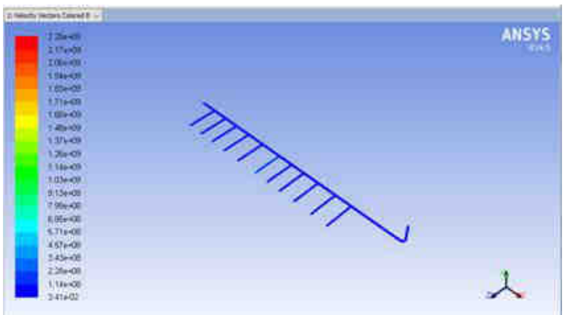

Fig. 13. Dynamic pressure [Pa]

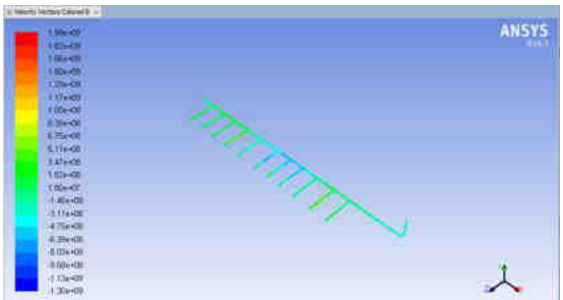

Fig. 14. Total pressure [Pa]

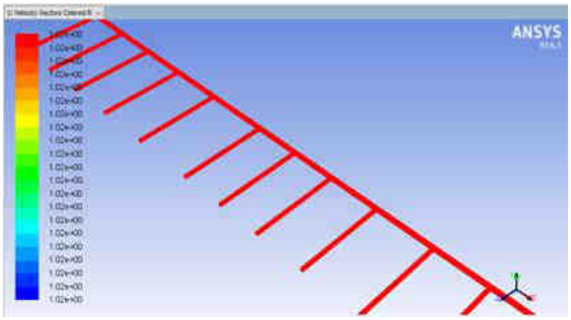

Fig. 15. Velocity vectors coloured by Density [kg.m^3]

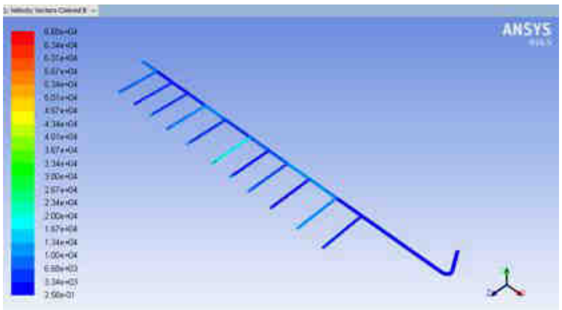

Fig. 16. Velocity vectors coloured by Velocity magnitude [m/s]

5. Conclusions

The results obtained from the simulation were:

- The static pressure maximum 3.9 · 108 Pa;

- Dynamic pressure maximum 2.28 · 109 Pa;

-Total pressure maximum 1.99 · 109 Pa.

The Ansys Fluent module v. 14.5, which has been taken to resolve the proposed theme, consists of 6 individual programs that help us to solve the problem of water collection. The programs are interconnected.

Although a conclusion may review the main points of the paper, do not replicate the abstract as the conclusion. A conclusion might elaborate on the importance of the work or suggest applications and extensions.

In order to achieve the modeling of the sea water system through the washing facility, the Ansys-Fluent part is applied to the study of liquids, as this program offers a wide range of solutions for the simulation, engineering sets with access to almost the field of engineering simulation. For this simulation a design calculation process was required beforehand.

References

[1] ***. “Histria Gemma oil tanker (photo).” *FleetMon Tracking the Seven Seas,* February 23, 2019. Accessed February 23, 2019. https://www.google.com/search?q=foto+nava+Histria+gemma&tbm=isch&source=iu&ictx=1&fir=5PYmpkW7EiqUwM%253A%252CyO5lwmrWNRrz4M%252C_&usg=AI4_-kSXjEzXe_amqXlixPBgkbsH6lbutQ&sa=X&ved=2ahUKEwi1nqPMy9LgAhVJxIsKHbOhDDkQ9QEwAnoECAQQBg&biw=1280&bih=881#imgrc=5PYmpkW7EiqUwM:&spf=1552987971661

[2] Ctro, Catalin. "Mitsui-MAN B&W Diesel Engine Type MAN. BW. 6S50 MC.C", February 23, 2019. Accessed February 23, 2019. http:// marinepdms.blogspot.com/2011/09/mitsui-engineering-shipbuilding-co.html.

[3] Crawford, J. *Marine and Offshore Pumping and Piping Systems.* London, Billing & Sons Ltd., 1981.

[4] Panaitescu, M., F.V. Panaitescu, and G. Tudose. ”Modeling of Flow through Cooling Plant with Sea Water.” *“HIDRAULICA” Magazine of Hydraulics, Pneumatics, Tribology, Ecology, Sensorics, Mechatronics*, no.1 (March 2017): 16-20.

Influence and Effects of Pressure Variation on the Life Span of External Gear Pumps

Ph.D. Stud. Eng. **Polifron – Alexandru CHIRIȚĂ**[1], Ph.D. Eng. **Teodor-Costinel POPESCU**[1], Ph.D. Stud. Eng. **Alexandru - Daniel MARINESCU**[1], Dipl. Eng. **Constantin TEODORU**[2], Dipl. Eng. **Corneliu CREȚU**[2]

[1] Hydraulics and Pneumatics Research Institute INOE 2000-IHP, Bucharest, Romania, chirita.ihp@fluidas.ro

[2] HESPER S.A., Bucharest, Romania, hesper@hesper.ro

Abstract: *The article analyzes the effects of variable pressure on the life of hydraulic gear pumps using modern numerical simulation tools (CAE & CAD). It presents the results of a static and a dynamic analysis (fatigue) as well as experimentation, validating these simulations, with the ultimate goal of improving the operating time of the tested pump.*

Keywords: *External gear pumps, CAE & CAD, numerical simulation, fatigue, dynamic analysis.*

1. Introduction

External gear pumps are the simplest and most common oil hydraulic pumps operated by an electrical motor. Their success is accounted for by several advantages, like their extreme lightness, mechanical simplicity, wide-range viscosity, optimum suction, their wide range of flow rates, adaptability to any position and space and, finally, their cost, which makes them one of the cheapest types on the market. [1]

Yet, these pumps have some drawbacks too, i.e. a design focused on sustaining around 150 - 280 bar, their unsuitability for high flow applications, rather loud noise and a rather poor overall efficiency.

Nonetheless, the strong demand for these hydraulic generators prompts manufacturers to carry out research and improve their products by employing special materials, accurate heat treatments, minimum coupling tolerance between wheels and surface precise finish in order to reduce the drawbacks mentioned above.

External gear pumps (Figure 1) are essentially made up of two twin gearwheels geared with each other that are held in a totally smooth stator housing to prevent leakages between moving and fixed parts; the 8-shaped bearings (Figure 5), held in the stator along with gears, counterbalance side hydraulic thrusts by means of dedicated seals. [2]

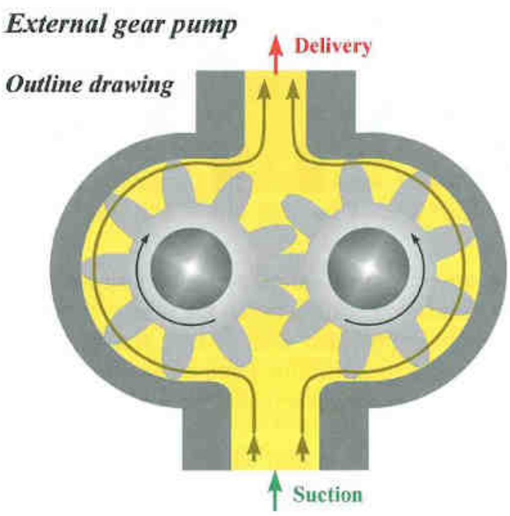

Fig. 1. External gear pump [2]

Axial and radial compensations are made possible by placing two balancing or compensation bearings opposite the plane faces of the gearwheels (Figure 2) and axially floating between the covers and the gears themselves (Figure 3).

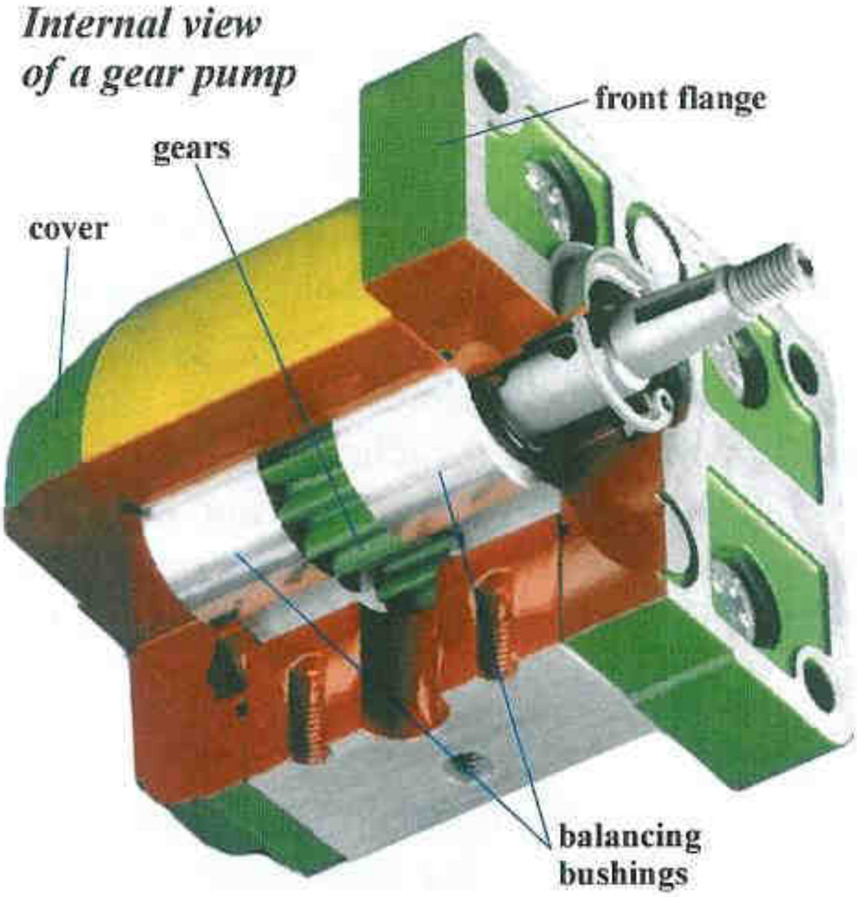

Fig. 2. Internal view of a gear pump [2]

In axial and radial balance (Figure 4), the pressurized fluid, pushed through tiny and accurately measured openings between the outlet and the bushings, exerts a thrust on their two back parts (cover sides). This keeps them solidly connected to the wheel but it allows an adequate lubrication thanks to an accurate design of the thrust force. As a result, gears perfectly mesh with bushings while the lubricating film prevents the faces of the parts from wearing out; the spindles solidly connected to the gearwheels do not need more bearings and the single bearing, if used, is positioned over the end of the transmission shaft.

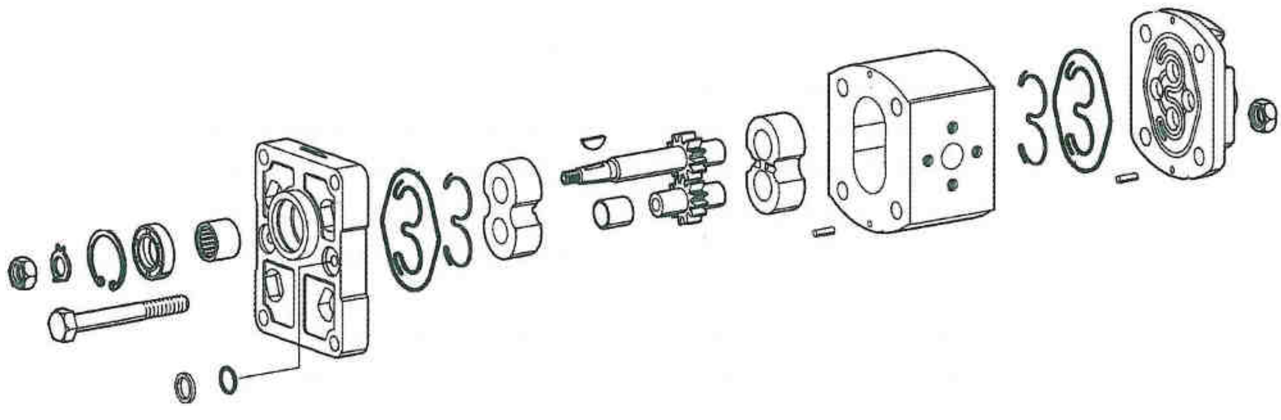

Fig. 3. Exploded view [2]

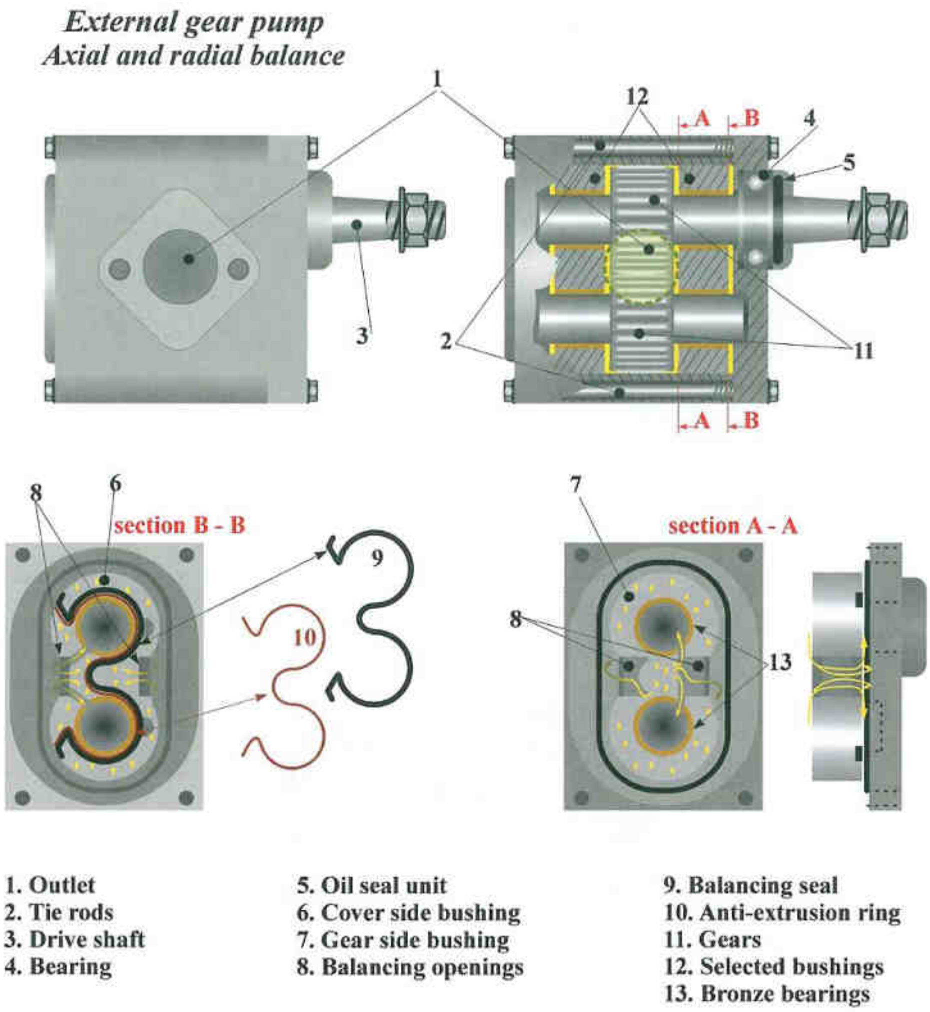

Fig. 4. Axial and radial balance [2]

Radial balance design must also consider the fact that teeth in mesh cannot fully expel oil. As a result, tiny fluid drops are 'squeezed' between the engaging wheels, thus entailing (depending on the incompressibility of the liquid) local overpressures that act in a radial manner vis-a-vis gear shafts. In addition, during gear disengagement, the volume between the teeth suddenly increases even before the contact with the sucked fluid.

Consequently, the central part of bushings must have some interstices in order to discharge this fluid; these are the only points where delivery and suction areas come into contact and the overpressure-prone fluid discharges in micro-areas subjected to early vacuum.

Fig. 5. Cover side bushing [2]

Bushing openings (Figure 5) play another important role as they allow leakages to pass from the delivery area to the suction area where the leaked fluid mixes with the fluid from the tank.

The "3-shaped" seal sets the balance area and separates the suction area from the delivery area. It is supported by an anti-extrusion ring, with the same shape as the seal, so as to avoid the extrusion of the seal parts where it is not supported due to clearance.

The pump leading gear is generally set to revolve clockwise; anticlockwise revolution occurs when the back cover is disassembled, and wheels are inverted (i.e. the leading wheel is replaced by the driven wheel and vice versa). [2]

2. Numerical simulation of pressure effects on the pump body

Given that type of pumps has radial and axial compensation, the forces discharging into the body are relatively small relative to the pressure action on the pump body. Therefore, the pressure action on the pump body will be analyzed using the CAE & CAD simulation software, Solidworks 2019.

2.1 Static analysis of the pump body

For static analysis with finite element, the 3D model was executed of the pump body (Figure 6) according to the execution documentation. The pump cap is not analyzed because for this construction it shows no significant deterioration but consider its presence during the simulation. The pump body shown below is made of an aluminum alloy which is poured under pressure into the mold.

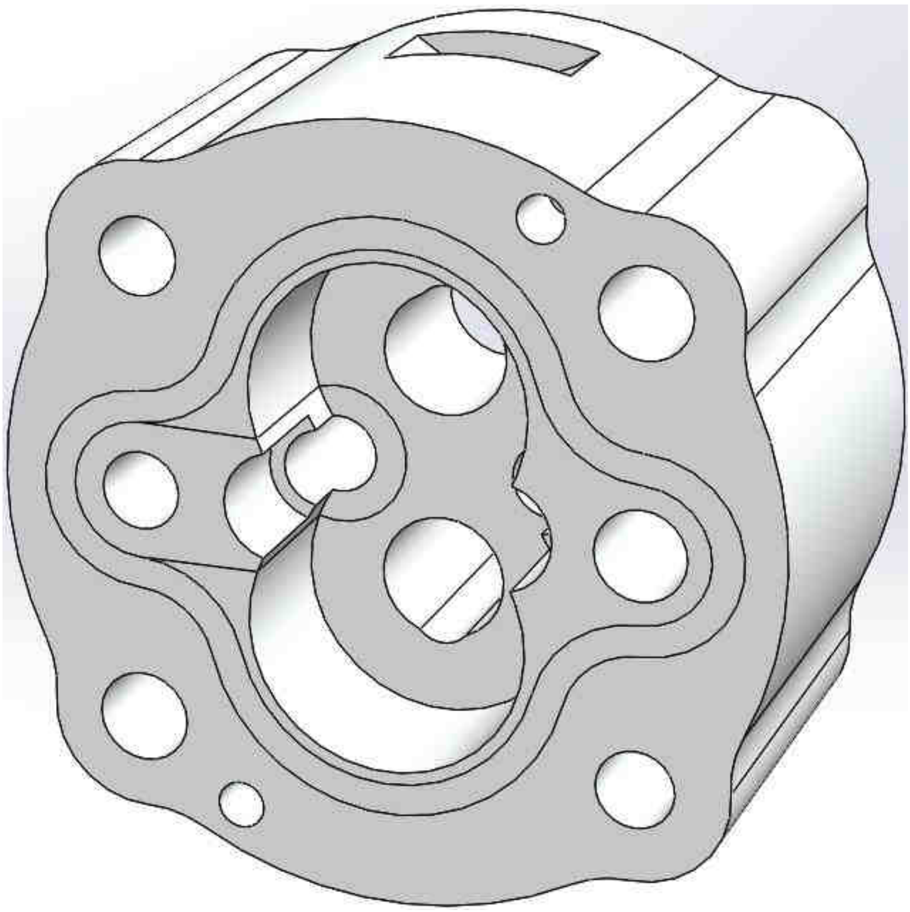

Fig. 6. The 3D model of the pump body

Figure 7 shows the mesh and the variation of its dimensions in the areas of interest, and in figure 8 the surfaces on which the pressure of 25 MPa acts are indicated with red arrows.

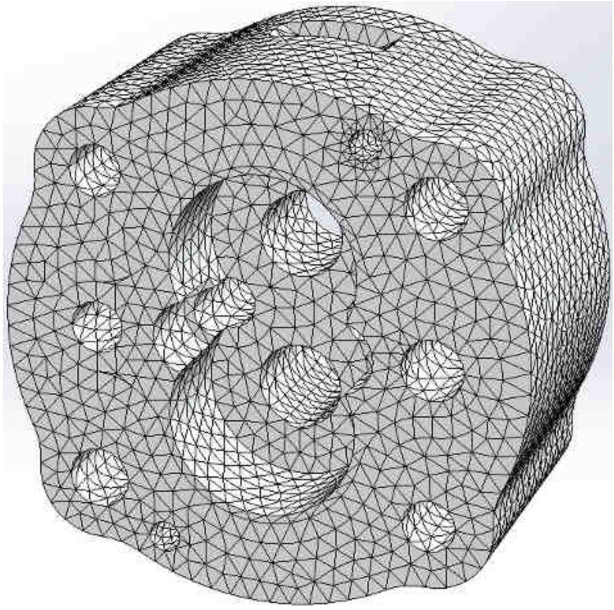

Fig. 7. The mesh

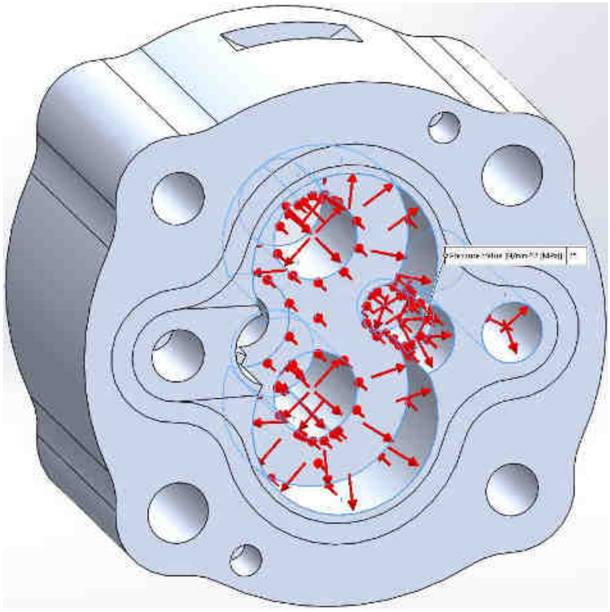

Fig. 8. Surfaces on which the pressure acts

Following the von Mises yield criterion analysis (Figure 9), the maximum stress on the body is 124 MPa, and it does not deform permanently up to a value of 140 MPa.

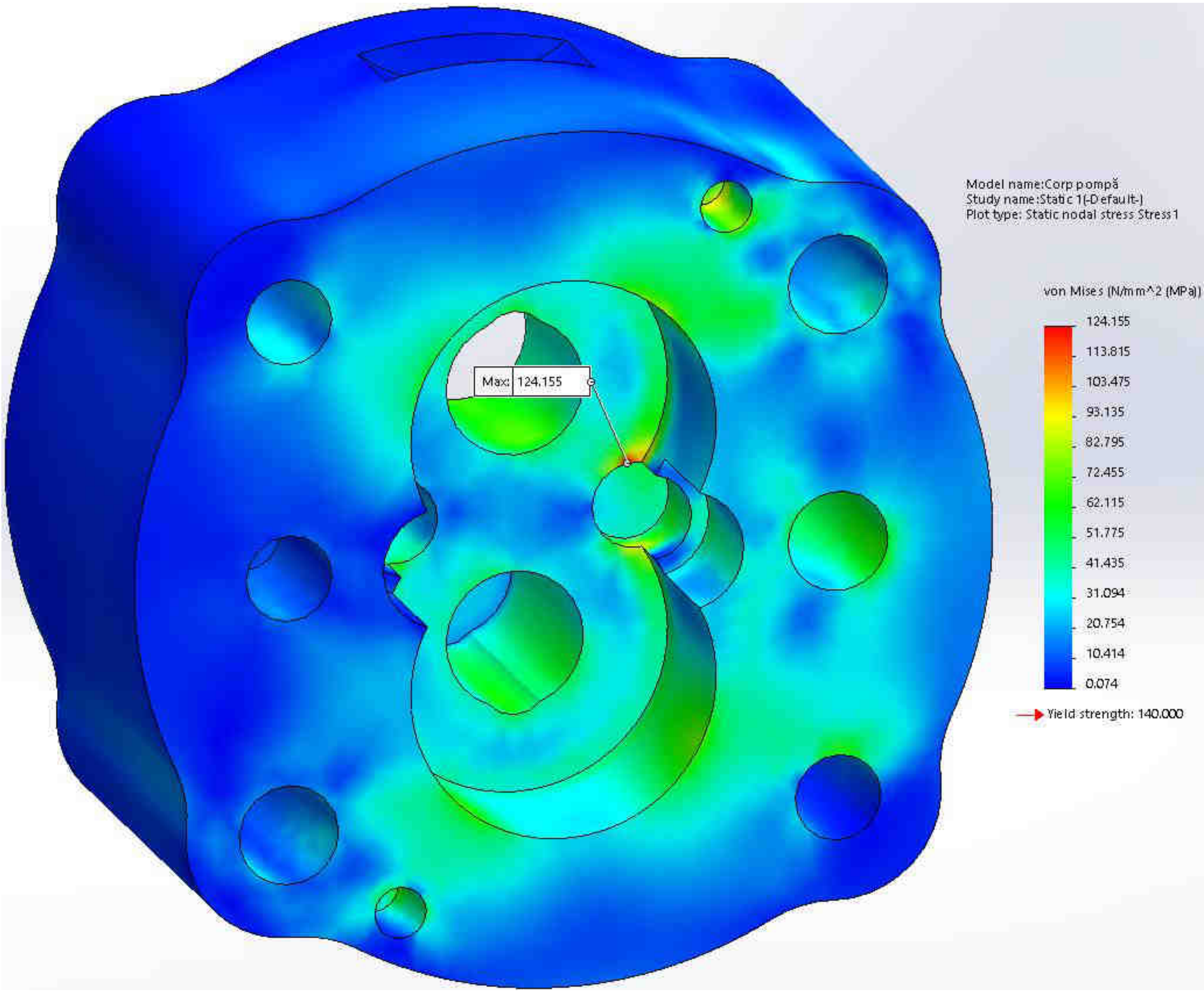

Fig. 9. The von Mises yield criterion analysis

Figure 10 shows a volume of 0.41% of the element's geometry of the pump body that is stressed with a value greater than 70 MPa.

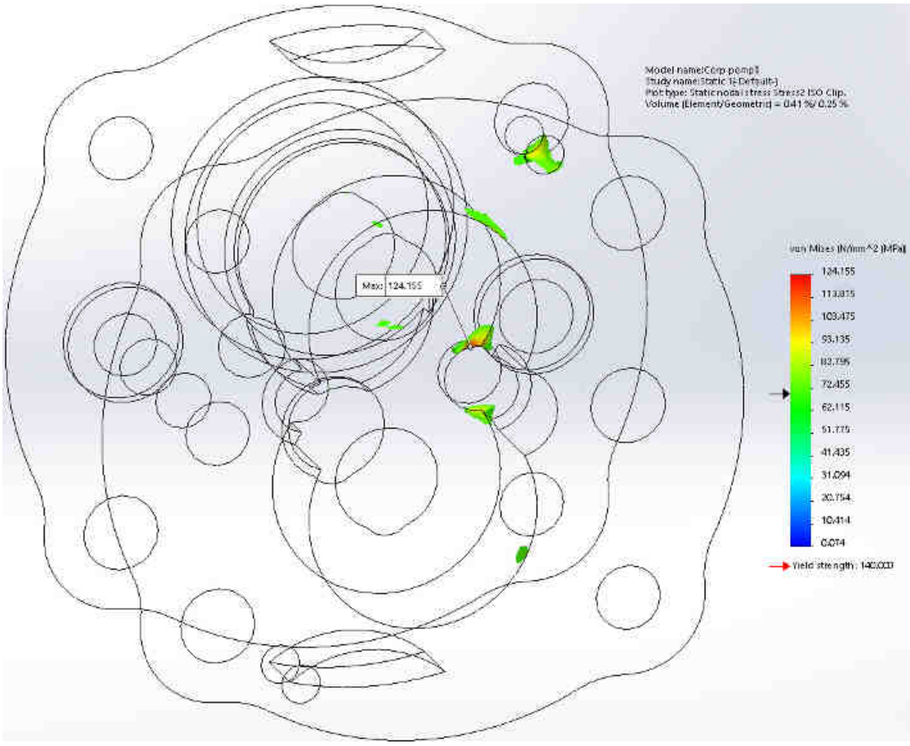

Fig. 10. The von Mises yield criterion analysis – Iso Clipping

Figure 11 shows the strain in the material of the pump body. On this diagram one can easily see the areas with the most mechanical demands.

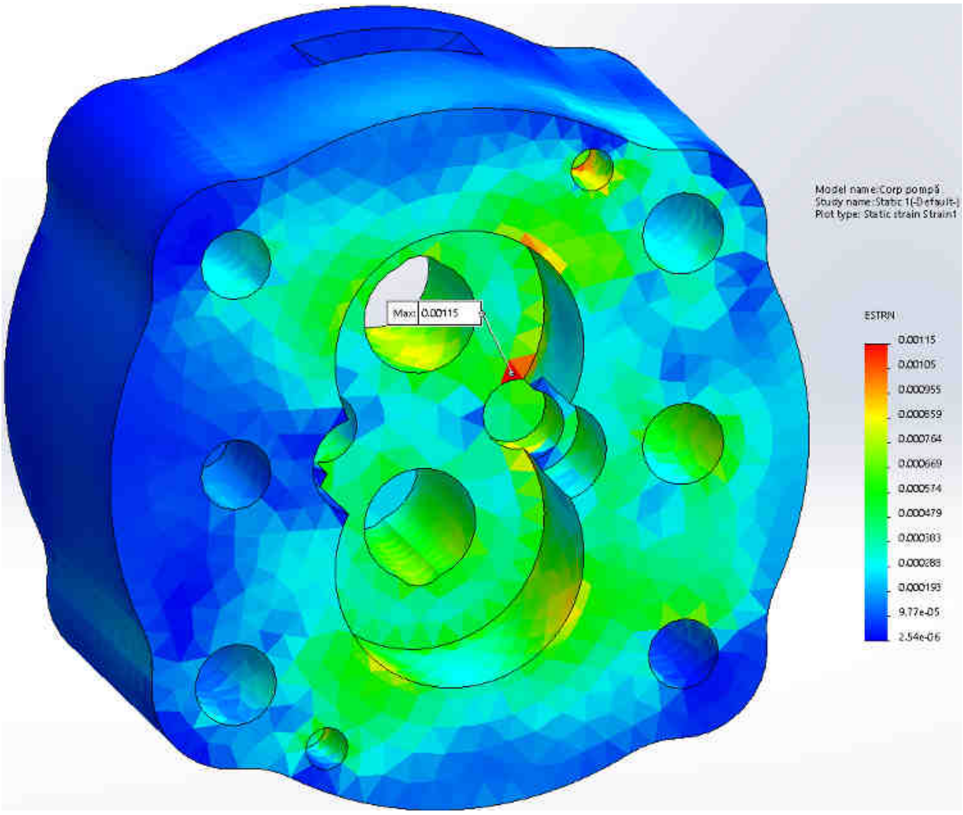

Fig. 11. The strain analysis

The deformations of the pump body are shown in Figure 12, where it can be seen that in the pump discharge zone the deformation has a maximum value of 0.0131 mm; on the same figure it can also be observed that the pressure deformation is not symmetrical compared to any main plane of the body, asymmetry due to the way the body cap is fastened.

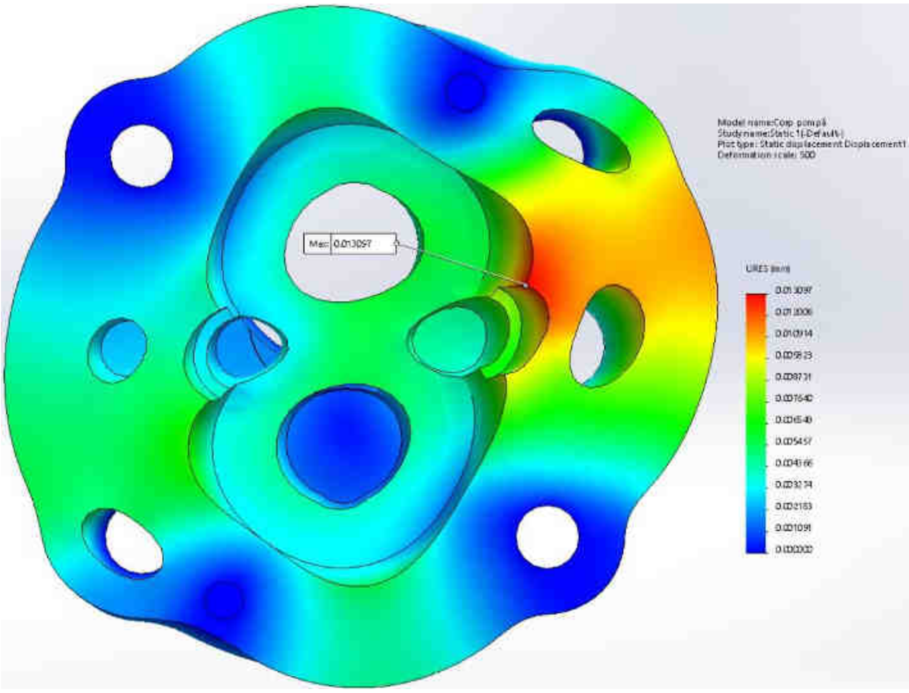

Fig. 12. The deformations of the pump body

After the static analysis of the pump body it can be concluded that it is well sized, no effort exceeds the critical value but there are minor problems with the stress concentrators in the pump discharge zone.

2.2 Dynamic analysis of the pump body

This subchapter is dedicated to the fatigue analysis of the pump body, the initial conditions of the simulation remain the same as in the previous subchapter, different from this is the load cycle, which in this case is pulsating-null cycle (R = 0), as exemplified in Figure 13.

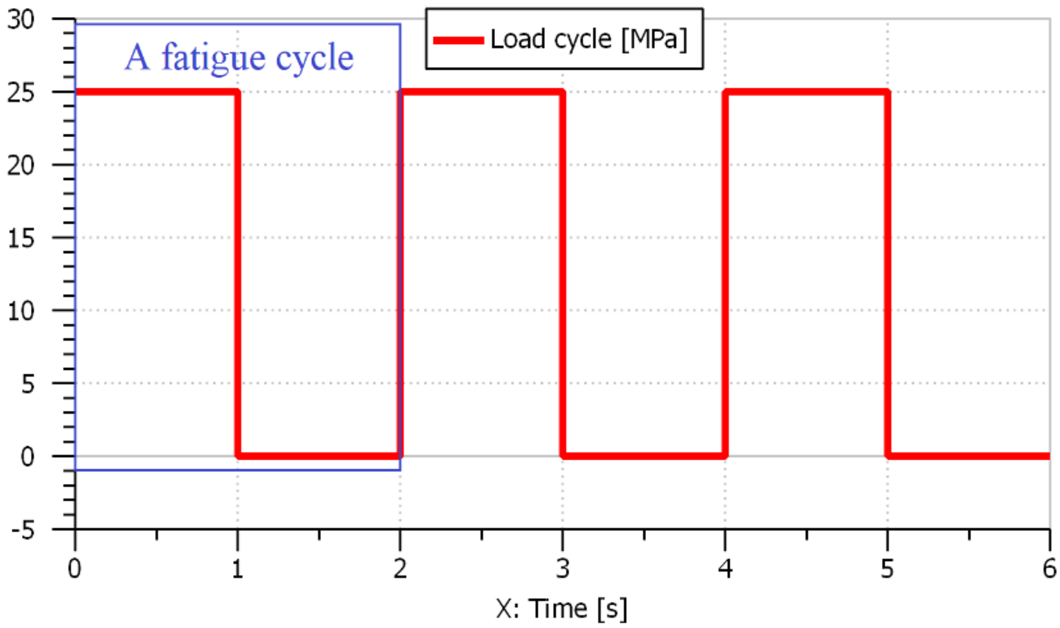

Fig. 13. The load cycles

After performing the analysis in Figures 14 and 15, the pump body resists along a number of 10.777.972 load cycles until in the discharge zone the destruction of the material reaches 100% where the material yields.

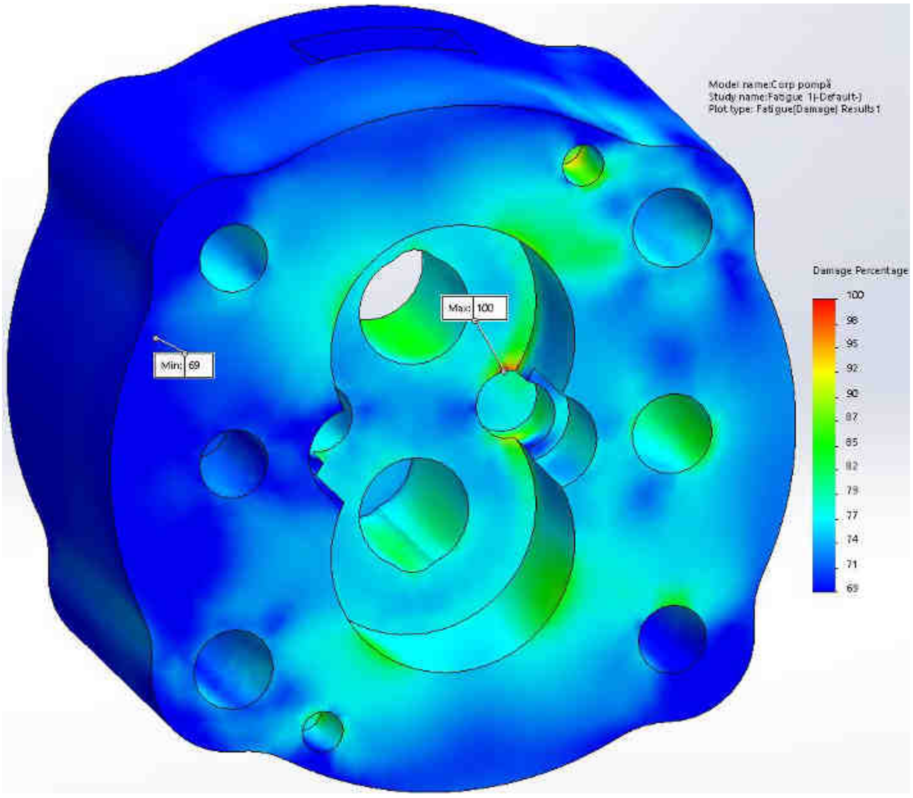

Fig. 14. Variation of material damage due to variation in pressure

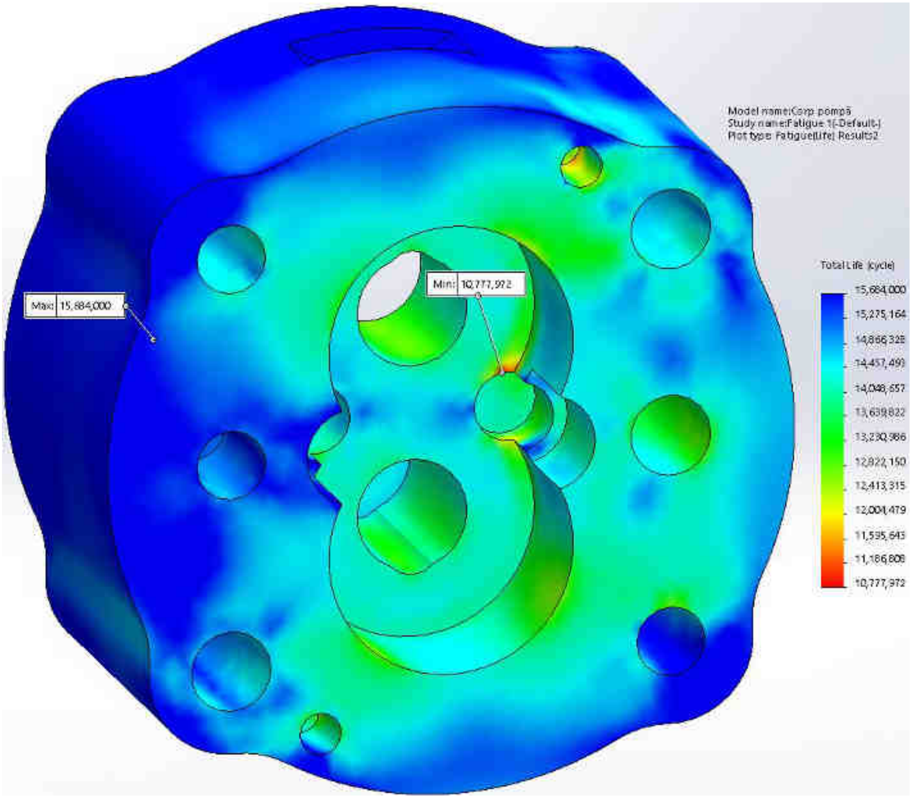

Fig. 15. Total life (fatigue)

3. Experimenting and validating numerical simulation results

Experimenting took place in the HESPER S.A. pump testing laboratory, where the pump was subjected to the same mechanical stress cycle as in Figure 13. The pump was driven at a speed of 3000 rpm for about 240 days.

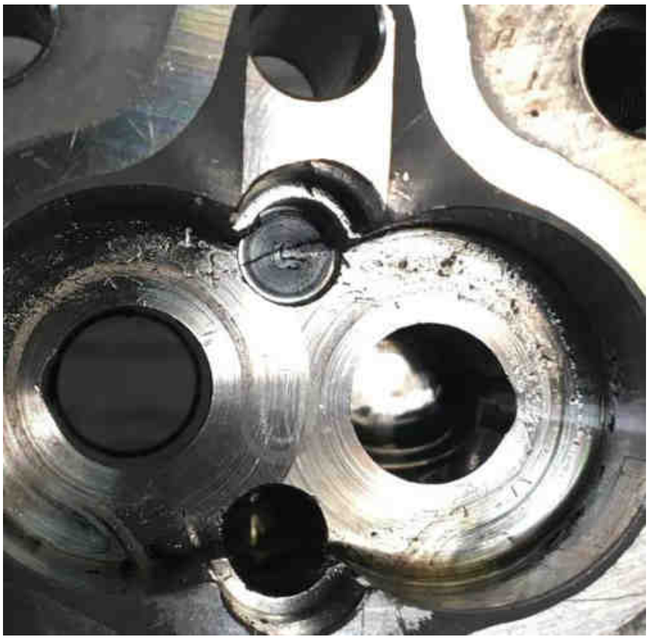

Fig. 16. The fissure

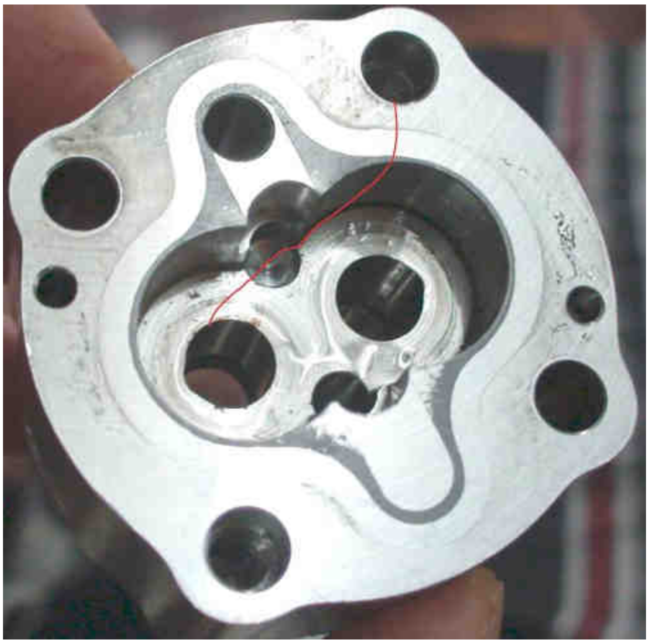

Fig. 17. The fissure route

After 10.413.376 cycles, a longitudinal fissure on the flange was observed in the discharge area, the crack (Figure 16 and 17) starting from the pump collar to the pump clamping screw (the crack is visible from the inside). When the pump was dismantled, it was found that the pump was working properly (Figure 18), the pinion shafts were free of wear, the gear toothing and the pump cover did not show significant wear. [3]

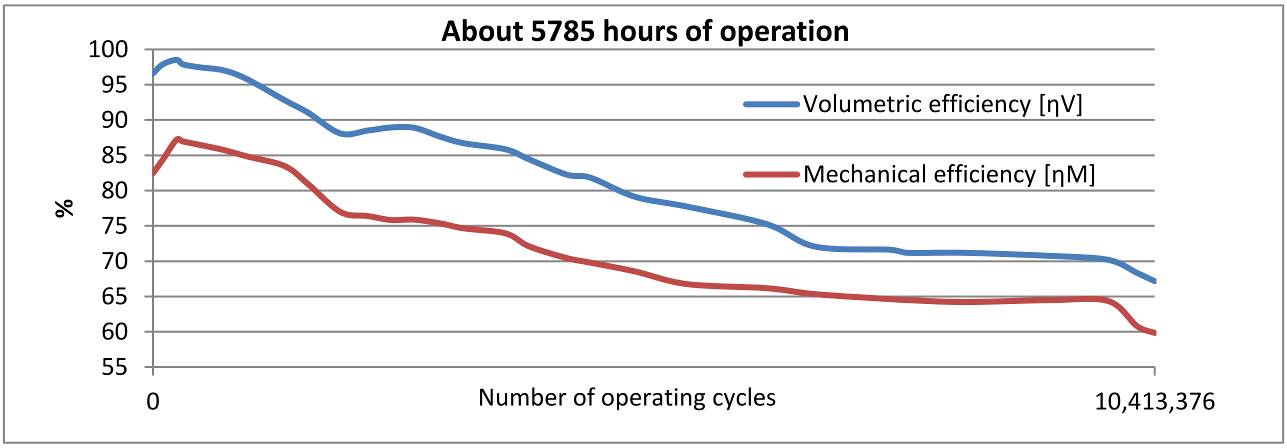

Fig. 18. The evolution in time of the pump's volumetric and mechanical efficiency

4. Conclusions

- It can be concluded that the numerical simulation is validated by the experimental results, with a difference of only 3.4%. Moreover, it can be noticed that both in simulation and in reality, the areas with stress concentrators coincide. The simulation can be used later to check different constructive variants to improve pump reliability.

- Most likely, the crack has emerged from the pump discharge zone due to a crack priming produced by mechanical machining by cutting and expanding outward. The development of this crack can be stopped by practicing a small diameter hole on the cracking route, or it would be much better if the machining in the troubled area would be done with a spherical head cutter that would reduce the number of stress concentrators and surface quality.
- The reliability of this hydraulic pump is very good, but there is still room for improvement in the future.

Acknowledgments

Thanks to HESPER S.A. company for the collaboration, expertise and data provided.
This paper has been developed in INOE 2000-IHP, supported by a grant of the Romanian Ministry of Research and Innovation, under the National Research Programme NUCLEU, project title: "Advanced research on developing synergic border architectures used in solving global challenges and improving knowledge-based competitiveness", Phase 4, Stage 1: 'Theoretical and experimental research on dynamic behaviour of hydrostatic equipment and transmissions on mobile machinery', Financial agreement no. 18N/08.02.2019

References

[1] Vasiliu, Nicolae and Daniela Vasiliu. *Fluid Power Systems/ Acţionări hidraulice şi pneumatice*. Bucharest, Technical Publishing House, 2005.
[2] Assofluid. *Hydraulics in Industrial and Mobile Applications*. Milano, Grafiche Parole Nuove s.r.l., 2007.
[3] ***. *Pump endurance test report HP05-0.8-A*. Pump Testing Laboratory - HESPER S.A. – Bucharest.

Computer Analysis of Water Flow Transition under Existing Conditions on a River Sector in the Range of a Bridge Structure

Lect.dr.eng. **Şerban-Vlad NICOARĂ**[1], Assoc.prof.dr.eng. **Gheorghe I. LAZĂR**[2], Lect.dr.eng. **Albert Titus CONSTANTIN**[3]

[1] POLITEHNICA University Timişoara, serban.nicoara@upt.ro

[2,3] POLITEHNICA University Timişoara

Abstract: *The paper presents a 2D numerical modelling of water flow transition on a sector of Strei River in the range of the DN7 national driveway bridge at km.376+818, outside the built-up area of Deva Town (upstream of Simeria), Romania, in case of a special highwaters phenomenon. The considered synthetical hydrograph follows an exceptional hydrologic event that occurred in the last days of April 2000 on the studied river sector. The numerical simulation looks to estimate (reconstruct) the water levels evolution and velocity distributions under the bridge and on the influenced upstream/downstream river stretches.*

Keywords: *River flow, highwaters flow, bridge hydraulics, numerical model.*

1. General considerations

The presented numerical model of Strei River sector in the range of the DN7 bridge at km.376+818, vicinity of the built-up area of Deva Town (Simeria), Romania, considers a formerly developed technical expertise [1] and feasibility study [2] upon the analysed site regarding the state and reconstruction of a river bottom step and the time affected riverbed. The Strei River crossing by the national driveway DN7 is accomplished by a concrete bridge of four gaps, the central two in the riverbed limit and the side ones towards the bordering floodplains (Figure 1).

Fig. 1. Driveway bridge on DN7 at km.376+818 Strei River
left - upstream view, right - downstream view

The two middle spans have an opening of about 28m between the abutment piers and showing a foundation spacing of about 24m, while the sides spans presenting a 19m abutments opening and a 17m foundations spacing. The bridge leans against the two side abutments, the total span being supported by the three intermediate abutment piers. The side abutments have a geometry upstream / downstream extended by cone quarters. The abutment piers have a thickness of about 1.60m, a length of 8.00m and an above foundation height of 2.60m (foundation block top level at 93.90mSL, to abutment level at 96.50mSL). The actual ground surface configuration under the bridge and for its upstream / downstream river stretches (figure 2) was supplied according to topographic measurements performed after the highwaters event that occurred on Strei receiving basin in December 2003.
The following data was required for the hydraulic approaches that looked to establish the overall flow transition– water levels and velocities time development – on the bridge river sector: maximum flow values of specific overrunning probabilities, the synthetic highwaters hydrograph, streambed and river banks roughness coefficients, and flow hydrodynamic gradient (at high waters especially).

The maximum flow values on the analysed sector of Strei River, as supplied by the Mureș Regional Water Branch of Romanian Waters National Administration, are: $Q_{5\%}$ = 480 m^3/s, $Q_{2\%}$ = 590 m^3/s, $Q_{1\%}$ = 680 m^3/s and $Q_{0,1\%}$ = 695 m^3/s. As about the development of the highwaters hydrograph, its shape was provided as associated to the 1% overrunning probability water flow. Regarding the hydrodynamic gradient, it was estimated as 0.62‰ associated to usual low levels flow and as 2.4‰ correlated to high water levels flow. The roughness coefficient corresponding to the riverbed was estimated at about 0.025…0.040 while corresponding to the river banks about 0.040….0.060.

Fig. 2. Site view of the DN7 bridge over Strei River as supplied by topographical measurements

The study of the flow regime under the existing geometry configuration was performed by developing a numerical simulation of the river sector discharging capacity. The river geometry modelling considers the specific upstream/downstream sector of about 447 m in length. The numerical simulation was developed by the help of HEC-RAS 5.0.6 [3]. A specific data base reflecting the terrain configuration (as shown by the Stereo 70 topographic measurements containing 7848 points) was created to cover the regular flow path and neighbouring floodplains. Six cross views (two on the upstream side of the bridge, PT4 and PT2, and four along its downstream side, PT1, PT3, PT6 and PT5, respectively) were organized in order to better point out the geometrical configuration of Strei River streambed and floodplains.

2. Development of the 2D numerical model

A "satellite" graphics given by Earth Explorer is usually employed as a common approach for the graphic accomplishment of a 3D ground configuration. Nicoară et.al. [4] follows a facile graphic processing of given (measured) topographic data. There is engaged a 2D graphic interpolation method able to generate a 3D surface in a shape type file (extension .shx) – the topography data base for the analysed surface is comprised from 7848 measurement points of coordinates x and y, and level z (figure 3.left). The surface uploaded by ArcMAP 9.3 [5] was meshed by discrete triangulated elements resulting a digitized shape in a 3D space, type **T**riangulated **I**rregular **N**etwork (TIN, figure 3.right). The created shape was then converted into an accessible Digital

Terrain Model file in order to be recognisable by RAS Mapper graphic module in HEC-RAS 5.0.6 [6,7]. The geographic coordinates system was considered and then the final converted ground configuration in an .FLT extension file was uploaded in RAS Mapper (figure 4). Specific information and approaching sequential procedure with respect to geometrical data conversion can be obtained from the mentioned documentation [4,7].

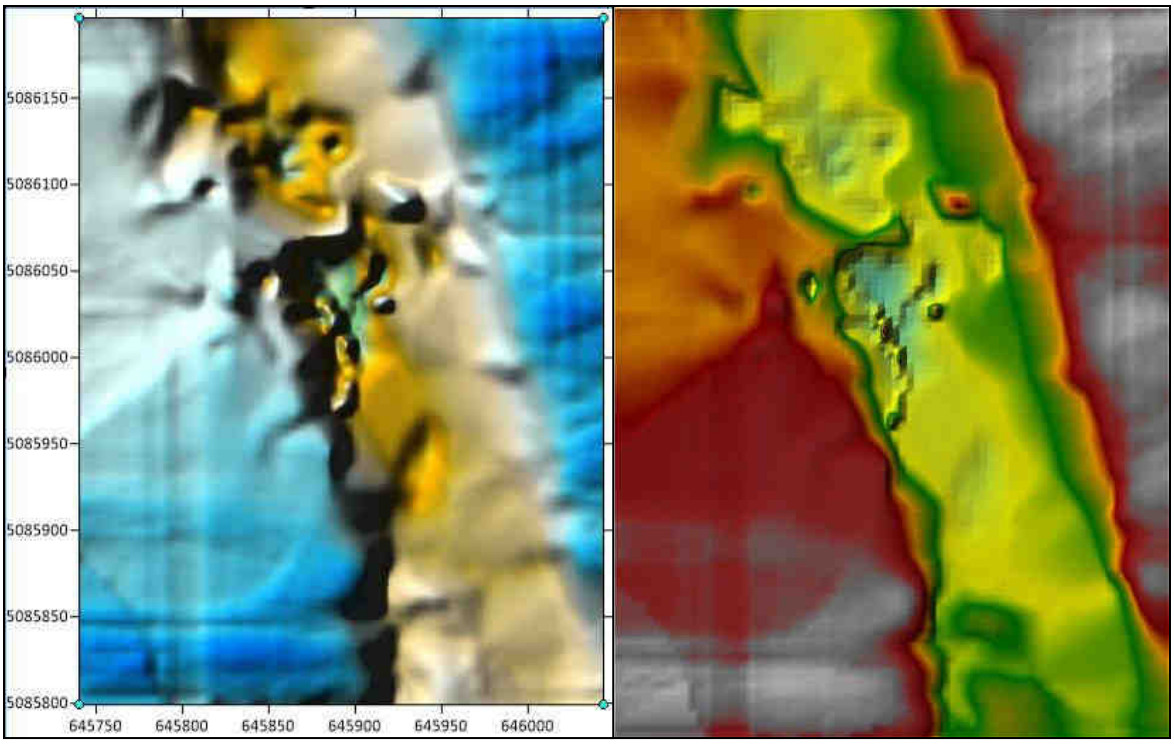

Fig. 3. Graphic view of the analysed site on the range of Strei River crossing bridge:
left - coloured processed 3D surface of topographic measurements, right - processed surface

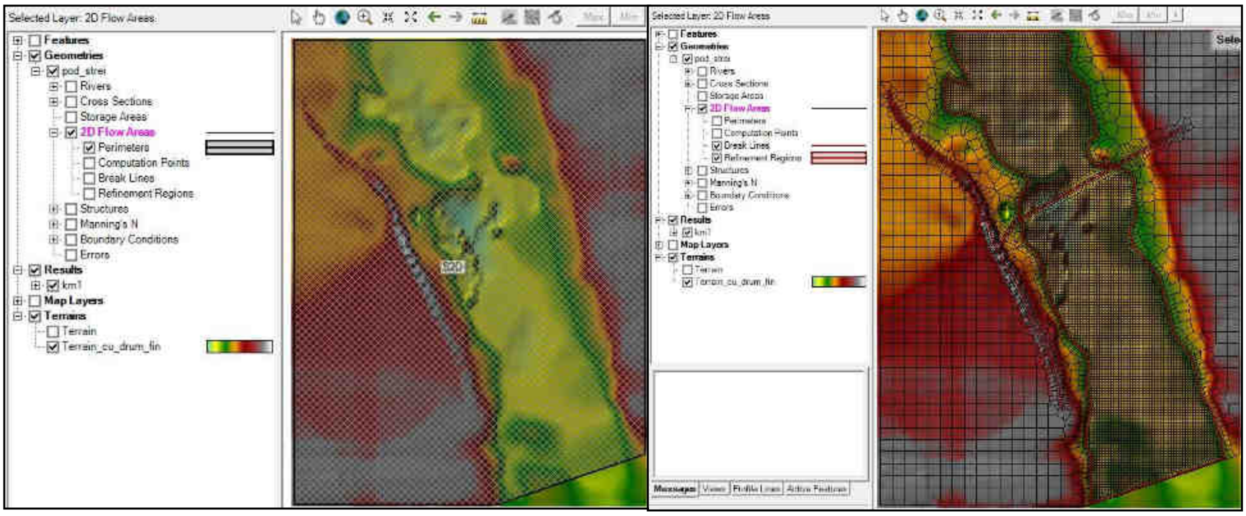

Fig. 4. Processed 3D analysed site on the range of Strei River crossing bridge:
left - general meshing, right - enhanced in the riverbed area

There can be appreciated that the 3D representation "satellite" model gives an adequate, quite realistic, digitized ground configuration (excepting the left bank roads outline that required a significant further improving alteration following updated procedures for flood protection embankments [8]). Even if the numerical geometry model is constructed on a relatively reduced number of topographical measured points – 7848, it still reasonably fulfils most of the natural terrain details as a 3D surface shape.

Accordingly, the digitized terrain model (figure 3.right) of the cut-out sector from Strei River covering the specific driveway bridge was considered in the 2D analysis domain of HEC-RAS 5.0.6 under the name "pod_strei". The 2D Flow Areas layer is accessed in the explorer type window in order to draw the 2D analysis domain contour (labelled S2D in figure 4.left). There was considered a general mesh of 10m × 10m grid size for which the associated points and their accompanying properties tables were generated (Generate Computations Points, Compute Property Points) and saved. A grid enhancing step was performed for the river-course area to engage a 2m×2m grid size (figure 4.right).

A grid break line was defined on the bridge axes direction in order to even more enhance the meshing of this important zone to 1.5m × 1.5m (figure 5) by considering additional points. The grid break line helps also to align the neighbouring grid cells on its defined direction, but even more important it allows to define a joining structure. So, by employing the SA/2D Area Conn facility in the main menu (Geometries), there was inserted a specific structure (overlaying with the defined grid break line) that connects the two adjoining zones of the numerical model.

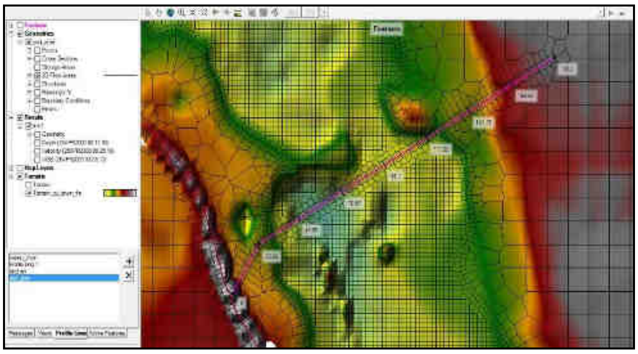

Fig. 5. Site detailed view in the immediate bridge area

There was defined the bridge geometric shape with its accompanying hydraulic conditions (figure 6).

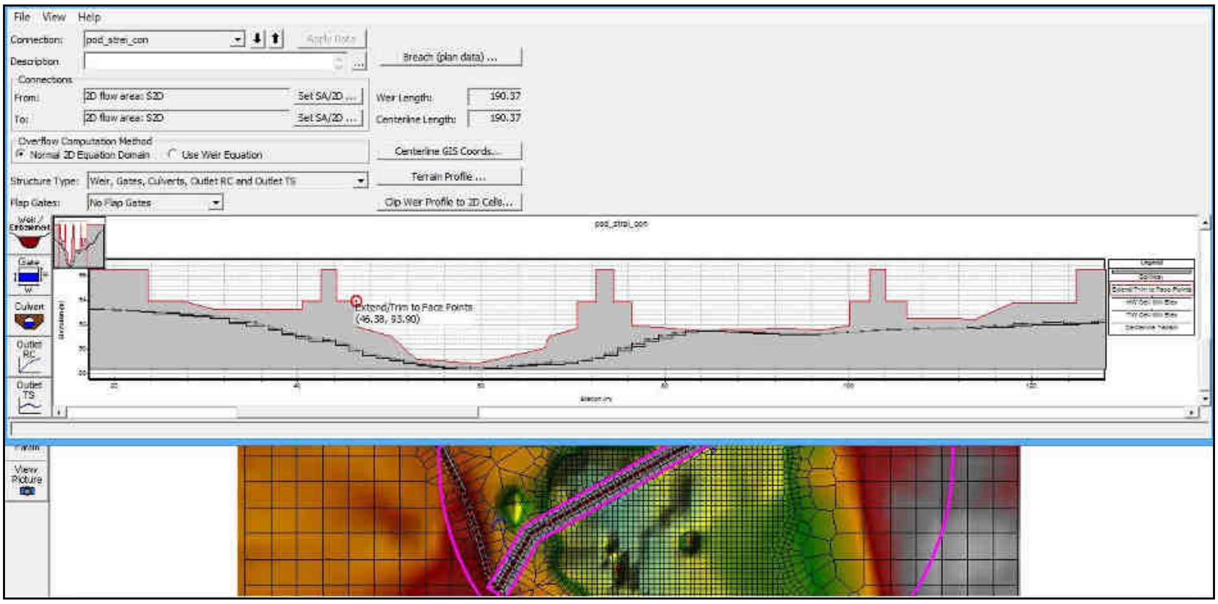

Fig. 6. Definition of the geometric and hydraulic conditions of the bridge axis river cross section

As about the 2D numerical model required boundary / initial conditions, they were defined in the Geometric Data main menu by the help of BC Line facility (SA/2D Area BC Lines option, figure 7). Two border lines were considered for this specific 2D domain, one on the river upstream entering model edge (BC_S2D_11) to which the highwaters hydrograph is to be assigned, and a second one upon the corresponding downstream edge (BC_S2D_22) which is to receive the hydrodynamic gradient of the water surface. Explicitly, the considered highwaters hydrograph on the specific site of Strei River corresponds to the maximum water flow $Q_{0,1\%}$= 695 m^3/s and the accompanying energy gradient 0.0024 (value by which the software will conclude the flow time distribution), as assigned to BC_S2D_11 edge line (figure 7). A hydrodynamic gradient value of 0.0024 was assigned to the downstream BC_S2D_22 line.

The actual numerical simulation of the flow transition was performed over a given time period that corresponds to a significant hydrological event of highwaters, meaning from 00:00 on April 24th to 16:00 on April 25th, 2000 (even if the entire phenomenon went on decreasing for another four days).

The analysis was set to run with a time step of 0.2 seconds and a mapping time step of 10 seconds, while the results were to be registered at each 10 minutes.

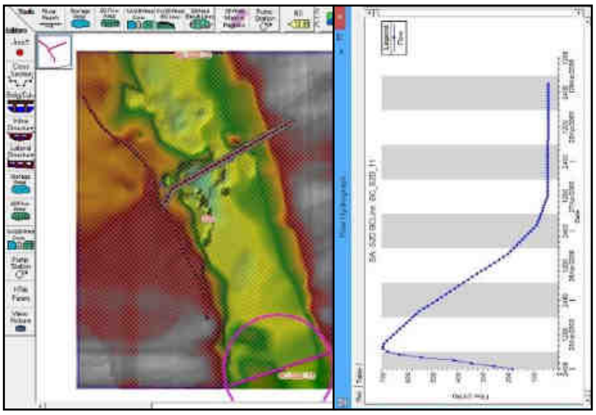

Fig. 7. Upstream/downstream boundary conditions assignment on the analysis domain and the upstream attached hydrograph development over the considered period (00:00 24th to 03:00 29th, April 2000)

3. Significant results of the numerical simulation

The following steady or time dependant water course parameters were reached in each 2D model cell by running the numerical simulation: surface levels, flows and velocities. Following certain graphic post-processing operations, the numerical results were stored in distinct files that can be afterwards visualized with respect to any required cell or along paths as defined by the user, by engaging the RAS Mapper options [7].
Several graphic depictions are further on selected for significant preestablished moments (figure 8), specifically when the water flow successively reaches the values approximately corresponding to the start moment (Q_{start} = 180m^3/s) and the mentioned standardised overrunning probabilities (i.e. $Q_{5\%}$ = 490 m^3/s; $Q_{2\%}$ = 590 m^3/s; $Q_{1\%}$ = 680 m^3/s and $Q_{0.1\%}$ = 695 m^3/s). There were also selected some noteworthy features, such as water surface elevation, particle tracking visualization or water surface longitudinal profile configuration.
As it is known, the water flow transition by the analysed river sector is influenced by the bridge structure, firstly meaning a water elevation increase. Specifically, the water surface elevations shown in the significant river cross sections – upstream model entering border, immediately upstream and downstream of the bridge structure and downstream model outgoing border – at the five specified moments along the simulated time periods are presented by the following table no.1 (as illustrated by figure 8 longitudinal development).

Table 1: Significant water levels along the modelled river sector

station / moment	Water Surface Elevation [mSL]			
	model entering	upstream bridge	downstream bridge (drop, cm)	model outgoing
00:10 (180m^3/s)	93.656	93.654	93.648 (6)	92.296
03:40 (498.6m^3/s)	94.587	94.562	94.533 (29)	92.951
04:30 (585.7m^3/s)	94.786	94.753	94.716 (37)	93.076
06:10 (680m^3/s)	94.980	94.946	94.910 (36)	93.231
07:40 (695m^3/s)	95.008	94.977	94.936 (41)	93.243

Figure 9 shows the particles tracking detailed visualization overlaid to water depth image for the immediate bridge area at the specific moment of maximum 695m^3/s flow, 07:40 on April 25th, 2000, while the next figure 10 brings as trajectories background the velocities distribution for the same river stretch aside with velocity longitudinal development at the mentioned significant time moment.

The last figure indicates also the bridge structure influence with respect to the water level rise in the immediate upstream cross section and consequently the increased water velocity that reach the maximum value of about 7.10 m/s in the immediate downstream area.

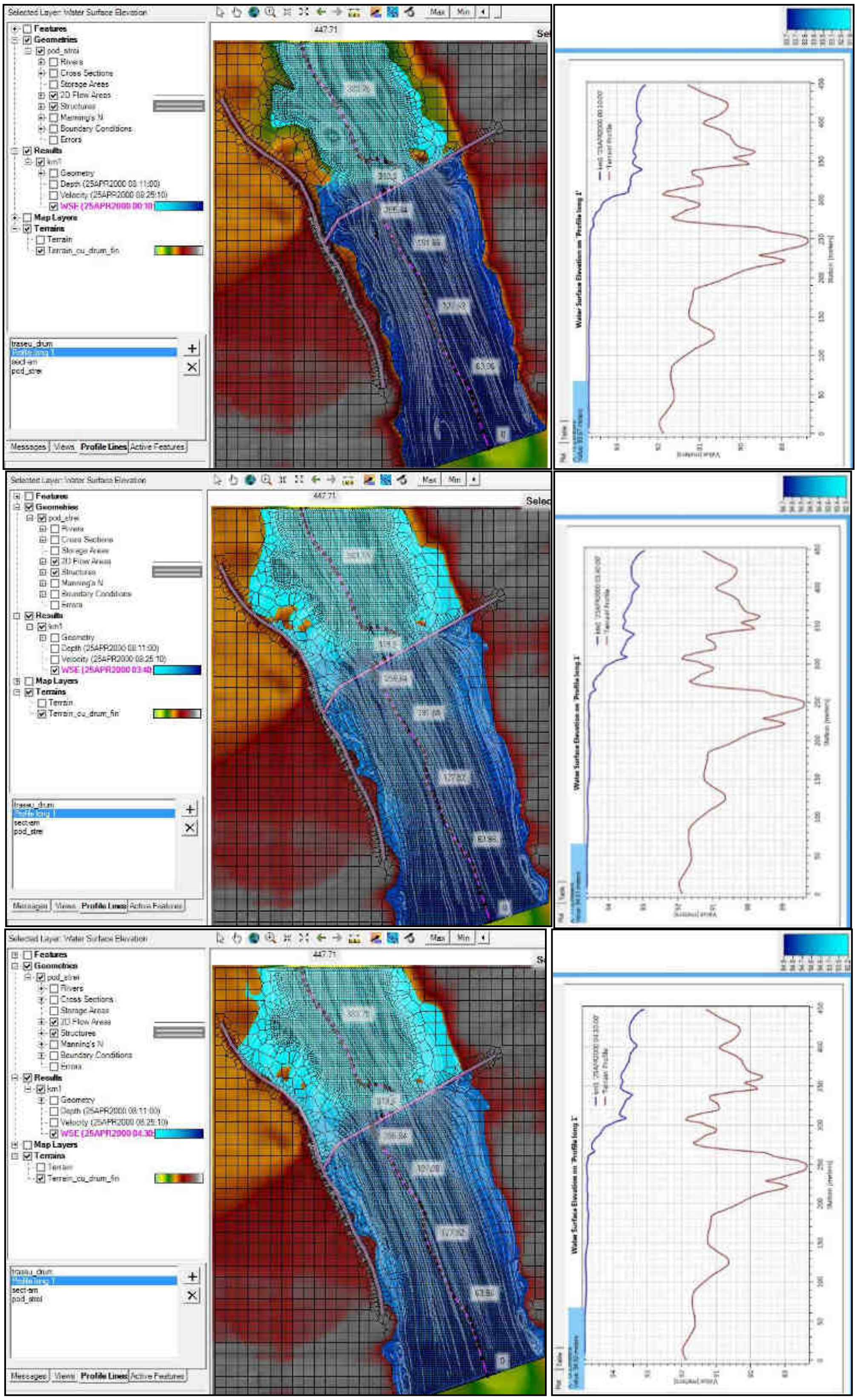

Fig. 8.a. Particles trajectories overlaid to water surface elevation development and thalweg longitudinal view of water surface at five specifically defined moments on April 25th: 00:10 (corresponding to the start flow value 180m^3/s), 03:40 (498.62m^3/s reached flow), 04:30 (585.68m^3/s)

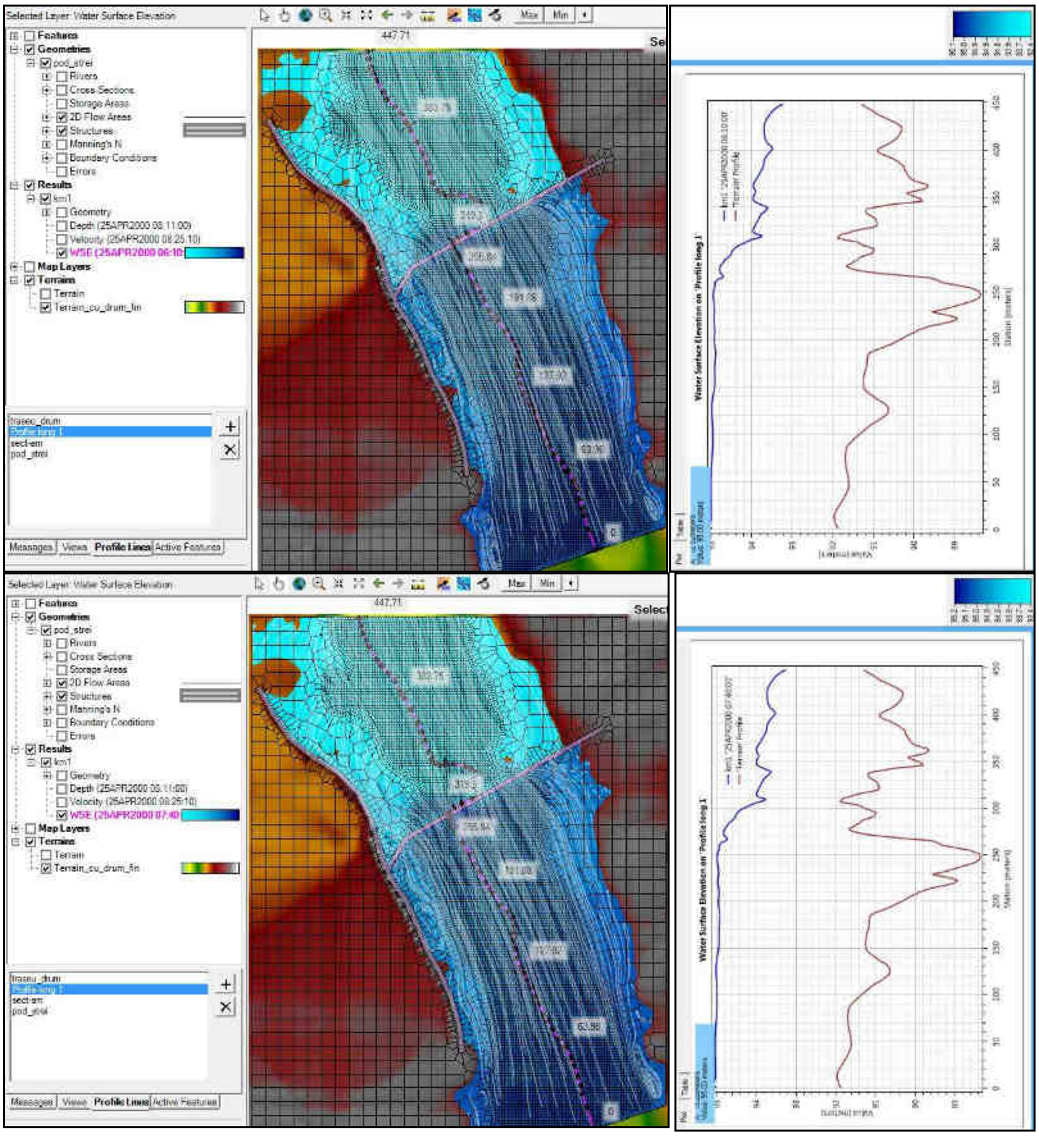

Fig. 8.b. idem previous: 06:10 (679.96m^3/s) and 07:40 (695.01m^3/s)

4. Conclusions

Based on the field observations and supplied topographical measurements, the performed hydraulic numerical modelling of Strei River sector in the range of the bridge at km.376+818 on DN7 driveway brings us to the following main conclusions with respect to the streambed state and processes:

● The bridge area streambed, both towards upstream and downstream, used to show at that time as silted on the central-right part, fact that pushed the main stream flow mostly under the central-left span where it generated important scourings, especially heightened against upstream of the central abutment pier foundation (thalweg level with about 5.46m below foundation top level and ground level near foundation block with only about 1.96m above thalweg);

● Due to alluvia deposits developed in the bridge downstream area, the streambed got an altered plan geometry, as the numerical model accordingly considered. Consequently, the flow stream was not anymore aiming towards the central span of the railway bridge following at about 300m downstream (not covered by the present model) but was tending instead against the left bank access ramp of this second bridge;

● The major river course in the analysed area proves to have the discharge capacity even under the maximum forecasted flow of 1‰ overrunning probability, $Q_{0,1\%}$ = 695 m^3/s.

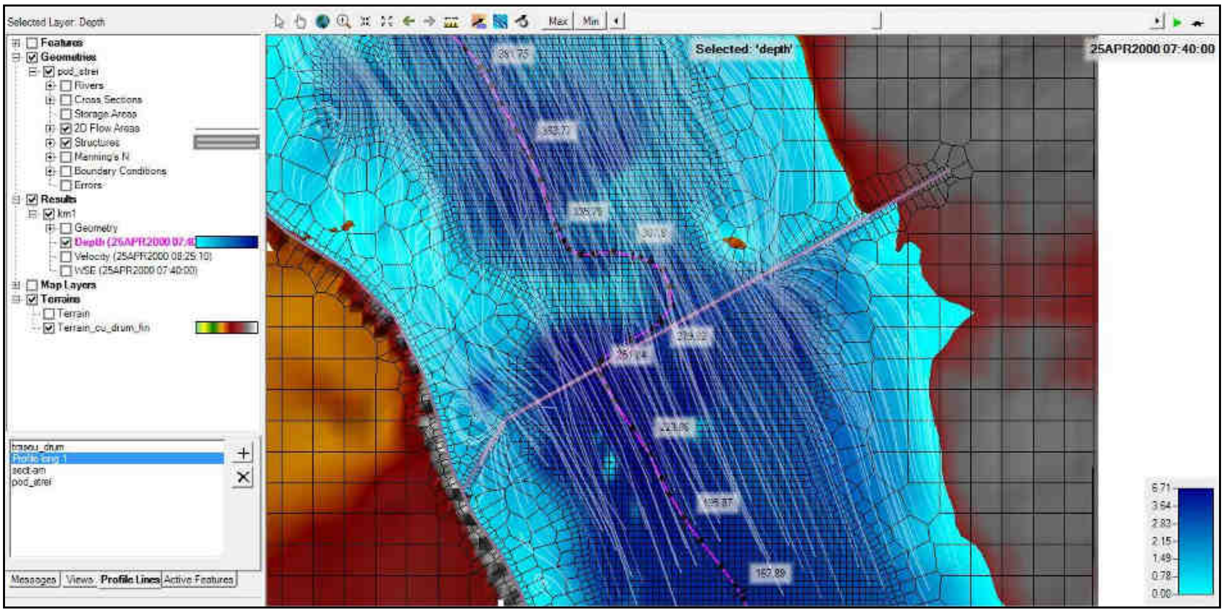

Fig. 9. Detailed particle tracking visualization overlaid to water depth image in the bridge area at 07:40 on April 25th, 2000, of maximum 695.01m^3/s flow

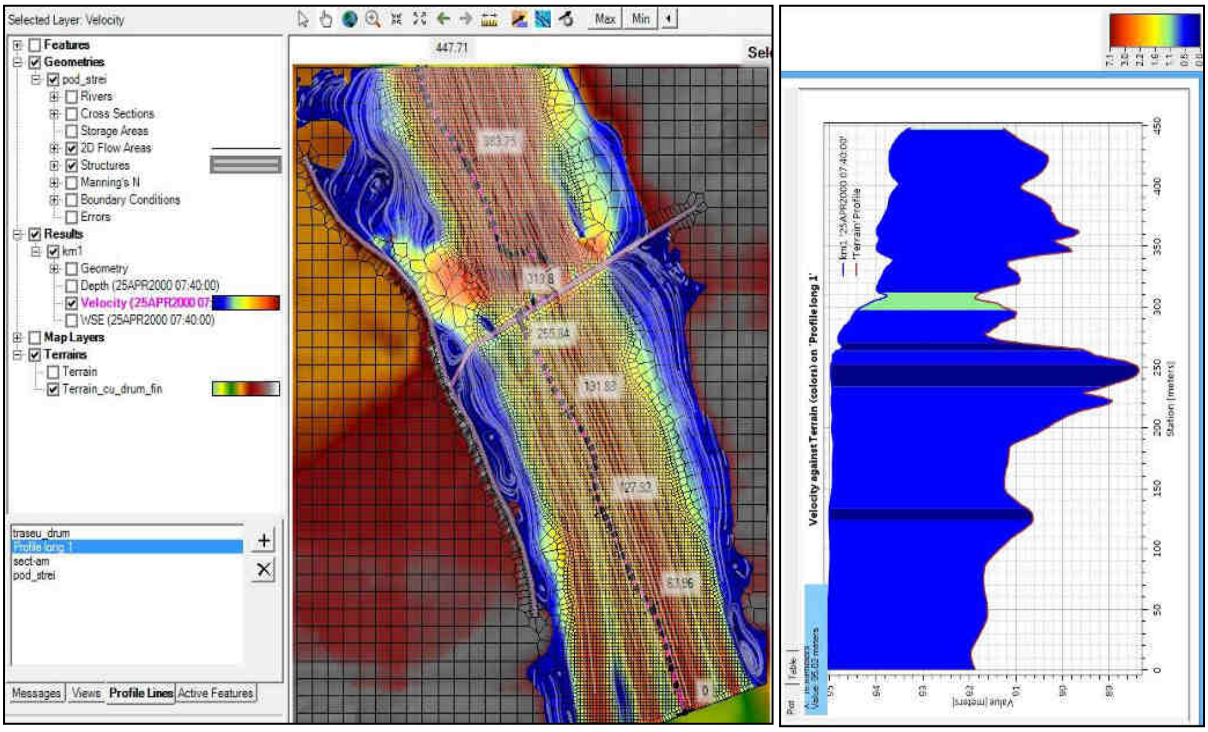

Fig. 10. Detailed particle tracking visualization overlaid to water velocities image in the bridge area and thalweg longitudinal view of water velocity development at 07:40 on April 25th, 2000, of maximum 695.01m^3/s flow

Further on, in order to achieve the general streambed balance in the analysed river sector under the reasonable requirement of improving the under-bridge water discharge capacity, one can suggest some measures for plan shape correction and riverbed processes diminishing:

● Accomplishment of a bottom step downstream side of the bridge that would re-silt the central-left span and would stop the general scourings under the crossing structure;

● Accomplishment of side-bank protections on the resulting bridge - bottom step stretch and also for a length of about 50 to 100m on both directions, downstream of the bottom step and upstream of the bridge;

● Remove of the worthless and abandoned concrete blocks from the riverbed in the bridge area, which would improve the flow pattern;
● Upstream and downstream streambed calibration by removing the developed alluvia deposits, which beside a flow pattern improvement would also help to point the main stream flow towards the central part of the downstream railway bridge;
● Accomplishment of at least two river groins about the left bank downstream of the suggested bottom step, which would ensure the stream flow pointing towards the central part of the railway bridge and so would remove the threat upon the bridge left access ramp.

References

[1] Lazăr, Gh.I., and E. Fülop. *Technical Expertise at river bottom step, DN7 bridge on Strei River at km.376+818 – Regarding the riverbed and layer processes in the bridge area / Expertiză tehnică la prag de fund, pod Strei pe DN 7 la Km.376+818 - Referitor la albie şi procese de albie în zona podului*. Beneficiar EUROPROIECT Timişoara, N.C./2003.
[2] Lazăr, Gh.I., and E. Fülop. *Feasibility Study at DN7 bridge on Strei River at km.376+818 – river bottom step and riverbed reconstruction in the bridge area / Studiu de fezabilitate, pod Strei pe DN 7 la Km.376+818 - prag de fund şi amenajare albie în zona podului*. Beneficiar EUROPROIECT Timişoara, N.C./2003.
[3] Brunner, G.W. *HEC–RAS 5.06*. US Army Corps of Engineers, November 2018.
[4] Nicoară, Ş.V., Gh.I. Lazăr, and A.T. Constantin. "Comparative study of a 1D and 2D numerical analysis modelling a water flow at a river confluence under accidental high waters." *Hidraulica Magazine*, no. 4 (December 2018): 90-97.
[5] ∗∗∗. *HEC–GeoRAS GIS Tools for Support of HEC-RAS using ArcGIS User's Manual, Version 4.3.93*. US Army Corps of Engineers, Institute for Water Resources Hydrologic Engineering Centre, February 2011.
[6] ∗∗∗. *HEC-RAS River Analysis System, Supplemental to HEC- RAS Version 5.0 User's Manual Version 5.0.4*. US Army Corps of Engineers, April 2018.
[7] Brunner, G.W. *Combined 1D and 2D Modelling with HEC–RAS, v.5*. US Army Corps of Engineers, 2016.
[8] Kiers, G. *Lifting Terrain in HEC-RAS 5.0*. VIZITERV Consult Kft., Hungary, Copyright © The RAS Solution and Gerrit Kiers 2015.
[9] Brunner, G.W. *HEC–RAS 4.1*, *River Analysis System Hydraulic Reference Manual*. US Army Corps of Engineers, November 2002.

Researches on the Operation of a Fine Bubble Generator and Oxygen Concentrators

PhD Student **Rareș Dumitru PĂUN**[1], Prof. Dr. Eng. **Nicolae BĂRAN**[1]

[1] Politehnica University of Bucharest, n_baran_fimm@yahoo.com

Abstract: *Two water treatment procedures are presented in the paper:*
- a process for aerating the water with the help of a fine bubble generator;
- a process for waters oxygenation by means of oxygen concentrators.
In both processes, the flow rate of the conveyed gas is the same: 600 dm³ / h.

Keywords: *Fine bubbles generators, waters oxygenation, oxygen concentrators.*

1. Introduction

Considering the multitude of types and forms of gas bubble generators that are introduced into the water, there is a need for theoretical and experimental researches to treat the entire water aeration system unitarily. The literature [1] [2] [3] uses the term aeration or oxygenation; it is proposed to make the following distinction:

• Water aeration means the introduction of atmospheric air into the water (21% O_2 + 79% N_2);
• Water oxygenation means introducing a gaseous mixture as follows:
- Atmospheric air + oxygen from a cylinder in volumetric ratio (25%, 50%, 75%, 100%),
- Air with low nitrogen content (r_{O2} = 95%; r_{N2} = 5%) supplied by oxygen concentrators.

Fine bubble aeration is more efficient than the one made with coarse bubbles because the interfacial specific area between the two fluid systems (air-water) is higher. The interfacial specific area (a) is defined as the ratio between the gas particle area and volume V; a = A / V [5] [6].
In order to intensify the oxygen mass transfer phenomenon from air to the water it is necessary to achieve a maximum interphase contact surface, therefore a smaller diameter of the gas bubble.

➢ Water aeration is carried out in the following fields [7] [8]:
• In sewage treatment plants;
• In water treatment processes, removal of dissolved inorganic substances or chemical elements such as iron, manganese, etc., by oxidation and formation of sedimentable compounds or which can be retained by boiling;
• On biological treatment of waste water, either through the activated sludge process or with bio filters;
• In disinfection processes, by ozonisation of raw water captured from a source in the purpose of its drinking;
• In separating and collecting emulsified fats from wastewater.

Water oxygenation is a mass transfer process with wide application in water treatment. Oxygenation equipment's are based on the dispersion of one phase into the other, for example gas in the liquid, energy consuming process.

➢ Water oxygenation is carried out in the following fields [9] [10]:
• Maintaining an oxygen concentration in aquariums;
• The operation of swimming pools;
• In the medical field in the supply of oxygen to some lung patients.

2. Presentation of the fine bubble generator

Figures 1, 2, 3 show constructive details of the fine bubble generator (FBG).

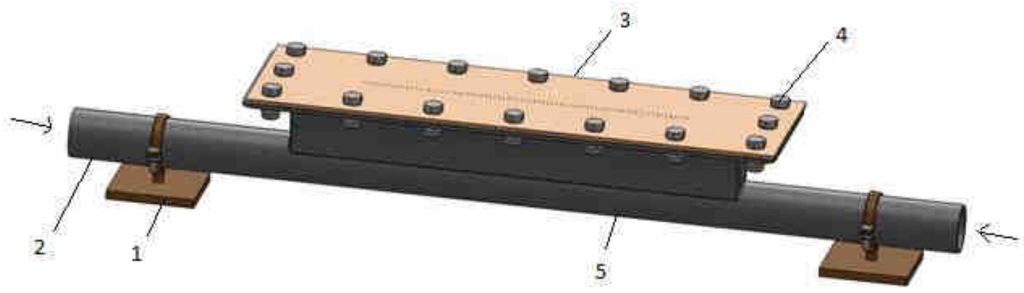

Fig. 1. Rectangular shaped fine bubble generator
1 - support, 2 - compressed air supply pipe, 3 - orifice plate, 4 - FBG body fixing screws, 5 - the body of the fine bubble generator

The 37 Φ 0.5 mm nozzles were disposed on a sole row, so that the bubble columns create a bubble curtain similar to the one formed by a planar jet with a rectangular shape transversal section [11][12]. The repartition of the Φ 0.5mm nozzles can be noticed in Figure 2.

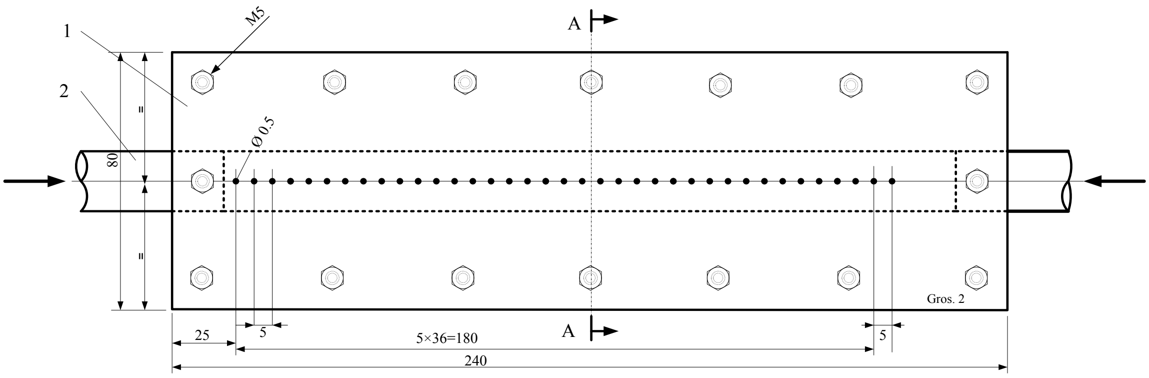

Fig. 2. Sketch of the rectangular shaped fine bubble generator perforated plate
1- orifice plate; 2- compressed air feed pipe.

A cross section through FBG it is seen in Figure 3, where the gas bubbles exit the orifices formed in a rectangular shaped plate.

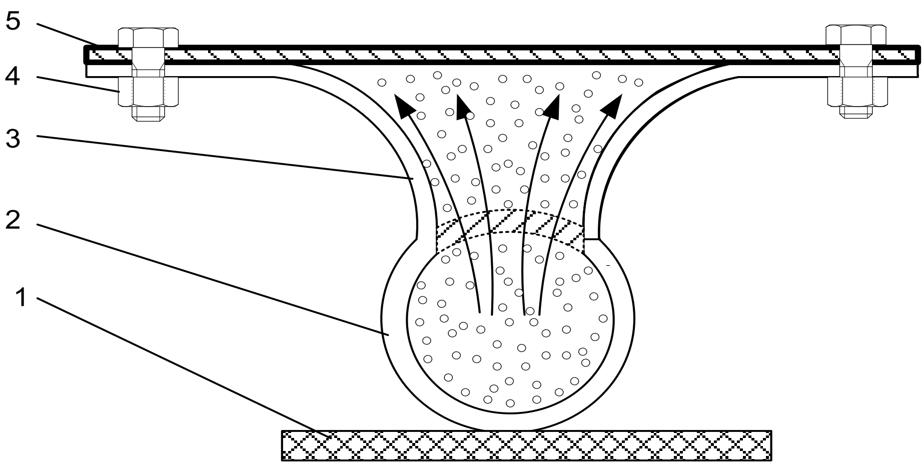

Fig. 3. Section from the rectangular shaped FBG.
1 – support; 2 – compressed air feed pipe; 3 – FBG body; 4 – screws for fastening the plate on the body; 5 – orifice plate.

This type of fine gas bubble generator will be used in experimental researches.

3. Experimental installation provided with a single fine bubble generator

The FBG is fed by its two ends, namely through the pipes 16 and 17.

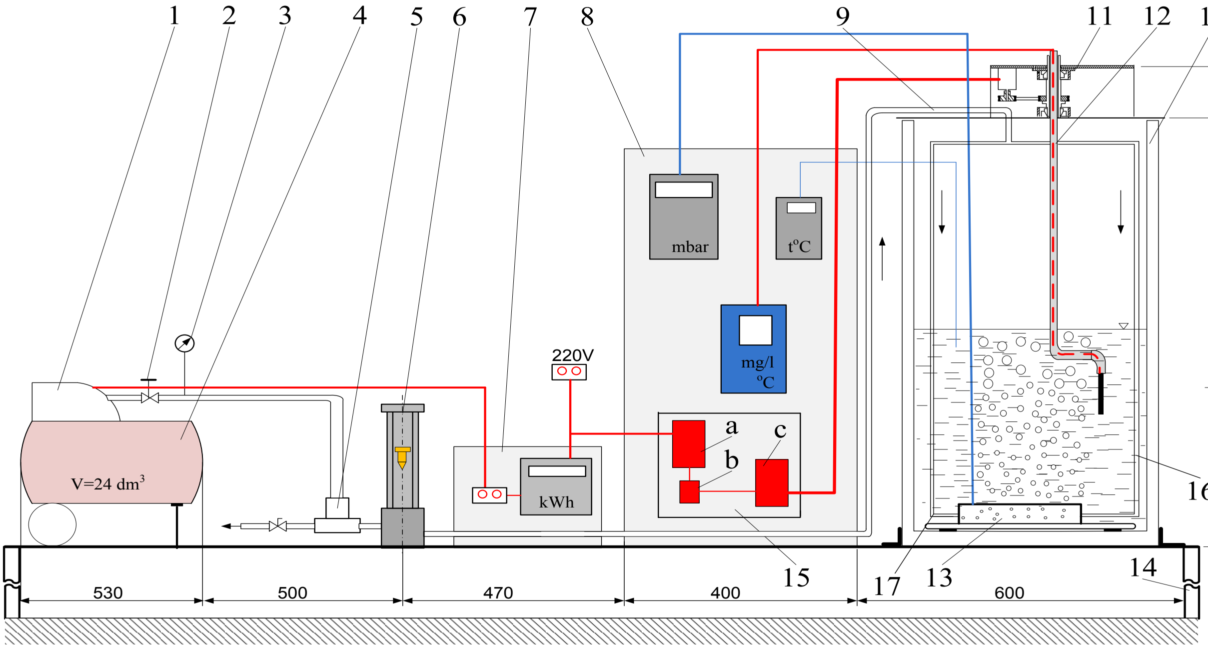

Fig. 4. Sketch of the experimental installation for researches regarding water oxygenation
1- electro compressor with air tank; 2- pressure reducer; 3-manometer; 4-compressed air tank V = 24 dm^3; 5-T joint; 6- rotameter; 7- electric panel; 8-panel with measuring devices; 9-compressed air pipeline to FBG; 10 - water tank; 11 - probe actuation mechanism; 12 - Oxygen probe; 13- rectangular shaped FBG; 14 - support for the installation; 15- electronics command: a - power supply, b - switch, c - control element; 16, 17 - compressed air supply pipes to FBG

Figure 5 shows the air bubble column emitted by the fine bubble generator.

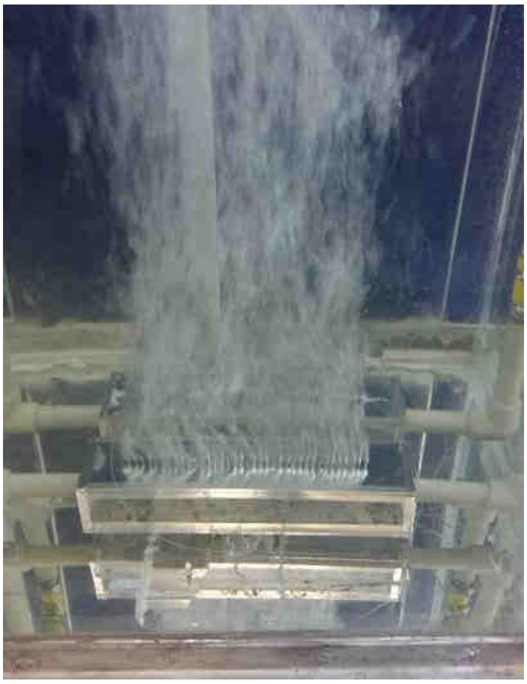

Fig. 5. Water oxygenation installation with one FBG in operation

Referring to the experimental installation of Figure 4, it is stated:
- It is possible to measure the flow rate and the pressure of the gas that ensure the oxygenation of

the water:
- atmospheric air;
- atmospheric air with low nitrogen content.

- Hydrostatic load can be changed in range of 0.5; 1.0; 1.5 m;
- It can be precisely measured with digital indicating devices: pressure, temperature and flow rate of gas introduced into the water tank;
- One can measure the instantaneous change of dissolved oxygen concentration in water or at time Δt with the oxygenometer whose probe is actuated by an electric mechanism.

For the installation operation electric current is needed to operate the electro compressor and for the mechanism of rotation of the oxygen sensor probe in the water tank.
The installation works as follows: compressed air from an electro compressor 1 (figure 4) accumulates at p = 1.5-2 bar in a 24 dm^3 tank. Subsequently, the air passes through the reducer 2 through the manometer 3 and reaches the FBG.
During an experiment, the volumetric air flow rate ($\dot{V}$), the pressure at the entrance at the FBG (p_{FBG}) and hydrostatic load (H) are kept constant.
The panel 15 with the control electronics provides, through the mechanism 11, the rotation of the oxygen sensor probe in the water tank at a speed of 0.3 m / s.

3.1 List of measuring devices provided on the installation scheme

For measuring the pressure and temperature of the air and the dissolved oxygen concentration in the water, there are provided digital indicating devices located on the panel (8) of Figure 4, namely:
a) A flow meter with a scale of 0 ÷ 2200 dm^3 / h for air was provided for the measurement of the flow rate.
b) A manometer with a digital indication in the range 0 ÷ 190 mbar was provided for the pressure measurement.
c) Measurement of temperature was performed with a digital thermometer with a scale of 50÷150ºC.
d) The dissolved oxygen concentration in water was measured using the electric method [13] [14] using a polarographic probe oxygen sensor.
For the measurements, the oxygen sensor is rotated in the water tank with 2 rot / s; for its rotation an electro-mechanical mechanism was designed in the Department of Thermotechnics, Engines, Heat and Refrigeration Equipment's.

4. Experimental researches on the operation of a fine bubble generator

The fine bubble generator has 37 orifices Ø 0.5 mm; the air flow rate was 600 dm^3/h and the duration of the experiments was two hours.
The results of the measurements are shown in Table 1.

Table 1: Experimental data obtained for one FBG

No.	0	1	2	3	4	5	6	7	8
τ [min]	0	15	30	45	60	75	90	105	120
t_{H2O}[ºC]	23	23	23	23	23	23	23	23	23
t_{air}[ºC]	25	25	25	25	25	25	25	25	25
OD[mg/dm^3]	3.65	5.75	6.90	7.55	7.97	8.11	8.21	8.45	8.58

Based on the data in Table 1, function C= f (τ) was plotted (Figure 6).

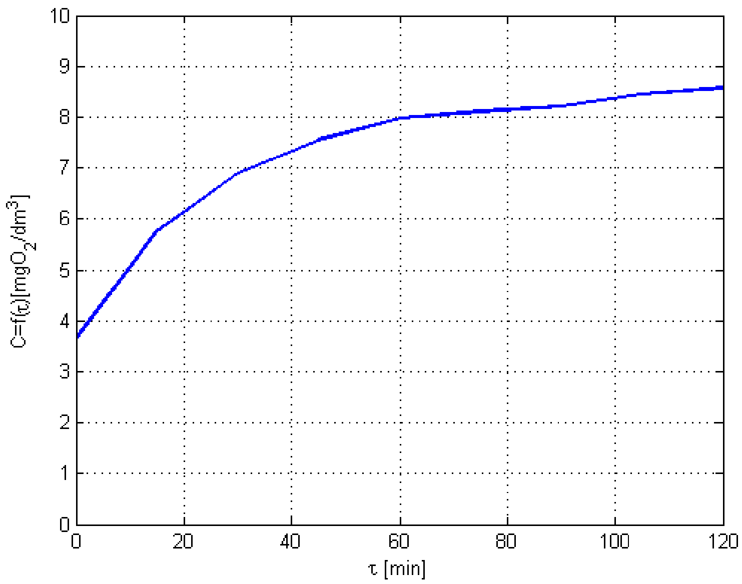

Fig. 6. The dependence C = f (τ) at the operation of a single FBG.

For a water temperature of 23 °C the value of C_s = 8.60 mg / dm^3.

5. Oxygen Concentrators

Two oxygen concentrators were used in the experimental installation each delivering a flow rate of 300 dm^3 / h.
Figure 7 shows the DeVilbis oxygen concentrator.

Fig. 7. Components of the DeVilbis oxygen concentrator

The technical data of this concentrator are shown in Table 2.

Table 2: DeVilbiss Concentrator technical data

DEVILBISS 5-LITER COMPAC T Concentrator		
Catalog Number	**525DS**	**525KS**
Delivery Rate	1 to 5 LPM	
Maximum Recommended Flow	5 LPM	
Outlet Pressure	58.6 kPa	
Electrical Rating	115V~, 60 Hz 3.3 A	220-230 V~, 50 Hz, 1.55 A 230 V~, 60 Hz 1.9 A
Operating Voltage Range	97-127 V~, 60 Hz	187-255 V~, 50 Hz 195-255 V~, 60 Hz
Oxygen Percentage	1-5 LPM = 93% ± 3%	

6. Experimental installation for the oxygen concentrators testing

Figure 8 shows the scheme of the experimental installation.
Oxygen concentrators (1) deliver 5 dm^3 / min ie 300 dm^3 / h each, so the installation delivers a flow rate of 600 dm^3 / h at $p > p_{atm}$.
This gas passes through the rotameter (4) and enters in the fine bubble generator on the position (12) located on the bottom of the water tank (10).
The air (5) (6) and water 8 (b + c) pressure and temperature are measured. For the operation of the air compressors within the oxygen generators 220V electric current is needed. Also, for the movement of the oxygen probe in the water tank it is necessary to operate a mechanism for rotating the probe in the water tank.

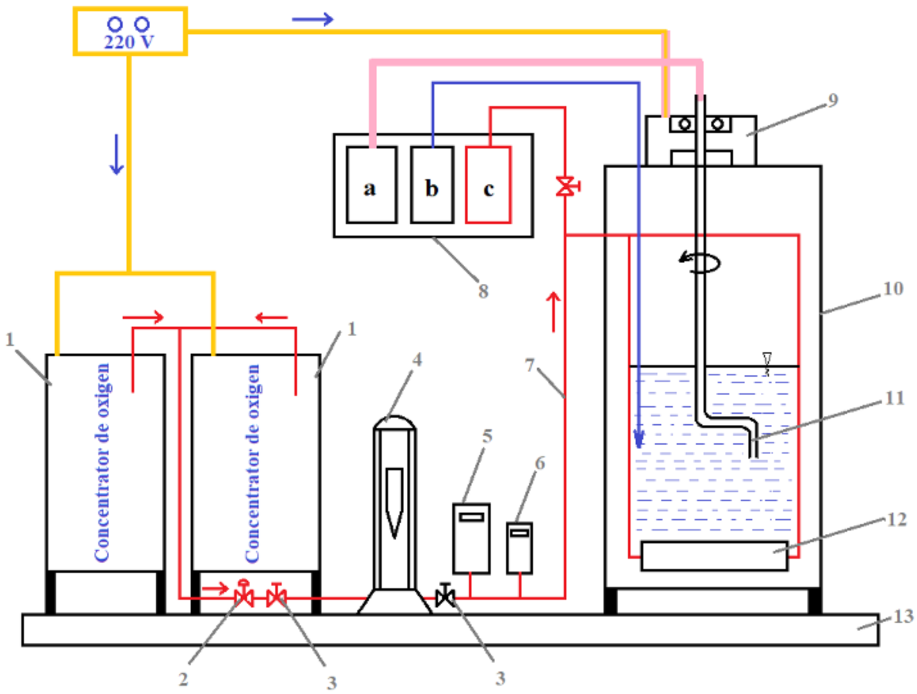

Fig. 8. Scheme of the experimental installation for researches on water oxygenation with oxygen concentrators
1 - oxygen concentrators; 2 - pressure regulator; 3 - valves; 4 - rotameter; 5- manometer with digital indication; 6 - digital thermometer; 7 - compressed air duct; 8 - panel with devices; a-oxygen meter; b - thermometer; c-manometer; 9 - electromechanical mechanism for probe oxygen sensor actuation; 10- water tank; 11 - oxygen probe; 12 - fine bubble generator; 13 - experimental installation support plate.

Figure 9 shows a general view of the two oxygen concentrators supplying a immersed FBG into the water tank.

Fig. 9. Overview of the experimental installation with two oxygen concentrators

Figure 10 shows the water tank with:
- digital indicating thermometer;
- oxygen measuring probe removed from the water.

Fig. 10. Details of the oxygen sensor probe removed from the water tank

7. Experimental researches on the operation of two oxygen concentrators

For the gas mixture the value of C_s is calculated with the relation:

$$C_s = C\frac{k\%}{21\%} \tag{1}$$

where k represents the volumetric ratio of oxygen that diffuses in water.
The results of the measurements for the operation of two parallel-bound oxygen concentrators are given in Table 3.

Table 3: The values of C measured by τ

τ [min]	0	30	60	90	120
C [mg/dm³]	2.57	23.97	31.98	36.59	38.10

The measurements were made on 29.01.2019 and the results are:
- Volumetric gas flow rate: $\dot{V}$ = 600 dm³ / h;
- The gas pressure at the entrance at FBG: p = 583 mmH_2O;
- Water temperature: t_{H2O} = 18 °C.

For t_{H2O} = 18 °C from [4] results C_0 = 2.57 mg / dm³.
If k = 0.93 ±3% is taken as a k = 0.9, the value of C_s is changed as follows:

$$C_s = 9.28\frac{0.9}{0.21} = 39.77 \approx 40\frac{mg}{dm^3} \tag{2}$$

So the function C_s = f (τ) will be framed in a rectangle:
- on the abscissa τ = 0 ÷ 120 [min];
- on the ordinate C = 0 ÷ 40 [mg / dm³].

Based on the data in Table 3 the function C = f (τ) is graphically represented in Figure 11.

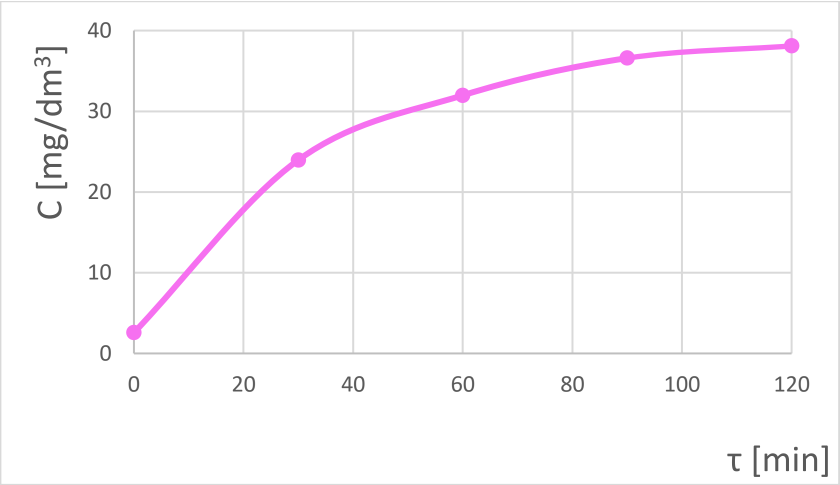

Fig. 11. The graphical representation of the function C = f (τ)

The experimental obtained data is similar to other scientific researches.
Figure 12 overlaps the two graphical representations for C= f (τ) in the cases:
- of the operation of a FBG (curve 1);
- of the operation of two oxygen concentrators (curve 2).

In both cases, the gas flow rate was 600 dm³ / h.
On the ordinate, the right scale refers to Curve 2.
Figure 12 shows the following:
After 20 minutes from the beginning of the FBG experience, the C value reaches 6 mg / dm³, and for the two oxygen concentrators C reaches 20 mg / dm³. As a result, the operation of oxygen concentrators is more efficient.

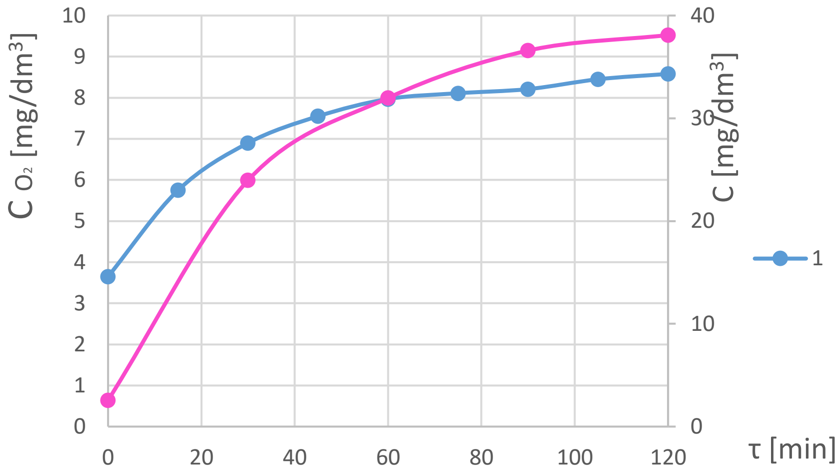

Fig. 12. The graphical representation of the function C= f (τ) for:
1 - fine bubble generator; 2 - two oxygen concentrators.

8. Conclusions

- Increasing the dissolved oxygen concentration in water is faster in the case of oxygenation with oxygen concentrators.
- It is necessary to analyse the consumption of electricity in the two versions.

References

[1] Oprina, G., I. Pincovschi, and Gh. Băran. *Hidro-Gazo-Dinamica Sistemelor de aerare echipate cu generatoare de bule*. Bucharest, Politehnica Press Publishing House, 2009.
[2] Robescu, D., and D.L. Robescu. *Procedee, instalaţii şi echipamente pentru epurarea apelor*. Bucharest, Lithography of Politehnica University of Bucharest, 1996.
[3] Oprina, G. *Contribuţii la hidro-gazo-dinamica difuzoarelor poroase*. PhD. Thesis. Bucharest, Politehnica University of Bucharest, Faculty of Power Engineering, 2007.
[4] Călușaru, I. *Influenţa proprietăţilor fizice ale lichidului asupra eficienţei proceselor de oxigenare*. PhD. Thesis. Bucharest, Politehnica University of Bucharest, Faculty of Mechanics and Mechatronics, 2014.
[5] Pătulea Al.S. *Influenţa parametrilor funcţionali şi a arhitecturii generatoarelor de bule fine asupra eficienţei instalaţiilor de aerare*. PhD. Thesis. Bucharest, Politehnica University of Bucharest, 2012.
[6] Miyahara, T., Y. Matsuha, and T. Takahashi. "The size of bubbles generated from perforated plates." *International Chemical Engineering* 23 (1983): 517-523.
[7] Robescu, D., D.L. Robescu, and A. Verestoy. *Fiabilitatea proceselor, instalaţiilor şi echipamentelor de tratare şi epurare a apelor*. Bucharest, Technical Publishing House, 2002.
[8] Tănase, B., M. Constantin, R. Mlisan (Cusma), R. Mechno, and N. Băran. "Water oxygenation using gas mixtures." Paper presented at the Septième edition du COlloque FRancophone en Energie, Environnement, Economie et Thermodynamique - COFRET'16, Bucharest, Romania, June 29–30, 2016.
[9] Constantin, M., N. Băran, and B. Tănase. "A New Solution for Water Oxygenation." *International Journal of Innovative Research in Advanced Engineering (IJIRAE)* 2, no. 7 (2015): 49-52.
[10] Băran, N., M. Constantin, E. Tănase, and R. Mlisan. "Researches regarding water oxygenation with fine air bubbles." *Buletinul Științific al Universității Politehnica din București, seria D, Inginerie Mecanică* 78, no. 2 (2016): 167-178.
[11] Băran, N., I.M. Căluşaru, and G. Mateescu. "Influence of the architecture of fine bubble generators on the variation of the concentration of oxygen dissolved in water." *Buletinul Stiintific al Universitatii Politehnica din Bucuresti*, *seria D, Inginerie Mecanică* 75, no. 3 (2013): 225-236.
[12] Căluşaru, I.M., N. Băran, and Al. Pătulea. "The influence of the constructive solution of fine bubble generators on the concentration of oxygen dissolved in water." *Advanced Materials Research* 538-541, Trans Tech Publications, Switzerland (June 2012): 2304-2310.
[13] Mateescu, G.M. *Hidro-gazo-dinamica generatoarelor de bule fine*. PhD. Thesis. Bucharest, Politehnica University of Bucharest, Faculty of Mechanics and Mechatronics, 2011.
[14] Căluşaru, I.M., N. Băran, and A. Costache. "The determination of dissolved oxygen concentration in stationary water." *Applied Mechanics and Materials* 436, Trans Tech Publications, Switzerland (October 2013): 233-237.

A Review & Progress on Digital Hydraulic Pumps and Valves

Asst. Prof. **Darshan KATGERI**[1], Dr. **Basavaraj HUBBALLI**[2]

[1]JGI's Jain College of Engineering, darshankatgeri@gmail.com

[2]JGI's Jain College of Engineering, bvhubliabhi@gmail.com

Abstract: *The main challenge in design of hydraulic circuits is to obtain desired flow rate and maintain required pressure, this is accomplished by using various types of hydraulic valves and other hydraulic elements. In this review paper work carried out by authors on valves with special emphasis on Digital Valves and Digital Hydraulic Power Management System (DHPMS) is presented. Digital valves are state valves (ON/OFF Valves), these valves give better control at low speeds. The state-of-the-art methodologies like inverse techniques, and use of commercially available software packages seem to make great impact on research.*

Keywords: *Digital fluid Power, Digital Hydraulic valves, Digital Hydraulic Power Management system*

1. Introduction

Digital hydraulics is an evolving field. Digital fluid power is briskly achieving a status of potential and sought-after technology for fluid power control. The reasons for use of Digital Fluid systems are encouraging because it presents exciting new solutions such as switching converters and Digital Hydraulic power management systems. Digital Displacement is a fundamental advance in field of fluid power, it is a promising technology which significantly improves efficiency and controllability of hydraulic pumps and motors.
As a technology it comprises many discrete valued components however essential feature of digital systems is its intelligent control [1]. Digital Fluid power systems is divided into two branches Parallel Connection and Switching Technologies. In parallel connection response is controlled by changing the state combination of components whereas in switching technologies output is controlled by pulse width ratio.

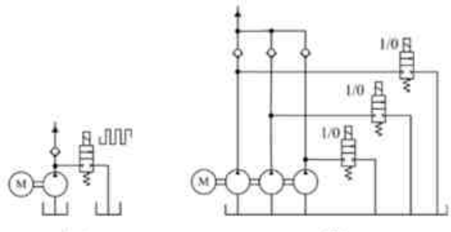

Fig. 1. (a) Switching pump; (b) parallel connected pumps [1]

2. Digital Displacement Pumps

Ehsan et al [2] the authors have used time domain modelling of pump-motor system to predict the performance under variable-demand, variable-speed at different control modes. The authors describe a new technique of digital-displacement to transfer energy between mechanical and fluid power. The digital-displacement pump-motor system is compatible with microprocessor which permits use of advanced control logic. These units are found to be more efficient than their conventional counter parts. The authors have discussed control techniques and basic algorithm which enables the controller to make a decision. The authors have concluded that the units are fast enough to achieve pressure control despite variable demand or variable speed. A schematic diagram of digital displacement pump-motor is shown in figure 2.

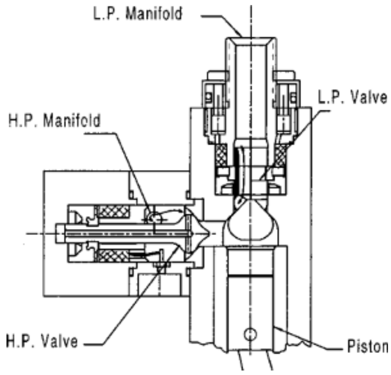

Fig. 2. Cylinder head arrangement of a digital-displacement pump-motor [2]

Wieczorek and Ivantysynoa [3] have used a CAE tool named CASPAR (Calculation of Swash Plate Axial Piston Pump/Motor) for design of hydrostatic machines. Caspar is developed at the Institute for Aircraft Systems Engineering of the Technical University of Hamburg-Harburg. It is a stand-alone tool developed using C++. It considers the time-dependent change of gap height, interaction between machine parts. There is also a module to incorporate spherical valve parts. CASPAR is designed to handle macro-geometry alterations. It presents the user with a GUI to accept inputs files, the inputs like oil properties, temperature, and machine geometry can be controlled, various types of outputs from pressure and gap flow modules can be obtained. A disadvantage of CASPAR is that it focuses on swash plate and axial pumps. To analyze gear pump performance another tool named HYGESim (Hydraulic Gear machines Simulator) can be used.

3. Digital Hydraulic Power Management System (DHPMS)

The conventional solution to meet power requirements is use of pumps and motors connected suitably in the Hydraulic circuit, but this not only increases the complexity of the circuit but also increases the installation and maintenance costs.
Digital hydraulic presents a new approach to meet the power demand. In DHPMS a centralized pump-motor transformer with many independent outlets is used. This approach greatly simplifies the mechanical design. The system variables pressure and flow can be controlled independently and there is no limitation on the pressure amplification which can be used for high pressure applications. In DHPMS flow is possible from prime mover to outlet, from one outlet to another outlet in any direction.

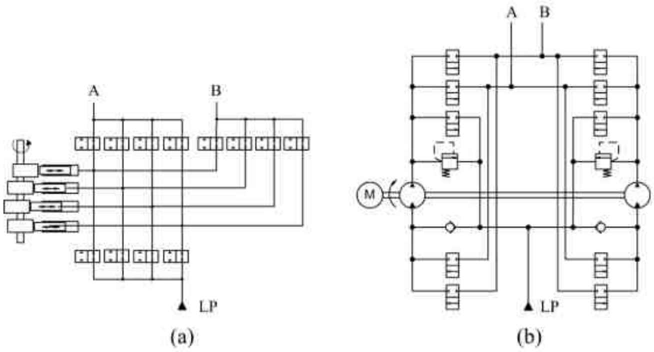

Fig. 3. (a) Two-outlet piston type DHPMS; (b) DHPMS based on fixed-displacement units [1]

4. Digital Hydraulic Valves

In digital hydraulic systems solenoid operated directional seat valves are used to control system variables namely pressure and flow. The valves have two possible states ON or OFF. A distinguishing feature of digital valves is that they are able to perform all valve functions such as pressure regulation, direction and flow control by using only ON/OFF type valves unlike traditional hydraulic system which utilize different type of valves to perform different functions. A group of ON/OFF valves connected in parallel make a Digital Flow Control Unit (DFCU) and at least 4 of

such units are required to substitute a proportional valve. In digital hydraulics circuit there may be numerous control lines. These control lines are independent and the ability to control each edge independently provides better control. This not only reduces power loss but also enables precise control. An additional advantage is that seat valves have zero leakage as opposed to traditional proportional valves. In digital hydraulics each valve needs to be controlled individually this results in a large number of possible valve combinations but it increases the complexity of control algorithm.
Conventional Servo valves are highly reliable hydraulic components that exhibit good response when compared to ON/OFF type valves, but when the spool gets stuck in one position a high frequency jitter has to be used to bring it back; When the same problem is encountered in ON/OFF valves a lesser technology and thus less cost is required to retract the spool [4], hence ON/OFF valves are used in digital valve technology. These valves are often used in slow moving loads and fast switching times.
Digital valves provide better control on pressure applied for precise control or movement of the machine elements. This is achieved by a bank of ON/OFF valves. These valves also simplify the architecture or circuitry by integrating the functions which were performed by proportional valves. The valves are controlled through a software. There could be many miniaturized valves in a digital bank, to accommodate these valves a manifold may be designed. The benefit of these valves are energy efficiency, speed, durability, accurate movements of elements and low initial investment.

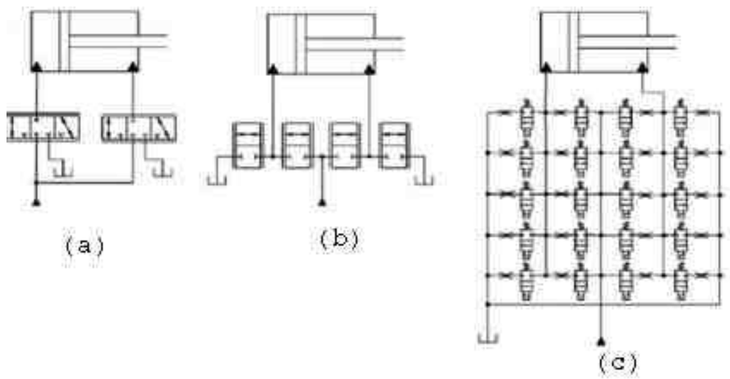

Fig. 4. (a) 2-three-way proportional valve distributed system; (b) 4- two-way valve system; (c) a digital on-off valve system [1]

5. Literature Survey

Linjama [1] presents two implementation approaches of DHPMS one using reciprocating piston unit and the other using fixed displacement unit. A piston type DHPMS is similar to switching system because continuous valve switching is needed. A DHPMS based on fixed displacement unit is a true parallel connected system and no valve switching is needed to maintain any flow combination of outlets. Fixed units provide better controllability because each fixed unit can have different displacement this in turn allows control on flow rates, but controlling pressure is challenging as only certain values are available. It is not possible to maintain pressure at target value; however, pressure can be driven towards target values leading to fluctuation in pressure around target values. In order to maintain hydraulic power author suggests certain strategies such as using more fixed displacement units to increase resolution of flow rate, maintaining correct average flow rate and pressure by using switching between two closest flow rates this can be achieved by using distributed valves together with DHPMS. A high-pressure accumulator can be used to meet peak power requirements. The salient feature of DHPMS is that it can fully utilize the energy storing capacity of accumulator. The efficiency achieved through DHPMS is reported to be much better than traditional approach.
Payne et al [5] have studied the application of digital displacement technology for wave enegy conversion. The technology is mainly based on radial piston layout. It provides faster response than conventional machines. The authors have analyzed the response of system for step up and step down command and investigated the change in flow rates. The efficiency of digital

displacement was about 90% where as for bent-axis machine it dropped to 80%. In the study it was found that digital displacement was well suited for wave energy conversion.

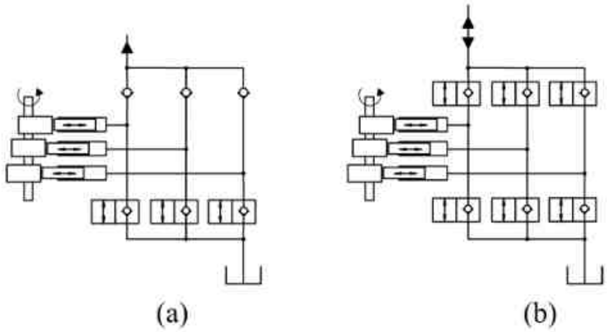

Fig. 5. (a) Piston type digital pump; (b) pump-motor [1]

Gradl and Scheidl [6] have suggested the application of Pulse Frequency control system instead of conventional Pulse Width Modulation system the authors have modelled the dynamic response behavior of systems. Authors have investigated control strategies in digital hydraulics using pulse Frequency Control (PFC) and pulse width modulation (PWM).

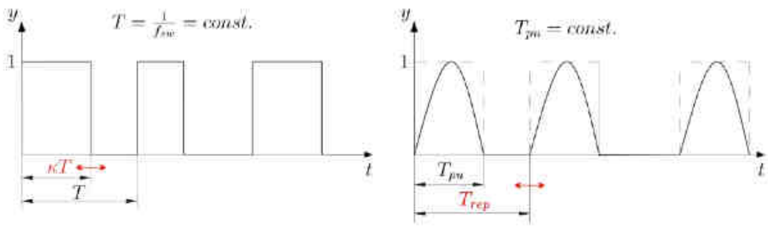

Fig. 6. PWM (left) and PFC (right) and their characteristic values [6]

In PFC input is applied in the form of a flow pulse to a digital flow unit such as a digital pump only after the previous pulse is finished. In PFC the pulse quantity and maximum repeating frequency are fixed. Theses pulses may interact with the plant and hence the whole plant needs to be analyzed.

Palonitty et al [7] have studied the feasibility of pulse frequency modulation to improve controllability of equally coded valve system at velocities below minimum velocity of Pulse number modulation (PNM) control. The authors have extensively conducted experiments to measure improvement of the PFM method on tracking the control performance. It was reported that simultaneous control on pressure and velocity is not possible, authors used a single cylinder drive in two edge connections. The authors have also discussed the challenge of accurate position tracking at low velocities using digital hydraulic valve control and suggested using a greater number of valves or to use 4-edge control and exploit cross flow. The PFM may be used to track control at low velocities and conclude that PFM can be used to improve controllability at least of single acting cylinder.

Sell et al [8] report development of a valve that combines high flowrate and switching speeds required for switched Reactance Hydraulic Transformer (SRHT)

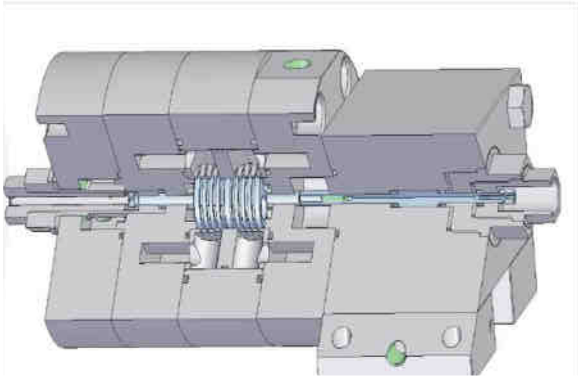

Fig. 7. CAD model of the fast switching linear valve [6]

Yang & Pan [9] have studied recent developments in the field of hydraulics especially in China. The authors enlist the future trends and discuss the challenges and recommendations in fluid power. The main challenges include its efficiency, compactness, and environmental impact. The authors present hydraulically driven robots and machines namely BigDog, Hydraulic Quadruped (HyQ), qRT-2, Baby Elephant and John Deere’s walking harvester. The author concludes that in spite of the challenge there is a very promising future for fluid power.

Liu et al [10] carried out research using proportional relief valve and reported that steady state error can be reduced by dynamic positioning. A conventional PID controller is used in closed-loop to control the pressure. The authors discovered that the system flow does not affect the actual pressure in closed loop system. The variation in actual pressure and set pressure for various input signal is discussed, for step and ramp signal actual pressure can be adjusted to set pressure and for sine and ramp signals actual pressure fluctuates around set pressure.

Dasgupta and Watton [11] have used the bond-graph technique without linearization. The pressure setting is achieved by current-controlled proportional solenoid or by pilot-spring pre-compression. A bond-graph model of proportional solenoid controlled piloted relief valve and various mathematical equations have been presented in the paper. The developed model takes into account laminar and turbulent flow through valve ports. Symbols 2000 software is used, it incorporates a facility called Encapsulation. Sub-systems called as capsules can be created in the software for additional control. The experiments reveal good agreement between calculated values with 95% confidence level. Transient response uncovers the increase in working range of hydraulic systems where such valve is used. The authors conclude that pre-compression of pilot spring and diameter of damping orifice are important design variables.

Pindera et al [12] the authors have used Co-Simulation to analyze the system. In Co-Simulation a complex multi-component system can be analyzed by further dividing it into sub-systems and components, it is well suited for analysis of Digital systems. The success of this is based on effective and efficient data exchange and communication among the modules. These are achieved by using middleware called as CoSim and CORBA protocol. A 2-way axisymmetric Hydraforce SV08-20 valve is used. The model is divided into sub-models like solenoid, fluid dynamic and dynamic motion sub-models which consider three types of forces acting on the poppet. These sub-models are intended to take into account electromagnetic force, inductance, flow-force, friction force, spring force and valve gain. The forces responsible for piston motion are also studied. As a result of this motion 5-piece of data is generated from position of piston and pressures from upper and lower cylinder chamber. The control is accomplished through Bang-Bang Standard (BBS) controller and Bang-Bang Model Based (BBMB) Controller. The authors have proved that Bang-Bang control strategies can track a square wave in non-oscillatory manner. The errors were less than 3%.

Heikkilä et al [13] have studied a mobile boom. The boom is slightly modified i.e. bucket is replaced by a mount to incorporate different weights required for the study. The pressure and displacement control using DHPMS, proportional and digital valves is delineated in the paper. The authors have considered different combinations of pumping and suction for selection of a combination in which the pressure error is minimum, further for displacement control the volume errors in the cylinder chambers should be minimum. To calculate volume errors the geometric piston development along with compressibility of the fluid has been considered. A control algorithm is used to control the cylinder back pressure. The control performance of DHPMS is studied for proportional controlled and direct displacement controlled system. The authors conclude that DHPMS is suitable for displacement controlled systems, however, if small number of pumping pistons with insufficient displacements are used controllability at low velocities is difficult. The authors report 50% energy savings was achieved by using direct displacement control when compared with proportional ELS control.

Vukovic and Murrenhoff [14] the authors have emphasized on holistic design methodologies that not only increase the energy efficiencies of the system, but also improves the system architecture. The authors are of the view that energy recovery especially in machines that involve frequent cyclic motion is important. This may be achieved through a control software.

Vescovoa & Lippolis [15] the authors have carried out axis-symmetric and 3D-analyses on Directional Control valve. In the study the flow is separated by zones, a zone near to walls of the valve and another zone in the center of flow; this is known as "Two Layer Zonal model". This model uses damping functions and classical turbulence model RNG K–ε. In axis-symmetric analysis, velocity and pressure contours are plotted. It is observed that in restricted section where pressure energy is converted into kinetic energy there is abrupt variation in acceleration. The velocities in the zones are found to be different, it is characterized by a high velocity zone at center surrounded by a very low velocity zone. A gradual deceleration at the core is caused because of interaction between the zones this also results in great shear forces, however no appreciable pressure recovery is reported. The authors have proposed a new parameter viz. equivalent hydraulic diameter, it is a non-dimensional parameter that considers flow force and flow rate. The authors have discussed the effect of pressure drop on various parameters like discharge coefficient, K-parameter (average static pressure acting on single spool face), flow coefficient have been studied. The velocity and pressure contours for sufficient meridian planes are plotted to obtain a complete image of three-dimensional field. In comparison it is observed that the axis-symmetric model does not consider circumferential pressure loses and lays more importance on velocities in metering sections, whereas 3D model reveals greater radial velocity than axis-symmetric model. It is clear that 3D model considers various parameters which were not considered by axis-symmetric analysis. 3D model gives a comprehensive means to understand the flow, pressure distribution and its effect.

M. Erhard et al [16] the authors have applied FEM and DOE approach to predict the geometrical shape of solenoid. The concepts of Response surface methodology and Monte-Carlo simulations are used in this paper. The models developed using DOE are generally robust. Usually, in industries the process of development is based on trial and error basis; in this paper the authors propose a holistic simulation approach to overcome the existing gap. The authors discuss the application of inverse simulation approach which involves calculation of subsystem characteristics at component level and thus predicting the geometrical shape fulfilling the subsystem requirement. The subsystems involved are hydraulic, mechanical and solenoid subsystems, their inverse model equivalents are flowrate, solenoid current, valve displacement and pressure. The authors have analyzed a direct-operated proportional pressure relief valve and are of the view that in geometrical valve design the concept of control orifice is important, the characteristics curves for zone, piston and sphere concepts are studied. The cone concept is favorable because the cone shape facilitates smaller actuator design. Various other force characteristic including spring forces are also studied. The results agree well at low pressure. In measurement and simulation, it was observed that material properties are deciding factors in solenoid design. The verification of hydraulic sub-system design is done through optic measurement and displacement of armature is done by laser vibrometer. The authors conclude that measured and simulated results are in good

agreement. Robustness analysis reinforces and ensues the same. Inverse simulation approach supports virtual product development.
Digital displacement has become the heart of Industry 4.0. Artemis a world leader in Digital Displacement technology. According to Artemis, "A new generation of digitally enabled smart machines is transforming industrial processes" [17]. Digital Displacement pumps (DDP's) offer improved productivity at reduced costs, pressure, and energy loses. DDP's respond to load changes rapidly than conventional hydraulic machines.
Artemis is working with major aircraft OEM's to determine potential for replacement of conventional hydraulic pumps by DDP's. DDP's can be used in ground based and distributed propulsion applications like flight simulators, fatigue testing rigs and heavy lift quadcopter. Artemis has conducted field tests of 16-ton excavator fitted with DDP's instead of conventional standard axial-piston pump. It was observed that fuel consumption was reduced between 16-21% and productivity increased by 11-12%, the company estimates that Digital Displacement technology will reduce fuel consumption by 50% resulting in significant reduction in engine size. Artemis and Quoceant are working on a project that concerns with making electricity from waves. They have developed a technology called 'Quantor' which includes use of digital displacement hydraulics.

6. Conclusion

Digital Hydraulics is a relatively new field of research with promising and application-oriented solutions. Digital pump-motor, transformers, multi-chamber cylinders and DHPMS are some of the newer trends of digital fluid power all of these promise better energy efficient solutions. A disadvantage is the commercial unavailability of valves and valve packages. The application of DOE, inverse techniques and the advanced software packages enable calculation of various parameters that were difficult to calculate previously. These developments in various domains are taking research to a new level and aimed at improving the productivity and yield better energy efficient solutions.

References

[1] Linjama, Matti. "Digital Fluid Power – State Of The Art." Paper presented at The Twelfth Scandinavian International Conference on Fluid Power, Tampere, Finland, May 18-20, 2011.
[2] Ehsan, Md., W.H.S. Rampen, and S.H. Salter. "Modeling of Digital-Displacement Pump-Motors and Their Application as Hydraulic Drives for Nonuniform Loads." *Journal of Dynamic Systems, Measurement, and Control* 122, no. 1 (March 2000): 210-215.
[3] Wieczorek, Uwe, and Monika Ivantysynova. "Computer Aided Optimization of Bearing and Sealing Gaps in Hydrostatic Machines—The Simulation Tool Caspar." *International Journal of Fluid Power* 3, no. 1 (2002): 7-20.
[4] Raghuraman, D.R.S., S. Senthil Kumar, and G. Kalaiarasan. "Simulation of proportional control of hydraulic actuator using digital hydraulic valves." *IOP Conf. Series: Materials Science and Engineering* 263 (2017).
[5] Payne, Grégory S., Uwe B.P. Stein, Mohammad Ehsan, Niall J. Caldwell and W H.S. Rampen. "Potential of Digital Displacement Hydraulics For Wave Energy Conversion." Paper presented at The 6th European Wave and Tidal Energy Conference, Glasgow, United Kingdom, August 29 - September 2, 2005.
[6] Gradl, Christoph, and Rudolf Scheidl. "A pulse-frequency controlled hydraulic drive for the elastic deformation of a structure." Paper presented at The 9th International Fluid Power Conference, 9. IFK, Aachen, Germany, March 24-26, 2014.
[7] Paloniitty, M., M. Linjama, and K. Huhtala. "Equal coded digital hydraulic valve system – improving tracking control with pulse frequency modulation." Paper presented at the 2nd International Conference on Dynamics and Vibroacoustics of Machines (DVM2014), Samara, Russia, September 15-17, 2014.
[8] Sell, N.P., N. Johnston, A.R. Plummer, and S. Kudzma. "Development Of a Position Controlled Digital Hydraulic Valve." Paper presented at the ASME/BATH 2015 Symposium on Fluid Power and Motion Control, Chicago, Illinois, USA, October 12-14, 2015.
[9] Yang, Hua-yong, and Min Pan. "Engineering research in fluid power: a review". *Journal of Zhejiang University Science A* 16, no. 6 (June 2015): 427-442.
[10] Liu, Yong, Bin Yang, Zhensong Wu, and Meng Chen. "Experimental Study on Closed Loop Simulated Loading of Proportional Relief Valve." *Chemical Engineering Transactions* 46, (December 2015): 1153-1158.

[11] Dasgupta, K., and J. Watton. "Dynamic analysis of proportional solenoid controlled piloted relief valve by bondgraph." *Simulation Modelling Practice and Theory* 13 (2005): 21–38.
[12] Pindera, Maciej Z., Yuzhi Sun, Jean-Jacques Malosse, and Jose M. Garcia. "Co-simulation based design and experimental validation of control strategies for digital fluid power systems." Paper presented at the ASME/BATH 2013 Symposium on Fluid Power & Motion Control, Sarasota, Florida, USA, October 6-9, 2013.
[13] Heikkilä, Mikko, Matti Karvonen, Matti Linjama, Seppo Tikkanen, and Kalevi Huhtala. "Comparison of proportional control and displacement control using digital hydraulic power management system." Paper presented at the ASME/BATH 2014 Symposium on Fluid Power & Motion Control, Bath, United Kingdom, September 10-12, 2014.
[14] Vukovic, Milos, and Hubertus Murrenhoff. "The next generation of fluid power systems." Paper presented at the 2nd International Conference on Dynamics and Vibroacoustics of Machines (DVM2014), Samara, Russia, September 15-17, 2014.
[15] Del Vescovoa, Giuseppe, and Antonio Lippolis. "Three-Dimensional Analysis of Flow Forces on Directional Control Valves." *International Journal of Fluid Power* 4, no. 2 (2003): 15-24.
[16] Erhard, M., J. Weber, and G. Schoppel. "Geometrical Design and Operability Verification of a Proportional Pressure Relief Valve." Paper presented at The 13th Scandinavian International Conference on Fluid Power, SICFP2013, Linköping, Sweden, June 3-5, 2013.
[17] http://www.artemisip.com/sectors/industrial.

From Human-Environment Interaction to Environmental Informatics (III): the Social-Ecological Systems dynamics in Knowledge-based Society

Assoc. prof. PhD. eng. **Mirela COMAN**[1], PhD stud. **Bogdan CIORUȚA**[1,2]

[1] Technical University of Cluj-Napoca - North University Centre of Baia Mare, Faculty of Engineering, str. Victor Babeș 62A, 430083, Baia Mare; comanmirela2000@yahoo.com

[2] Technical University of Cluj-Napoca - North University Centre of Baia Mare, Office of Information and Communication, str. Victor Babeș 62A, 430083, Baia Mare; bogdan.cioruta@staff.utcluj.ro

Abstract: *Since its inception, human society has noticed that there is a close relationship between the activities it carries out and the way in which the environment behaves; however, attempts to adjust activities to health and environmental integrity have been delayed even in this Knowledge-based Society.*
Nowadays, the environment, as a third part of sustainable development modern concept, plays a crucial role in people's physical, mental and social well-being. Despite significant improvements, major differences in environmental quality and human health remain between and within countries.
The complex relationships between environmental factors and human health, taking into account multiple pathways and interactions (natural-human-human made), should be seen in a broader spatial, socio-economic and cultural context. In this sense, the present paper focuses on the Human-Environment Interaction (HEI) and the Social-Ecological Systems (SESs) dynamics.

Keywords: *Human-environment interaction, Bronfenbrenner's theory, analytic framework, system dynamics*

1. Introduction

The modern society consumer's most pressing problems (environmental pollution, urban sprawl, excessive industrialization and urbanization) - as the results of the Human-Environment Interaction (HEI) - are complex and often transcend spatial and temporal scales [1]. They also do not fall cleanly within the boundaries of a single area of interest, because of the Social-Ecological Systems dynamics (as presented in Fig. 1) - which we see as being an expansion of Bronfenbrenner's environment theory, under different thinking systems approaches [2].

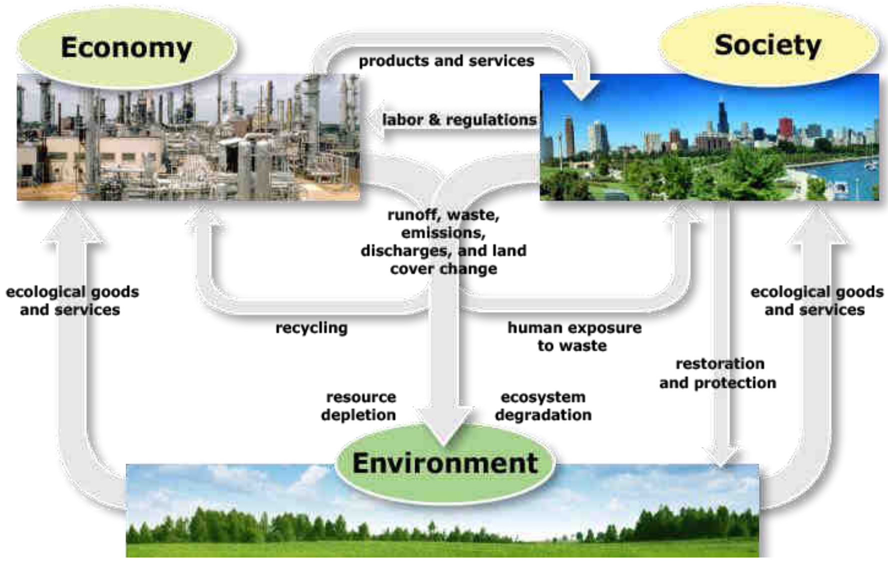

Fig. 1. The Human-Environment Interaction view as a sustainability framework [3]

Thinking system is an approach to problem solving [4] that is based on the belief that the component parts of a system are best understood in the context of their relationships and interactions with one another and with other systems.

Since its inception, human society has noticed that there is a close relationship between the activities it carries out and the way in which the environment behaves; however, attempts to adjust activities to environmental integrity have been delayed even in the Knowledge-based Society.
Expansion of cultivated areas, intensification of agricultural production process, irrational exploitation of forests, excessive industrialization and urbanization, etc. there are so many causes that cause the entire habitat, to be enable to fulfil, in part or in full, its fundamental functions [1].
The unity of the human body with the environment as the fundamental law of life, requires habitat protection against pollution, rational exploitation of resources and, as far as possible, increasing them to meet the increasing needs of humanity. These issues, together with others, require a detailed understanding of the structure, interactions and dynamics existed in our environment.

2. Exploring the Human-Environment Interaction (HEI)

The environment is our basic life support system which provides the air for breathing, the water for drinking, the food for eating and the land for a living. It is collectively portrayed all the external forces and conditions, which influences the life, nature, growth and maturity of living organism, whereas "ecology' is the scientific analysis and study of interactions among organisms and their environment [5]. Much more, understanding the dynamics of Human-Environment Systems (HESs) and developing strategies that promote their sustainability, requires a holistic, integrated approach. Although many frameworks have been developed over time [7, 8], that include social and environmental or, in other words, natural, human and human-made components (Fig. 2), managing social and environmental systems as integrated systems has been difficult in today's practice.

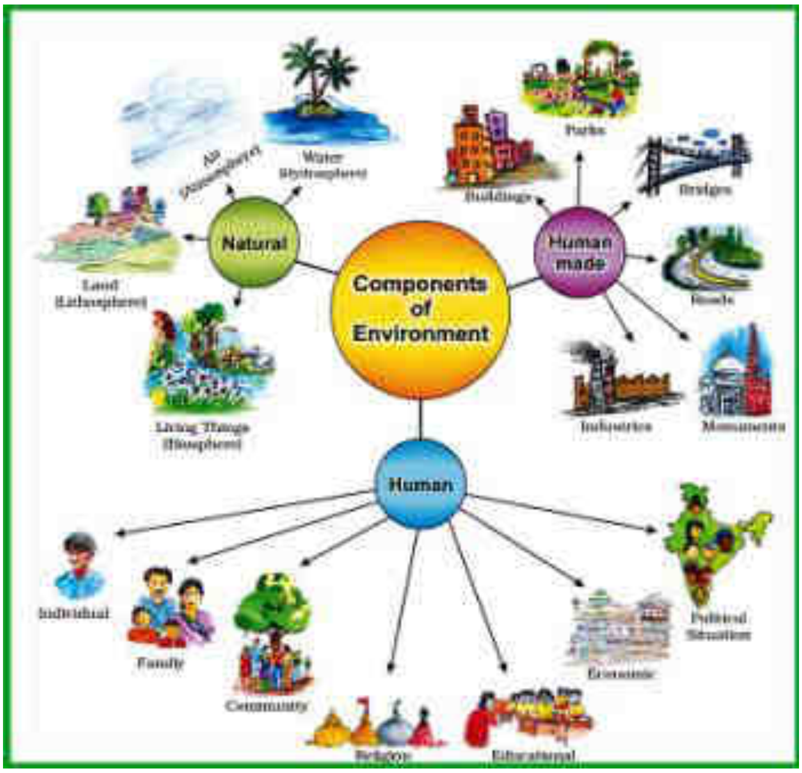

Fig. 2. Illustrated diagram version of components and structures that constitute the environment [5]

Starting from point of view expressed by *ecology* as the science of relationships between living organisms and their environment [1] and *human-ecology* as about relationships between people and their environment [9], an *ecosystem* is everything in a specified area - the air, soil, water, living organisms and physical structures, including everything built by humans. The living parts of an ecosystem - microorganisms, plants and animals (including humans) - are its biological community. The *Social System* is perceived as being everything about people, their population and the psychology and social organization that shape their behavior [9], as presented in Figure 3.

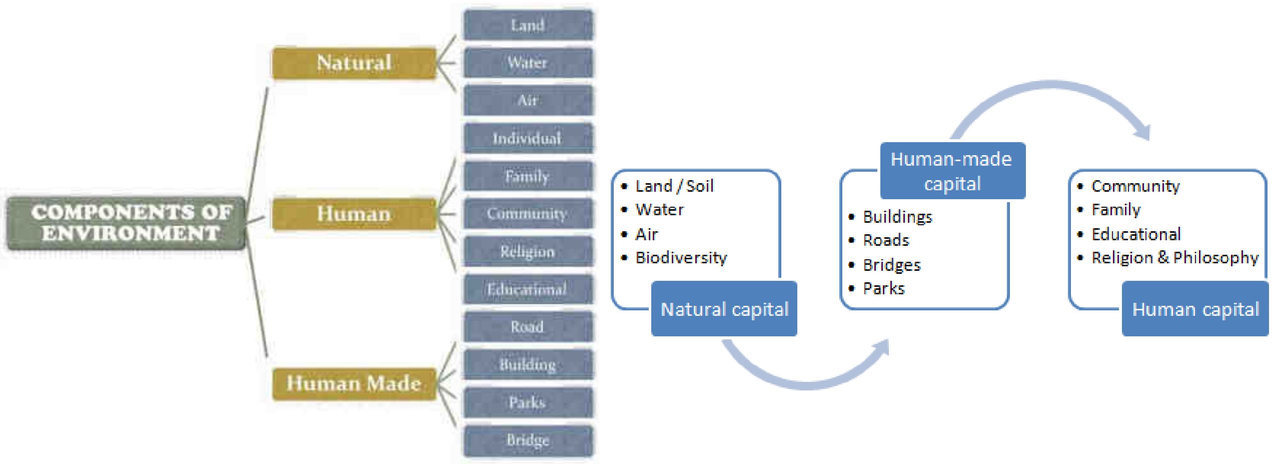

a) b)

Fig. 3. Simple diagram versions and different perspectives for the components of the environment [5, 6]

Human-Environmental Interactions (HEI) in line with the idea presented in Fig. 2 and Fig. 3 can be defined as interactions between the human social system and (the “rest” of) the ecosystem [9].
Human-Social Systems and ecosystems are complex adaptive systems, complex because ecosystems and human social systems have many parts and many connections between these parts (see Fig. 4), and adaptive because they have feedback structures that promote survival in a constantly changing ecosystem or environment [9].

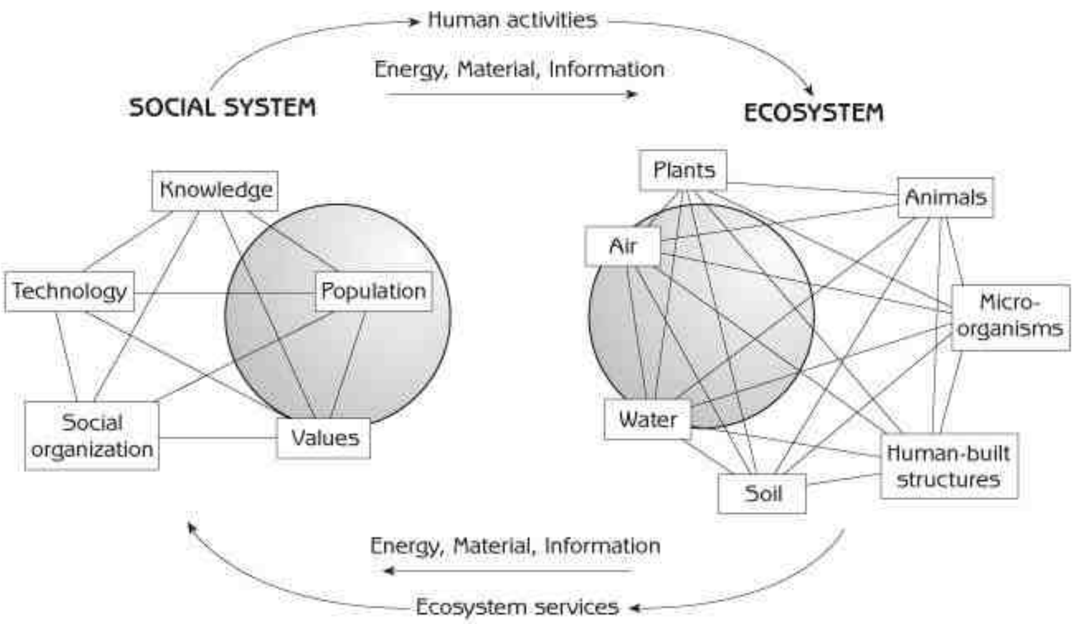

Fig. 4. Interaction of the Human Social System with the Ecosystem [9]

The Social System is a central concept in human ecology because human activities that impact on ecosystems are strongly influenced by the society in which people live. Values and knowledge - which together form our worldview as individuals and as a society - shape the way that we process and interpret information and translate it into action.
Technology defines our repertoire of possible actions, and the social organizations shape the possibilities into what we actually do. Like ecosystems, social systems can be on any scale - from a family to the entire human population of the planet (see Fig. 5). The ecosystem provides services and not only services to the social system by moving materials, energy and information to the social system to meet people’s needs - in this sense we are talking about Social-Ecological Systems dynamics.

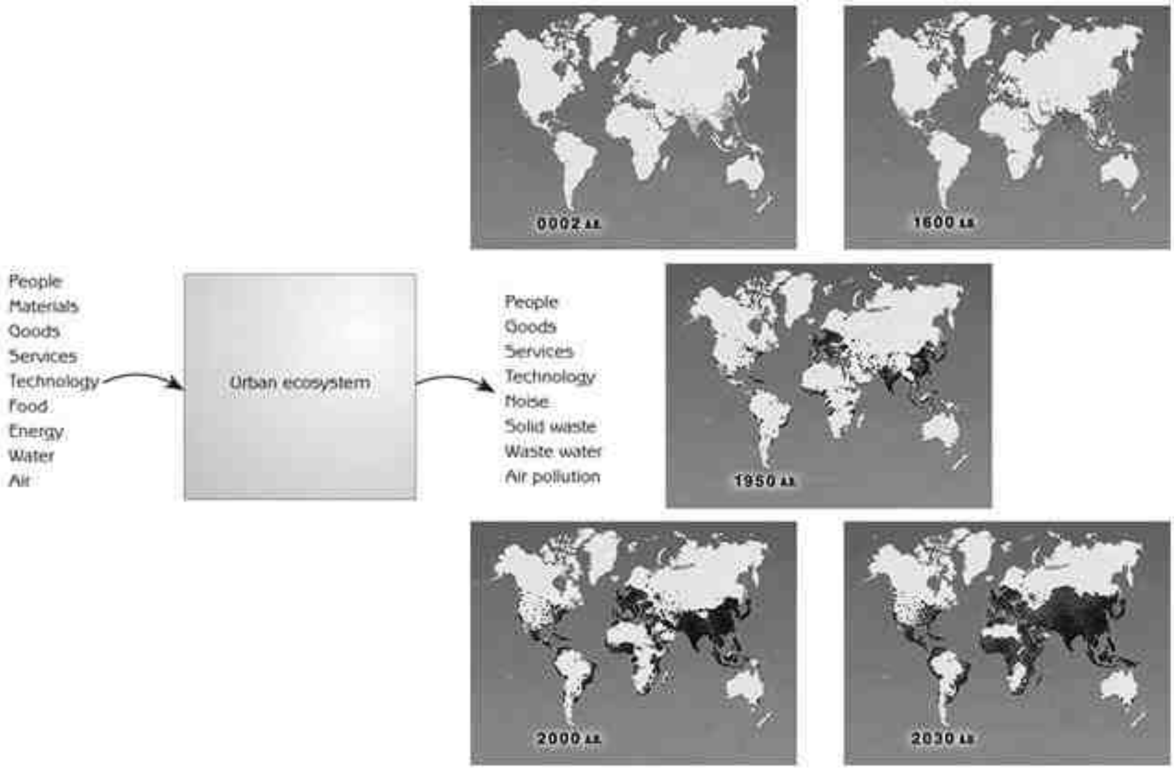

Fig. 5. Inputs and outputs of the urban ecosystem [9]

Material, energy and information move from Social System to Ecosystem (see Fig. 6) as a direct and intimate consequence of human activities that impact the ecosystem - people affect ecosystems when they use resources, after using materials from ecosystems, people return the materials to ecosystems as waste.

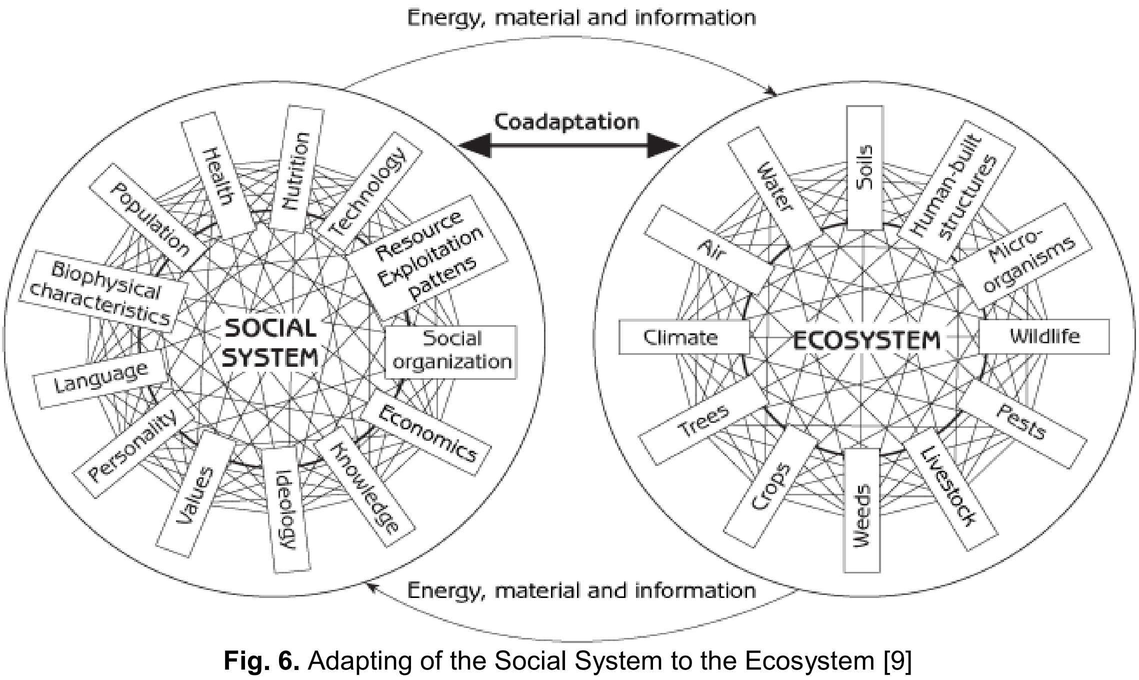

Fig. 6. Adapting of the Social System to the Ecosystem [9]

People intentionally modify or reorganize existing ecosystems, or create new ones, to better serve their needs (see Fig. 7). With machines or human labor, people use energy to modify or create ecosystems by moving materials within them or between them. They transfer information from social system to ecosystem whenever they modify, reorganize or create an ecosystem.

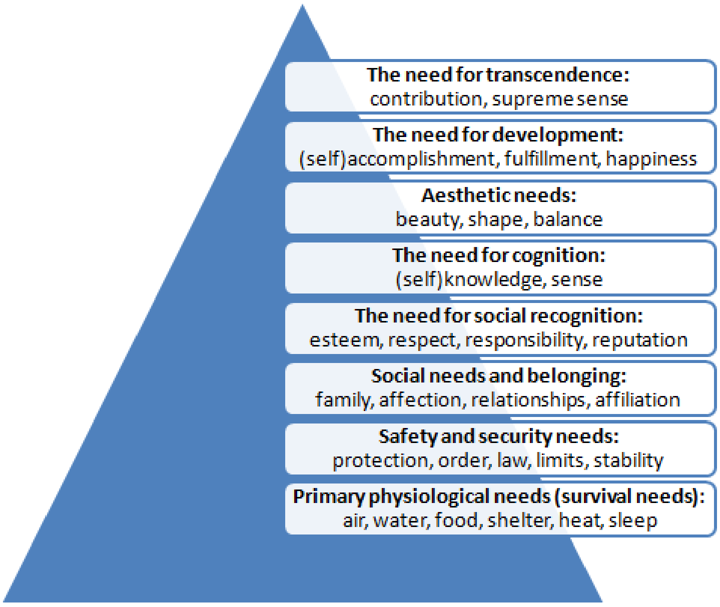

Fig. 7. The need for environmental protection from the perspective of the Maslow Pyramid [6]

Depending on the momentary needs, due to adapting attempts of the Social System to the Ecosystem we are talking about the three hypostases presented in Fig. 8, which, at a certain level, we can say they overlap the Eco-Anthropo-Techno hypostases presented in Fig. 9, within the complex relationship between Social System and Ecosystem.

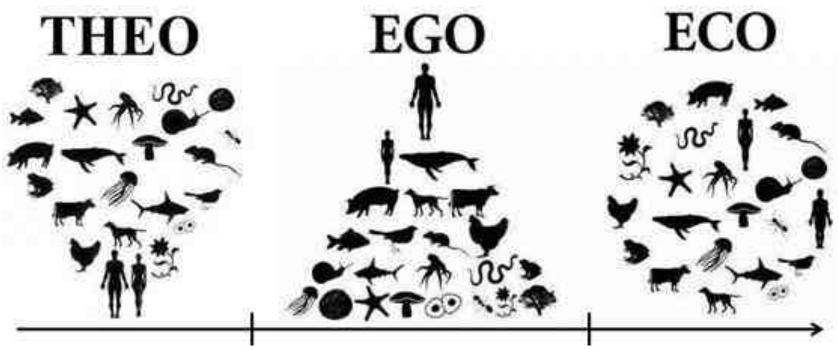

Fig. 8. Overview of human reporting to nature - the 3 hypostases [6]

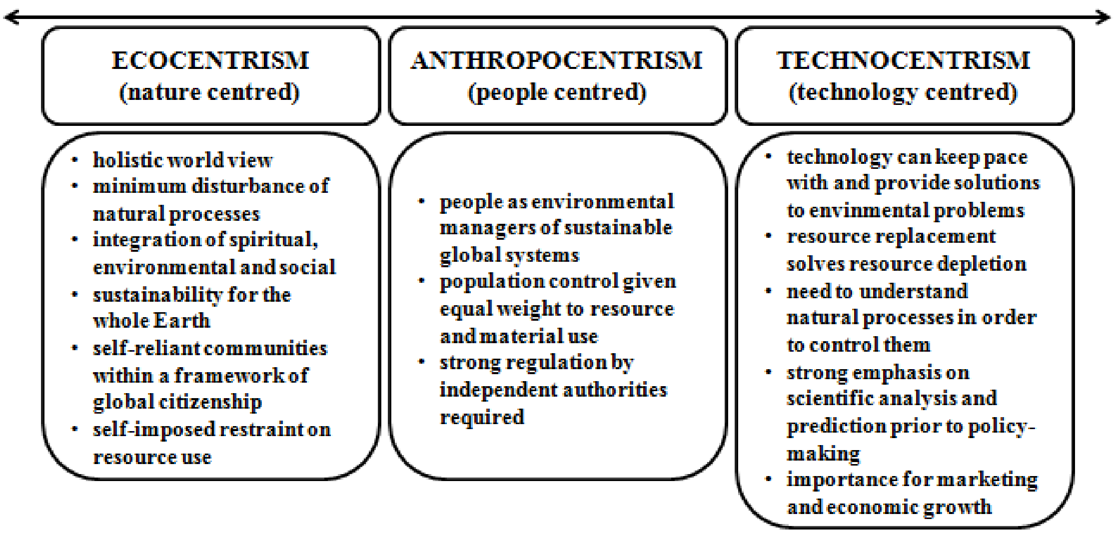

Fig. 9. Overview of human reporting to nature - the Eco-Anthropo-Techno hypostases

3. Bronfenbrenner's Ecological Theory from Human-Environment Interaction perspective

The *ecological systems theory* was developed by Urie Bronfenbrenner, who believed that a person's development was affected by everything in their surrounding environment, starting with the individual level (Fig. 10) - the child's personality, the elements of temperament and attitude.

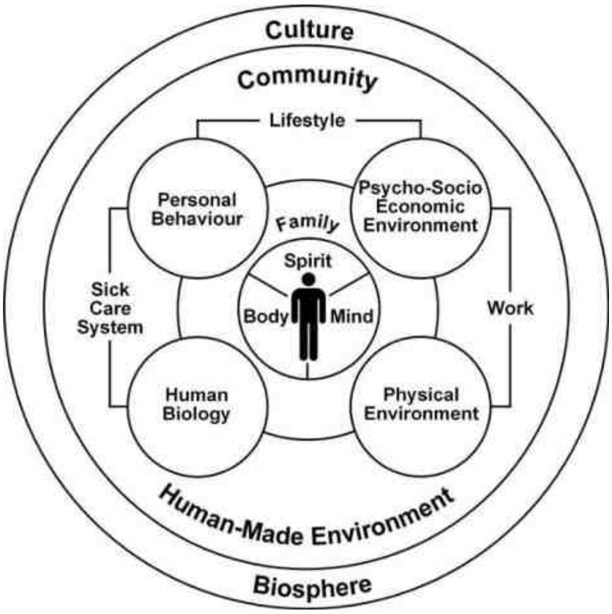

Fig. 10. Ecological Systems Theory at individual level [10]

At this point we talk about 4 aspects as follows:

- *social* - a lot of time spent with friends as well as staying connected via internet and mobile;
- *confident* - with the ability to converse with students and adults alike with ease;
- *mature* - well-mannered and appropriately behaved when required;
- *responsible* - is well presented and understands his responsibilities in the family.

Urie Bronfenbrenner divided the person's environment into five different levels (see Fig. 11):

a) *the microsystem* (*interpersonal processes* and *primary groups*) - is the environment closest to the person, the one in which they have direct contact and where is educated about the world physically, socially and psychologically.

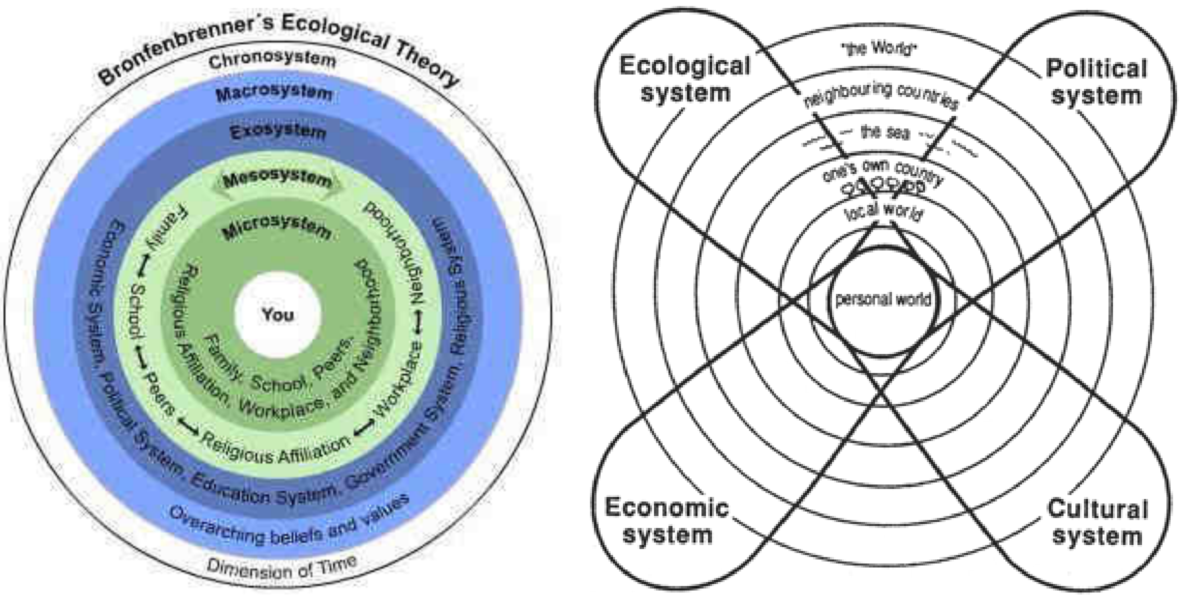

Fig. 11. Different perspectives of Ecological Systems Theory [11]

Some examples would be: *home/family* - values and beliefs are derived from here that he chooses to follow and live by and where support and nurture is found; *school/university* - place where he is uducated and embraces opportunity of education; *daycare/friends* - a diverse range of nationalities where he has learnt to acknowledge and appreciate different cultures; *work* - learning the difficulties that are part of life and the hard work that comes with everyday necessities.

b) *the mesosystem* - consists of the interactions between the different parts of a person's microsystem. The mesosystem is where a person's individual microsystems do not function independently, but are interconnected and assert influence upon one another.
c) *the exosystem* (*organizational factors*) - refers to a setting that does not involve the person as an active participant, but still affects them. This includes decisions that have bearing on the person, but in which they have no participation in the decision-making process.
d) *the macrosystem* (*community factors*) - this layer may be considered the outermost layer in the child's environment. While not being a specific framework, this layer is comprised of cultural values, customs, and laws. The effects of larger principles defined by the macrosystem have a cascading influence throughout the interactions of all other layers.
e) *the chronosystem* (*public policy*) - this system encompasses the dimension of time as it relates to a child's environments. Elements within this system can be either external, such as the timing of a parent's death, or internal, such as the physiological changes that occur with the aging of a child. As children get older, they may react differently to environmental changes and may be more able to determine more how that change will influence them.

In order to analyze Human-Environmental Interactions it is important to be aware of specific characteristics of the human social system. The type of society strongly influences people's attitude towards nature, their behavior and therefore their impact on ecosystems. Important characteristics of human social systems are population size, social organization, values, technology, wealth, education, knowledge and many more.

Especially values and knowledge strongly influence peoples "view of life" and consequently define the way people act. The choice of possible actions is then limited by the available technology, so people modify the environment for their purposes and obtain benefits - Ecosystem Services (see Fig. 12) from it.

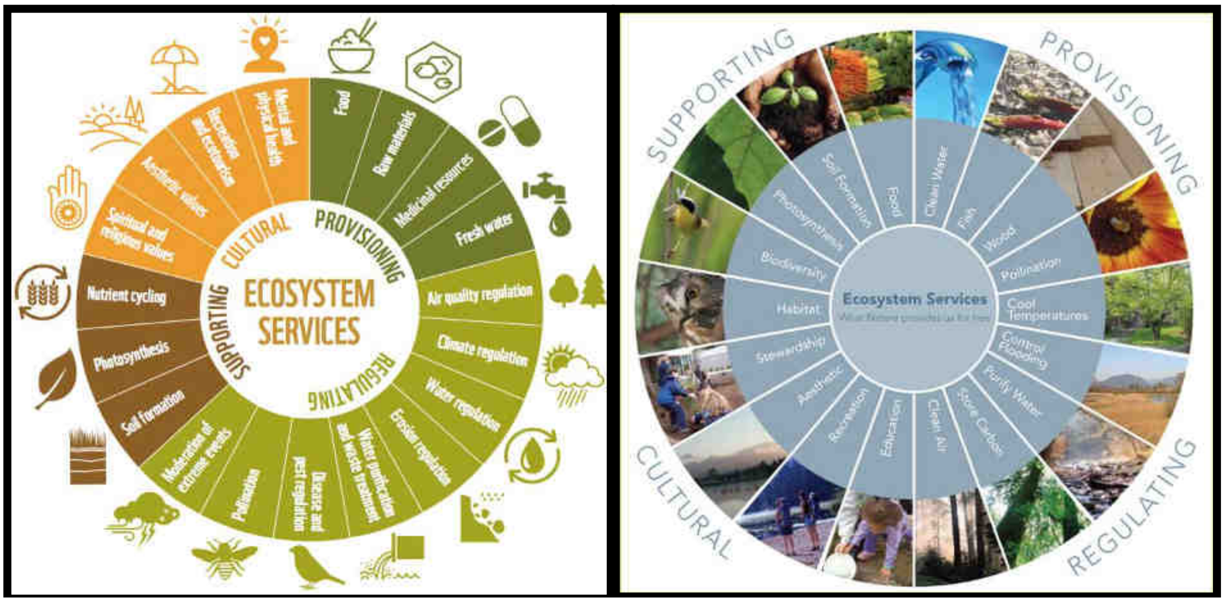

Fig. 12. Different perspectives of Ecosystem Services [12, 13]

These Ecosystem Services are essential for human well-being and include for example the provision of resources like water, timber, food, energy, information, and land for farming and many more. Obviously by using these resources people affect the environment in a lot of ways. Furthermore people often reorganize existing ecosystems to achieve new ones that seem to be more effective in serving their needs.

4. From frameworks typologies for analyzing the Social-Ecological Systems dynamics to the need for Environmental Big Data

Existing frameworks for the analysis of complex systems come in different forms, reflecting differences in the state of knowledge and different understandings of what constitutes a framework. Published frameworks range from systems of equations derived from first principles through to relatively simple box and arrow diagrams that explain quite loosely how different pieces of a system are expected to fit together. They may also be developed for different reasons.
Frameworks for social-ecological systems can be broadly grouped into five categories [8]:

a) *hypothesis-oriented frameworks* - are quite specific, focusing on pairs of variables or clearly defined theoretical questions (e.g. the landscape disturbance framework);
b) *assessment-oriented frameworks* - help people to think in a structured way about a system but are relatively mechanism-free. They are used to summarize key attributes of a social-ecological system for the purpose of describing it, typically for stock-taking or evaluative exercises (e.g. the Millennium Ecosystem Assessment Framework);
c) *action-oriented frameworks* - these recommend a particular course of action by an established set of actors in response to a particular kind of problem. They are usually focused on implementing solutions rather than establishing the causes of problems (e.g. the Nature Conservancy's 5-S framework for conservation, the Driving forces-Pressure-State-Impacts-Responses framework);
d) *problem-oriented frameworks* - have mostly been developed to initiate and facilitate the process of solving a particular kind of problem. They focus more on problem identification and problem-solving processes than on prescribing the actual actions that are to be undertaken; unlike action-oriented frameworks, they do not start with a clear definition of the solution; and
e) *theory-oriented or overarching frameworks* - are the frameworks that attempt to define and connect different pieces of theory within the domain of a particular area of research. There have been a number of attempts at producing general frameworks which either deal directly with SES theory or with relevant aspects of related theories.

The modern society - Knowledge-based Society - in accordance with the actual changes and preoccupations in the environment domain, such as Human-Environment Interaction frameworks and sustainable development [14, 15], has provided various types of informatics resources (tools, methodologies, procedures) to manage and support the ideas and actions related to the environmental issues [16, 17, 18]. The specialists that activates in the environmental protection or other connected domains needs more and more information (Environmental Big Data pool) and knowledges at every level of environmental processes management and evaluation (see Fig. 13).

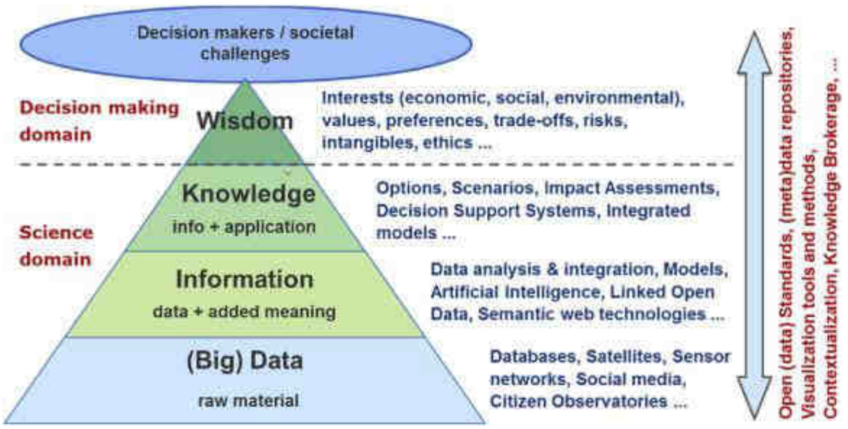

Fig. 13. DIKW hierarchy, from Big Data to decision making for societal challenges [19]

At the same time, in order to elaborate and development a sustainable development project, they need to know and to understand the environmental and phenomena conditions. The analysis used must be based on the best available techniques (B.A.T.), methods and data, and the knowledges get from self experince or from another specialists.

Traditionally, these information and knowledges - part of Environmental Big Data river (see Fig. 14) - are obtained, in accordance with the temporar requirements, by accessing directly databases, reports and documents, by transfering/sharing information and knowledge with specialists or by the contacs extablished at the workshops, conferences and simposions [16, 17, 18].

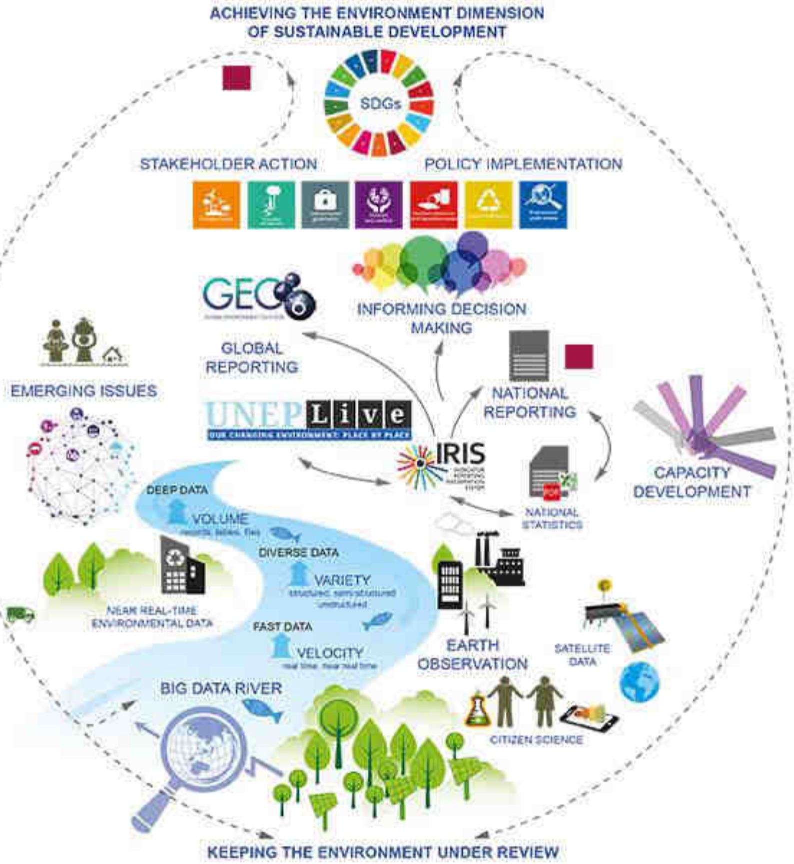

Fig. 14. From Environmental Big Data to Sustainable Development goals [23]

To improve the management capabilities and environmental assessment is necessary for specialists to be able to manage and implement concepts for effective and efficient environment that can be achieved through information software environment. They must also have a simple and efficient access to knowledge and current information enabling them to take the best decisions for sustainable development for both developed economies and those in transition [20, 21, 22].
The current approach starts from the few Romanian contributions in Environmental Informatics domain, trying to rally to the main concerns of the international level. Without going into detail to show all of the specific aspects of Environmental Informatics, we propose, for the next articles, an integrative vision on the subject of discussion as an open and dynamic system, able to perform multiple functions, particularly research, to meet the goals and needs of users.
Knowing that the environmental protection activitivity is just at the beginning in our country, with a major involvement responsiveness and only in the last two decades and that requires a comprehensive approach, multidisciplinary, I tried in these few lines to lay the foundations of future actions research and environmental protection through the tools provided by the Environmental Informatics [20, 21, 22]. The potential beneficiaries of structured information during this project are students and teachers in environmental engineering departments of universities from the country, engineers, computer programmers and support staff involved in specific environmental activities.

5. Conclusions

In our current society, regardless of how developed it is technologically speaking, the dependence on the environment is a current issue. The element that is most notable subjected to change is our vision regarding man and his' environment. If this was seen until recently as man against nature, nowadays we talk about his integration with the environment or rather his good management of it.
This new vision, *part of Knowledge-based Society* is, as we've presently shown in this paper, in very tight relationship with the environment in which man works, with local traditions and most notably his formal and informal education. In his historic context, the ecological education process is a relatively new one, and as such, a need to insist on recent results and the refinement of interdisciplinary models appears.

References

[1] Coman, M. *General and Applied Ecology / Ecologie generală și aplicată*. Cluj-Napoca, Risoprint Publishing House, 2010.
[2] Brondízio, E.S., and E.F. Moran (eds.). *Human-Environment Interactions: Current and Future Directions*. Dordrecht, Springer Science+Business Media, 2012.
[3] ***. www.epa.gov/report-environment/sustainability-and-roe.
[4] ***. environment-ecology.com/general-systems-theory/379-systems-thinking.html.
[5] ***. www.jagranjosh.com/general-knowledge/ecology-and-ecosystem-a-complete-overview.
[6] Mesaroș, M., B. Cioruța, and M. Coman. "Protected natural heritage on route from philosophy to environment engineering." *Scientific Bulletin of North University Center of Baia Mare, Series D, Mining, Mineral Processing, Non-ferrous Metallurgy, Geology and Environmental Engineering* 32, no. 1 (2018): 63-72.
[7] Stave, K., G. Yemer, and S. Aynelem (eds.). *System Dynamics as a Framework for Understanding Human-Environment Dynamics*. AESS Interdisciplinary Environmental Studies and Sciences Series. Swizerland, Springer International Publishing, 2017. www.springer.com/gp/book/9783319457536.
[8] Cumming, G.S. *Theoretical Frameworks for the Analysis of Social-Ecological Systems*. Japan, Springer, 2014. www.researchgate.net/.../Theoretical Frameworks for the Analysis of Social-Ecological Systems.
[9] Marten, G. *Human Ecology - Basic Concepts for Sustainable Development*. Canada, Earthscan Publications, 2001. gerrymarten.com/human-ecology/tableofcontents.html.
[10] ***. http://isecn.org/2013/05/07/vision-and-values-matter-and-so-do-sailing-lessons.
[11] ***. https://sites.google.com/site/dsmktylenda/content/bronfenbrenner-s-ecological-theory.
[12] ***. https://blog.nus.edu.sg/myhornisnotforsale/2016/11/08/ecosystem-services.
[13] ***. http://soscanvairet.blogspot.com/2011/07/intentos-de-valoracion-de-los-servicios.html.
[14] Cioruța, B., M. Coman, A. Cioruța, and A. Lauran. "From Human-Environment Interaction to Environmental Informatics (I): Theoretical and Practical Implications of Knowledge-based Computing." *Magazine of Hydraulics, Pneumatics, Tribology, Ecology, Sensorics, Mechatronics (Hidraulica®)*, no. 1 (March 2018): 71-82. http://hidraulica.fluidas.ro/2018/nr1/71-82.pdf.
[15] Cioruța, B., M. Coman, and A. Lauran. "From Human-Environment Interaction to Environmental Informatics (II): the sustainability evolution as requirement of Knowledge-based Society." *Magazine of Hydraulics, Pneumatics, Tribology, Ecology, Sensorics, Mechatronics (Hidraulica®)*, no. 2 (June 2018): 33-42. hidraulica.fluidas.ro/2018/nr2/33-42.pdf.
[16] Cioruța, B., M. Coman, and A. Cioruța. "Studying Environmental Problematics and Hazards with help of Informatics Applications." Paper presented at the International Conference "Scientific Research and Education in the Air Force" (AFASES®), Braşov, Romania, May 22-24, 2014. www.afahc.ro/.../2014/Cioruta_Coman_Cioruta.pdf.
[17] Cioruţa, B., M. Coman, and V. Mateșan. "Environmental Information Systems: solutions and emerging challenges for modern strategic development of Romanian local communities." Paper presented at the International Conference "Scientific Research and Education in the Air Force" (AFASES®), Braşov, Romania, May 23-25, 2013. www.afahc.ro/.../Cioruta_Coman_Matesan.pdf.
[18] Coman, M., and B. Cioruţa. "Environmental Information Systems as a possible solution for strategic development of local and regional communities." Paper presented at the International Conference „Air and Water - Environmental Components'/ „Aerul şi Apa – componente ale mediului", Cluj-Napoca, Romania, March 22-23, 2013.
[19] Lokers, R., R. Knapen, S. Janssen, Y. Randen, and J. Jansen. "Analysis of Big Data technologies for use in agro-environmental science." *Environmental Modelling & Software* 84 (2016): 494-504. www.sciencedirect.com/science/article/pii/S1364815216304194.

[20] Cioruţa, B., A. Cioruţa, and M. Coman. "Pleading for an environmental informatic culture forming need." /„Pledoarie pentru necesitatea formării unei culturi informaţionale environmentale." *Journal of Environmental Research and Protection* 30 (2012): 31-39. www.ecoterra-online.ro/files/1339069625.pdf.
[21] Cioruţa, B., and M. Coman. "The evolution, definition and role of EIS in the development of environmental protection strategies." /„Evoluţia, definiţia şi rolul Sistemelor Informatice de Mediu în dezvoltarea strategiilor pentru protecţia mediului." *Journal of Environmental Research and Protection* 27 (2011) : 11-14. www.ecoterra-online.ro/files/1321371401.pdf.
[22] Cioruţa, B., and M. Coman. "A forey in modern scientific research of the environment. From SIM to environmental informatics." /„Incursiune în cercetarea ştiinţifică modernă a mediului înconjurător. De la Sistemele Informatice de Mediu la Informatica Mediului." *Journal of Environmental Research and Protection* 29 (2011): 17-20. www.ecoterra-online.ro/files/1330955124.pdf.
[23] ***. www.unenvironment.org/environment-under-review/why-does-environment-under-review-matter.

UNIUNEA EUROPEANĂ

Instrumente Structurale 2014-2020

Comunicat de presă

București, martie 2019

ANUNȚ PUBLICITAR PROIECT POC - Axa G

Firmele producătoare de subansambluri mecano-hidraulice la cerere (netipizate sau cu destinații speciale), firmele producătoare sau care se ocupă cu repararea de aparatură, echipamente și instalații hidraulice, firmele care se ocupă cu vânzarea, montarea, întreținerea și exploatarea unor astfel de produse *sunt invitate să participe la work-shopurile și evenimentele tematice* organizate la sediul Filialei Institutul de Cercetări pentru Hidraulică și Pneumatică a INOE 2000, în scopul informării privind oportunitățile de colaborare ce se pot dezvolta între firmă și institut, în cadrul contractului nr. 6/AXA1/1.2.3G/25.06.2018, încheiat între **MCI** în calitate de **Organism Intermediar (OI)** pentru Programul Operațional Competitivitate (POC), în numele și pentru **Ministerul Fondurilor Europene (MFE)** în calitate de **Autoritate de Management (AM)** pentru Programul Operațional Competitivitate (POC) și **INSTITUTUL NAȚIONAL DE CERCETARE-DEZVOLTARE PENTRU OPTOELECTRONICĂ INOE 2000**, contract aflat acum în derulare.

Transferul de cunoștințe (know-how, produse și servicii) pe care institutul îl furnizează firmelor interesate are loc în baza unor contracte subsidiare de tip B, C sau D, care constau în realizarea de activități specifice fiecărui tip de contract, după cum urmează:

- Contractele de tip B permit accesul întreprinderilor la facilitățile, instalațiile, echipamentele de cercetare ale INOE 2000 Filiala IHP, în scopul realizării unor analize, testări, experimente etc. necesare pentru dezvoltarea unor produse /tehnologii /metode noi sau îmbunătățite.

- Contractele de tip C constau în transfer de abilități /competențe de cercetare-dezvoltare și de sprijinire a inovării, inclusiv cercetare contractuală executată la cererea întreprinderii (activități de CD oferite de INOE 2000-IHP) și detașare de personal specializat dinspre INOE 2000-IHP spre întreprindere.

- Contractele de tip D au ca obiect derularea de activități de cercetare-dezvoltare în colaborare efectivă cu o întreprindere, prin care se urmărește realizarea unui obiectiv comun pe baza diviziunii muncii, ambii parteneri concepând de comun acord activitățile, contribuind la punerea lor în aplicare și împărțind riscurile financiare, tehnologice, științifice și de altă natură, precum și rezultatele obținute.

Vă invităm să urmăriți pe site-ul proiectului http://menteh.ihp.ro și alte informații utile, precum și anunțurile de lansare a competițiilor pe proiectele subsidiare tip B, C sau D.

Proiect cofinanțat din Fondul European de Dezvoltare Regională prin Programul Operațional Competitivitate 2014-2019

Date de contact:
INOE 2000 Filiala IHP, cu sediul în București, sector 4, str. Cuțitul de Argint nr. 14, cod postal: 040558
Telefon: 0213363991, Fax: 0213373040,
www.ihp.ro

Director de proiect:
Dr. Ing. Cătălin DUMITRESCU
Telefon: 0727391783
E-mail: dumitrescu.ihp@fluidas.ro

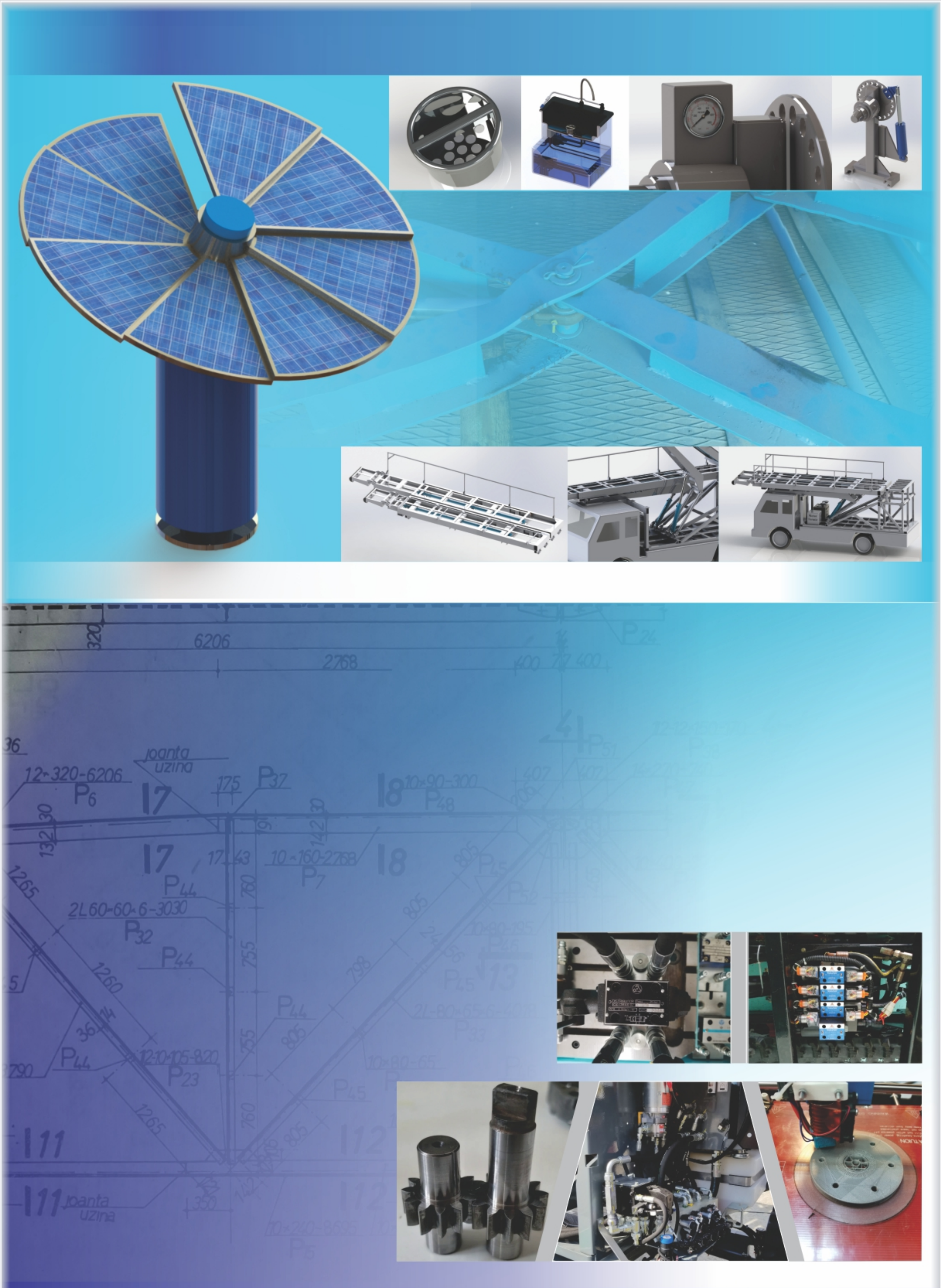

hidraulica.fluidas.ro